

# Sequence Synchronisation in Chaos-based Direct Sequence Spread Spectrum Communication Systems

Ramin Vali

*A thesis submitted in partial fulfilment of the requirements for the degree of  
Doctor of Philosophy in Electrical and Electronic Engineering,  
The University of Auckland, New Zealand.*

February 2012



# Abstract

This thesis presents an investigation into the modelling and performance of sequence synchronisation in Chaos-based Direct Sequence Spread Spectrum (CDS-SS) communication systems with the aims of identifying the existing gaps in research and suggesting a new and accurate modelling approach. The CDS-SS systems offer physical layer security without the need for a significant increase in computation or power requirements. This is significant when conventional encryption techniques cannot be used on secure communication systems because of their high power requirements as well as computational intensity.

The main focus of this thesis is the problem of synchronising chaos-based spreading sequences. The modelling approaches previously used for chaos-based spreading codes do not take their non-binary nature into account and are not accurate as a result. This thesis extends the existing analysis in the literature to include CDS-SS synchronisation in presence of channel fading. Subsequently, an accurate approach is developed for modelling the synchronisation block of a CDS-SS system. This approach is based on the statistical description of chaos-based spreading codes cross- and auto-correlation functions and is termed chaos correlation statistics (CCS). To verify the validity of this approach, the acquisition stage of a CDS-SS synchronisation block is modelled using three scenarios: noise, fading and interleaving. It has been shown that the CCS method makes an accurate prediction of the acquisition phase performance for all three scenarios considered. The CCS method is also used to model a CDS-SS tracking loop statistically with high accuracy as verified by comparison with numerical analysis results. The effects of tracking loop errors and timing jitter on the probability of error have been derived for the same three scenarios mentioned above. These newly derived probability of error equations are verified by extensive simulation results.

Overall it is concluded that sequence synchronisation for CDS-SS systems is possible and the CCS method is a suitable tool for accurate prediction of synchronisation performance in CDS-SS systems. Also, the CCS approach can be used in any scenario in which accurate modelling of the correlation function of non-binary spreading sequences is needed.



# List of Publications

This thesis has inspired the following.

## Journal Papers

- J1      **Ramin Vali**, Stevan Berber, and Sing Kiong Nguang. Effect of Rayleigh fading on non-coherent sequence synchronization for multi-user chaos based DS-CDMA. *Elsevier Signal Processing*, vol.90, pp1924-1939, 2010.
- J2      **Ramin Vali**, Stevan Berber, and Sing Kiong Nguang. Analysis of Chaos-based Code Tracking Using Chaotic Correlation Statistics. *IEEE Transactions on Circuits and Systems I*, 2012
- J3      **Ramin Vali**, Stevan Berber, and Sing Kiong Nguang. Accurate Derivation of Chaos-based Acquisition Performance in a Fading Channel. *IEEE Transactions on Wireless Communications*, 2012
- J4      **Ramin Vali**, Stevan Berber, and Sing Kiong Nguang. Accurate Performance of Chaos-based Code Tracking In Presence of Multipath Fading. *IEE Electronics Letters*, 2012. (Accepted for publication).
- J5      **Ramin Vali**, Stevan Berber, and Sing Kiong Nguang. Comparing DSP Realizations of Correlator and SVM Receivers for Chaos-based Multi-user DS-SS. *Elsevier Signal Processing*. (Submitted for publication).
- J6      **Ramin Vali**, Stevan Berber, and Sing Kiong Nguang. Performance of Chip Interleaved Partially Synchronised Chaotic DS-SS Systems. *IEEE Transactions on Wireless Communications*. (Submitted for publication).
- J7      **Ramin Vali**, Stevan Berber, and Sing Kiong Nguang. Chaos-based Code Tracking Performance Improvement Using Chip Interleaving. *IEEE Communication Letters*, 2011. (Submitted for publication).

## Book Chapter

- BC1     **Ramin Vali**, Stevan Berber, and Sing Kiong Nguang. *Planning and Optimization of 3G and 4G Wireless Networks*, chapter 14, pages 445-479. River Publishers, 2009.

## Conference Papers

- C1      **Ramin Vali** and Stevan Berber. Analysis of non-coherent code tracking for NPSK systems in presence of noise and fading. *In IEEE International Conference on Acoustics, Speech and Signal Processing, 2011. ICASSP'2011.*
- C2      **Ramin Vali** and Stevan Berber. Noise-based DS-CDMA System Performance with Timing Jitter. *In WSEAS International Conference on Communications, 2011.*
- C3      **Ramin Vali** and Stevan Berber. Fading Mitigation in Interleaved Chaos-Based DS-CDMA Systems for Secure Communications. *In WSEAS International Conference on Communications, 2011.*
- C4      **Ramin Vali**, Stevan Berber, and Sing Kiong Nguang. Analysis of a chaos- based non-coherent delay lock tracking loop. *IEEE International Conference on Communications 2010, ICC '10.*
- C5      **Ramin Vali** and Stevan Berber. Noise based DS-SS acquisition performance in presence of fast fading. *In Asia Pacific Conference on Communications, 2010. APCC '2010.*
- C6      **Ramin Vali** and Stevan Berber. Chaos-based DS-CDMA acquisition performance in presence of fast fading. *In Wireless @ Virginia-Tech, 2010.*
- C7      **Ramin Vali** and Stevan M. Berber. Secure communication in asynchronous noise phase shift keying CDMA systems. *In Spread Spectrum Techniques and Applications, 2008. ISSSTA '08. IEEE 10th International Symposium on*, pages 528-533, Aug. 2008.

# Dedication

*I dedicate this thesis to my mother Giti, my father Hamid and my lovely sister Hideh.*

*I wish you all the best in the world.*



# Acknowledgements

First, I would like to thank my supervisors, Dr. Stevan Mirko Berber and A/Prof. Sing Kiong Nguang, for their guidance throughout my research.

I also wish to acknowledge:

- Dr. Michael Neve, A/Prof. Kevin Sowerby, Dr. Bernard Guillemin and Dr. Mark Andrews for many interesting and instructive discussions as well as their continued assistance and support.
- The other two members of the exclusive “The three witches of the Scottish play club”, Andrew and Salim.
- Claudio, Hazim, Iman, Nasser, Rachita, and Rav for many laughs, their friendship and  $10^3 \pm 6$ , tea breaks.

Last, but most definitely not the least, I wish to thank my family for their never ending support, care and love. I could never do this without them.



# Contents

<b>1</b>	<b>Introduction</b>	<b>1</b>
<b>2</b>	<b>Wireless Communications Using Chaos</b>	<b>7</b>
2.1	Introduction . . . . .	7
2.2	Multi-User Wireless Communications — A Background . . . . .	7
2.2.1	A simple communication model . . . . .	7
2.2.1.1	Transmitter . . . . .	8
2.2.1.2	Channel . . . . .	9
2.2.1.3	Receiver . . . . .	10
2.2.2	Resource sharing for multi-user wireless systems . . . . .	10
2.2.3	Spread spectrum techniques . . . . .	13
2.3	Chaotic Systems and Wireless Communications . . . . .	15
2.3.1	History of chaos . . . . .	15
2.3.2	Why chaos-based communications? . . . . .	17
2.3.3	Chaos-based wireless communication schemes . . . . .	18
2.4	Summary . . . . .	22
<b>3</b>	<b>Chaos-based DS-SS (CDS-SS) Communications</b>	<b>25</b>
3.1	Introduction . . . . .	25
3.2	Existing CDS-SS Communication Methods . . . . .	28
3.3	Systems Model for Investigation . . . . .	29
3.3.1	Transmitter structure . . . . .	30
3.3.2	Channel model . . . . .	31
3.3.2.1	Noise . . . . .	31
3.3.2.2	Multi-path fading . . . . .	32

3.3.2.3	Inter-user interference . . . . .	35
3.3.2.4	Time delay . . . . .	36
3.3.3	Receiver structure . . . . .	36
3.4	The Need for Synchronisation . . . . .	41
3.5	Thesis Contributions . . . . .	43
3.6	Summary . . . . .	43
<b>4</b>	<b>Sequence Synchronisation in CDS-SS Communications</b>	<b>45</b>
4.1	Introduction . . . . .	45
4.2	Sequence Acquisition . . . . .	46
4.2.1	Sequence acquisition for DS-SS systems — A survey . . . . .	46
4.2.2	Sequence acquisition for chaos-based spreading sequences . . . . .	51
4.3	Sequence Tracking . . . . .	52
4.3.1	Sequence tracking for DS-SS systems—A survey . . . . .	53
4.3.2	Sequence tracking for chaos-based spreading sequences . . . . .	54
4.4	Discussion . . . . .	56
4.4.1	CDS-SS sequence acquisition shortcomings . . . . .	56
4.4.2	CDS-SS sequence tracking shortcomings . . . . .	56
4.5	Summary . . . . .	57
<b>5</b>	<b>Sequence Synchronisation of CDS-SS System in Presence of Fading</b>	<b>59</b>
5.1	Introduction . . . . .	59
5.2	System Overview . . . . .	59
5.3	Sequence Acquisition in Presence of Fading . . . . .	61
5.4	Sequence Tracking in Presence of Fading . . . . .	71
5.4.1	Control law derivation . . . . .	80
5.4.2	Effects of filtering and noise on the tracking loop properties . . . . .	81
5.5	Summary . . . . .	84
<b>6</b>	<b>Statistical Analysis of CDS-SS Acquisition</b>	<b>87</b>
6.1	Introduction . . . . .	87
6.2	Chaotic Correlation Statistics (CCS) . . . . .	87
6.3	Accurate Analysis of Code Acquisition Using CCS . . . . .	91

---

6.3.1	Scenario 1, noise only . . . . .	92
6.3.2	Scenario 2, noise and fading . . . . .	94
6.3.3	Scenario 3, noise and fading with interleaving . . . . .	98
6.3.4	Probability of false alarm, accurate statistical analysis . . . . .	101
6.3.5	Probability of detection, accurate statistical analysis . . . . .	101
6.4	Results and Discussion . . . . .	103
6.5	Summary . . . . .	105
<b>7</b>	<b>Statistical Analysis of CDS-SS Tracking</b>	<b>109</b>
7.1	Introduction . . . . .	109
7.2	Code Tracking, An Accurate Statistical Analysis Using CCS . . . . .	109
7.3	Theoretical Findings . . . . .	117
7.4	Summary . . . . .	123
<b>8</b>	<b>CDS-SS Performance with Tracking Errors</b>	<b>125</b>
8.1	Introduction . . . . .	125
8.2	System Outline . . . . .	125
8.3	Chip Misalignment . . . . .	127
8.4	Derivation of the BER Expression With Partial Chip Overlap . . . . .	128
8.4.1	Scenario 1, AWGN . . . . .	129
8.4.2	Scenario 2, AWGN and fading . . . . .	130
8.4.3	Scenario 3, AWGN and fading with interleaving . . . . .	132
8.5	Derivation of the BER for Constant Tracking Errors . . . . .	134
8.6	Derivation of the BER for Random Tracking Errors . . . . .	135
8.7	Theoretical Findings . . . . .	138
8.8	Summary . . . . .	139
<b>9</b>	<b>Implications and Prospects</b>	<b>143</b>
9.1	Introduction . . . . .	143
9.2	The Effects of the Findings on the State of the Art . . . . .	143
9.3	Possible Enhancements to the Existing Work . . . . .	144
9.3.1	Expansion to QPSK . . . . .	144
9.3.2	Use of RAKE receiver . . . . .	145

9.3.3	Adaptive chaos-based synchronisation . . . . .	145
9.3.4	Other non-binary spreading sequences . . . . .	145
9.3.5	Hardware implementation and design . . . . .	145
9.4	Summary . . . . .	146
<b>10</b>	<b>Conclusions</b>	<b>147</b>
<b>A</b>	<b>Logistic map</b>	<b>151</b>
<b>B</b>	<b>Statistical derivations</b>	<b>153</b>
B.1	Derivation of $E[x_k^2]$ . . . . .	153
B.2	Derivation of $E[x_k^4]$ . . . . .	154
<b>C</b>	<b>Mean and Variance of the Rayleigh Random Variable</b>	<b>155</b>
<b>D</b>	<b>Product of Rayleigh and Gaussian Distributions</b>	<b>157</b>
<b>E</b>	<b>Chip-interleaving</b>	<b>161</b>
<b>F</b>	<b>BER Derivation</b>	<b>163</b>
F.1	In presence of noise . . . . .	163
F.2	In presence of noise and fading . . . . .	164
F.3	In presence of noise and interleaved fading . . . . .	164
<b>G</b>	<b>DSP Design</b>	<b>165</b>
G.1	DSP Specification and Justification . . . . .	165
G.2	Design and Implementation of the CDS-SS System . . . . .	166
G.3	System Results . . . . .	167
G.4	Acquisition Results . . . . .	168
G.5	Visual Transmission Results . . . . .	168
G.6	Speed Test Result . . . . .	168
<b>References</b>		<b>173</b>

# List of Figures

2.1	Simplified communication model.	8
2.2	FDMA.	11
2.3	OFDMA.	11
2.4	TDMA.	12
2.5	CDMA.	12
2.6	Spread spectrum signal power and noise floor.	13
2.7	Spread spectrum in time domain.	14
2.8	The Lorenz attractor.	16
2.9	The “Double Scroll” attractor.	16
2.10	Rössler attractor.	17
2.11	Random-like nature of a chaotic sequence generated by the Logistic map.	20
2.12	Sensitivity to initial conditions for chaotic sequences.	20
2.13	The cross-and auto-correlation of chaotic sequences.	22
3.1	The block diagram of the transmitter with signal representations.	31
3.2	AWGN in time and frequency domain.	32
3.3	Rayleigh fading	34
3.4	Receiver block diagram.	37
3.5	Distribution of the correlator output for BPSK modulation and the threshold chosen.	38
3.6	Distribution of the correlator output (no synchronisation).	38
3.7	System model.	40
3.8	Thesis structure and contributions, a graphic representation.	42
4.1	Tree diagram for search strategies.	47
4.2	Block diagrams for different implementations of the serial search algorithm.	49

---

4.3	Sliding correlator output waveform for serial search algorithm. . . . .	50
4.4	Tree diagram for acquisition schemes. . . . .	51
4.5	Block diagrams of two tracking loop configurations. . . . .	54
4.6	Early-late gate output waveform. . . . .	55
4.7	Tree diagram for Tracking. . . . .	55
5.1	Synchronisation system model in the presence of fading. . . . .	60
5.2	Correlation illustration. . . . .	62
5.3	ROC in presence of noise (SNR = 0 dB), for 0 to 12 users and fading . . . . .	68
5.4	ROC in presence of noise (SNR = 4 dB), for 0 to 12 users and fading . . . . .	68
5.5	ROC in presence of noise (SNR = 8 dB), for 0 to 12 users and fading . . . . .	69
5.6	ROC in presence of noise (SNR = 12 dB), for 0 to 12 users and fading . . . . .	69
5.7	ROC with different correlation periods. . . . .	70
5.8	Tracking loop output for a chaotic pilot when $\Delta = 1$ . . . . .	75
5.9	The PDF of $\epsilon_{\text{filtered}}(t, \delta)$ . . . . .	77
5.10	Timing jitter, $T_d$ and its estimation $\hat{T}_d$ . . . . .	79
5.11	Non-coherent tracking loop error curve with filtered pulses for $\Delta = 0.5$ . . . . .	81
5.12	Non-coherent tracking loop error curve with filtered pulses for $\Delta = 1$ . . . . .	82
5.13	Non-coherent tracking loop error curve with filtered pulses for $\Delta = 1.5$ . . . . .	82
5.14	Non-coherent tracking loop error curve with filtered pulses for $\Delta = 2$ . . . . .	83
5.15	Tracking loop error signals. . . . .	84
6.1	Comparison between the statistical models and simulated distributions of $Z_{h_0}$ and $Z_{h_1}$ . .	90
6.2	Synchronisation system model in presence of fading. . . . .	93
6.3	The chaotic correlator output for many experiments. . . . .	93
6.4	Comparison between the statistical models and simulated distributions of $Z'_{h_0}$ and $Z'_{h_1}$ . .	95
6.5	Comparison between the exact distribution of $Z$ . . . . .	96
6.6	Comparison results for $P(Z'_{h_1}, 1, \lambda)$ . . . . .	99
6.7	Visual representation of $P_D$ and $P_F$ based on $P(Z'_{h_0}, 1)$ and $P(Z'_{h_1}, 1, \lambda)$ . . . . .	103
6.8	ROC plot with three scenarios, for SNR = 2 dB and correlation length = 100 chips. . . . .	105
6.9	ROC plot with three scenarios, for SNR = 8 dB and correlation length = 100 chips. . . . .	106
6.10	ROC plot with three scenarios, for SNR = 8 dB and correlation length = 300 chips. . . . .	106

6.11 Percentage improvement for $P_D$ . . . . .	107
7.1 Normalised correlation function square of the correlation function. . . . .	111
7.2 The outputs of the square-law devices for the two branches of the tracking loop. . . . .	112
7.3 Upper and lower limits of the S-curve as well as the chosen points for the distribution. . .	112
7.4 Early and late correlation functions before the square law device. . . . .	115
7.5 Early and late correlation functions after the square law device. . . . .	115
7.6 $D_{\Delta_b}(\delta)$ for correlation lengths of 8, 16, 32, 64 and 128. . . . .	118
7.7 Theoretical values for $D_{\Delta_b}(\delta)$ in a non-coherent scenario. . . . .	118
7.8 CCS tracking comparison results before square-law device. . . . .	119
7.9 CCS tracking comparison results after square-law device. . . . .	120
7.10 $\mathbf{D}_{\Delta}(\delta)$ in the chaos-based non-coherent tracking loop, noiseless (a) and SNR= -12dB (b)	121
7.11 The distribution of $\mathbf{D}_{\Delta}(\delta)$ for $\delta = 0, 0.5T_c$ . . . . .	122
8.1 System block diagram. . . . .	126
8.2 Chip misalignment . . . . .	128
8.3 Probability of error given $z_i^{(g)}$ . . . . .	134
8.4 3D BER for various $\frac{\tau}{R_s}$ values. . . . .	139
8.5 BER performance for AWGN, 1 and 16 user, constant jitter case. . . . .	140
8.6 BER performance for AWGN and fading, 1 user, uniform jitter case. . . . .	140
8.7 BER performance for fading and interleaved scenarios, 1 user, uniform jitter case. . .	141
8.8 BER performance for AWGN and fading, 1 user, Gaussian distributed jitter case. . . .	141
A.1 The Logistic map function. . . . .	152
A.2 The bifurcation diagram for the Logistic map. . . . .	152
D.1 Theory and simulation comparison for the product of Rayleigh and Gaussian. . . . .	158
D.2 Theory and simulation comparison for Rayleigh $\times$ Gaussian+Gaussian. . . . .	159
E.1 Block chip interleaver/de-interleaver pair. . . . .	161
G.1 The functional block diagram of the DS-SS system as implemented on the DSP. . . . .	169
G.2 Comparison between a theoretical Gaussian PDF and the DSP implementation. . . . .	170
G.3 BER for a 1, 5, 10 and 15 user DS-SS system, spreading factor of 100. . . . .	170
G.4 BER for a four-user DS-SS system using spreading factors 20, 32, 64 and 100. . . . .	171

G.5 ROC results form the DSP. . . . .	171
G.6 Visual results for transmission of information. . . . .	172
G.7 Bit rate comparison for correlator and SVM receivers for various number of users. . . . .	172

# List of Abbreviations and Acronyms

AM	Amplitude Modulation
AMPS	Advanced Mobile Phone System
AWGN	Additive White Gaussian Noise
BER	Bit Error Rate
BPSK	Binary Phase Shift Keying
CCS	Chaos Correlation Statistics
CDMA	Code Division Multiple Access
CDS-SS	Chaos-based Direct Sequence Spread Spectrum
CDSK	Correlation Delay Shift Keying
CLT	Central Limit Theorem
CPSK	Chaos Phase Shift Keying
COOK	Chaotic On Off Keying
CSK	Chaotic Shift Keying
DCSK	Differential Chaps Shift Keying
DDL	Double Ditter Loop
DE	Differential Equations
DLL	Delay Locked Loop
DSP	Digital Signal Processor
DS-SS	Direct Sequence Spread Spectrum
FDMA	Frequency Division Multiple Access
FH-SS	Frequency Hopping Spread Spectrum
FM	Frequency Modulation
FM-DCSK	Frequency Modulated DCSK
HPF	High Pass Filter
IUI	Inter User Interference
ISI	Inter Symbol Interference
LPF	Low Pass Filter
MCTL	Modified Code Tracking Loop
OFDMA	Orthogonal Frequency Division Multiple Access
PDF	Probability Density Function
PLL	Phase Locked Loop
PM	Phase Modulation
PN	Pseudo Noise

PNRZ	Polar Non Return to Zero
PRBS	Pseudo Random Binary Sequences
QPSK	Quadrature Phase Shift Keying
ROC	Receiver Operating Characteristics
SMS	Short Message Service
SNR	Signal to Noise Ratio
SS	Spread Spectrum
SVM	Support Vector Machine
TDL	Tau Ditter Loop
TDMA	Time Division Multiple Access
UMTS	Universal Mobile Telecommunications System
UWB	Ultra Wide Band
VCO	Voltage Controlled Oscillator
WCDMA	Wide Band CDMA
Wi-Fi	Wireless Fidelity
WiMAX	Worldwide Interoperability for Microwave Access

# Chapter 1

## Introduction

“See if you can hear anything, Mr. Kemp.”

Guglielmo Marconi’s face showed no evidence of excitement as he said these words on December 12, 1901. Mr. Kemp took the receiver, and a moment later, faintly and yet distinctly and unmistakably, came the three little clicks – the dots of the letter S, tapped out an instant before from Cornwall, England and received at Signal Hill, Newfoundland [1]. This was the first instance of wireless transatlantic signal transmission. The immensity of transmitting a wireless signal over a distance of more than 3000 kilometers was so great that Marconi hesitated to release the news for two days lest it seem too extraordinary for belief [1]. This was an important milestone for wireless communications.

The immediate years following this event saw an increase in the customer base for wireless signalling (all in the form of wireless telegraphy). Navies were the primary contractors for wireless signalling installations in the form of land to warship communications [2, pp-69]. Through the 1910s, all intercontinental transport remained marine and the primary customers for wireless telegraphy were in the shipping segments [2, pp-69]. In 1912 the distress signals transmitted by the Marconi wireless operators in the *Titanic* were received by nearby ships resulting in saving 700 people from that disaster. Britain’s postmaster-general summed up, referring to the Titanic disaster, “Those who have been saved, have been saved through one man, Mr. Marconi... and his marvelous invention.”

Like many other technological arenas communications has been driven, to a great extent, by the military. Both wireless and wired signalling techniques were utilised by both sides of the conflict in WWI [3, pp-406]. The fragility of cables and the possibility of line tapping by the enemy, drove the British forces to adopt wireless techniques in WWI. The extent of German wiretapping was so great that the entire movements of the British forces were known. The Germans used wireless signals to guide their airships for their bombing runs [4] and both sides used them for sighting and correcting artillery fire as well as assisting the air force [3, pp-407]; interestingly, reports that emerged after the war indicate that the French were successful in confusing the German airships by sending them phony wireless signals [5]. These are the first instances of information transmission security becoming important in a military situation.

The reliance on telecommunications grew during the intervening years between the first and second world wars. As a result transmission security requirements became more stringent. New methods of using radio waves to transmit coordinates, and military messages were developed by both Axis and Allied nations,

but because both sides of the conflict had the same technological base, the systems were similar. The most noteworthy development which was extensively utilised during this conflict was spread spectrum (SS) communication. The first publicly available patent on the use of SS in military application was given to Hedy Lamarr and George Antheil. This patent was granted in 1942, but the details were a closely held military secret for many years [6, pp-3]. The inventors turned their invention over to the US Government for use in the war effort, and commercial use was delayed until after the patent had expired [6, pp-3]. The SS technique was used to send secure messages in WWII and to guide torpedoes, but most of the information regarding the use of this technique is still not available [6, pp-4]. From 1948 to 1968, the commercial use of wireless communication was driven by the development of Frequency Modulation (FM) which was an improvement over the Amplitude Modulation (AM) that had been used since the beginning of wireless signalling right up to the end of WWII [2, pp-35].

The communication technology was opened for public use after WWII. The wireless communication specifically was opened to the mass usage in the 1980s by the introduction of the first cellular phones. The first cellular system launched in the early 1980s was analogue and it has been termed the first generation or 1G. These systems only managed voice transmission and were very expensive for subscribers. The US introduced the Advanced Mobile Phone System (AMPS) while Europe adopted a multitude of standards fragmenting its cellular market [2, pp-35].

In 1989, a pan European standard for digital cellular communication was launched. This heralded the 2G era which brought smaller handsets, more capacity and its killer application - the ability to send data in the form of Short Message Service (SMS). The name of the pan European system was chosen to be GSM (Global System for Mobile Communications, originally Groupe Spécial Mobile). A Finnish mobile operator, Radiolinja, launched the first GSM network in 1991 [2, pp-49]. Now it was the turn of the US to have different competing digital and analogues standards, while GSM enjoyed 98% deployment share in western Europe. Towards the end of the 1990s, the growth of SMS exploded in advanced markets such as the Nordic countries [2, pp-49].

As the demand for faster mobile data rates and increase in subscription capacity continued, the third generation of cellular systems, known collectively as 3G, was introduced in Europe, US and Japan. The 3G cellular system has effectively brought the ability to use the Internet to mobile subscribers using wide-band techniques to achieve higher data rates as well as higher capacity. Unlike many of the early 2G systems, the 3G networks across the globe are compatible with each other making inter-standard roaming possible. More recent developments in the cellular technology are striving for even faster data rates and are collectively known as 4G. Recently, the number of cellular subscribers has been estimated to be over 5 billion [7] and is forecast to reach six billion in the middle of 2012. The current 6 billion mark means there are more than three times as many phones as personal computers [7].

The use of wireless systems to communicate between users has not been only for cellular systems, other forms of wireless networking also exist. For example wireless local area networks (WLANs) exist that follow Wi-Fi<sup>1</sup> standards. Also, mobile broadband Internet access is possible and is governed by WiMAX<sup>2</sup> protocols. One of the emergent technologies that has benefited immensely from the recent advancements in the field of wireless communications is the wireless sensor network (WSN). These

---

<sup>1</sup>Wi-Fi stands for Wireless Fidelity.

<sup>2</sup>WiMAX stands for Worldwide Interoperability for Microwave Access.

---

cheap and easily deployed sensors can be placed anywhere and gather data using each other as relays to get their collected data across to a storage/processing unit. There are many different military/civilian applications for WSN and the number of these applications increases as the robustness of the networks improves.

Throughout the history of wireless communications, transmission security and robustness have been very important factors. As the reliance on wireless communications for transmitting sensitive data increases and the transmission devices become battery reliant, some scenarios arise in which using conventional encryption techniques become too computationally expensive to be viable. For example, secure WSNs have to have a way of securing their transmissions that does not involve complex calculations. Even some variants of the cellular wireless networks that rely on handsets can benefit from security with less power consumption compared to the conventional encryption techniques. As a result of this, there is a need for some form of technique which offers wireless transmission security that is based on the actual modulation techniques.

Of the various wireless communication methods that have been developed, the SS still holds a lot of value in terms of jamming resistance and security. However, secure SS systems today utilise encryption because the transmitter and receiver have access to high computational power. In low power scenarios, a new approach to SS has to be used which incorporates some form of physical layer security. This need has given rise to the development of chaos-based communications, a branch of which is developed for use on a SS system.

Nearly all the digital communication schemes that exist today have to have some degree of timing alignment between the transmitter and receiver, and the SS systems are no exception. The process of acquiring and maintaining such a timing alignment is known as synchronisation. The chaos-based SS system also needs to have an accurate and secure timing estimation between the transmitter and receiver to be effective as a communication tool. The nature of chaos-based SS signals<sup>3</sup> is such that it makes their synchronisation a non-trivial problem.

The preliminary focus of this thesis is to explore the current state of the art in synchronisation of chaos-based SS systems and to find the shortcomings therein. Having achieved that, this thesis focuses on suggesting a new approach for modelling the synchronisation process of a chaos-based SS system that overcomes these shortcomings. This suggested new approach is tested using different communication channel scenarios and verified using extensive simulation. Finally, this thesis analyses theoretically the effect of imperfect synchronisation on the system performance and presents mathematical expressions that are used to gauge the performance of a chaos-based SS system. Overall, this thesis extends significantly the previous works presented in literature by suggesting a new analytical approach and fills the research gap that exists for modelling the synchronisation block of a chaos-based SS system accurately.

Chapter 2 covers multi-user wireless communications in its modern form by presenting a simple communications model and spelling out the roles of transmitter, channel and receiver in a communication model. The concept of resource sharing for accommodating a number of users in a communication system as well as detailed explanation of the SS concept are then covered. This chapter continues with a brief history of chaotic phenomena and detailed discourse on the co-existence of chaos and wireless

---

<sup>3</sup>There will be a more detailed discussion about SS and chaotic signals in §2

communications. Finally, various chaos-based communication schemes are covered narrowing the topic to chaos-based direct sequence spread spectrum (CDS-SS) systems.

Chapter 3 explores the chosen CDS-SS concept and provides a literature review on the existing communication systems that are based on CDS-SS. The coherent CDS-SS system which is chosen for further investigation is then introduced. The transmitter and receiver structures are explained along with a detailed examination of the wireless channel corrupting effects. The method for benchmarking the system performance in terms of the probability of occurrence for bit errors is discussed. The need for synchronisation between the transmitter and receiver in the CDS-SS systems is then highlighted as being critical for system performance. The contributions of this thesis, within the context of synchronisation in CDS-SS systems, are then pointed out and explained in detail.

Chapter 4 discusses the various synchronisation schemes in existence for conventional DS-SS systems as well as the previous research in the specific field of sequence synchronisation for CDS-SS systems. The problem of sequence synchronisation is broken down into sequence acquisition and sequence tracking for acquiring and maintaining synchronisation respectively. The various acquisition and tracking stages present in the literature are then categorised and their merits and disadvantages are discussed. Finally two discussion sections are presented dealing with the shortcomings of the present literature for chaotic code acquisition and tracking to justify the need and motivation for the contributions of this thesis.

Chapter 5 introduces the synchronisation block of a CDS-SS system and quantifies its performance in the presence of channel noise and fading. The acquisition performance is quantified by deriving the upper bounds for the probability of detection  $P_D$ , which is the probability of correct acquisition, and the probability of false alarm  $P_F$ , which is the probability of erroneous declaration of synchronisation, for the acquisition stage. The tracking loop performance and the subsequent control law for the tracking phase are also examined in channel fading conditions. It is shown that the performance of the acquisition and tracking stages of the synchronisation block is affected adversely by the fading in the channel.

Chapter 6 begins by introducing the new statistical approach that is one of the main contributions of this thesis. This approach is termed the chaotic correlation statistics (CCS). Once CCS is explained in detail it is used to model the correlation function of an arbitrary chaotic pilot with three channel scenarios of Additive White Gaussian Noise (AWGN), fading, and interleaving. For each scenario the correlator output is modelled and is used to extract  $P_D$  and  $P_F$ . The analytical expressions for  $P_D$  and  $P_F$  are then derived in closed form. The theoretical results are confirmed using numerical analysis for each of the three channel scenarios mentioned previously.

Chapter 7 modifies the CCS method introduced in chapter 6 to make it usable on the tracking stage of a CDS-SS synchronisation block. The tracking stage consists of a delay lock loop using two correlators, where one is advanced in time for half a chip length, and the other one is delayed in time for the same amount. The subtraction of these two correlation functions is known as the S-curve and is the main tool used for correcting the timing errors that are smaller than a chip duration. This chapter compares the tracking S-curves of a conventional loop which uses m-sequences with the S-curve of a chaos-based loop. It is shown that unlike the conventional S-curves, the chaos-based S-curve changes slightly from one spreading sequence to the next. The CCS approach is employed to model the salient points of the S-curve statistically. The analytical results presented are then verified with simulation results for the

statistical distribution of the same salient points. It is also shown that the tracking loop does not perform ideally when noise is present and a residual tracking error occurs as a result.

Chapter 8 takes a system-wide approach to the problem of synchronisation. It assumes that the acquisition phase has finished successfully and the delay is known to within one chip duration. This chapter begins by deriving the effect of chip misalignment on the energy per chip and uses that to find the probability of error when the system is exposed to AWGN and all the bits have the same amount of timing mismatch. This derivation is repeated for the fading and interleaving scenarios as well. As the next step, the tracking error is assumed to be a random variable that changes from bit to bit. The new probabilities of error are then derived assuming that the tracking error follows a uniform and a Gaussian distribution. The validity of the derivations are then confirmed by the simulation results.

Chapter 9 presents the implications of the contributions of this thesis on the state of the art and the wider literature. It also points out various directions that can be taken for further research in this topic in the future. This is followed by concluding remarks in Chapter 10.



# Chapter 2

## Wireless Communications Using Chaos

### 2.1 Introduction

The use of chaos for covert communications has attracted scientists and researchers since the early 90s. The idea of using chaos for communications coincided with spread spectrum systems becoming commercially available and has resulted in a large volume of research which tries to exploit both these concepts in various ways. Providing sufficient information about wireless communications and the place of chaos within this arena is the primary goal of this chapter. To achieve this goal, the chapter has been divided into two separate parts.

The first part (§2.2) provides a background for wireless communications. This background consists of examining the communication model and resource sharing techniques enabling multi-user wireless communications. The discourse is then narrowed to list the characteristics of ideal codes/sequences at the end of §2.2. The second part (§2.3) is dedicated to the examination of the usage of chaos in communication systems. In this part, the merits of communication using chaos are examined based on the criteria provided in literature. The discussion is then narrowed down to focus on chaos-based spreading codes and suggests that they can be a practical substitute for conventional spreading codes.

### 2.2 Multi-User Wireless Communications — A Background

#### 2.2.1 A simple communication model<sup>1</sup>

The main purpose of any communication system is to send messages from a source to one or more destinations with the highest possible accuracy. This section examines a communication system in its simplest and broadest possible sense.

In order for information to be sent, there needs to be an information source. In some definitions the information source is not included in the communication system; however, there is still a need to examine

---

<sup>1</sup>This thesis examines and uses the communication model excluding coding (both source and channel coding). For more information about coding in communication systems the reader can refer to one of many excellent text books on coding within digital communications including [8–10].

it. The information obtained from the information source could be in the form of voice (speech), plain text in any language, image etc. The primary characteristic of the information obtained from the information source is that it must be random. This means that it has to be impossible for the recipients of the message to determine what the message was without the communication system in place. If the output of the information source is deterministic, then there is no need to send the message in the first place. Once the message is received, it is fed into the information sink which could take the form of a human being, or electronic/computer equipment which may act on the information received. Fig. 2.1 depicts a simplified communication model.

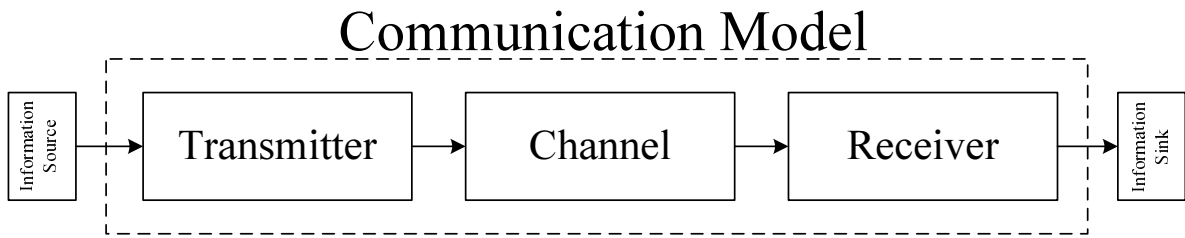


**Figure 2.1:** Simplified communication model.

The main components of the communication system are the transmitter, the channel, and the receiver. Each of these will be explained in more detail and the concepts and terminology related to them is introduced in the following.

### 2.2.1.1 Transmitter

The transmitter has the task of converting the signals fed into it by the information source to a form that can be transmitted [10, 11]. For both analogue and digital forms of communication, the transmitter has the task of placing the message into a frequency range which is chosen for transmission, and to send these messages at certain times. The message frequency conversion is required to match the signal to the transmission medium and is known as *modulation*. The frequency and time chosen for transmission are regulated by the broadcast authorities in every country as well as transmission standards which have been agreed upon previously [10, 11].

The modulation of signals can be done in several ways. In analogue communication, the amplitude, frequency or phase of a carrier can be changed according to the message signal. For example in amplitude modulation (AM), the message signal is contained in the amplitude of the transmitted signal which has a centre frequency on the band allocated to it by the radio transmission station. In frequency modulation (FM), the message is embedded in the frequency changes in the sinusoidal carrier being transmitted. In phase modulation (PM), the phase of the sinusoidal signal is changed based on the message signal. The choice of modulation depends on several factors, including the allocated band-width, the level and types of noise and interference the signal is likely to encounter and the type of signal amplifier being used [10, 11].

Apart from the modulation of signals, the transmitter has the tasks of filtering and amplifying the modulated signal. In the case of digital communication systems, the information bearing signal is sampled

and quantised into *bits* of information, which are then encoded into *symbols* through various encoding methods. These symbols are then transmitted through the communication medium. In the case of a wireless communication system, the transmitter has the additional task of radiating the message into the atmosphere using a transmission antenna.

### 2.2.1.2 Channel

The channel is the physical medium that the message signal traverses to reach the receiver. In wired communication, the channel can be in the form of a variety of physical media, including copper wire and optical fibres. In wireless communications however, the channel is the free space (atmosphere) between the transmitter and receiver antennas [10, 11].

Irrespective of the physical medium of the channel, the transmitted signal is corrupted in a random fashion when going through the channel. There are many different corruption mechanisms present in the channel. The most common corruption mechanism is the additive noise which is normally taken into account in the front end of the receiver where received signal amplification is performed. In general, the channel models lump all the atmospheric noise and thermal noise (generated in electrical devices in transmitter and receiver) into one additive noise source and place that just before the front end of the receiver [10, 11].

Another corruption mechanism is the interference by other communication users. Given that the channel is shared by many users who want to send their own messages, the transmitted signal is subject to interference from other users of the channel. This type of corruption can often be modelled as a random additive process as well, irrespective of the transmission medium. The system performance is normally examined at a certain *signal to noise ratio* (SNR), which is a standardised measure of signal power over noise power [10, 11].

In wireless communication channels, the transmitted signal will be reflected by various obstacles in the environment. This results in the signal taking multiple paths and the received signal being a summation of reflected signals all taking different paths and arriving at the receiver at slightly different times. This summation over multiple paths gives rise to the *multi-path* phenomenon, which physically manifests itself as a non-additive effect on signal power known as *multi-path fading*. The time that the signal takes to go through the channel is known as the *propagation time* and is normally made up of small timing variants added to a very slowly changing larger delay component [12]. More information regarding the corruptive mechanisms in the channel is provided in §3.3.2.

All channel corruptive mechanisms are normally modelled as random processes irrespective of additivity. The effects of these random processes are taken into account by the system designer. The system designer normally works with the statistical models of these corruptive mechanisms. The statistical characterisations that are used in the mathematical model of the system are normally justified by empirical measurements. Sometimes the channel characteristics are time varying and the system parameters have to be adjusted using information obtained from the channel [10, 11].

### 2.2.1.3 Receiver

The role of the receiver is to recover the message from the received signal. For every type of modulation employed by the transmitter, the receiver performs a specific demodulation process to extract the intended message and pass it to the information sink/s. Since the signal that is demodulated is corrupted by additive and non-additive effects of the channel, the extracted message may be different to that originally sent from the transmitter. The fidelity of the received message is dependant on the modulation scheme, the strength of corruptive mechanism in the channel, and the accuracy of the receiver components.

In digital communications, when the fidelity in the transmission of data in the form of bits is concerned, the performance is normally measured as the number of erroneous bits over the total number of transmitted bits. This measure is known as the bit error rate (BER) and allows various communication techniques to be compared. Given that the transmitted message, as well as the corruptive channel effects are essentially random and are represented by statistical distributions, a probability for wrong *a priori*<sup>2</sup> estimation of bits can be defined. This probability is known as the probability of error and is discussed further in §3.3.3.

Apart from demodulating the received signal, the receiver has the roles of filtering the received signal as well as noise suppression.

## 2.2.2 Resource sharing for multi-user wireless systems

There has been a sharp increase in demand for mobile wireless services since the late 1980s. At the end of 2005 there were approximately 2 billion wireless subscribers worldwide, and this number is projected to increase to approximately 5 billion by the end of 2011 [13]. With the increase in subscribers and the subsequent increase in uptake of mobile wireless technology, the issue of servicing many users in a densely populated urban area becomes very important. Given that the band-width is a finite resource, there is a need for efficient ways of accommodating more users in the communication channel. This part of the thesis provides an explanation for various forms of multi-user wireless systems that have been developed for such a purpose.

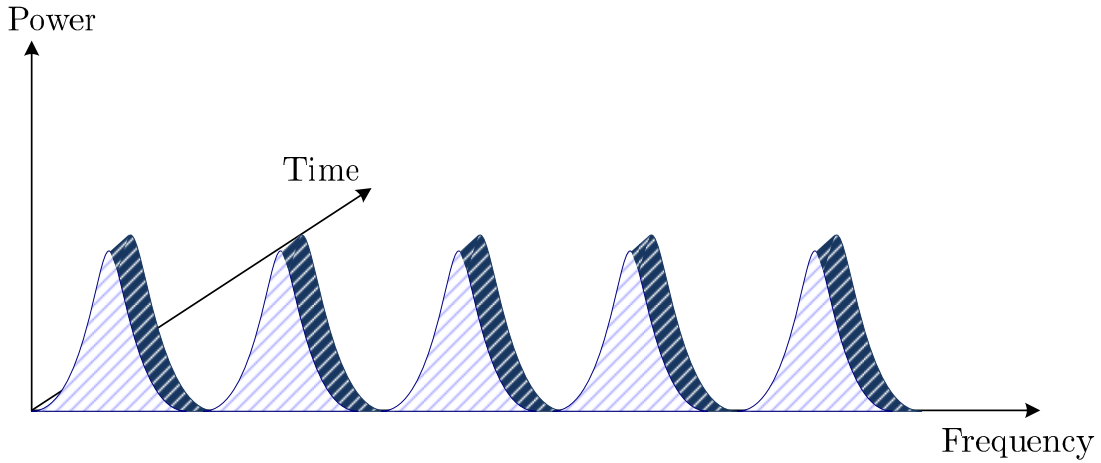
When separating the users for a multi-user system is concerned, one way is to separate them in frequency. That is, to allocate a part of the band-width to each user to transmit freely at any time. This way each user has its own band-width to use and the intended receiver can tune into that particular frequency. Assuming there is enough separation between the different users' frequencies, there would be no interference. In formal terms, separating multiple users in frequency is termed Frequency Division Multiple Access (FDMA). FDMA is not a band-width efficient multiple access method because when a user is transmitting in a certain frequency, that frequency becomes unusable for any other user within the area. The diagram presented in Fig. 2.2 shows the operation of an FDMA system in a conceptual way.

OFDMA or Orthogonal Frequency Division Multiple Access is the multi-user version of the OFDM<sup>3</sup> communication scheme. The OFDM system achieves a high throughput by transmitting the data at a

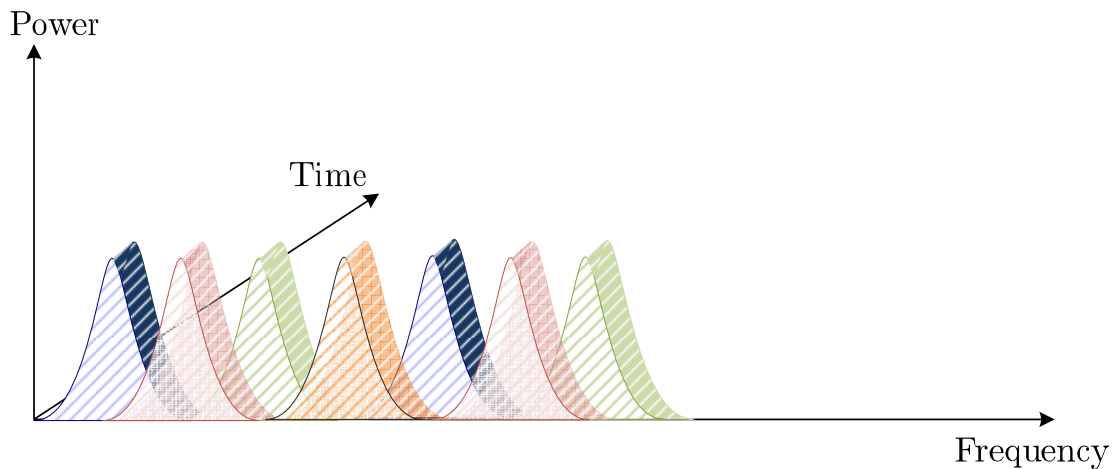
---

<sup>2</sup>*Apriori* determination of the received message is independent of the previous messages or any other information whereas *aposteriori* determination of a received message includes information obtained from previous messages.

<sup>3</sup>OFDM stands for Orthogonal Frequency Division Multiplexing

**Figure 2.2:** FDMA.

low rate using carrier frequencies (known as sub-carriers) that are orthogonal to each other. Both FDMA and OFDMA divide users in frequency but the concept of orthogonality is only used by the latter. The user then combines the data from each sub-carrier achieving a high data rate. Different number of sub-carriers can be assigned to different users enabling different rates of transmission. However, if the number of sub-carriers assigned to a user is small, then the OFDMA resistance to frequency selective fading will be adversely affected. Moreover, from a security standpoint, it is easy to use narrow-band jammers and disable a few of the sub-carriers and affect the system performance significantly. Fig. 2.3 presents a conceptual diagram of how OFDMA uses sub-carriers to share the channel between users.

**Figure 2.3:** OFDMA.

Another way to separate the users in a multi-user scenario is to separate them in time. This means that each user has access to the transmission channel for a short time while they are transmitting. In formal terms this is known as Time Division Multiple Access or TDMA. For TDMA to work efficiently, a robust mechanism for determining the time slots each user can transmit in has to be in place. The diagram presented in Fig. 2.4 shows the operation of a TDMA system in a conceptual way. As the number of users increases, the demand for time slots for transmission also increases, eventually reaching a point where more users cannot be allowed to transmit. Another disadvantage arises because of the “dead time”

between the transmission time slots which reduces the efficiency of the TDMA systems. Also, moving mobile devices have to take the change in the propagation delay into account as their distance to base stations changes since the ability to keep to the allotted timing slot is very important in a TDMA system.

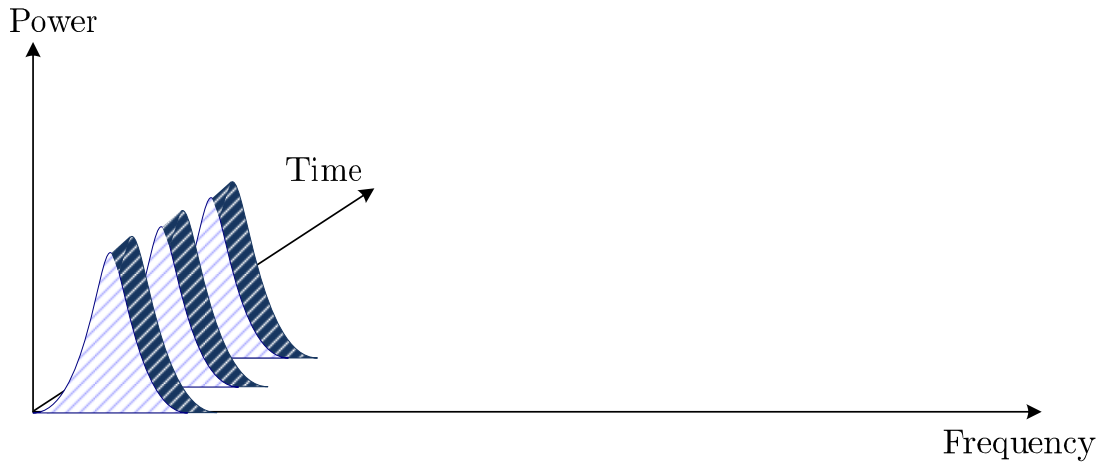


**Figure 2.4:** TDMA.

In a Code Division Multiple Access (CDMA) system, the users share the same channel band-width at the same time while they are separated by a set of orthogonal sequences/codes. The concept of CDMA in terms of resource sharing is shown in Fig. 2.5. Each user's data is modulated by a code portion unique to that user and recognised by the receiver. CDMA both as a channel access form, and a mobile communication system, is in very wide use today because of its practical band-width efficiency. Asynchronous CDMA is used for dynamic allocation of resources to various users within a certain geographical area (a cell site etc.).

In CDMA the band-width occupied by the transmitted signal is several times larger than the actual message band-width. Conceptually speaking, using wide-band signals to transmit narrow-band messages is not new. The technique which is employed for increasing the bandwidth, or in other words spreading the signal power over a wide band-width, is known as spread spectrum (SS). The core idea of SS as a signalling method has been around in patent form since 1903 [14].

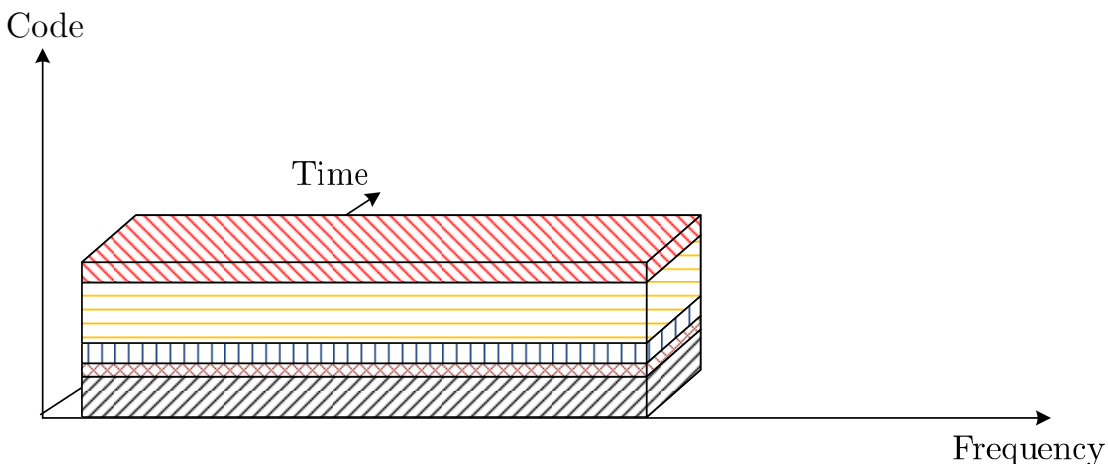


**Figure 2.5:** CDMA.

### 2.2.3 Spread spectrum techniques

The SS technology was developed and used during World War II where anti-jamming and security capabilities for communication systems were paramount. The SS techniques can be classified into two broad categories. The first one is the *frequency hopping spread spectrum* (FH-SS) technique, in which the message is transmitted in seemingly random parts of a preassigned band-width. This can be visualised as the transmitted signal hopping in frequency domain. If the receiver knows the time and the exact frequency of the hops, then the message can be de-spread. A jammer will have difficulties in interfering with the signal if the time and frequency of the hops are unknown to it.

The second technique is the *direct sequence spread spectrum* (DS-SS), where the message is directly spread into a larger band-width and transmitted. This technique is used in the CDMA technologies today. The effects of spreading the message are two fold. The first is that it will become more difficult for a narrow-band jammer to interfere destructively with the signal because the signal power is spread across a large band-width and jamming a wide band-width is not practical in terms of power. The second claimed effect is that the signal power can be spread so much that it effectively goes under the channel noise floor and is therefore masked from the unintended receiver. Fig. 2.6 presents the concept of DS-SS in the frequency domain in a visual way. The time domain visualisation of spreading the message signal is presented in Fig. 2.7. The system chosen for investigation in this thesis is DS-SS because this thesis is concerned with security and stealth in communications and a DS-SS is a logical choice for this matter.

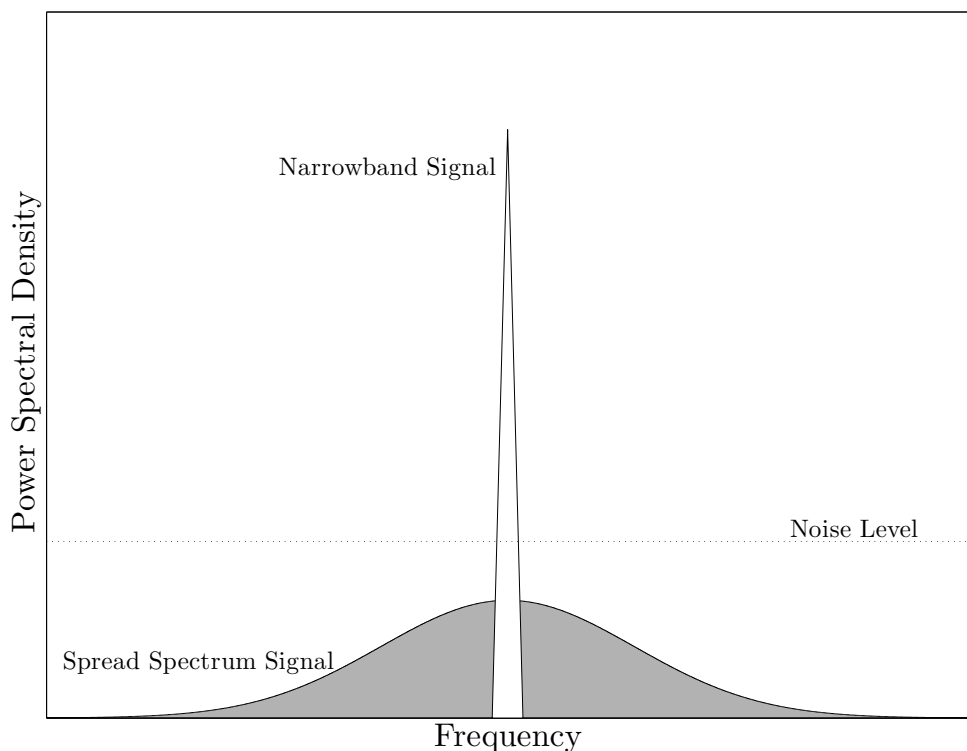


**Figure 2.6:** Spread spectrum signal power and noise floor.

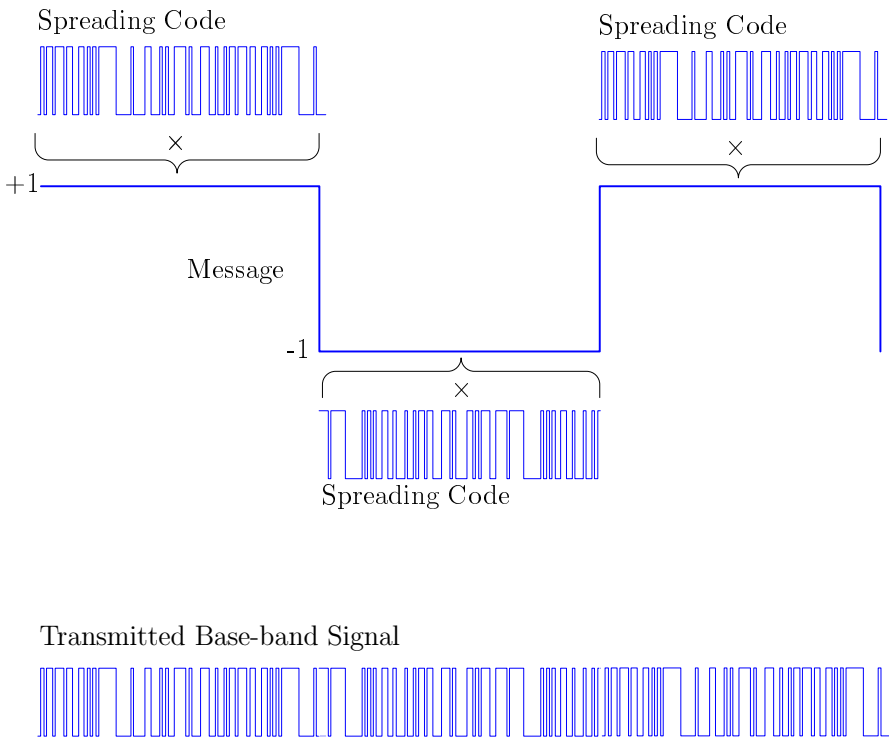


**Figure 2.7:** Spread spectrum in time domain.

It is important to explain the characteristics of a good spreading code/sequence<sup>4</sup> at this stage. Given that the DS-SS relies on the orthogonality of the codes, there is a need for codes that ideally have (a) impulse-like auto-correlation and (b) a zero or near zero cross-correlation function. Some examples of spreading codes are (Pseudo Noise) PN codes, Walsh sequences, Gold codes, m-sequences etc. These codes have near zero cross-correlation functions and an auto-correlation function which resembles an impulse [8]. These codes belong to the binary category- this means that they take only one of the two available values of +1 or -1. Another important issue regarding the choice of spreading codes is the ability to generate many orthogonal codes easily to accommodate many users.

Summarising the above, the characteristics of ideal code that can be used for DS-SS schemes can be listed as:

1. Zero or near zero cross-correlation and impulse like auto-correlation function.
2. The codes need to be wide-band to spread the signal energy over a wide section of the spectrum.
3. The codes need to be easy to generate.

This part has given background information about wireless communication techniques in use today and has narrowed the scope to DS-SS systems. In doing so, the characteristics of good spreading codes have been explained and listed. The following part gives background information about the chaotic phenomenon and introduces various ways it is used for masking information to provide security for communication systems.

---

<sup>4</sup>In this thesis spreading code and spreading sequence are used interchangeably and have the same meaning.

## 2.3 Chaotic Systems and Wireless Communications

### 2.3.1 History of chaos

Chaos is the highly complex behaviour of non-linear dynamical systems which are very sensitive to their initial conditions. Historically, the first experiment that showed the existence of chaos in a scientific sense was done by Faraday in 1831. He discovered the occurrence of sub-harmonic components of frequency in the vertical variations of water in a shallow container. This experiment was then repeated and published by Lord Rayleigh in his discourse on theory of sound in 1877 [15]. The Faraday experiment was repeated in 1981 with modern equipment and it was observed that the subharmonics will subdivide until they turn into a noise-like output with a continuous frequency spectrum. Other examples of chaos occurring in nature can be found in the shape of leaves, clouds and weather patterns [15].

The word 'chaos', as an apparently random phenomenon, first appeared in a scientific context in L. Boltzmann's assumption of molecular chaos in his derivation of the H-theorem. However, the modern use of the word 'chaos' began to be employed in mathematical journals around 1975 [15]. For the time being, there is no universally accepted formal definition of chaos and the working definition used here is deemed sufficiently accurate for the purposes of this thesis.

A process must have two important characteristics to be considered chaotic:

1. The future states of the process have to be deterministic if the initial condition is exactly known.
2. The future states of the process have to be unpredictable if the initial condition is not known.

Mathematically speaking, the dynamical systems that exhibit chaotic behaviour can be represented with differential equations (DEs). Chaotic behaviour manifests itself when the parameters within the DEs are set to certain values. The resulting oscillations from the iterative solution of these differential equations are known as attractors. There are many different attractors in existence but the three most famous are introduced in the rest of this section.

The first, is the Lorenz attractor introduced by E.N. Lorenz in 1963 from the simplified equations of the thermal convection problem in the atmosphere. This attractor is three dimensional with the following set of differential equations [16].

$$\begin{aligned}\frac{dx}{dt} &= \sigma(y - x) \\ \frac{dy}{dt} &= x(\rho - z) - y \\ \frac{dz}{dt} &= xy - \beta z,\end{aligned}\tag{2.1}$$

where  $\sigma$ ,  $\rho$  and  $\beta$  are control parameters. The oscillations of the Lorenz attractor can be seen in Fig.2.8. If the initial condition of the equations changes by a small number, the same attractor will be acquired; however, the oscillation trajectories will be completely different.

The second attractor is known as the "Double Scroll" because of its shape. This attractor is the output of the circuit proposed by L. Chua in 1983 [17]. Because of its simplicity, this circuit has become a very

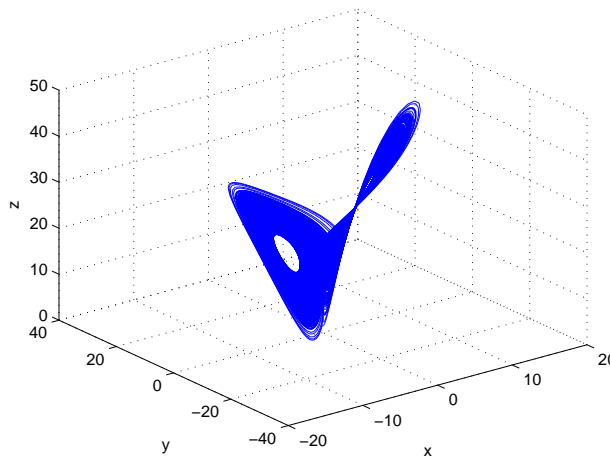


**Figure 2.8:** The Lorenz attractor.

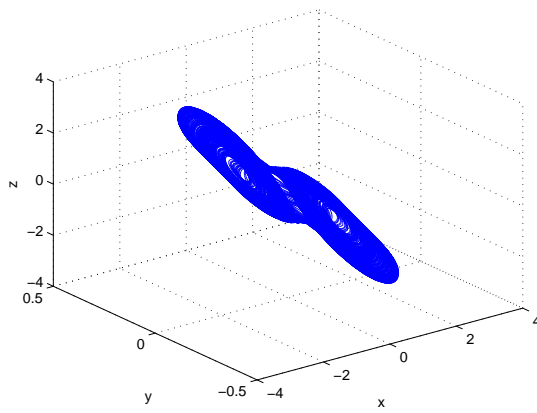


**Figure 2.9:** The “Double Scroll” attractor.

popular example of chaotic behaviour. The circuit dynamics can be described with a set of three differential equations resulting in a three dimensional attractor shown in Fig. 2.9. The differential equations are

$$\begin{aligned}\frac{dx}{dt} &= \alpha [y - x - f(x)] \\ \frac{dy}{dt} &= x - y + z \\ \frac{dz}{dt} &= -\beta y,\end{aligned}\tag{2.2}$$

where function  $f(x)$  describes the electrical response of the nonlinear resistor used in the Chua’s circuit. The shape of  $f(x)$  depends on the particular configuration of the circuit components. The parameters  $\alpha$  and  $\beta$  are determined by the particular values of the circuit components.

The final attractor was designed by O. Rössler in 1976 [18]. The differential equations governing this attractor were found to be useful in describing chemical reactions. This attractor is shown in Fig. 2.10.

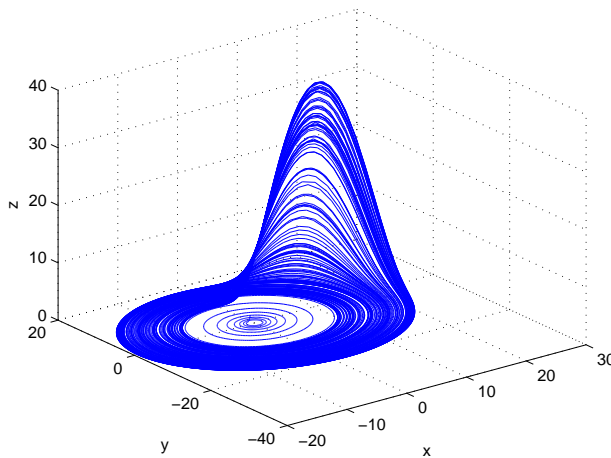


**Figure 2.10:** Rössler attractor.

The governing differential equations for the Rössler attractor are

$$\begin{aligned}\frac{dx}{dt} &= -y - z \\ \frac{dy}{dt} &= x + \alpha y \\ \frac{dz}{dt} &= \beta + z(x - c).\end{aligned}\tag{2.3}$$

From what is presented above, it is easy to discern that chaotic systems are hard to predict and aperiodic and are outputs of the differential equations that look random and are very sensitive to their initial conditions.

The next part examines the reasons for adoption of chaos in communications given their above mentioned properties.

### 2.3.2 Why chaos-based communications?

In his pioneering paper, “Communication Theory of Secrecy Systems” [19], Shannon discussed the three fundamental aspects of secret communication systems which are: concealment, privacy and encryption. In this part each of these aspects will be discussed in the context of chaos-based communications.

Concealment refers to hiding the existence of a transmitted message from potential eavesdroppers. Concealment of a message using a chaotic carrier signal is possible because the chaotic carrier has an irregular shape when viewed in the time domain and it is ideally<sup>5</sup> aperiodic. As a result, the concealment of the existence of a message in the transmitted signal can be achieved using chaotic signals [15, 20].

The privacy aspect of communication is primarily concerned with requiring the recipient of the message to possess special information or equipment to be able to detect and receive the message. This is to keep the information transmitted private from other non-intended recipients. Chaos-based communication can

---

<sup>5</sup>The hardware implementation of chaotic signals is not being considered at this stage.

address this aspect since the receiver requires to match exactly the chaotic parameters to the transmitter's chaotic signal generator to be able to extract the message correctly [15, 20].

The last aspect of security examined by Shannon is the encryption. Encryption is the act of using a common "key" and an encryption scheme in communication. The transmitter and receiver share this "key" and as a result the receiver can decrypt the messages. Encryption normally occurs in the higher communication layers. However, chaos-based communications add a physical encryption layer to the transmitted signal. Essentially, the transmitter acts as a "dynamical key generator" and the receiver has to have the matching parameters to be able to extract the message. Using a chaotic carrier does not stop the system designer from applying higher level encryption techniques as well [15, 20].

The main focus of chaos-based communications is the security/privacy issue as indicated above. The next part gives an overview on the various schemes that use chaotic carriers to transmit messages.

### 2.3.3 Chaos-based wireless communication schemes

Chaos-based communication schemes can be classified into two broad categories. The first one is the chaos-based communication through attractor synchronisation, and the second is chaos-based spread spectrum communication. The following is an explanation regarding each of these categories and their relative advantages and disadvantages.

The idea of attractor synchronisation was first mentioned by Pecora and Carroll in 1990 and 1991 [21, 22]. The main idea was that two attractors could be made to go through the same trajectories by linking them with common signals. That is, one of the attractors will eventually converge on the other if a parameter of the first attractor is continually fed to the second. After this idea was published, there was a large amount of research dedicated to making use of this concept for chaos masking for communication purposes. The following is a representative survey of the publications related to attractor synchronisation sorted by publication date.

One of the first publications in this category was [23] which suggested a circuit implementation of synchronised chaos with applications to communications. This was followed by [24] which used self-synchronising Chua's circuits for communication. [25] suggested the concept of chaotic digital encoding as an approach to secure communications and [26] examined the transmission of signals by synchronisation in a chaotic van der Pol-Duffing oscillator. [27] presented methods for chaotic signal estimation and [28] unified many of the previous approaches into a general approach for communication using chaotic synchronisation.

A year later, [29] elaborated on statistical analysis and spectral estimation of chaotic signals while [30] defined methods for controlling chaos and oscillations and using them for communication. [31] presented a communication system based on chaotic synchronisation of concentration maps; [32] examined the extraction of information masked by chaos in noisy environments; [33] explored the possibility of using multiple attractors for masking the information; [34] explained the implementation of self synchronising chaotic encoder/decoders in a digital signal processor (DSP).

In [35], Kohda *et al.* give a complete overview of the methods for using chaotic dynamics to encode information sources for communication purposes; [36] elaborates on the concept of ergodic chaos-based

communication systems in general; [37] explores the usability of a unified chaotic system for applications in secure communications; [38] proposes a secure digital communication system based on the discrete time synchronisation of chaotic attractors; [39] extends the previous work by proposing an adaptive synchronisation scheme; [40] presents schemes to control chaotic attractor synchronisation for applications in secure communication; [41] examines a scheme which uses the delay time in delayed synchronisation of attractors as a communication key; [42] proposes a multiple access chaotic digital communication scheme based on generalised synchronisation; [43] presents a method for adaptive tracking control of chaotic systems which can be used for synchronisation of attractors.

One method of synchronising attractors for communication purposes that has received some attention recently is the master-slave method. Of course, the concept is not very new and dates back to [33] where it was introduced as a drive-response unit. Recent publications by Jovic *et al.* in [44, 45] have basically reintroduced that concept with some expansions. In [44], it is shown that two attractors can be synchronised if one drives another. However, it is shown that such a system is not at all robust in the presence of noise and other channel effects are not even considered. The analysis presented in [45] describes a control law for another master-slave system. Interestingly, in this analysis the noise is ignored altogether and it is claimed that the system can be used for secure communications. No information regarding the robustness of such a system is given.

Secure communication through synchronisation of chaotic attractors declined as the time went by. The reason for this is the lack of robustness in the presence of noise and other channel impairments. Essentially, all of the secure communication schemes that have their roots in attractor synchronisation rely solely on some form of driving signal to be given by the transmitter to the receiver without being corrupted by noise. However, in practical applications this is not possible, as a result, all these schemes suffer heavily in the presence of moderate amount of noise in the channel [46].

As mentioned above, the second category of chaos-based communication involves using chaotic signals as spreading sequences for SS communication. As indicated in §2.2.3, SS signals are used to spread the message power over a large band-width to achieve jamming resistance as well as potential transmission security by being masked by the channel noise. Conventionally, the spreading codes used for such a task are binary signals generated using various methods.

Once the idea of chaos-based communication was pointed out as a means for securing the transmission, the researchers saw a potential advantage in using the chaotic signals in SS systems. As a result the concept of Chaos-based DS-SS or CDS-SS was born. The first report of such a scheme was by Heidari-Bateni and McGillem in 1994 [47]. After that a large number of publications was dedicated to proposing new techniques for using chaotic sequences in DS-SS type communications. Some noteworthy examples are [48–53].

These systems rely on correlation properties of chaotic spreading codes to detect and de-spread messages. Overall, they have been proven to be robust in terms of noise because they use the DS-SS principles which are inherently robust in the presence of noise and jamming. As a result, the CDS-SS methods are far more practical than the attractor synchronisation methods mentioned previously.

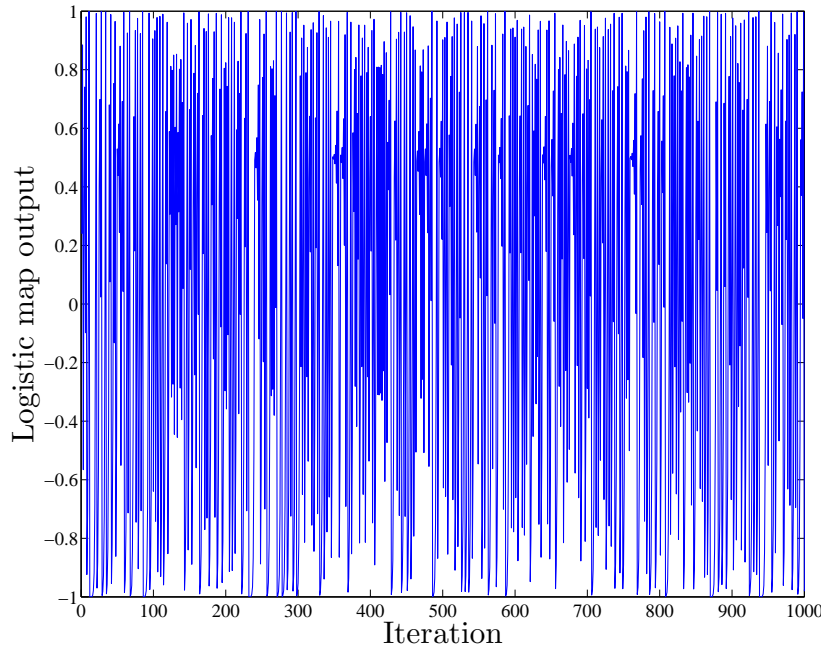


**Figure 2.11:** Random-like nature of a chaotic sequence generated by the Logistic map.

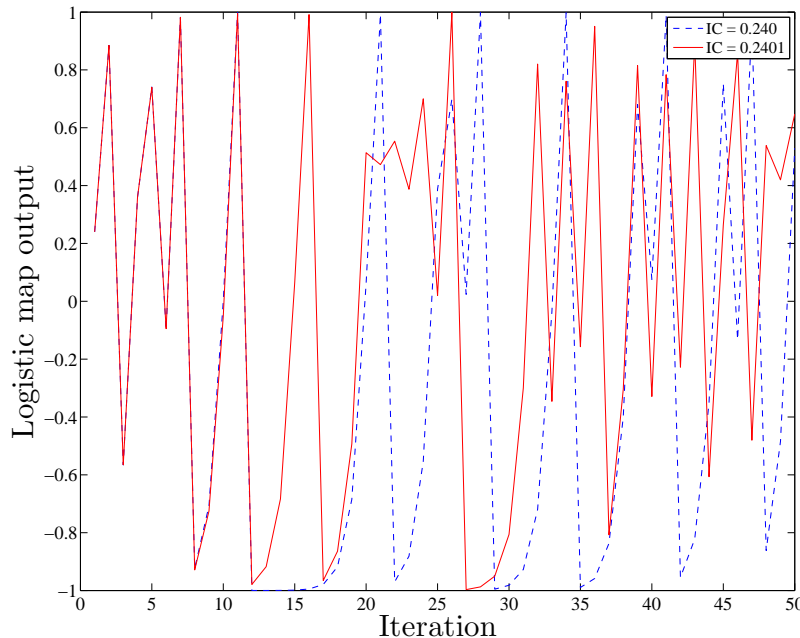


**Figure 2.12:** Sensitivity to initial conditions for chaotic sequences.

The issue that naturally arises here is the generation of chaotic sequences from chaotic processes. Moreover, the characteristics of chaos-based spreading codes are of interest. The generation of chaos-based spreading sequences is facilitated by using one dimensional difference equations that exhibit non-linear dynamical behaviour. These normally take the form of an iterative function in which the next value is dependant on the previous value/s. To start generation, an initial condition is needed, and since these iterative generators are chaotic, they are very sensitive to this initial condition. In literature these generating functions are known as *maps*. This is because they map the chaotic process into one dimension.

One of the most famous chaotic maps is the Chebychev polynomial which arises as the solution of the Chebychev differential equations and can be defined by recursive equations.

Some of the Chebychev polynomials (of both first and second kinds) exhibit chaotic behaviour. That is, they are very sensitive to their initial conditions, and the output of the generating function is bounded to certain limits. The chaotic map chosen for this thesis is the third Chebychev polynomial of the first type which, in literature, is known as the *Logistic map*. The generating function of the Logistic map is

$$x_{n+1} = 2x_n^2 - 1. \quad (2.4)$$

More information about the other places the Logistic map is used is contained in Appendix A.

The sequences generated by the Logistic map have the following characteristics:

1. They appear random in the time domain; however, they are bounded as shown in Fig. 2.11.
2. They are sensitive to their initial conditions, as shown in Fig. 2.12. Hence they are easy to generate since infinite initial conditions exists for the Logistic map.
3. They have near zero cross-correlation and impulse-like auto-correlation, as shown in Fig. 2.13.
4. They have a wide band-width.

As can be seen, clearly the chaotic sequence characteristics mentioned here are similar to the ones listed in §2.2.3. Also the sensitivity of the Logistic map to its initial condition is an additional feature which makes the generation of orthogonal spreading sequences possible. Moreover, unlike the conventional spreading codes mentioned in §2.2.2 the chaotic sequences are non-binary, taking any value between two bounds which makes them appear random in time domain.

It is time to revisit Shannon's requirements for a secret communications in a CDS-SS context. The chaotic spreading codes add to the security on the physical layer, because they make the shape of the transmitted signals difficult to interpret. In a situation where binary spreading sequences are transmitted, their binary nature can act as a flag for the transmission of the message. A chaotic non-binary sequence however, has infinite levels between its two bounds and will be more difficult to recognise and flag as a genuine transmission as opposed to noise. Moreover, if a set of messages is spread using chaotic sequences, it cannot be de-spread if the map and the exact initial condition used is not known. Moreover, many different initial conditions are available, and because of that, there will be no shortage of spreading codes for multi-user scenarios.

Given the discussion above, it is justified to pursue a CDS-SS system as a valid and practical system with additional physical layer security. As a result, this thesis identifies the CDS-SS type systems as the ones to examine and will present the details of the CDS-SS systems which have been proposed before in the next chapter.

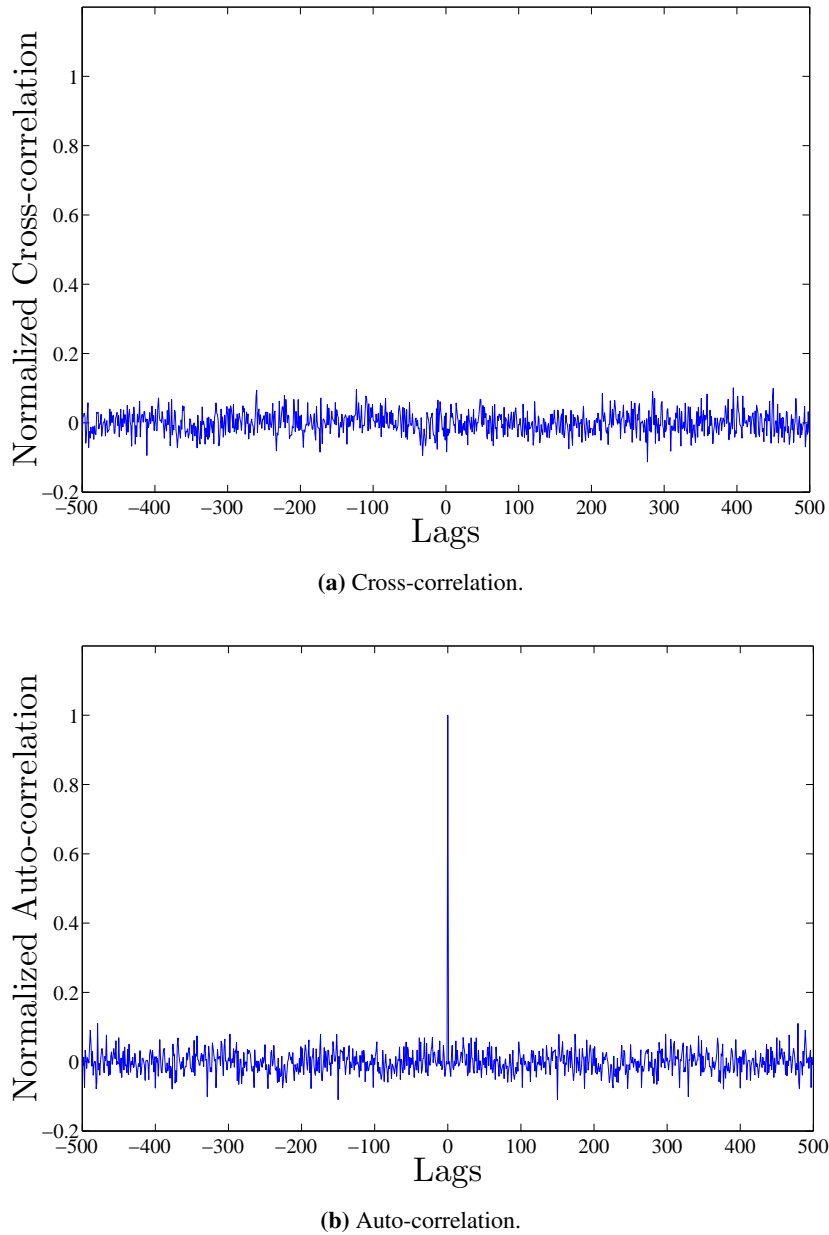


**Figure 2.13:** The cross-and auto-correlation of chaotic sequences.

## 2.4 Summary

This chapter described the fundamentals of wireless communications and presented the conventional multiple access schemes. The use of chaos in wireless communications was then introduced and it was shown that the interest in using chaos in communication arises from chaotic signals satisfying the characteristics indicated to be fundamental by Shannon. The uptake of chaos in communications has resulted in the emergence of two broad categories of chaotic communication systems. The first category attempts to establish secure communication by synchronising chaotic attractors. This method was shown not to be robust in the presence of noise and other channel impairments. The CDS-SS method however, was shown to be robust in presence of channel impairments because it used the DS-SS principles but

replaced the conventional binary spreading codes with chaotic spreading codes generated from maps. The chaotic sequences exhibit characteristics which make them desirable as spreading codes in existing DS-SS systems. Therefore, it was argued that a CDS-SS system using chaos-based spreading codes was deemed the best possible way to use chaos theory in wireless communications. The next chapter will survey the various CDS-SS systems presented in the literature and focuses on a particular method deemed the most suitable.



# **Chapter 3**

## **Chaos-based DS-SS (CDS-SS) Communications**

### **3.1 Introduction**

So far, §2 has given an overview of the use of chaotic signals in communications, and has identified the Chaos-based Direct Sequence Spread Spectrum (CDS-SS) as a practical way of using the virtues of chaotic signals for communication purposes. Because of the large amount of research conducted in the chaos-based spread spectrum field, CDS-SS has come to encompass a complex collation of different communication schemes which have the utilisation of chaotic sequences as their common point.

The aims of this chapter are twofold. The first aim is to present a concise and representative (but by no means exhaustive) literature review of the CDS-SS communication schemes and to categorise them based on their coherence, synchronicity and robustness. The second, and more important, aim of this chapter is to identify the problem of synchronisation as fundamental to the working of the CDS-SS communication schemes. To demonstrate the importance of synchronisation, a Chaos Phase Shift Keying (CPSK) system is considered as an example and all its components, as well as the channel impairments, are explained. The system performance is then compared for the synchronised and non-synchronised case in theoretical and visual ways.

The rest of this chapter is organised as follows. §3.2 presents a concise but representative survey of CDS-SS systems that exist in the literature. §3.3 presents the CPSK system model chosen for demonstrating the need for synchronisation and the justification for choosing such a system. §3.4 elaborates on the need for synchronisation in CDS-SS systems and gives more supporting information; §3.5 presents the thesis contribution both in textual and visual ways and finally §3.6 summarises this chapter.

System Name	Year	Author	Coherent \ Non-coherent	Features and Remarks
Chaotic DS-SS	1994	Heidari-Bateni and McGillem [47]	✓	First use of chaos as spreading sequences. No BER derivation.
DCSK <sup>1</sup>	1996	Kolumban <i>et al.</i> [54]	✓	No need for locally generated chaotic sequence.
FM-DCSK <sup>2</sup>	1997	Kolumban <i>et al.</i> [55]	✓	Transmission is achieved with constant bit energy.
COOK <sup>3</sup>	1997	Kolumban <i>et al.</i> [56]	✓	Introduction of null transmission for bit '0'.
Unipodal CSK <sup>4</sup>	1998	Kolumban <i>et al.</i> [57]	✓	Varying bit energies is taken into account.
FM-DCSK in multi-path Conditions	1999	Kennedy <i>et al.</i> [58]	✓	The first examination of DCSK in multi-path environment.
Enhanced DCSK and FM-DCSK	1999	Kolumban <i>et al.</i> [59]	✓	Enhancement achieved by using a single reference bit for multiple data bits.
CDSK <sup>5</sup>	2000	Sushchik <i>et al.</i> [51]	✓	Delayed versions of the chaotic sequence are summed and transmitted.
Quadrature CSK (QCSK)	2001	Galias and Magio [60]	✓	Doubling the throughput for fixed BER and band-width.
Multiple Access DCSK	2001	Lau <i>et al.</i> [61]	✓	Multiple access capability for DCSK.
CDS-SS	2001	Chen and Yao [62]	✓	SS system using chaotic with Lebesgue spectrum.
Ergodic Chaos Communication	2002	Leung <i>et al.</i> [36]	✓	Chaotic sequence estimation.
Non-coherent CSK	2002	Tse <i>et al.</i> [63]	✓	First proposal of regression and probability approaches for detection.
Optimum CSK Receiver	2002	Lau <i>et al.</i> [64]	✓	Optimum receiver for correlator type CSK systems.
Multiple Access CSK and DCSK	2003	Tam <i>et al.</i> [65]	✓	Gaussian Approximated Solutions for AWGN channel.

<sup>1</sup>DCSK stands for *Differential Chaos Shift Keying*

<sup>2</sup>FM-DCSK stands for *Frequency Modulated DCSK*

<sup>3</sup>COOK stands for *Chaotic On Off Keying*

<sup>4</sup>CSK stands for *Chaotic Shift Keying*

<sup>5</sup>CDSK stands for *Correlation Delay Shift Keying*

Multiple Access CSK	2004	Tam <i>et al.</i> [66]	✓	Exact BER solution for AWGN channel.
DCSK	2004	Xia <i>et al.</i> [67]	✓	Approximate BER solution for DCSK in fading conditions.
CSK	2004	Xia <i>et al.</i> [68]	✓	Examination of CSK in multi-path environment.
CSK	2005	Yao and Lawrance [69]	✓	Maximum likelihood approximation optimal receiver.
DCSK	2005	Yao and Lawrance [70]	✓	Examination of the optimal spreading factor value.
Binary Chaotic Codes	2005	Wang <i>et al.</i> [71]	✓	Use of binary chaotic codes for communication.
CDS-SS Receiver	2005	Luca <i>et al.</i> [72]	✓	Complete CDS-SS receiver.
Non-linear Chaotic Receiver	2006	Wang and Zhang [52]	✓	Nonlinear auto-regressive filter with changeable parameters.
Chaotic TDMA	2006	Jovic and Unsworth [73]	✓	Chaotic users separated in time.
DS-UWB <sup>6</sup>	2007	Cimatti <i>et al.</i> [74]	✓	Use of chaotic sequence in UWB communications.
CDS-SS	2009	Yu <i>et al.</i> [75]	✓	Use of real sequences with realisable band-width.
SVM Receivers for Chaos <sup>7</sup>	2010	Kao <i>et al.</i> [76]	✓	Using support vector machines as receivers.

**Table 3.1:** CDS-SS communication methods, adapted from [77] and [78].<sup>6</sup>UWB stands for *Ultra Wide Band*<sup>7</sup>SVM stands for *Support Vector Machine*

### 3.2 Existing CDS-SS Communication Methods

As explained in §2, CDS-SS systems work by masking the information to be sent by a set of chaotic basis functions, which are chaotic spreading sequences. The existing CDS-SS communication methods can be broadly classified into two categories, namely, coherent and non-coherent systems [78, 79]. In this context, coherence refers to the need for the chaotic basis functions to be available in the receiver. That is, in coherent CDS-SS systems, both transmitter and receiver have access to the same spreading sequences. Non-coherent systems on the other hand do not have such a need. This means that the receiver in a non-coherent system does not need to have the replica of the transmitter's spreading sequence and can use any means of detection [78, 79]. Most non-coherent systems use a transmitted reference method to de-spread the information. It has to be noted that some CDS-SS techniques can be realised in both coherent and non-coherent forms.

One important point to consider is that different signalling schemes can be used in different CDS-SS communication methods. For example, the binary-phase-shift-keying (BPSK), quadrature phase shift keying (QPSK), and M-ary modulation schemes have all been reported in the literature before.

Another way to classify CDS-SS systems is to see if they use analogue or digital methods to encode the message in chaotic signals. Techniques which involve chaotic masking, chaotic modulation and signal reconstruction fall into the analogue category. These techniques have been described in §2.3. On the other hand most of the techniques that have been followed up in the literature have been digital techniques e.g. shift-keying and differential techniques.

Tabulation is by far the best way to present a concise survey of CDS-SS systems given the large number and the varied categories. So Table 3.1 presents a representative survey of all the work that has been done in the CDS-SS arena with remarks and explanations on what makes each of them unique. Some of the contents of this table are adapted from [77, 78] which contains surveys into CDS-SS systems. However, these surveys have been updated with material which has been published since then.

There are certain trade-offs between coherent and non-coherent communication methods. In general coherent communication is robust in the presence of noise and is more band-width efficient than non-coherent communication [78, 79]. The receivers for coherent communication are also relatively simple and do not require much processing [78, 79]. However as mentioned above, coherent systems rely on the exact replica of the transmitter spreading sequences to be available to the receiver. On the other hand by observing the cross- and auto-correlation properties of chaotic spreading shown in Fig. 2.13, it can be seen that the peak of the auto-correlation function happens when the relative delay between the two sequences is zero. This means that the sequences have to be aligned or *time-synchronised* for the auto-correlation peak to emerge and the data to be de-spread. Furthermore, the synchronisation has to be accurate to allow correct de-spreading of the message. The main complexity of a coherent system is the synchronisation block which is the central topic of discussion in this thesis [78, 79]. The need for synchronisation will be discussed further in §3.4.

Non-coherent systems, on the other hand, are shown not to be as efficient in the band-width usage. They rely on a reference signal to be transmitted with the message, and also for the transmitter to let the receiver know when each bit finishes and the new one starts [78, 79]. The additional overhead and the fact that a reference has to be sent for each message bit adversely affects the throughput; moreover, the robustness

of the non-coherent systems is shown to be less than their coherent counterparts due to the fact that both the information bearing and reference signals are corrupted by noise and channel impairments [78, 79].

Table 3.1 shows that the first system that used chaotic codes as a spreading sequence was a coherent system, however the subsequent systems that were introduced were mostly non-coherent. This is the result of the perception that coherent CDS-SS systems are not possible because it is very difficult or impossible to synchronise the transmitter and receiver sequence generators [79]. As a result, more research effort was put into non-coherent systems. However, the band-width efficiency and robustness concerns meant that a lot of research effort [36, 51, 59–61, 63, 70] had to be directed into improving the BER performance of non-coherent systems. However, the performance improvement came at the cost of more complexity and often the benefits gained were not significant compared to the costs.

The survey and discussion above shows that, the synchronisation issue aside, a coherent CDS-SS system is the optimal choice for a chaotic communication system in terms of band-width efficiency, simplicity of implementation and BER performance. As a result, a variant of coherent CDS-SS system is chosen as the communication system in this thesis and the sequence synchronisation of such a system will be examined. One reason for choosing this particular system is that the BER expression for this system has been already derived and the system has been shown to be robust. This will be discussed more in §3.3.

The modulation scheme used in this CDS-SS system is BPSK because it is preferable to keep the primary system simple in order to focus more on the synchronisation part. Using higher modulation schemes over-complicates the already involved problem of sequence synchronisation unnecessarily. Consequently, the real part of the signals is used for this BPSK modulated CDS-SS system and the data symbols are the same as bits throughout this thesis<sup>8</sup>. Once the problem of synchronising chaotic spreading codes has been solved, the results can be expanded to obtain performance measures for more complicated synchronisation systems and algorithms.

The following section will give details of the coherent CDS-SS system chosen in this thesis including various components and the channel models used.

### 3.3 Systems Model for Investigation

The coherent base-band CDS-SS system variant presented here was first examined by Tam *et al.* in [66] and is a multi-user CSK system. This section presents the various system components, as well as the channel model used, except the synchronisation block which is the subject of the following chapters. Each subsection includes a block diagram of the component being examined as well as the time domain representation of signals flowing through the system. The mathematical expressions for the inputs and outputs of each of the system components are provided and the procedure for deriving the probability of error is explained. It has to be noted that what follows is a simplified derivation of the probability of error and is used for the sole purpose of better understanding the system. Interested readers can find an advanced discourse on the subject in [66].

---

<sup>8</sup>It should be noted that such an assumption only holds for BPSK modulation. For QPSK and above the conventional relationship between bits and symbols has to be observed.

To be able to simulate the behaviour of this system the Matlab<sup>TM</sup> software is employed. This is deemed sufficiently flexible for development and is acceptable in terms of speed if efficient coding practices are used. The simulation setup for each system component is explained step by step alongside the discussion for that system component. The whole system block diagram is presented and discussed at the end of the section.

### 3.3.1 Transmitter structure

The transmitter block diagram is presented in Fig. 3.1. The message bits have to be encoded into the polar non return to zero (PNRZ) form, that is the bit '1' remains unchanged and the bit '0' changes to '-1'. From here on the bit stream of the first user is shown by  $\gamma^{(1)}$ . Once the encoding is performed each bit is multiplied, or spread, using a certain number of chaotic values coming from the chaotic sequence generator. Each single value of the spreading code is known as a chip. The  $t$ -th chip for the 1-st user is shown by  $x_t^{(1)}$ . It has to be noted that  $t$  is a discrete notation for showing time.

The number of chips used to spread a particular bit is known as the spreading factor or the processing gain. The chip duration is denoted as  $T_c$  as opposed to the bit duration which is  $T_b$ . Generally, in noisy conditions a larger spreading factor results in improved performance because there is more information available to the receiver.

By multiplying the chaotic spreading sequence with 1s and -1s, the phase of the sequence either remains the same or changes by  $180^\circ$ . It has to be noted that the blocks shown here are for a single user and the full system contains a cascade of these spreading code generators and all of their outputs are summed before being sent to the channel.

As a result the transmitter output can be written as

$$S_t = \sum_{g=1}^N \gamma_i^g x_t^g, \quad (3.1)$$

where  $N$  is the number of users,  $g$  denotes the user index, and  $i$  is the bit index. This means that the transmitter output is the sum of the  $t$ -th chip of the  $i$ -th bit of all users and the system is synchronous.

Given that  $\forall g, i \ \gamma_i^g = \begin{cases} -1 \\ +1 \end{cases}$ , therefore

$$S_t = \begin{cases} -x_t^g \\ x_t^g. \end{cases} \quad (3.2)$$

The transmitter simulator in Matlab<sup>TM</sup> consists of an iterative function that generates a string of chaotic spreading values stored as a matrix. This matrix is then multiplied with a data matrix which is generated by a random process and contains the bits to be transmitted which have equal probability. The result of this multiplication is added to the rest of the spread messages and then sent to the next part of the simulator.

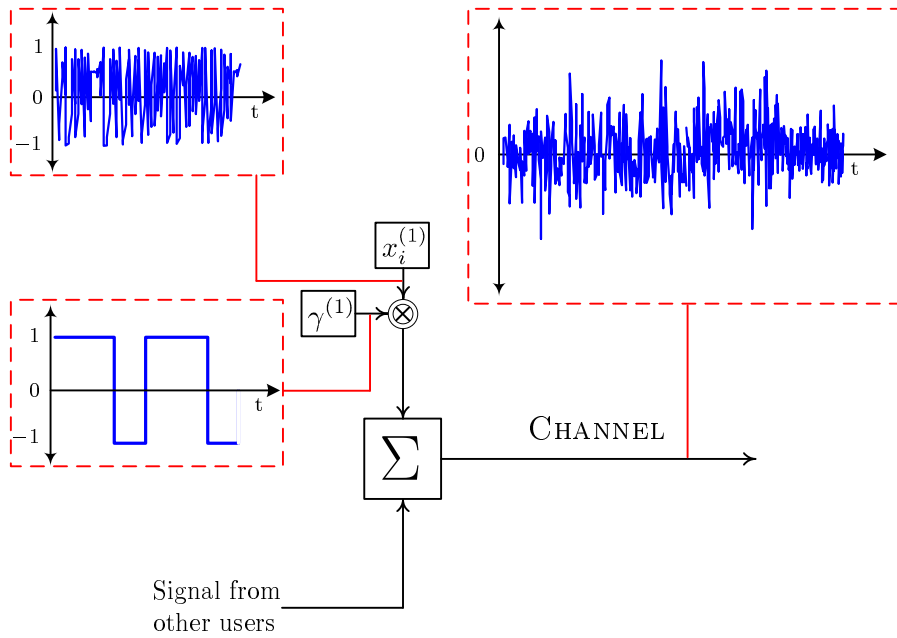


**Figure 3.1:** The block diagram of the transmitter with signal representations.

### 3.3.2 Channel model

This part presents the various assumptions made for the channel model used, including the noise, fading, inter-user interference, and propagation delay.

#### 3.3.2.1 Noise

The performance of the various digital communication systems is normally evaluated when the transmitted signal is exposed to noise. The noise model which is used as a benchmark is the Additive White Gaussian Noise (AWGN). This is an idealised form of noise which is added to the output of the transmitter [80]. The term 'white' refers to the assumption that this type of noise has a large band-width and its power spectral density is the fixed value of  $\frac{N_0}{2}$  over this band-width; this is illustrated in Fig. 3.2(a) [80]. The noise power spectral density,  $N_0$ , has dimensions of watts per Hertz. The inverse Fourier transform of the power spectral density is the noise auto-correlation function which, ideally, can be shown as  $R_{noise} = \frac{N_0}{2}\delta(t)$ , where  $\delta(t)$  is an impulse function. It should be noted that the bandwidth in this case is normalised to 1. The ideal auto-correlation is presented in Fig. 3.2(b).

The term Gaussian refers to the statistical distribution of the noise values, given that most natural phenomena have a Gaussian distribution, the AWGN is also assumed to have a Gaussian distribution [80]. The time domain representation of the Gaussian noise as well as the probability distribution function (PDF) are shown in Fig. 3.2(c) [80]. There are many different ways to generate noise for simulation purposes. The noise simulator in Matlab<sup>TM</sup> uses a fast algorithm to generate AWGN values that can be used in simulations.

For simulation purposes, the noise power is altered by adjusting the variance of the noise generator output. The noise variance is denoted as  $\sigma_\xi^2$  and can be calculated using the relationship between the

SNR (in linear terms), the energy per bit (denoted as  $E_b$ ) and one sided noise power spectral density (denoted as  $N_0$ ). Since  $\text{SNR} = \frac{E_b}{N_0}$ , and the noise power is the same as the variance for an ergodic process, the noise variance can be calculated as  $\sigma_\xi^2 = \frac{N_0}{2}$ . This is the value used to scale the AWGN values generated in the simulator for the SNR value of choice [81].

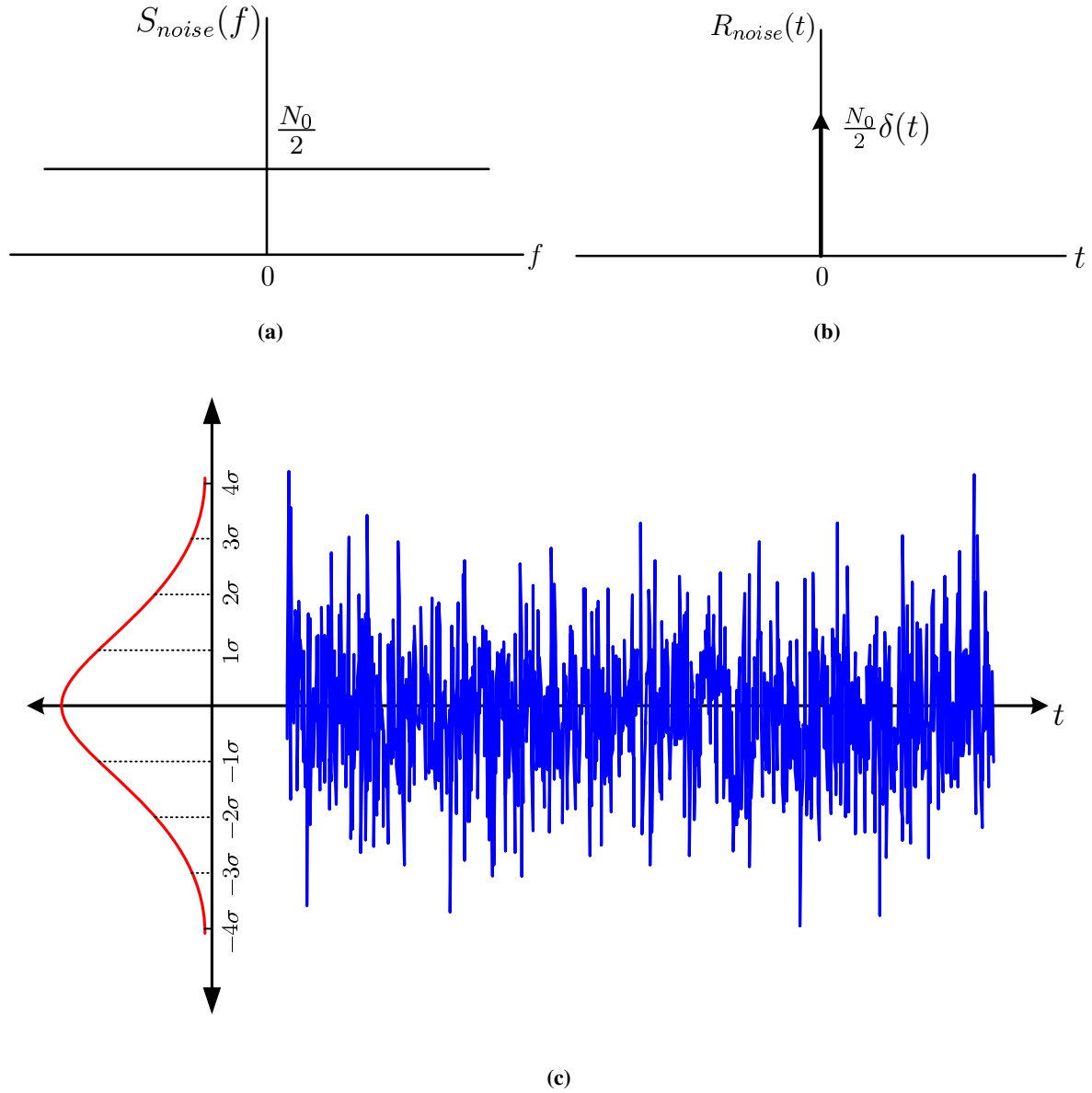


**Figure 3.2:** AWGN in frequency domain with infinite band-width (a); AWGN auto-correlation function (b); AWGN in time domain and PDF (c); adapted from [80].

### 3.3.2.2 Multi-path fading

The short-time variations in the received signal strength are normally known as multi-path fading. These occur because the received signal is a summation of various reflected replicas of the transmitted signal that arrive at the receiver with different time delays. The relative time delays result in constructive or destructive collation of these signals, a schematic model of which is shown in Fig. 3.3 (a). It has been

shown in the literature [82, 83] that, assuming there is no line of sight signal component present, the short term variations of the received signal can be modelled with a Rayleigh distribution with the following PDF

$$f_A(a) = \frac{a}{b^2} \exp\left(\frac{-a^2}{2b^2}\right), \quad (3.3)$$

where  $a$  is the received signal strength (in units of voltage and always positive) and  $b$  is the mode of the Rayleigh distribution. The Rayleigh distribution is a theoretical outcome of Clarke's model, which assumes that the received signal is a summation of replicas with equal magnitude and random phases where phases are statistically independent and uniformly distributed between 0 and  $2\pi$  [82, 83].

If the received signal power (in mW) is to be considered then (3.3) changes to an exponential distribution where

$$f_{A_p}(a_p) = \frac{1}{\bar{a}_p} \exp\left(\frac{-a_p}{\bar{a}_p}\right) \quad (3.4)$$

where  $a_p$  is the received signal power (in mW), and  $\bar{a}_p$  is the local mean of the received signal strength (in mW). Presented in a log scale, the received signal power can be plotted as shown in 3.3 (b) and the phase in 3.3 (c). One way to generate the Rayleigh fading envelope is to use two Gaussian distributions as documented in [84] by Arredondo *et. al.*, a modified version of which is used for simulating the Rayleigh envelope in this thesis.

The Rayleigh fading model is valid for narrow-band systems (where the transmission band-width is “narrow”). Spread spectrum systems, however, spread the message power over a band-width larger than the message signal. As a result, the summation of individual signal paths maybe be frequency dependent [82, 83]. This phenomenon can be examined in both time and frequency domains.

In the frequency domain, a *coherence band-width* is defined which designates the frequency range over which the signal components will not differ much in the amount of frequency distortion they are exposed to. This means that the multi-path fading has the same effect on all the frequencies giving rise to the *flat fading* phenomenon [82, 83]. Flat fading is the model chosen for narrow-band systems given the small frequency range they operate on. On the other hand, spread spectrum systems normally have an operating frequency range greater than the coherence band-width of the channel. As a result, the spread spectrum systems undergo *frequency selective fading* which means that different frequency ranges of these signals will have different frequency distortions [82, 83].

In the time domain, a *power delay profile* is defined for the channel. This is measured by a channel sounder setup where a wide-band code is transmitted and continuously correlated with the receiver generated code resulting in a set of delayed and attenuated auto-correlation functions which show when each of the significant signal components has arrived.

In indoor environments, the significant component and the secondary components all arrive at the receiver in a time window smaller than a symbol duration. However in outdoor environments, where there is large propagation delay, the significant component of one symbol might arrive “late” and interfere with the signal belonging to a later symbol. This phenomenon is known as inter-symbol-interference (ISI)

and has a direct relationship with frequency selective fading as explained above [82, 83, 85]. The multi-path phenomenon can be exploited for increasing the system performance. Various diversity techniques, the most notable of which are RAKE receivers, are used to extract individual signal components and combine them to increase the accuracy of estimation in spread spectrum systems [85].

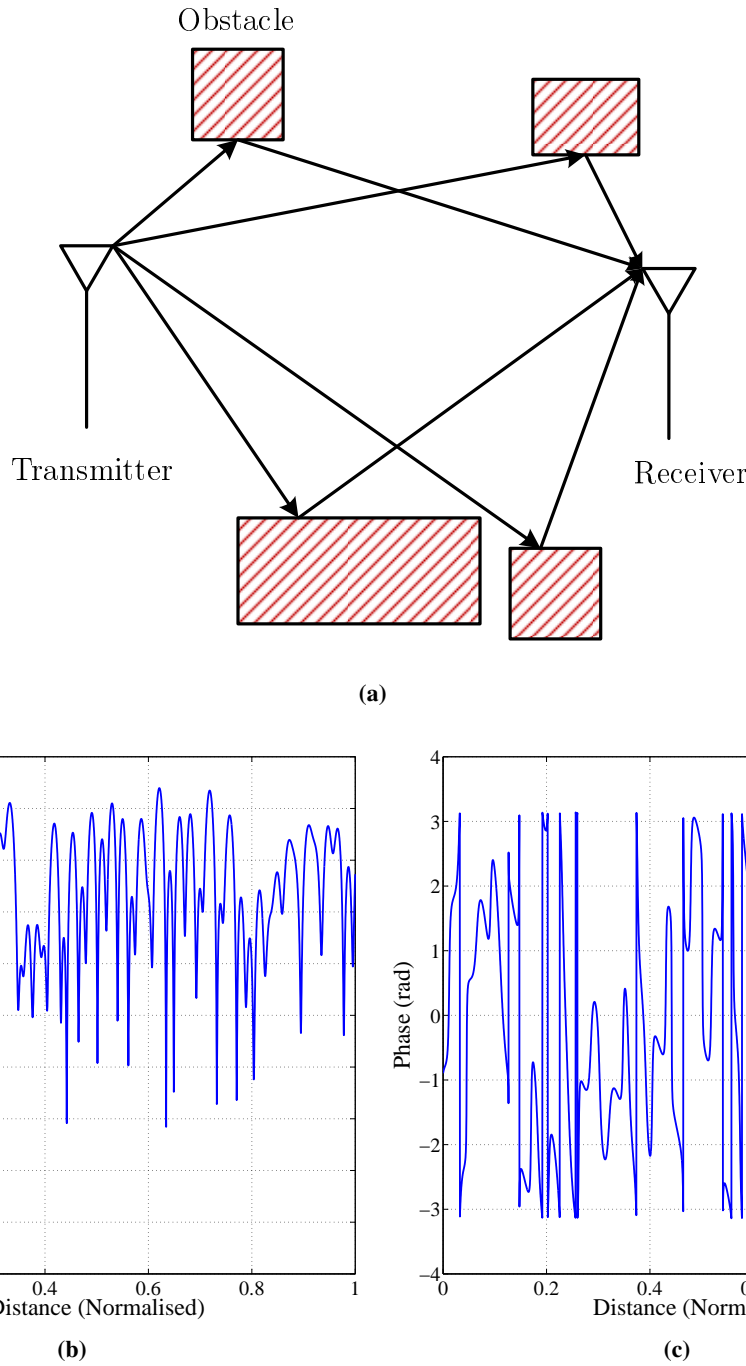


**Figure 3.3:** Multi-path model (a); Rayleigh fading envelope model (2.5 GHz) (b); Rayleigh fading phase model (2.5 GHz) (c).

In DS-CDMA systems such as WCDMA<sup>9</sup> and UMTS<sup>10</sup>, the chip rate is specified at 3.83 Mcps. Therefore it is possible for the chips from the previous symbol to arrive and interfere with the ones belonging to the next symbol, and causing ISI, if the environment is sufficiently large. However, for DS-CDMA systems this is merely a summation of delayed versions of the received signal and since there is no (or very small) correlation between the chips, no equalisation is needed. Other wide-band systems that do not use DS-SS require channel equalisation to deal with the ISI [82, 83, 85].

In order for a RAKE receiver to distinguish between the multi-path components, the chip time resolution has to be at least as much as a one chip duration which is 260 ns for DS-CDMA systems. This means that if the distance between transmitter and receiver is less than 78 meters, the RAKE receiver cannot distinguish between the reflected components of the signal and the probability of ISI occurring becomes low enough to warrant the use of a frequency flat Rayleigh fading model [86].

This thesis assumes that the propagation distances are short enough for the ISI not to be an issue (e.g. indoor environments). Even if this assumption is relaxed, the instances of using RAKE for dealing with ISI are very well documented in literature [87–89]. As a result, the approach presented in [86], that is using a frequency flat Rayleigh model, is used for this thesis.

### 3.3.2.3 Inter-user interference

The CDS-SS system that is being described here uses the orthogonality of chaotic sequences to accommodate several users in the same frequency at the same time. However, as shown in Fig. 2.13, the cross-correlation of chaotic sequences is only close to zero and not exactly zero. As a result, the addition of users (each with a residual cross-correlation value) in the system will cause inter-user-interference (IUI). It is shown that for a small number of users the effect of IUI is negligible [66]. However, for a larger number of users the system performance will be adversely affected. In order to achieve the same BER performance with more users, at the same SNR, the spreading factor has to be increased which in turn increases the band-width requirements.

If the desired user<sup>11</sup> is the first one ( $g = 1$ ), the IUI can be mathematically shown in the transmitted signal as

$$S_t = \gamma_i^1 x_t^1 + \underbrace{\sum_{g=2}^N \gamma_i^g x_t^g}_{\text{IUI}}. \quad (3.5)$$

Given that each user has its own separate sequence generator and the spreading sequences have a small cross-correlation, the spreading sequences for different users can be assumed to be statistically independent. Because the signal at the output of the transmitter is the summation of spreading sequences of various users, the end result can be assumed to be a summation of independent identically distributed random variables. Invoking the central limit theorem (CLT), it can be concluded that the IUI follows a Gaussian distribution. This is useful later on when the probability of error for the system is to be defined.

---

<sup>9</sup>WCDMA stands for Wide Band CDMA.

<sup>10</sup>UMTS stands for Universal Mobile Telecommunications System.

<sup>11</sup>The desired user is the one for whom the probability of error is defined.

The IUI has been implemented as a summation of chaotic sequences generated from random initial conditions modulated with random sequences of PNRZ bits in the simulator. The IUI is then added to the spread bits of the desired user.

### 3.3.2.4 Time delay

As explained above, radio signals take some time to propagate between the transmitter and receiver. This is known as the *propagation time* or *propagation delay*. Knowing the exact amount of time taken for the signal to travel between the transmitter and receiver is not possible most of the time due to the existence of various attenuating, reflecting, refracting and scattering objects in the propagation path. As a result, in this thesis the propagation delay is assumed to be a random value several times larger than  $T_c$ . That is, if the propagation delay was denoted as  $\tau$  then,  $\tau \gg T_c$ .

Apart from the propagation delay, this thesis assumes the existence of timing jitter in the received signal, in the form of random timing misalignments which are smaller than a chip duration. An introduction to timing jitter in circuits can be found in [12]. In order to cope with the timing jitter in the received signal, the receiver has to have the ability of tracking the incoming signal and to extract the highest amount of auto-correlation between the local and incoming spreading sequences. The timing jitter is denoted by  $\tau_j$ .

The overall time delay is denoted by

$$\tau_{total} = \tau + \tau_j, \quad (3.6)$$

where  $\tau$  is the time delay as a whole multiple of chip and  $\tau_j$  is a fraction of a chip duration.

The time delay between the transmitter and receiver, its estimation and remedying its adverse effects are issues for the synchronisation part of the system which will be discussed in detail in later chapters.

### 3.3.3 Receiver structure

The receiver has the role of extracting the message from the received noisy signal. As shown in Fig. 3.4, in the multi-user CSK receiver configuration, detection and de-spreading are achieved by correlating the incoming signal with the various locally generated users' spreading codes. Remembering the synchronisation assumption mentioned previously, each locally generated spreading sequence is correlated with the incoming signal and the result of the correlation is sampled when all the energy of the particular bit/symbol has come through the system. A threshold device is then used after the accumulator to estimate the bits that were sent. Since PNRZ form is used to represent bits, the threshold is chosen to be zero.

Given that the received signal is typically corrupted by noise and the interference from other users, there will always be errors. Errors are instances of the wrong estimation of the transmitted signal by the receiver. Given that the received signal is random, a certain probability can be attached to this event which is known as the probability of error denoted by  $P_e$ . The performance of various systems are compared using their probabilities of error.

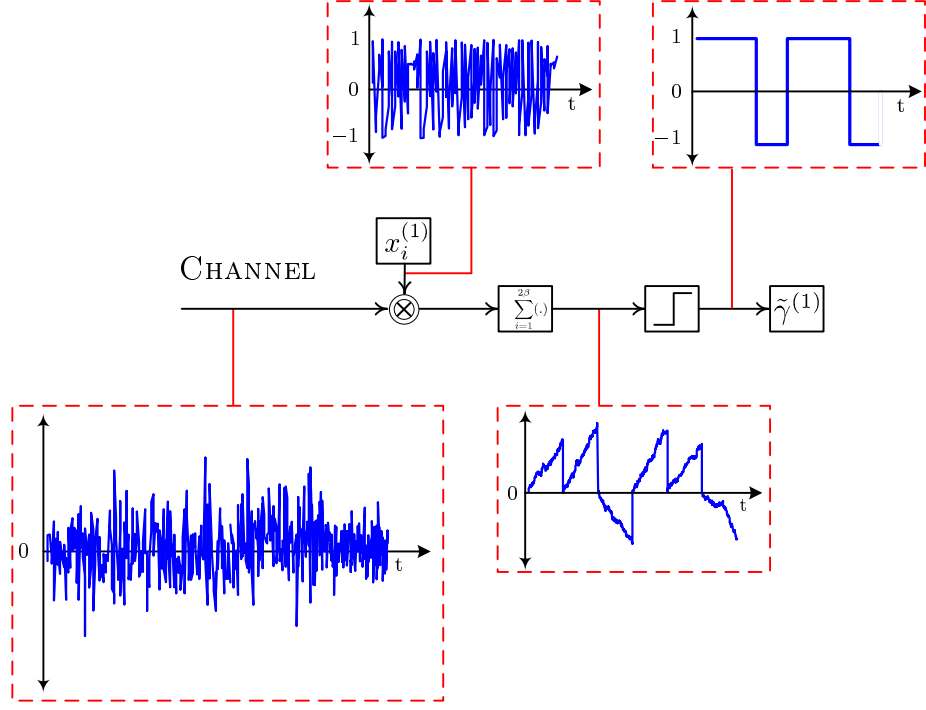


Figure 3.4: Receiver block diagram.

The received signal can be expressed as

$$r_t = S_t + \xi_t, \quad (3.7)$$

where  $S_t$  is defined in (3.5) and  $\xi_t$  is the AWGN the variance of which was explained in §3.3.2.1.

Since this is an introductory chapter and the goal is familiarisation with the system, the BER performance of the system in Rayleigh fading is not considered in the subsequent analysis. Interested readers can consult [46] for more information.

The correlator output for bit  $i$  can be written as

$$\begin{aligned} z_i &= \sum_{t=1}^{2\beta} r_t x_t^{(1)} \\ &= \sum_{t=1}^{2\beta} \gamma_i^{(1)} \left( x_t^{(1)} \right)^2 + \sum_{g=2}^N \sum_{t=1}^{2\beta} \gamma_i^g x_t^g x_t^{(1)} + \sum_{t=1}^{2\beta} \xi_t x_t^{(1)}, \end{aligned} \quad (3.8)$$

where  $2\beta$  is the spreading factor. It can be seen from (3.8) that the correlator output can be divided into three parts: the desired signal, the IUI term and the signal  $\times$  noise term. It is shown in [78, pp 46-48] that the last two of these parts can be considered a Gaussian random variable and as a result their summation is also Gaussian. In order to find  $P_e$ , the mean and variance of  $z_i$  have to be found. The final expression for the distribution of  $z_i^{(g)}$  ( $z_i$  for the  $g$ -th user) is found in [78, pp 58] to be a Gaussian distribution given by

$$z_i^{(g)} \sim G \left( 2\beta \text{VAR} \left[ x_t^{(1)} \right], 2\beta (N-1) (P_c)^2 + \beta N_0 P_c \right), \quad (3.9)$$

where  $P_c$  is the chip power.

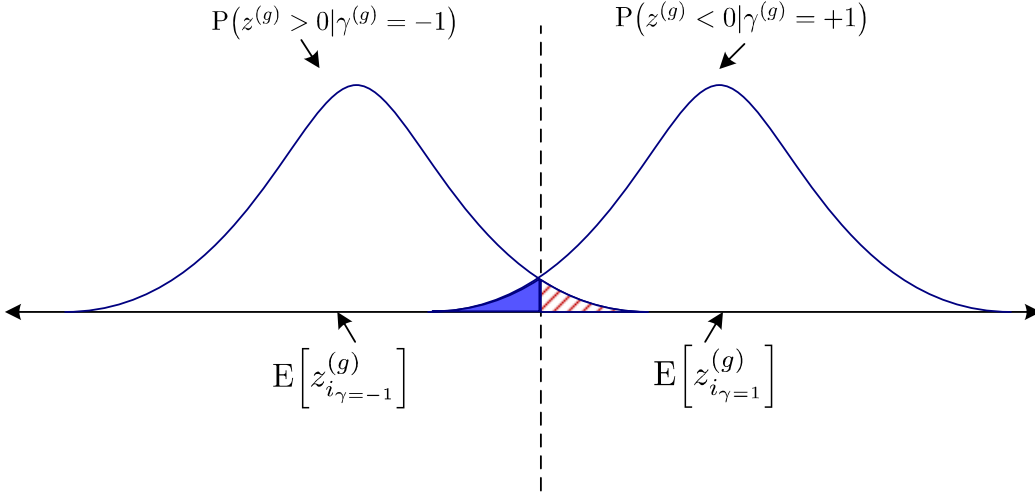


**Figure 3.5:** Distribution of the correlator output for BPSK modulation and the threshold chosen.

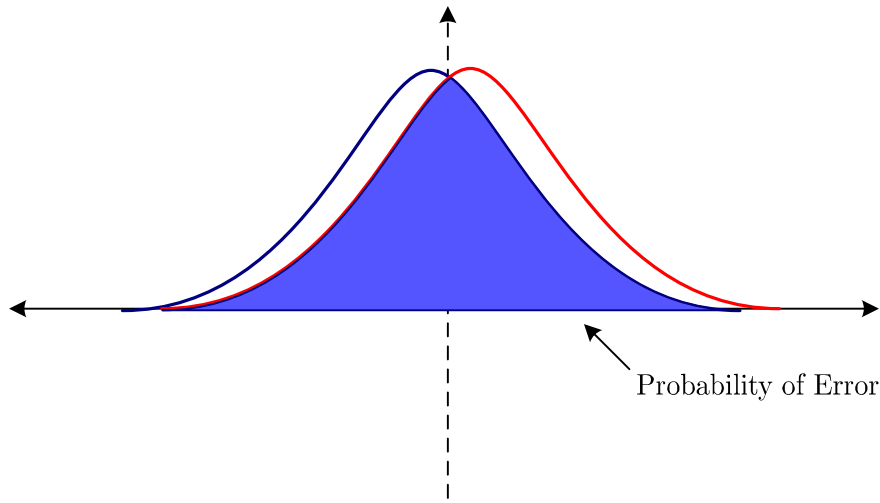


**Figure 3.6:** Distribution of the correlator output for BPSK modulation when no synchronisation is present.

It has been shown in [78, pp 46-48] that

$$\begin{aligned}
 P_e &= \frac{1}{2}P\left(z_i^{(g)} < 0 | \gamma_i^{(g)} = +1\right) + \frac{1}{2}P\left(z_i^{(g)} > 0 | \gamma_i^{(g)} = -1\right) \\
 &= \frac{1}{2}\text{erfc}\frac{\mathbb{E}[z_i^{(g)} | \gamma_i^{(g)} = +1]}{\sqrt{2\text{VAR}[z_i^{(g)} | \gamma_i^{(g)} = +1]}}, \tag{3.10}
 \end{aligned}$$

which indicates that  $P_e$  for the  $g$ -th user is the probability of detecting a bit 1 whilst a bit  $-1$  was sent or vice-versa. Given the Gaussian nature of the correlator output, the integration for  $P_e$  can be represented by a complementary error function or  $\text{erfc}(\cdot)$ . Fig. 3.5 gives a visual representation for the probability of

error as well as the distribution of the correlator output. The probability of error is the shaded area. The two possible outcomes are both on the real axis because BPSK modulation is used here. Observing Fig. 3.5 more carefully, it is clear that with more users, or with a lower SNR, the variance of the two Gaussian distributions increases and the area of overlap also increases which directly translates to the increase in the probability of error.

Substituting (3.9) into(3.10), the probability of error for an AWGN channel can be expressed as

$$P_e = \frac{1}{2} \operatorname{erfc} \left( \frac{\psi}{\beta} + \frac{(N-1)}{\beta} + \left( \frac{N_0}{E_b} \right) \right)^{-\frac{1}{2}}, \quad (3.11)$$

where  $\psi = \frac{\operatorname{VAR}[x_t^g]^2}{\operatorname{E}[(x_t^g)^2]}$  [78].

Fig. 3.6 is presented in order to visually show what happens when synchronisation is lacking in the coherent CSK system. As can be seen the two Gaussian distributions shown in Fig. 3.5 collapse into one because the mean of the correlator output is very close to zero. This maximises the overlap between the two distributions and the probability of error becomes half the area under the Gaussian distribution. Since the area under the PDF curve is equal to unity, the probability of error equals 0.5, which corresponds to a BER of 0.5.

The simulator for the receiver component works on an array of bits that have been corrupted in the channel. These are then correlated with the noise-free spreading sequences and the result is then accumulated for each bit. The estimation of the message is simply done by a threshold comparison function.

Fig. 3.7 presents the base-band multi-user CSK system except the synchronisation related blocks. As can be seen each user uses its own spreading sequence generator. The fading coefficients are denoted by  $a_k$ . It is assumed that  $k$  changes at every bit because the slow fading scenario is considered.

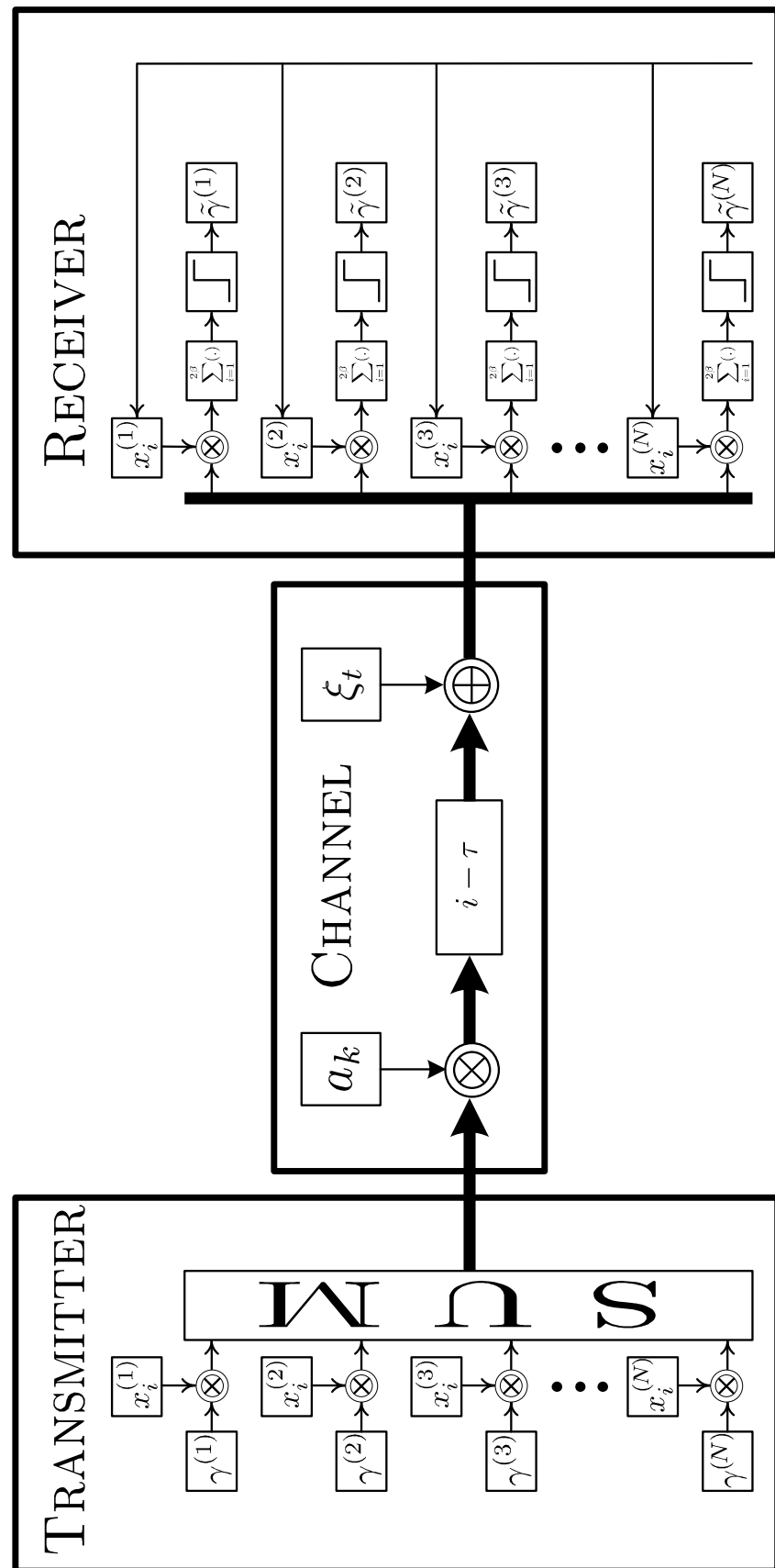


Figure 3.7: System model.

### 3.4 The Need for Synchronisation

Now that the coherent<sup>12</sup> CDS-SS CSK system has been examined, the significance of the synchronisation part becomes clear. The sequence generator in Fig. 3.1 generates a set of spreading sequences and its counterpart in Fig. 3.4 also starts generating the same sequence at the same time. However, it takes some time for the transmitter signal to reach the receiver. This time is known as propagation time and cannot be determined in advance. The propagation time forces a delay between the transmitter signal and the locally generated receiver sequence. This delay is normally several times larger than a chip duration. Moreover, the time delay between the transmitter and receiver changes in small increments in time. This means that the time delay between the transmitter and receiver sequence generators is essentially a random value several times a chip length, to which a small time-changing random value is added.

As shown in Fig. 2.13, if the corresponding transmitter and receiver chips have a time misalignment as much as one chip duration, the auto-correlation function will not be at its peak anymore. As a result, the correlator output is a value very close to zero and the receiver cannot determine if a 1 or  $-1$  was sent. In this scenario, the receiver becomes redundant and the BER will equal 0.5, which essentially is a random guess as to the nature of the bit sent. Fig. 3.6 illustrates the situation when there is no synchronisation and the distributions for both 1 and  $-1$  bits overlap. As can be seen the probability of error in this case equals to 0.5, which is half the area under the Gaussian curve presented in Fig. 3.6.<sup>13</sup>

Up to now, nearly all the work presented in the literature containing coherent CDS-SS communication, has done so by assuming that perfect synchronisation is achieved between the transmitter and receiver sequence generators [50, 60, 64, 65, 68, 69, 76, 77, 90]. However, none of these works present any insight into the synchronisation of chaotic sequences.

The first major piece of work that addressed the synchronisation issue in CDS-SS systems appeared in three successive papers by Kolumban *et al.* [57, 91, 92]. The main message of these series of papers was that the sequence synchronisation for coherent CDS-SS systems is very difficult if not impossible to achieve. These papers stated that the research has to be focused on the development of non-coherent systems which do not acquire synchronisation of sequence generators between the transmitter and receiver. This resulted in a shift in the research trend and the subsequent literature focused on the variants of DCSK systems which are non-coherent all citing the three papers by Kolumban.

Further research which originated in [93] and was continued in [93–95] set about proving that sequence synchronisation in coherent CDS-SS systems is possible. However, this research has limitations in both the scope of the channel characteristics considered as well as the way correlation function of the chaotic spreading sequences are modelled; addressing these limitations and extending the analysis is the primary goal of this thesis.

---

<sup>12</sup>Of course non-coherent systems also require synchronisation to be able to establish where the old bit finishes and the new one starts. To do this they exploit periodic signals at the beginning of every packet which adds to the overhead. However, these systems do not need sequence synchronisation as long as the transmitted reference part of the signal and the information bearing part can be distinguished. It is correct that sequence synchronisation is not needed for non-coherent systems but carrier synchronisation is still needed.

<sup>13</sup>The problem of synchronisation for conventional DS-SS has been solved and various trends and solutions are presented in §4. The current chapter highlights the need for synchronisation for coherent systems.

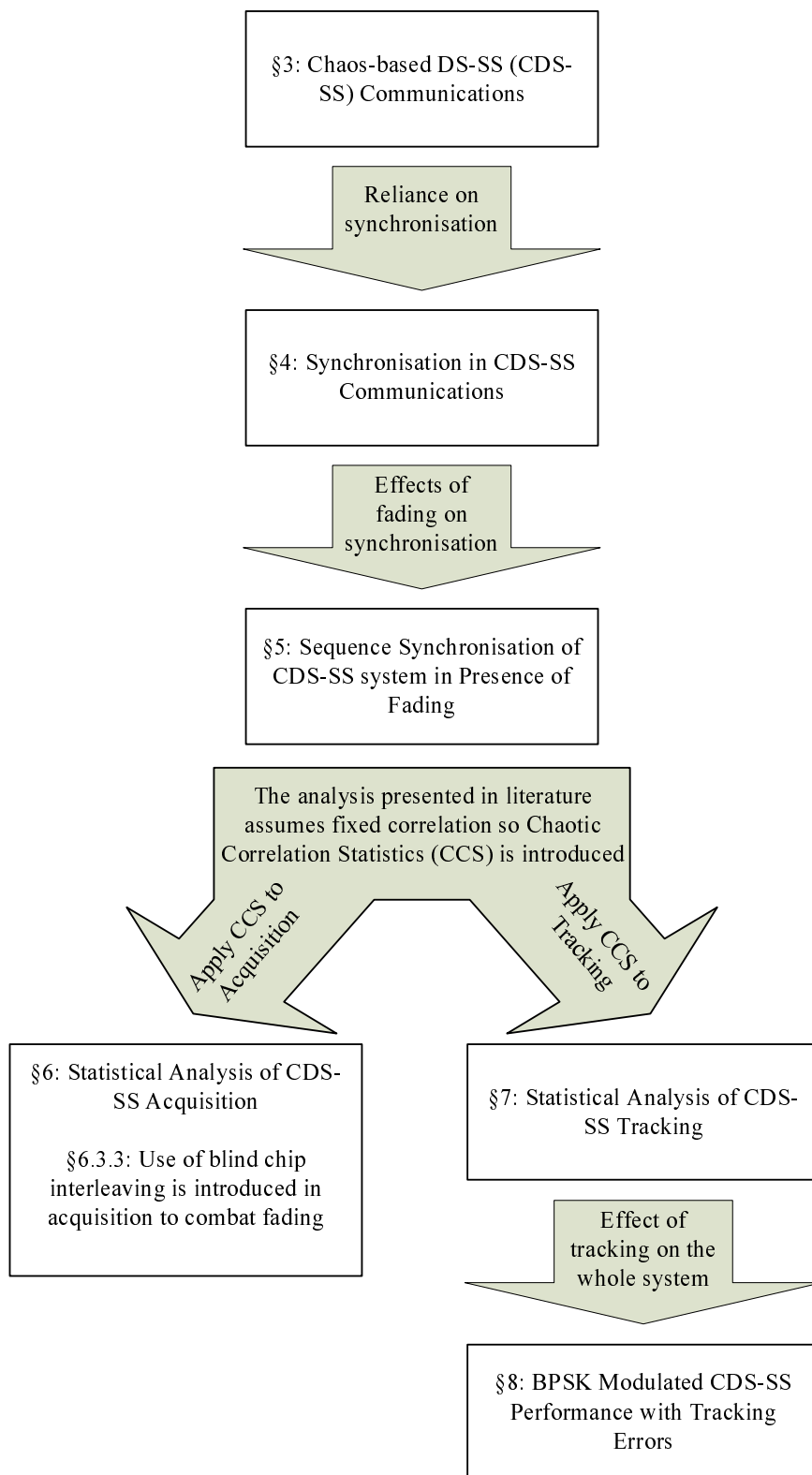


**Figure 3.8:** Thesis structure and contributions, a graphic representation.

The discussion above establishes the need for synchronisation in coherent CDS-SS systems and to some extent addresses the shortcomings in the current literature regarding this issue. The next section presents

the thesis contributions which are within the context of the need for synchronisation described in this section.

## 3.5 Thesis Contributions

Now that the need for synchronisation in coherent CDS-SS systems is established and the limitations of the previous research in this regard are exposed, it is time to present the contributions of this thesis. These are as follows:

1. In order to address the limited capabilities of the existing model for coherent CDS-SS synchronisation, a model which examines the effect of fading on chaotic sequence synchronisation has been considered in §5.
2. The existing analysis used for coherent CDS-SS synchronisation is inaccurate because it uses the theoretical model developed for conventional binary sequences instead of chaotic sequences. This has caused a gap between what the theoretical predictions are and what the system actually achieves. As a result, the development of a statistical approach for chaos-based spreading sequence correlation, termed chaos correlation statistics (CCS), was needed and was performed in §6.2.
3. The CCS was used for accurate analysis of chaos-based code acquisition in three different scenarios of AWGN, AWGN and fading, and AWGN, fading with blind interleaving in §6.
4. The CCS was used for accurate analysis of chaos-based code tracking and deriving the statistical properties related to chaotic sequence tracking in §7.
5. The bit-error-rate (BER) expression for a BPSK modulated CDS-SS system with tracking errors was derived for various distribution of tracking errors in §8 to examine the effect of tracking errors on the overall system performance.

The flowchart given in Fig. 3.8 gives a visual presentation of the thesis contributions within the general flow of this thesis. This flowchart is designed to give a one page overview of this thesis with the interconnections between the different chapters. The thesis chapters are connected with arrows which either emphasise the reason for the investigation or present the contribution made in going from one chapter to the following one.

## 3.6 Summary

This chapter presented the CDS-SS system with BPSK modulation and has highlighted the problem of synchronisation as an important issue with direct relation to the system performance. The synchronisation of CDS-SS systems has not been thoroughly investigated and the existing models are limited and inaccurate. As a result there needs to be a more in depth review of synchronisation for CDS-SS systems to examine the existing models and techniques, and to understand exactly what the limitations and inaccuracies are. This review is presented in the next chapter.



# **Chapter 4**

## **Sequence Synchronisation in CDS-SS Communications**

### **4.1 Introduction**

So far, §2 has identified the chaos-based direct sequence spread spectrum (CDS-SS) communication as a good way of utilising chaotic sequences, and §3 has highlighted the need for synchronisation as an important issue which is directly related to the working of CDS-SS systems. The need for synchronisation is universal amongst all DS-SS communication systems and it arises from the inherent time difference between the transmitter and receiver sequence generators. The main purpose of synchronisation, irrespective of the specific communication scheme, is to estimate and eliminate the time difference between the transmitter and locally generated receiver spreading sequences. In DS-SS systems sequence synchronisation is achieved in two stages of *acquisition* and *tracking*.

The aims of this chapter are threefold. The first aim is to present a general survey of existing DS-SS acquisition and tracking techniques which are not limited to the techniques already applied to CDS-SS systems. The second aim is to explain the concepts and assumptions related the treatment of these techniques. The third aim is to point out the acquisition and tracking techniques that have been applied to the CDS-SS systems and identify the shortcomings and limitations in the analysis that exists in literature. Once these shortcomings and limitations are identified, the next chapters will each deal with certain aspects of these shortcomings by extending the previous research.

The rest of this chapter is structured as follows. §4.2 and 4.3 present a concise but representative review of acquisition and tracking techniques presented in literature as well as introducing the concepts and terminologies related to the performance measurement of these techniques respectively. §4.4 identifies and discusses the shortcomings of the current models for CDS-SS synchronisation. §4.5 summarises the chapter.

## 4.2 Sequence Acquisition

The aim of the acquisition stage of a DS-SS system is to accurately estimate the time difference between the received spreading sequence and its replica generated in the receiver. The accuracy of this estimation has to be within one chip duration, otherwise the DS-SS system is not able to de-spread the received signal. To achieve sequence acquisition, the transmitter sends a periodic spreading sequence to the receiver which is normally called the *pilot*. The pilot period defines the *uncertainty region*, that is, the various timing offset values the pilot can possibly have. Each timing offset within the uncertainty region is called a *cell* and the role of the sequence acquisition is to find out what cell corresponds to the correct timing offset between the transmitter and receiver and then declare the achievement of synchronisation between the two.

Given that sequence synchronisation in noisy environments can be treated as a statistical problem [96], various probabilities can be assigned to different events and outcomes of the acquisition process. What follows is the introduction of the most important probabilities related to the sequence acquisition. The probability that the acquisition stage declares synchronisation correctly is called the *probability of detection* ( $P_D$ ). The probability that the acquisition declares synchronisation incorrectly is known as the *probability of false alarm* ( $P_F$ ) and the acquisition is said to be in a false alarm state. The time it takes for the acquisition stage to synchronise to the incoming signal is named the *acquisition time* ( $T_{acq}$ ). The probability that, upon sweeping the uncertainty region, the acquisition phase misses the correct timing offset is termed the probability of *missed detection* ( $P_M$ ).

### 4.2.1 Sequence acquisition for DS-SS systems — A survey

Sequence acquisition holds within it two separate concepts, the first is the *detection scheme* used for the incoming signal which is primarily concerned with detecting the arrival of a certain spreading sequence; the second one is the *search strategy*, that is, the algorithm with which the time difference between the received and local spreading sequences is estimated. Given the importance of sequence acquisition for DS-SS systems, a large amount of research has been dedicated to proposing and analysing various detection architectures and search strategies over the past three decades. This volume of research is so large that it makes an exhaustive literature survey impractical; however, a representative survey is given here alongside the relevant citations of the original and ground breaking works.

DS-SS sequence acquisition can be sub-categorised in many different ways. However, almost all these sub-categories share a common trait which is the usage of some measure of correlation between the incoming spreading sequence and its locally generated replica [97]. The correlation between the two sequences is measured using different methods based on the detection scheme. The search strategy then acts on the output of the detection scheme to declare whether synchronisation is achieved or not [97]. The survey presented here first examines various detection schemes and then focuses on various search strategies reported in the literature. The tree diagram presented in Fig. 4.1 gives a visual representation of the detection schemes which will be explained as well as the citations related to each of the subcategories.

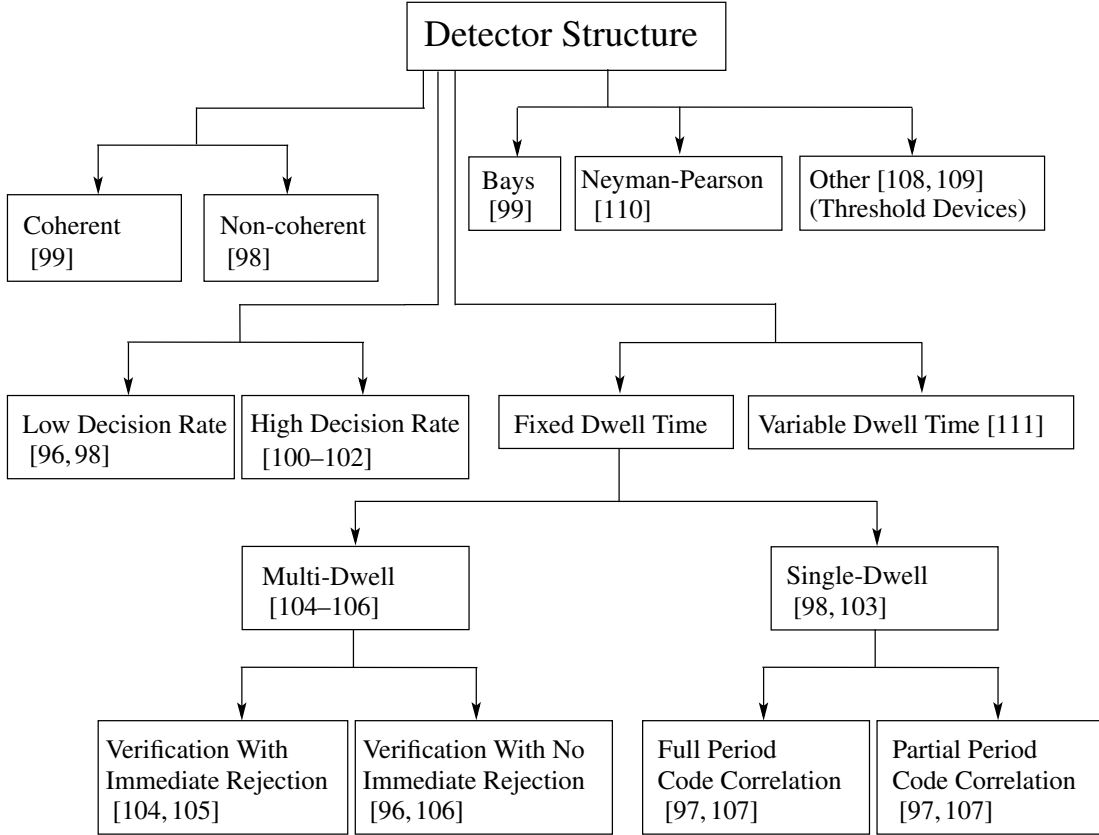


**Figure 4.1:** Tree diagram for search strategies, adapted from [112].

Detection schemes can be placed into the *coherent* and *non-coherent* categories. The coherent detection schemes assume that the receiver has reliable knowledge of carrier phase, that is, the carrier can be demodulated prior to de-spreading. Non-coherent detectors do not have any information regarding the carrier phase and they normally use band-pass filtering in conjunction with a square-law envelope detector. Detection schemes can be one of *fixed* or *variable* integration time types. The integration time is the time spent correlating the incoming sequence (with its arbitrary timing) to the receiver generated replica which has known timing offset. The fixed integration type detector is further differentiated into the *single-dwell* and *multi-dwell* categories. In this context, dwelling refers to the examination of each cell within the uncertainty region. In single-dwell detection schemes, each cell is examined only once, whereas in multi-dwell schemes this is performed multiple times. Depending on the length of the pilot sequence used for correlation, the single-dwell acquisition schemes can be sub-categorised into *partial* or *full period sequence correlation*. Multi-dwell schemes on the other hand can be categorised based on the way they make the final decision regarding the synchronicity of the two sequences. This type of decision making is referred to as the verification in the literature and has two broad categories of *immediate rejection verification* and *non-immediate rejection verification*.

The rate of decision making is important for detection schemes and, in general, the detection scheme can be *high rate* (like devices such as matched filters or passive detectors) or *low rate* (active correlators, or sliding correlators) which make the synchronisation decision at a rate much lower than the chip rate. Finally, detection schemes can be categorised based on the decision criterion used to declare synchron-

isation or lack thereof. This can be a simple *Bays* hypothesis which minimises the average risks, or the more complex *Neyman-Pearson* hypothesis.

Various search strategies in the literature can also be categorised using the same structure as detection schemes. The tree diagram presented in Fig. 4.4 gives a visual representation of the existing search strategies as well as the citations related to each of the sub-categories. These strategies fall into three broad categories of *sequential estimation*, *serial search* and *maximum-likelihood estimation*. The sequential estimation algorithm was first introduced in [108] with improvements in [109, 113]. This category of search strategy relies on very accurate estimation of the incoming spreading sequence which is then used as the initialising state for the receiver spreading sequence generator. The other major category of search strategies is the maximum-likelihood algorithm which, conceptually speaking, is the simplest form of search strategy [97]. The received spreading sequence is correlated with all possible sequence positions of the locally generated replica. The correlation is performed concurrently for all the spreading sequence positions, using a bank of matched filters individually tuned to every possible sequence timing offset, and the largest correlation result is chosen as the correct timing offset [97]. Finally, the most widely used search strategy is the serial search algorithm [97, 107] which was suggested in [114]. Usually the serial search algorithm achieves synchronisation using a sliding correlator and a threshold detector to find the correct timing offset. The serial search algorithm can also be implemented in a parallel<sup>1</sup> fashion. That is, the acquisition phase divides the uncertainty region into several smaller regions and uses one correlator per region. With this approach,  $T_{acq}$  is reduced but the system requires many more components.

Fig. 4.2a shows the block diagram of a base-band acquisition phase using the serial search algorithm while Fig. 4.2b depicts the parallel implementation of the serial search algorithm, the increase in complexity and components is evident. Fig. 4.3 presents the time domain waveform of the sliding correlator output and the threshold. This figure is designed to illustrate the concepts of detection, which happens when the threshold is crossed at the correct timing offset, and false alarm, where the output crosses the threshold in the incorrect timing offsets. The output of the square law device will be the square of every sample in Fig. 4.3.

The serial search algorithm<sup>2</sup> can be classified based on the allowable acquisition time, the way a false alarm state is treated and the sweep strategy for the uncertainty region. With respect to the allowable acquisition time, the serial search algorithm can be sub-divided into *limited* and *unlimited allowable time*. The false alarm situation can be treated by either *returning state*, which means that after declaring a false synchronisation, the acquisition phase will recover and resume the search for the correct timing offset, or the *absorbing state*, which entails a catastrophic unrecoverable false alarm state.

Based on the sweep strategies they employ, serial search algorithms can be sub-divided into the *continuous sweep* strategy, where the time difference between the two sequences is varied in a continuous manner or the *discrete step sweep* in which the time difference for the sweep is varied in discrete steps. The discrete steps can be of a *uniform* or a *non-uniform* size. The non-uniform step sized sweep strategies can be further divided into the *expanding window type*, where a part of the uncertainty region is chosen

---

<sup>1</sup>Parallel serial search should not be confused with the maximum-likelihood search strategy. In the maximum likelihood acquisition method, the sequence phase positions are tested with the same observation of the signal, whereas in the parallelised serial search different received signal observations are used.

<sup>2</sup>The serial search strategy is also known as serial search algorithm in the literature.

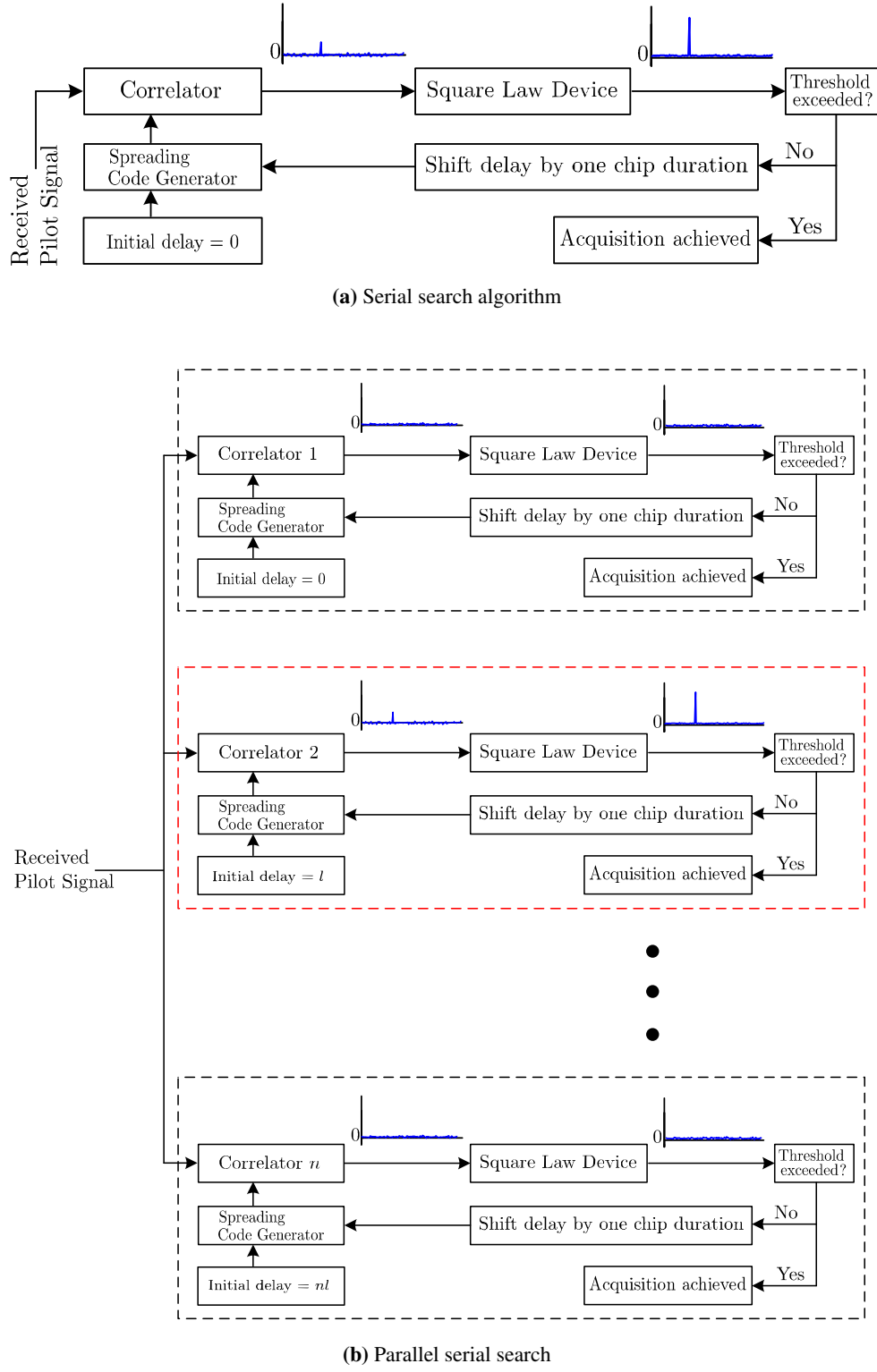


**Figure 4.2:** Block diagrams for different implementations of the serial search algorithm.

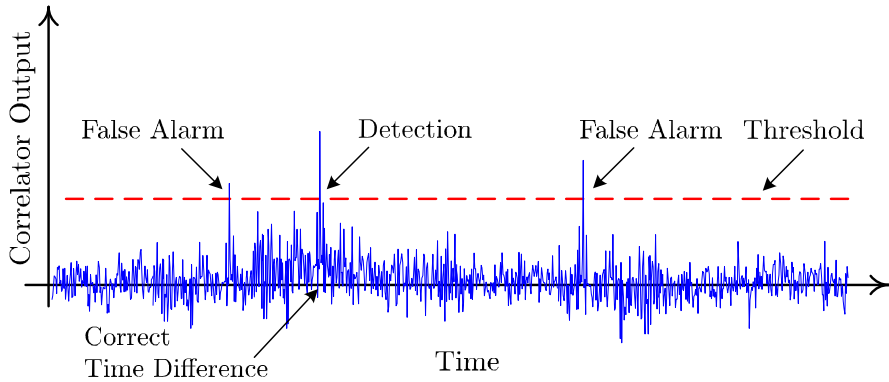


**Figure 4.3:** Sliding correlator output waveform for serial search algorithm.

based on the a priori information and the sweep is then expanded outwards from that, or the *z-type* sweep strategies that start the sweep from the middle of the uncertainty region.

All the works presented in the citations above assumed an AWGN channel scenario; however, an important issue that has to be considered in sequence acquisition is the multi-path channel. Given that the multi-path fading has a significant effect on the signal reception, it naturally follows that the performance of the acquisition stage under fading conditions has to be investigated. In fact, sequence acquisition performance in a multi-path channel has generated a lot of interest and what follows is representative of the diverse treatments of this problem for binary<sup>3</sup> spreading sequences in the literature. The performance of an acquisition stage for digital communication systems in general has been investigated in [119]. In [120] a differentially coherent acquisition system is investigated when the system is exposed to a fast Rayleigh fading channel, while the results in [120] are extended to include slow fading in [121]. The topic of non-coherent DS-SS acquisition in a frequency selective environment was first investigated in [122] with a comparison for fading/non-fading channels given in [123]. This was then continued by an investigation of the system performance for asynchronous case in time varying fading channels in [124]. The first derivation of  $P_D$  and  $P_F$  in a fading channel was presented in [125] and then expanded in [126] and [127].

Serial search algorithm in presence of fading has been investigated in [128–131] and the parallel search in [132]. Correlated fading scenarios and their effect on acquisition have been covered in [133] and [134]. Since the introduction of diversity techniques to mitigate fading in DS-SS systems, various treatments of sequence acquisition with diversity techniques has been put forward. Namely, [87] presents a RAKE receiver in a multi-path channel scenario; [135] discusses joint timing and pilot symbol channel estimation for frequency flat fading channels; and both [136] and [137] discuss multi-path utilisation techniques for frequency selective fading channels.

<sup>3</sup>Binary spreading sequences take only two values as their name suggests. These are distinguished from non-binary spreading sequences which can take any value between two set bounds. Chaos-based spreading sequences are in the category of non-binary spreading sequences.

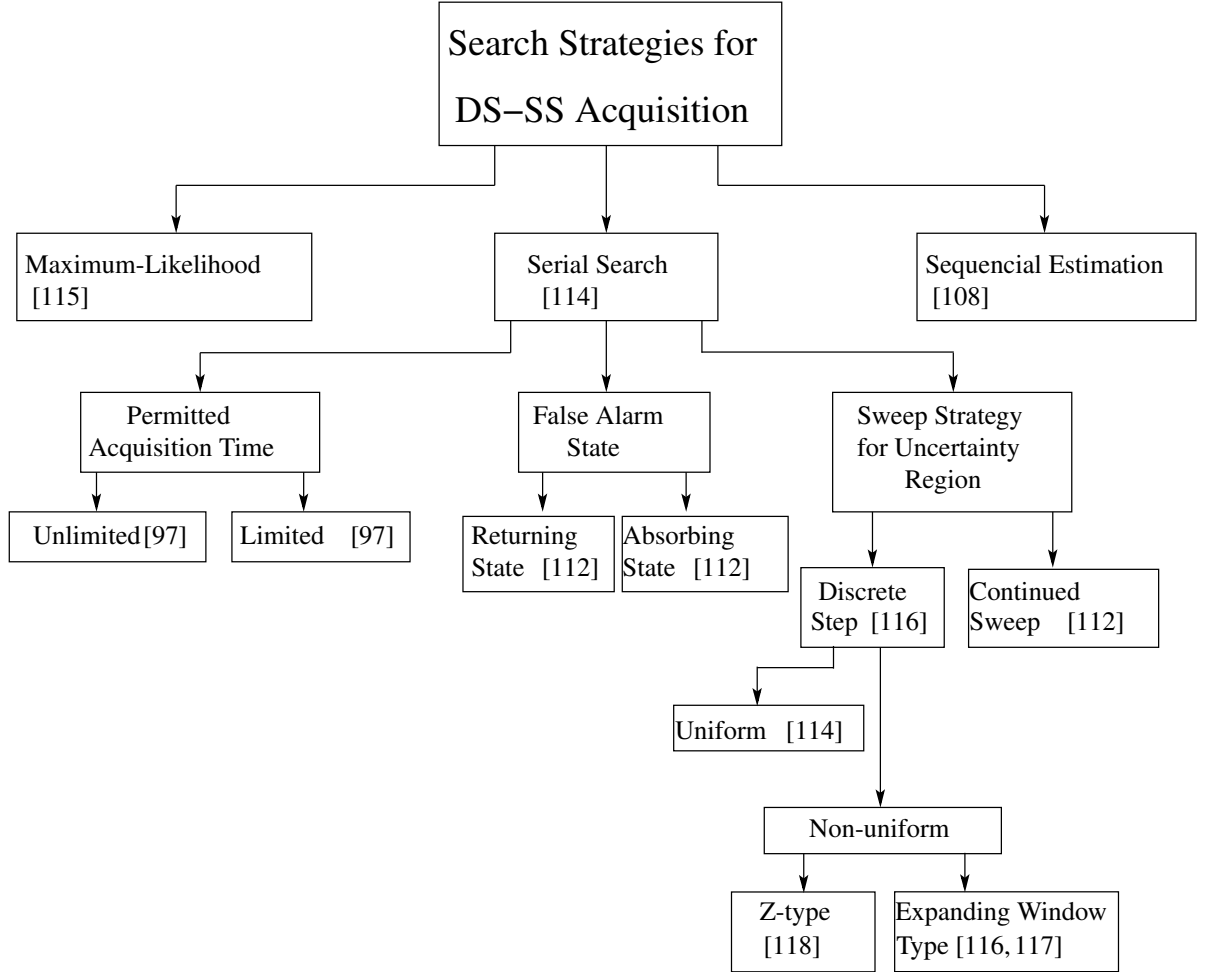


**Figure 4.4:** Tree diagram for acquisition schemes, adapted from [112].

### 4.2.2 Sequence acquisition for chaos-based spreading sequences

The citations in the survey presented in §4.2.1 assume that the spreading sequence is of a binary nature (PN, Gold codes or m-sequences). This section deals with the research concerning acquisition for *chaos-based* spreading sequences.

The body of research for CDS-SS sequence acquisition is more recent and far less voluminous. The first treatment for the sequence acquisition problem was presented in [138], which used the examination method suggested in [139, pp. 39–58] with a slight modification to derive  $T_{acq}$ . The acquisition method proposed in [139, pp. 39–58] uses non-coherent detection as well as serial search algorithm which was introduced previously. However, [138] did not present a study of the derivation of  $P_D$  and  $P_F$  nor did it shed any light on the role of the correlator receiver. The most relevant treatment of the sequence acquisition of CDS-SS systems with emphasis on chaotic sequence correlation, was presented in [93] and then expanded in [94]. Unlike [138], the treatment presented in [94] is based on the cross and auto-correlation of the chaotic spreading sequences which are used to derive  $P_D$  and  $P_F$ . Also, [94] claims to present the system performance in a multi-path Rayleigh fading channel. The method for deriving  $P_D$  and  $P_F$  in [94] is not proposed by Jovic *et. al.* and is a reproduction of what has already been presented in [8]. This acquisition stage is based on a non-coherent, single dwell, partial sequence

correlation detector and uses the serial search algorithm with unlimited allowable time, which is the most commonly investigated DS-SS acquisition stage. However, the sequence acquisition unit and its accompanying derivation presented in [94] has some significant shortcomings which can be summarised thus: first, although it is claimed that Rayleigh fading has been taken into account for the whole system, there is no evidence of its effects on the acquisition stage. Second, the method for deriving  $P_D$  and  $P_F$  in [94] needs to be adapted to sequences that are non-binary, this is the main reason for Jovic *et. al.* presenting only approximations and upper bounds instead of presenting accurate theoretical expressions for the acquisition phase performance. These shortcomings and motivations to continue this work will be discussed in more detail in §4.4.

Most recent publications such as [95, 140] that deal with CDS-SS systems, bypass the chaotic sequence acquisition issue altogether citing [94] as the research that has solved the synchronisation problem. [95] uses a PN instead of a chaos-based sequence in a chaos-based DS-CDMA setting and [140] does not use chaos-based spreading sequences leaving them in favour of Chua's attractor which have been shown not to be robust for noisy channel conditions [141].

### 4.3 Sequence Tracking

Once the acquisition stage has estimated the time difference between the transmitter and receiver to within one chip duration, the synchronisation block enters the tracking mode. The aims of the tracking stage are twofold; first, it is to estimate the time difference between the transmitter and receiver to a time resolution finer than the acquisition phase. As a result the tracking is sometimes referred to as *fine synchronisation*. The second goal is to maintain time synchronisation between the transmitter and receiver when timing jitter, which is a result of clock wander and oscillator discrepancies, is present in the system.

Most of the tracking stages in literature are feedback based and have a loop configuration. As a result they are often called *tracking loops*. This is because they use the carrier tracking phase locked loops (PLL) theory as the basis of operation. The main point of difference between the PLLs and the sequence tracking loops is the way phase discriminators are implemented in the tracking loops [97]. Tracking loops adjust the speed of the receiver sequence generators to stay synchronised with the incoming signal. This is achieved by calculating the timing error between the received signal and the locally generated one. This timing error is normally noted down as  $e(t)$ . Since  $e(t)$  is a voltage waveform, it is used to control a voltage controlled Oscillator (VCO). The value of  $e(t)$  is linked to the true timing error (denoted by  $\epsilon(t)$ ) by a function called the tracking loop phase characteristics or *S-curve*. All tracking loops have a range of operation which is termed the *pull-in region*. This is a region in time in which the estimation given by the acquisition stage can be tracked. If the spreading sequence timing offset falls outside this region, then the tracking stage is not able to achieve its aim and the system goes back to the acquisition stage. The maximum value for the pull-in region for all tracking loops is one chip duration. The duration of successful tracking until the system goes back to the acquisition stage is called *time to lose lock or slip time*.

### 4.3.1 Sequence tracking for DS-SS systems—A survey

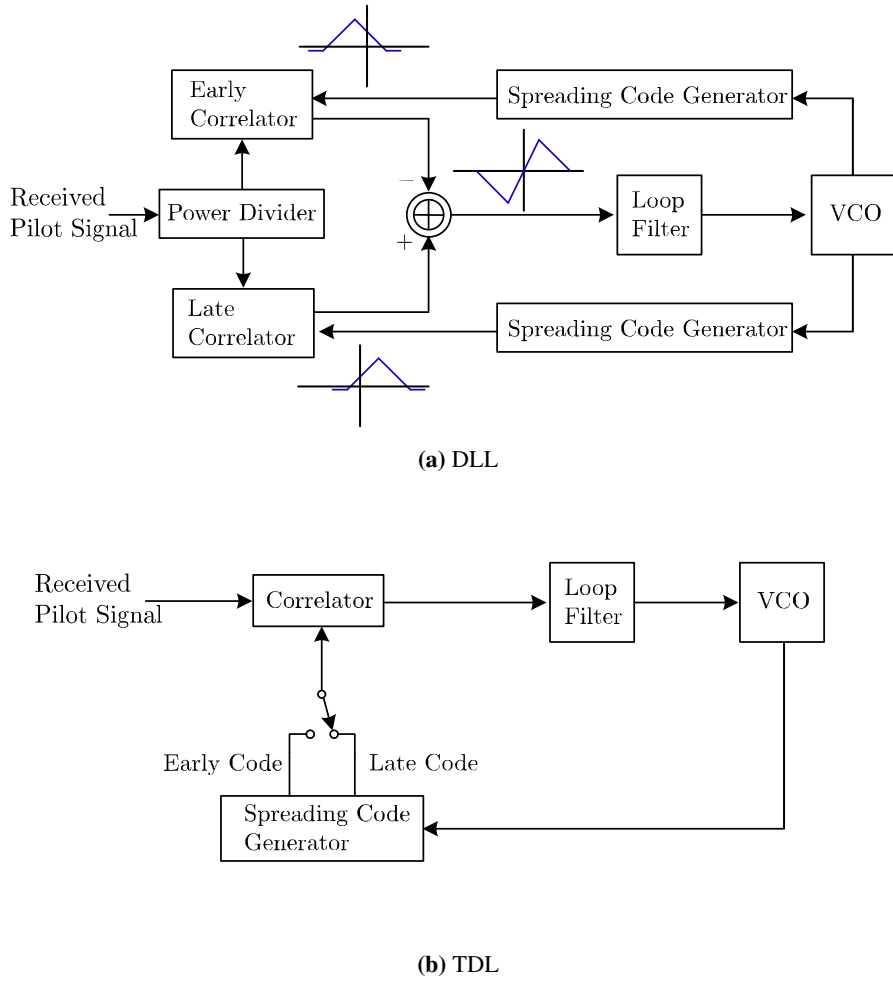
Similar to sequence acquisition schemes, the sequence tracking loops can be categorised as coherent and non-coherent loops depending on whether the carrier phase information is available to the tracking loop or not respectively. Various tracking loop configurations can be implemented in a coherent or non-coherent manner. Almost all tracking loops make use of correlators for phase discrimination in the form of finding the correlation between the incoming signal and two different phases of the locally generated spreading sequence. One of the phases is slightly early and the other one is slightly late with respect to the true timing of the incoming sequence. As a result these tracking loops are called *early-late gates*.

A tracking loop configuration that makes use of two independent correlators is called a *Delay-Lock Loop* (DLL) which was first introduced as an optimum tracking device in [142]. The DLL theory was then specialised for the tracking of binary signals in [143] and for stochastic signals in [144]. A good comparison and study of DLL implementations can be found in [145]. The mean slip time for both coherent and non-coherent DLLs has been treated in [146–149]. Apart from the early-late DLLs, the decision-directed [150–152] and data-aided [152] have also been proposed in the literature. The DLL performance in the presence of multi-user interference has been covered in [153] with interference reduction techniques proposed in [154]. The performance of coherent DLL has been investigated in [155] for a pilot symbol aided system. The coherent DLL performance has also been examined when using non-rectangular chip waveforms in [156]. Fig. 4.5a presents the block diagram of a base-band DLL with the associated waveform in various stages.

Another class of early-late gates is named *Tau-Dither Loop* (TDL) and it uses only one correlator which is shared by the advanced and delayed branches. This type of loop was first proposed in [157] and more detailed analysis was then presented in [97, 107]. Fig. 4.5b presents the block diagram of a base-band TDL, note the use of only one correlator compared to two for DLL. Fig. 4.6 presents the superimposed waveforms associated with coherent tracking of spreading sequence. The S-curve is extracted using the loop filter and its slope is used to increase or decrease the speed of the VCO in order to achieve fine synchronisation. The non-coherent tracking of PN sequences has been thoroughly examined in [158] for both DLL and TDL configurations.

There are reports of modified versions of the DLL and TDL configurations, namely the *double dither loop* (DDL) which was presented in [159], the *modified code tracking loop* (MCTL) introduced in [160], the *product of sum and difference DLL* ( $\Sigma\Delta$ DLL) and finally the *complex sums DLL* which is suggested for environments which are prone to fast fading. Various tracking loop configurations as well as their hierarchy are shown in Fig. 4.7.

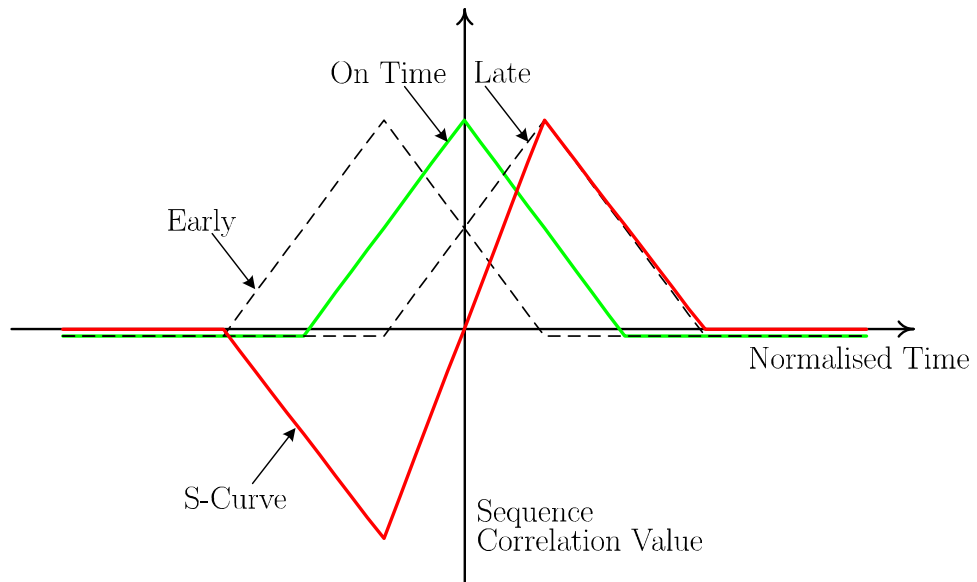
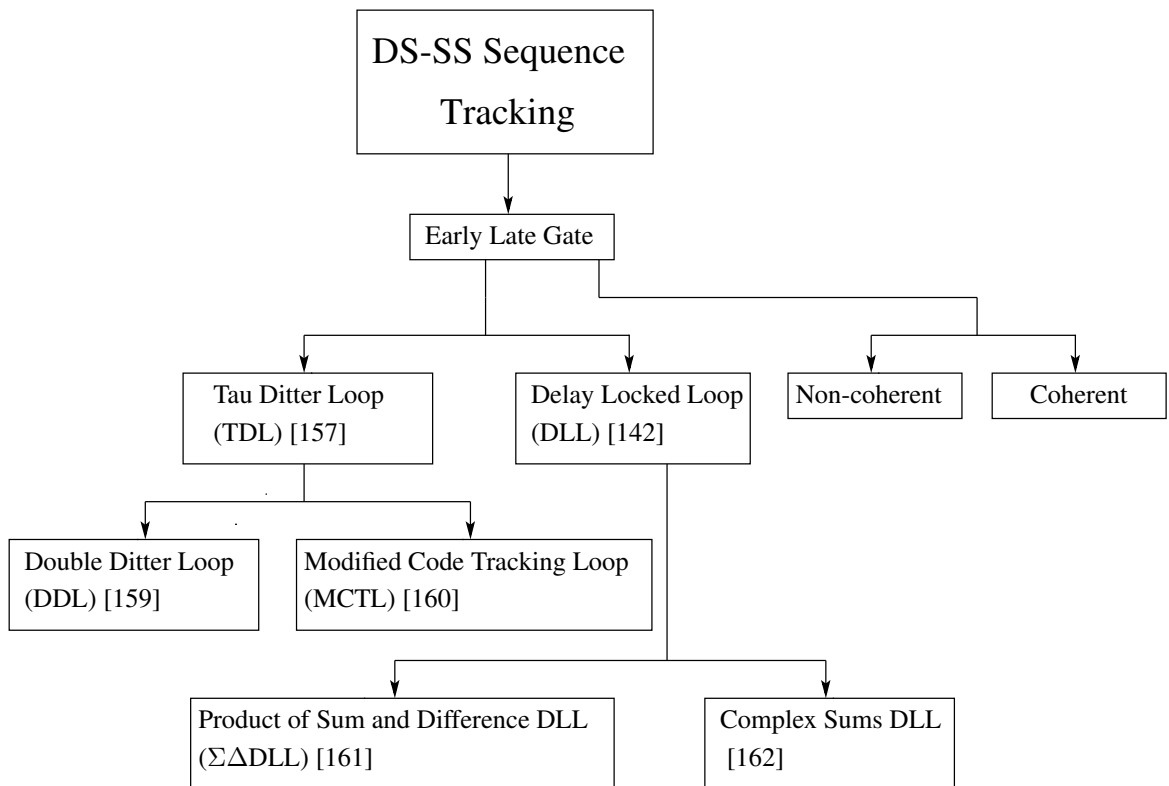
All the works mentioned in the citations above assumed an AWGN or AWGN and multi-user interference channel scenario. However, like the acquisition case, an important issue that has to be considered is the multi-path channel. The performance of both DLL and TDL in a Rayleigh fading channel has been investigated in [163]. Tracking loop configurations that have been modified to mitigate frequency selective and correlated fading can be found in [164, 165].



**Figure 4.5:** Block diagrams of two tracking loop configurations.

#### 4.3.2 Sequence tracking for chaos-based spreading sequences

The citations in the survey presented in §4.3.1 all assume that the spreading sequence is of a binary nature, (PN, Gold codes or m-sequences). However, since the pilot sequence is chaos-based, it has to be tracked to maintain synchronisation. There is not much research covering the tracking of chaos-based spreading sequences. There are only three papers that mention or treat the tracking of chaotic spreading sequences. Both [138] and [166] just assume that the tracking of the chaos-based spreading sequence is a part of the acquisition problem. Recently [94] has investigated sequence tracking of the chaos-based spreading sequences. However, the investigation of the chaos-based tracking loop presented in [94], although novel has some significant shortcomings which can be summarised thus: first, [94] has used a coherent tracking loop which is not consistent with the non-coherent acquisition used in the same paper. Second, [94] claims that fading has been investigated for the whole system but the effect of fading on chaos-based sequence tracking was not presented in [94]. Third, in [94] it was assumed that the correlation of chaotic spreading sequence remains the same no matter what sequence is used. This assumption is not accurate as the value of the correlation changes from sequence to sequence given the non-binary nature of the chaotic spreading sequences. These shortcomings are covered in greater detail in §4.4.

**Figure 4.6:** Early-late gate output waveform.**Figure 4.7:** Tree diagram for Tracking.

## 4.4 Discussion

Both §4.2 and §4.3 presented concise surveys for DS-SS acquisition and tracking methods. Moreover, in-depth surveys of the literature for CDS-SS acquisition and tracking were presented in §4.2.2 and §4.3.2 touching on some of the shortcomings in the treatment of both of these. The aim of this section is to discuss the shortcomings of the treatments of CDS-SS acquisition and tracking presented in the literature in more depth and justify the research path chosen to address these shortcomings. By the end of this section, the research path and the motivation will be clear to the reader.

### 4.4.1 CDS-SS sequence acquisition shortcomings

As shown by citations in §4.2.2, chaos-based sequence acquisition has been investigated previously; however, the research which claims to have taken account of Rayleigh fading in the system fails to address the acquisition performance for a fading scenario. Given that the performance of the acquisition phase has a direct impact on the overall system performance, it is imperative to have a good notion of the acquisition performance of a CDS-SS system in a fading scenario. Moreover, it is important to suggest and implement ways to mitigate the effect of fading on the sequence acquisition for CDS-SS systems. As a result, investigating the performance of the acquisition phase in a fading scenario and suggesting ways to mitigate it is a motivation for this thesis.

Another important issue is related to the chaotic sequence statistics. The papers that directly deal with chaos-based sequence acquisition have simply used the mathematical model which has been developed for binary sequences. This has resulted in discrepancies between the theoretical and simulation results. In order to have theoretical expressions which accurately predict the system performance, the mathematical model for sequence acquisition has to be developed for use with chaotic spreading sequences. Therefore, finding accurate expressions for the acquisition performance of chaos-based spreading sequences is another motivation for this thesis.

Now that the shortcomings of the acquisition stage have been stated, the research path chosen needs to be expressed and justified. In this thesis, the serial search algorithm with a modified non-coherent detector was chosen to investigate the acquisition phase of the CDS-SS system for several reasons. First, the serial search algorithm is one of the most widely used algorithms for SS systems in general. Second, all the results developed for the chaos-based acquisition using serial search algorithm (as well as the CCS), can be expanded into the more complex schemes which are already in existence. Third, all available results from previous investigations which are comparable to the current one use the same technique, which makes a direct comparison possible.

### 4.4.2 CDS-SS sequence tracking shortcomings

Chaos-based sequence tracking is less thoroughly investigated compared to chaos-based sequence acquisition as was shown in §4.3.2. However, since the sequence tracking is dependent on the correlation properties of the chaotic sequences, all shortcomings relating to the correlation mathematical model used for sequence acquisition exist for sequence tracking as well. This thesis will address that issue with the

use of CCS in the tracking stage analysis. Moreover, the performance of the chaos-based tracking stage in a fading scenario has not been investigated in the literature. These two issues are motivations for the investigation presented in this thesis for sequence tracking.

Another important point is the effect of sequence tracking on the overall performance of the communication system. In the investigation presented in [94], the system performance is presented without due attention to the partial synchronisation of the system. In other words, it is assumed that once the system is synchronised, the synchronisation mechanism aligns the sequences without any residual effects from jitter in the channel. In this thesis, this assumption is relaxed to include partially synchronised scenarios and by BER expressions that take into account partial synchronisation. These expressions are then further expanded to include random timing jitters with different distribution as well as fading. It is shown that the system performance in presence of tracking loop errors and fading can be found theoretically and the theoretical results are found to agree closely with the numerical ones.

Having covered the shortcomings of the tracking stage for chaos-based spreading codes, it is now time to justify the research path chosen for the investigation presented in this thesis. A DLL has been chosen to study the tracking of chaos-based sequences for the following reasons. First, the DLL is one of the most widely used tracking loop configurations. Second, the results of the investigation on the tracking loop can be easily expanded to any other configuration which uses the correlation of spreading sequences. Third, the DLL is the only tracking loop configuration that has been partially investigated in conjunction with chaos-based sequences. As a result, it is the best choice for continuation of the research and comparing the results with the previous investigation.

## 4.5 Summary

In this chapter, representative literature surveys of acquisition and tracking methods for DS-SS system were presented and an overview of the various techniques and their inter-relations was shown. A more in depth literature search was then presented on the extent of research already conducted for acquisition and tracking of chaos-based DS-SS systems. It was shown that the previous analysis has several shortcomings. First, the literature does not provide analysis for chaos-based acquisition and tracking in presence of fading. Second, it makes the inaccurate assumption that the correlation of chaos-based spreading sequences remains constant and applies the conventional acquisition and tracking theory used for binary signals. Third, it does not suggest any way of mitigating the fading effects on acquisition phase. The next chapter will address the shortcoming related to the analysis of chaos-based acquisition and tracking performance in presence of fading.



# Chapter 5

## Sequence Synchronisation of CDS-SS System in Presence of Fading

### 5.1 Introduction

So far §4 has introduced the concepts of acquisition and tracking and highlighted the shortcomings of the analysis presented in literature with regards to the CDS-SS systems. The first shortcoming relates to the problem of sequence acquisition and tracking in presence of fading which is going to be addressed in this chapter. First, a system overview as well as the block diagram will be presented in §5.2. Then the problems of acquisition and tracking will be addressed in §5.3 and §5.4 respectively and finally, §5.5 summarises the chapter. The contents of this chapter have been published in [46, 167].

### 5.2 System Overview

Fig. 5.1 illustrates the system model used. Essentially, the pilot is a set of +1 bits which is spread and sent to the channel in which it is delayed by  $\tau$  and corrupted by noise and fading. The time delay equation is (3.6) where  $\tau$  will be found using the acquisition phase and  $T_d$  is found using the tracking stage.

The reception quality is dependent on the SNR, the power of fades and the synchronisation quality in the channel. The fading phenomenon is modelled statistically as a Rayleigh distributed random variable which affects all the users' sequences as well as the pilot signal. Also, the fading coefficient is fixed for a bit period, that is, the fading duration is considered to be as long as a bit duration. The Rayleigh fading equation is given in (3.3).

It is assumed that the receiver has the initial condition of each of the users and that there is some residual phase difference between the received carrier and locally generate carrier. It is also assumed that the users will begin their transmission at the beginning of the pilot sequence.

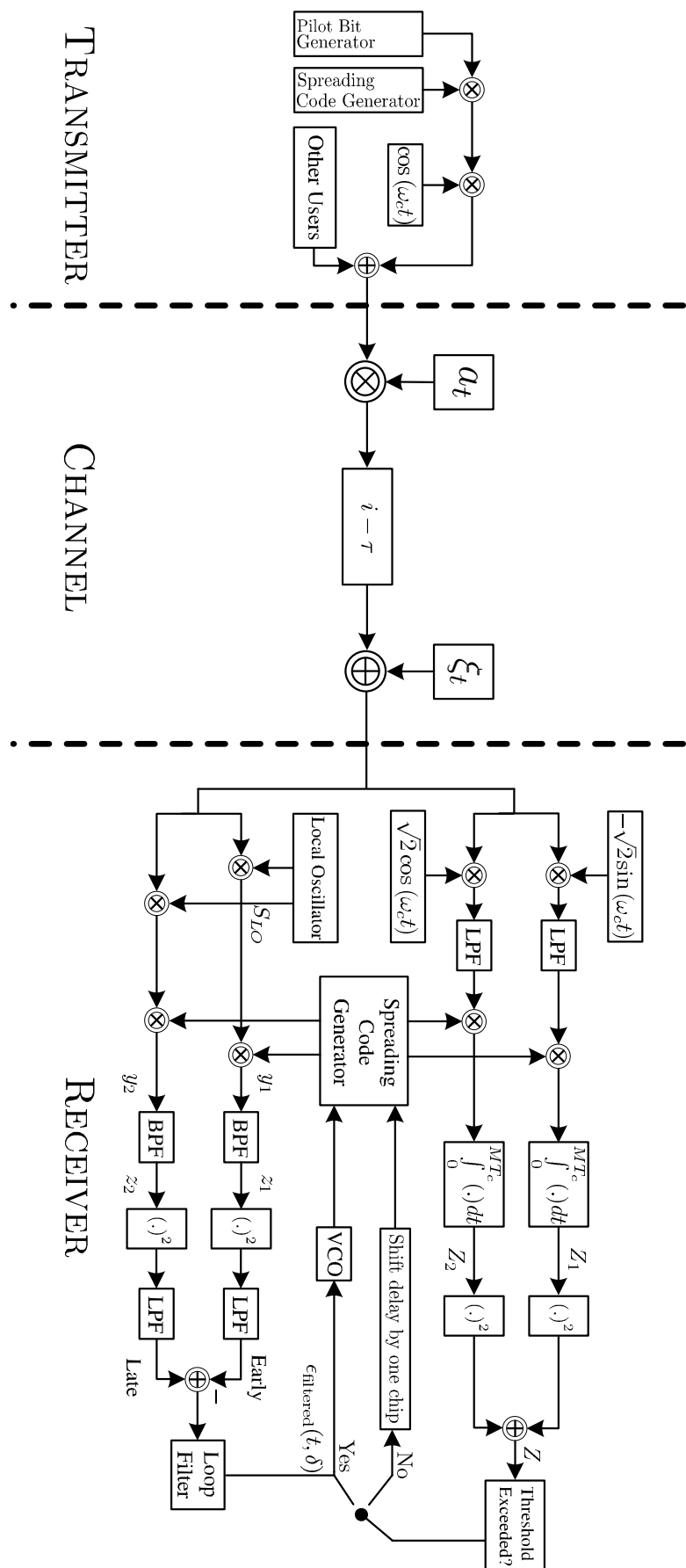


Figure 5.1: Synchronisation system model in the presence of fading.

### 5.3 Sequence Acquisition in Presence of Fading

This section is concerned with the first stage of the spreading sequence synchronisation known as acquisition stage in presence of noise and slow frequency flat Rayleigh fading. The noise only case is presented in [93] and some analysis with a Pseudo Random Binary Sequence (PRBS) pilot is included in [94]. In this section the acquisition stage is analysed in the presence of fading, the governing equations are then derived and the theoretical results are compared with the simulation results.

The acquisition stage is shown on the top part of Fig. 5.1. The mathematical model adopted is for bandpass since this is the standard method of analysing such techniques [97, 107, 168].

From Fig. 5.1 it can be seen that the received signal may be expressed as

$$r_{rec} = a_t \left( \sum_{g=0}^N \gamma_i^g x_i^g \right) \sqrt{2} A \cos(\omega_c t + \varphi) + \xi_t(t), \quad (5.1)$$

where  $N$  is the number of users using the channel at the same time,  $\gamma_i$  is the user data,  $x_i$  is the chaotic spreading code,  $A$  is the pilot amplitude,  $\omega_c$  is the angular frequency of the carrier,  $\varphi$  is the carrier phase shift between the transmitter and receiver,  $\xi_t(t)$  is the noise component and  $a_t$  is the fading coefficient that characterises fading influence of the channel on the received signal.  $a_t$  has a Rayleigh distribution given by (3.3).

After demodulation (multiplication with  $\cos(\omega_c t)$  and  $\sin(\omega_c t)$  and low pass filtering), the outputs of the in-phase branch of the demodulator can be expressed as

$$\begin{aligned} r_1 &= a_t \left( \sum_{g=0}^N \gamma_i^g x_i^g \right) A \cos(\varphi) + \xi_t^I(t) \\ &= a_t \gamma_i^0 x_i^0 A \cos(\varphi) + a_t \left( \sum_{g=1}^N \gamma_i^g x_i^g \right) A \cos(\varphi) + \xi_t^I(t), \end{aligned} \quad (5.2)$$

where  $x_i^0$  is the chaotic spreading code for the pilot which consists of a certain number of chips and is periodic and  $\gamma_i^0$  is the pilot data. The period of the pilot sequence is several times that of the spreading factor. The pilot period has a direct relationship to the range of delays that can be estimated by the system.  $\xi_t^I(t)$  is the in-phase component of noise after filtering.

Similarly

$$\begin{aligned} r_2 &= a_t \left( \sum_{g=0}^N \gamma_i^g x_i^g \right) A \sin(\varphi) + \xi_t^Q(t) \\ &= a_t \gamma_i^0 x_i^0 A \sin(\varphi) + a_t \left( \sum_{g=1}^N \gamma_i^g x_i^g \right) A \sin(\varphi) + \xi_t^Q(t), \end{aligned} \quad (5.3)$$

where  $\xi_t^Q(t)$  is the quadrature component of noise after filtering. Since the data pilot is always one, i.e.  $\gamma_i^0 = 1$ ,

$$r_1 = a_t x_i^0 A \cos(\varphi) + a_t \left( \sum_{g=1}^N \gamma_i^g x_i^g \right) A \cos(\varphi) + \xi_t^I(t). \quad (5.4)$$

This expression and its quadrature equivalent will be correlated by an  $m$ -bit reference sequence containing  $M$  chips. This sequence is the same as the transmitter pilot sequence, however, there is a time shift between the two. The time shift directly represents the delay between the transmitter and receiver and the role of the acquisition stage is to estimate this time delay. The time delay is expressed as  $\tau$ .

The correlation result is expressed as

$$\begin{aligned} Z_1 &= A \cos(\varphi) \int_{t=0}^{t=MmT_c} \sum_{j=1}^m a_j x_j(t - \tau) x_j(t) dt \\ &\quad + A \cos(\varphi) \int_{t=0}^{t=MmT_c} \sum_{j=1}^m \sum_{g=1}^N a_j (\gamma_i x_i^g)_j x_j(t - \tau) dt \\ &\quad + \int_{t=0}^{t=MmT_c} \xi_t^I(t) x(t - \tau) dt. \end{aligned} \quad (5.5)$$

The spreading sequence  $x_j(t)$  is defined as a sequence of  $M$  chaotic chips. This means that for each  $j$ ,  $x_j(t)$  is one bit long and the whole correlation period (to find the correct delay) consists of  $m$  bits. The time reference of  $x_j(t)$  is shown with  $t$  and the time delay between the respective transmitter and receiver sequences is shown as  $(t - \tau)$ , where transmitted sequences have a delay of  $\tau$  chips. The fading coefficients are assumed to change every bit period. Fig. 5.2 explains the correlation process.

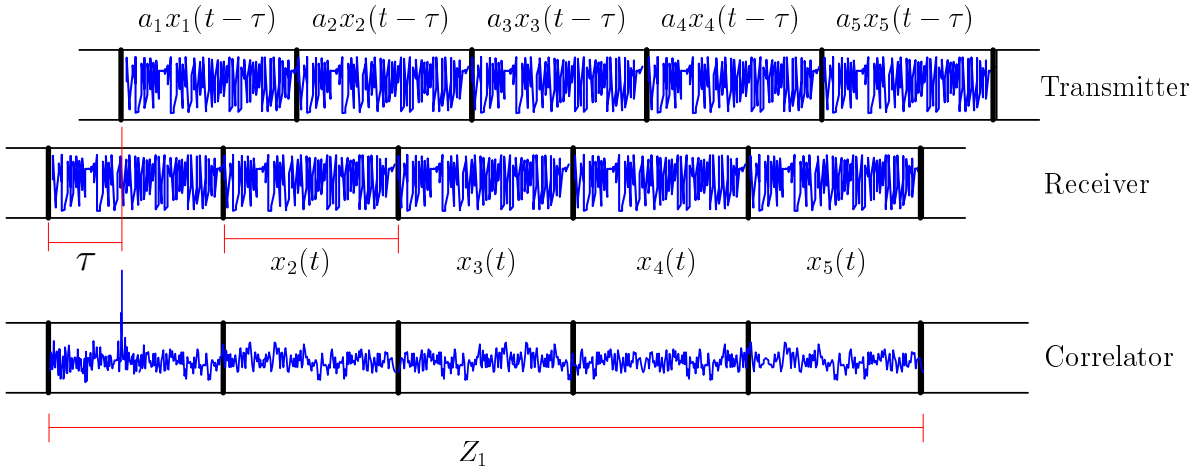


**Figure 5.2:** Correlation illustration.

The second and third lines of (5.5) are the interference and noise parts respectively and they constitute a random term which will be denoted with  $RT$  from now on.

As can be seen from above, the correlation period is divided into  $m$  equal sections each consisting of one bit.  $a_t$  has been replaced by  $a_j$  because  $a_t$  denotes a random variable with a Rayleigh distribution that varies with time and  $a_j$  is a single sample of that variable acting as a coefficient for one bit period of the transmitted pilot signal. The faded pilot signal is now used to calculate the correlation. Also  $x_j(t - \tau)$  and  $x_j(t)$  are the  $j$ -th bits of the correlation period.

In order to continue, a statistical characterisation of the correlator output ( $Z_1$ ) has to be performed. The same characterisation will apply for the output of the other branch ( $Z_2$ ). Once these two variables are statistically characterised in the presence of fading, the relevant performance measures for the acquisition scheme can be analytically expressed.

$Z_1$  can be formulated as

$$Z_1 = C \int_{t=0}^{t=mT=MmT_c} [a_1 x_1(t - \tau) x_1(t) + a_2 x_2(t - \tau) x_2(t) + \dots + a_m x_m(t - \tau) x_m(t)] dt + RT \quad (5.6)$$

where  $C$  is  $A \cos(\varphi)$ .

After expansion we have

$$\begin{aligned} Z_1 &= Ca_1 \int_0^{mT_c} x_1(t - \tau) x_1(t) dt + Ca_2 \int_{mT_c+1}^{2mT_c} x_2(t - \tau) x_2(t) dt + \dots \\ &\quad + Ca_m \int_{(M-1)mT_c+1}^{MmT_c} x_m(t - \tau) x_m(t) dt + RT \\ &= Ca_1 R_1(\tau) + Ca_2 R_2(\tau) + \dots + Ca_m R_m(\tau) + RT. \end{aligned} \quad (5.7)$$

For a large spreading factor  $R_1(\tau) = R_2(\tau) = \dots = R_m(\tau) = R(\tau)$ . These terms are correlations over one bit. One complete pilot correlation denoted by  $\mathbb{R}(\tau)$  which is the addition of  $m$  of the one bit correlations.

Based on the above,  $Z_1$  becomes

$$\begin{aligned} Z_1 &= CR(\tau) \{a_1 + a_2 + \dots + a_m\} + RT \\ &= CR(\tau) \sum_{j=1}^m a_j + RT, \end{aligned} \quad (5.8)$$

which is a sum of independent identically distributed (i.i.d) Rayleigh random variables multiplied by constants and added to a random term. The Rayleigh random variables are i.i.d because it is assumed that the duration of the fading is one bit interval long. This means that every bit is affected by different depth of fading (different  $a$  coefficient). Now that the statistical expression for  $Z_1$  is known, the mean and variance for it can be found. It should be noted that the synchronisation process is a statistical one and as a result  $a_j$ s are considered i.i.ds as the Rayleigh distribution used for each trial is independent from the previous one.

Mean of  $Z_1$  can be found as follows

$$\begin{aligned}
E[Z_1] &= E \left[ CR(\tau) \sum_{j=1}^m a_j + RT \right] \\
&= E \left[ CR(\tau) \sum_{j=1}^m a_j \right] + E[RT] \\
&= CR(\tau) E \left[ \sum_{j=1}^m a_j \right] \\
&= CR(\tau) m E[a_j] \\
&= CR(\tau) E[a_j] \\
&= CR(\tau) b \sqrt{\frac{\pi}{2}}, 
\end{aligned} \tag{5.9}$$

where  $\mathbb{R}(\tau)$  is the complete correlation function over a correlation period,  $b$  is the mode of the Rayleigh distribution, and  $C$  is a constant and  $E[RT]=0$ , because the interference is modeled as a zero mean Gaussian random process.

To find the variance of  $Z_1$  it is necessary to return to the original expression in (5.8). Invoking the central limit theorem (CLT) the addition of these random variables has a Gaussian distribution. Since  $E[a_j] = b\sqrt{\frac{\pi}{2}}$  and  $\sigma_{a_j}^2 = b^2(2 - \frac{\pi}{2})$  and if  $Y = \sum_{j=1}^m a_j$  we will have

$$E[Y] = mb\sqrt{\frac{\pi}{2}}, \tag{5.10}$$

$$\sigma_Y^2 = mb^2(2 - \frac{\pi}{2}). \tag{5.11}$$

Focusing on  $Z_1$  again

$$Z_1 = CR(\tau)Y + RT = Z_{11} + Z_{12} \tag{5.12}$$

in which  $CR(\tau)Y$  is denoted as  $Z_{11}$  and  $RT$  is denoted as  $Z_{12}$ .

Since  $Y$  is a Gaussian distributed random variable,  $Z_{11}$  is also a Gaussian distributed random variable. The  $Z_{11}$  term is also Gaussian by the virtue of the CLT because it is an addition of several independent identically distributed random variables. Therefore

$$\begin{aligned}
\sigma_{Z_{11}}^2 &= E[Z_{11}^2] - E^2[Z_{11}] \\
&= C^2 R^2(\tau) E[Y^2] - C^2 R^2(\tau) E^2[Y] \\
&= C^2 R^2(\tau) \{E[Y^2] - E^2[Y]\} \\
&= C^2 R^2(\tau) \sigma_Y^2 \\
&= C^2 R^2(\tau) mb^2 \left(2 - \frac{\pi}{2}\right).
\end{aligned} \tag{5.13}$$

Now the probability density function of  $Z_{11}$  can be expressed as

$$f_{Z_{11}}(z_{11}) = \frac{1}{\sqrt{2\pi\sigma_{Z_{11}}^2}} \exp\left(\frac{-(Z_{11} - C\mathbb{R}(\tau)b\sqrt{\frac{\pi}{2}})^2}{2\sigma_{Z_{11}}^2}\right). \quad (5.14)$$

For the  $Z_{12}$  term,  $E[Z_2] = 0$  and  $\sigma_{Z_{12}}^2 = \frac{N'_0 T}{2}$ , where  $\sigma_{Z_{12}}^2$  is the sum of the variance of noise ( $\frac{N_0}{2}$ ) and the variance introduced by IUI over time. Therefore  $Z_1$  can be written as

$$Z_1 \sim G\left(E[Z_{11}], \sigma_{Z_{11}}^2 + \sigma_{Z_{12}}^2\right). \quad (5.15)$$

Substituting for the mean and variances

$$Z_1 \sim G\left(C\mathbb{R}(\tau)b\sqrt{\frac{\pi}{2}}, C^2\frac{\mathbb{R}^2(\tau)}{m}b^2\left(2 - \frac{\pi}{2}\right) + \frac{N'_0 T}{2}\right), \quad (5.16)$$

where it is assumed that  $C^2\frac{\mathbb{R}^2(\tau)}{m}b^2\left(2 - \frac{\pi}{2}\right) + \frac{N'_0 T}{2} = \frac{N''_0 T}{2}$  from now on. That is,  $N''_0$  is the sum of the noise, IUI and fading variances all affecting the value of  $Z_1$ .

Because the amplitude of the pilot is  $A = \sqrt{\frac{2E_c}{T_c}}$  (where  $E_c$  is the energy per chip) and the number of chips in the interval  $T$  is  $M = \frac{T}{T_c}$ ,

$$\begin{aligned} Z_1 &\sim G\left(T\sqrt{\frac{2E_c}{T_c}}\cos(\varphi)\mathbb{R}(\tau)b\sqrt{\frac{\pi}{2}}, \frac{N''_0 T}{2}\right) \\ &\sim \sqrt{\frac{N''_0 T}{2}}G\left(2\sqrt{\frac{TE_c}{T_c N''_0}}\cos(\varphi)\mathbb{R}(\tau)b\sqrt{\frac{\pi}{2}}, 1\right) \\ &\sim \sqrt{\frac{N''_0 T}{2}}G\left(2\sqrt{\frac{ME_c}{N''_0}}\cos(\varphi)\mathbb{R}(\tau)b\sqrt{\frac{\pi}{2}}, 1\right); \end{aligned} \quad (5.17)$$

similarly

$$Z_2 \sim \sqrt{\frac{N''_0 T}{2}}G\left(2\sqrt{\frac{ME_c}{N''_0}}\sin(\varphi)\mathbb{R}(\tau)b\sqrt{\frac{\pi}{2}}, 1\right), \quad (5.18)$$

since  $M = \frac{T}{T_c}$ .

The decision variable that controls the synchronisation is  $Z = Z_1^2 + Z_2^2$ , which makes it  $\sigma^2 = \frac{N''_0 T}{2}$  times a non-central chi-squared random variable with two degrees of freedom. The non-centrality parameter is

$$\begin{aligned} \lambda &= \left[2\sqrt{\frac{ME_c}{N''_0}}\cos(\varphi)\mathbb{R}(\tau)b\sqrt{\frac{\pi}{2}}\right]^2 + \left[2\sqrt{\frac{ME_c}{N''_0}}\sin(\varphi)\mathbb{R}(\tau)b\sqrt{\frac{\pi}{2}}\right]^2 \\ &= \frac{2ME_c}{N''_0}\mathbb{R}^2(\tau)b^2\pi. \end{aligned} \quad (5.19)$$

Therefore the PDF of  $Z$  is

$$p_Z(z) = \left\{ \frac{1}{2\sigma^2} \exp\left(-\frac{1}{2}(\lambda + z/\sigma^2)\right) I_0\left(\sqrt{\frac{\lambda z}{\sigma^2}}\right), z > 0 \right\}, \quad (5.20)$$

which is a Rice distribution.

Now that the  $Z$  parameter is found, it can be used to decide if the synchronisation procedure was successful or not. Assuming that the decision is based on two hypothesis tests namely

$$\begin{aligned} H_0 & : |\tau| > T_c \Rightarrow \mathbb{R}(\tau) \approx 0, N_0'' > N_0 \\ H_1 & : |\tau| \leq T_c \Rightarrow \mathbb{R}(\tau) > 0, N_0'' \approx N_0. \end{aligned} \quad (5.21)$$

The two PDFs based on these hypotheses are

$$p_Z(z|H_0) = \frac{1}{2\sigma^2} \exp\left(-\frac{1}{2}(z/\sigma^2)\right), \quad (5.22)$$

$$p_Z(z|H_1) = \frac{1}{2\sigma^2} \exp\left(-\frac{1}{2}(\lambda + z/\sigma^2)\right) I_0\left(\sqrt{\frac{\lambda z}{\sigma^2}}\right). \quad (5.23)$$

It is clear that the non-centrality parameter is zero for the first hypothesis and different from zero in the second. The single attempt ( $k = 1$ ) false alarm probability is

$$\begin{aligned} P_F(k=1) & = p(Z > z_T|H_0) = \int_{z_T}^{\infty} \frac{1}{2\sigma^2} \exp\left(-\frac{1}{2}(z/\sigma^2)\right) dz \\ & = \exp\left(-\frac{1}{2}(z_T/\sigma^2)\right), \end{aligned} \quad (5.24)$$

hence the threshold value can be found as

$$z_T = -2\sigma^2 \ln P_F(k=1) = -N_0'' T \ln P_F(k=1); \quad (5.25)$$

now the single run detection probability can be found as

$$P_D(k=1) = P_D(Z > z_T|H_1) = \int_{z_T}^{\infty} \frac{1}{2\sigma^2} \exp\left(-\frac{1}{2}(\lambda + z/\sigma^2)\right) I_0\left(\sqrt{\frac{\lambda z}{\sigma^2}}\right) dz. \quad (5.26)$$

Using the change of variable  $z = x^2\sigma^2$ , the expression changes to

$$P_D(k=1) = \int_{\sqrt{z_T/\sigma^2}}^{\infty} x \exp\left(-\frac{1}{2}(\lambda + x^2)\right) I_0\left(\sqrt{\lambda}x\right) dx, \quad (5.27)$$

which is the Marcum's Q-function, so

$$P_D(k=1) = Q_M\left(\sqrt{\lambda}, \sqrt{z_T/\sigma^2}\right). \quad (5.28)$$

If the  $H_1$  hypothesis is valid then  $\mathbb{R}(\tau) > 0$ ,  $N_0'' \approx N_0$  and  $\sigma^2 = \frac{N_0 T}{2}$ ,

$$\lambda = \frac{2M E_c}{N_0} \mathbb{R}^2(\tau) b^2 \pi. \quad (5.29)$$

Inserting expressions from (5.25) and (5.29) into (5.28) results in

$$\begin{aligned} P_D(k=1) &= Q_M \left( b \mathbb{R}(\tau) \sqrt{\frac{2M\pi E_c}{N_0}}, \sqrt{-\frac{N_0'' T \ln p_F(k=1)}{N_0 T/2}} \right) \\ &= Q_M \left( b \mathbb{R}(\tau) \sqrt{\frac{2M\pi E_c}{N_0}}, \sqrt{-\frac{2N_0'' \ln p_F(k=1)}{N_0}} \right). \end{aligned} \quad (5.30)$$

The upper-bound in (5.30) is defined when the system is in synchronisation i.e. when  $\mathbb{R}(\tau) \simeq 1$ ,  $N_0'' \simeq N_0$ , so based on [94] the expression changes to

$$\begin{aligned} P_D(m=1) &\leq Q_M \left( b \sqrt{\frac{2M\pi E_c}{N_0}}, \sqrt{-2 \ln p_F(k=1)} \right) \\ &\simeq Q \left( \sqrt{-2 \ln p_F(k=1)} - b \sqrt{\frac{2M\pi E_c}{N_0}} \right). \end{aligned} \quad (5.31)$$

In the expression above,  $Q(\cdot)$  is a Gaussian Q-function that approximates the Marcum's Q function.

Comparing (5.31) with the expression for the upper bound of  $P_D$  in [93], the effect of fading in the theoretical expression can be observed. That is, the theoretical expression has a new variable which is the mode of the Rayleigh random variable used to model the multi-path fading effect. The power of the fades has a direct influence on the Receiver Operating Characteristics (ROC), which is a plot of  $P_D$  vs.  $P_F$  and is the main tool for observing the quality of acquisition.

The results presented in this section compare the simulated ROC of the acquisition stage in the presence of fading with the theoretical prediction of (5.30). This is performed for various number of users and SNR, using a correlator period of 200 ( $M = 100$ ) and a pilot period of 1000 ( $mM = 1000$ ) chips at the average fading power of 1 as explained in (3.3). As can be seen from Figs. 5.3-5.6, the simulated ROC in the presence of fading shows a close agreement with the analytical upper-bound predictions of (5.31). Also, as expected, the increase in number of users and noise in the channel decreases the  $P_D$  for a fixed  $P_F$ . However, as can be seen in Fig. 5.3 the effect of IUI is more pronounced when only noise is present [94]. When fading is present the effect of IUI is reduced and the ROC curves for different numbers of users come close to each other. This is attributed to the multiplicative effect of fading on the pilot sequence. It is assumed that the power of the pilot is the same as the power of each user. That is, the pilot can be considered an extra users as far as the power is concerned.

Next, the ROC when only noise and IUI are present in the channel are shown and compared with the ROC in the presence of fading. As can be seen from Fig. 5.7, the system performance generally degrades in the presence of deep fades which is expected. The reason is attributed to the multiplicative fading coefficients affecting the auto-correlation peak of the transmitted pilot with its locally generated replica.

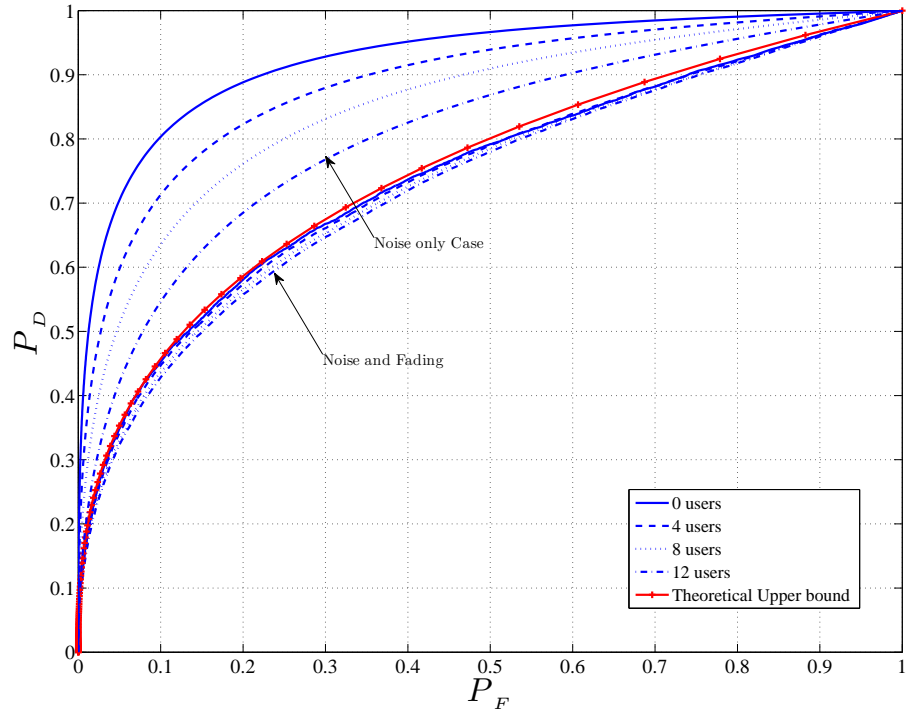


**Figure 5.3:** ROC in presence of noise (SNR = 0 dB), for 0 to 12 users and fading ( $E[a^2] = 1$ ), pilot length is ten times the spreading factor. The noise only results are shown here for comparison.

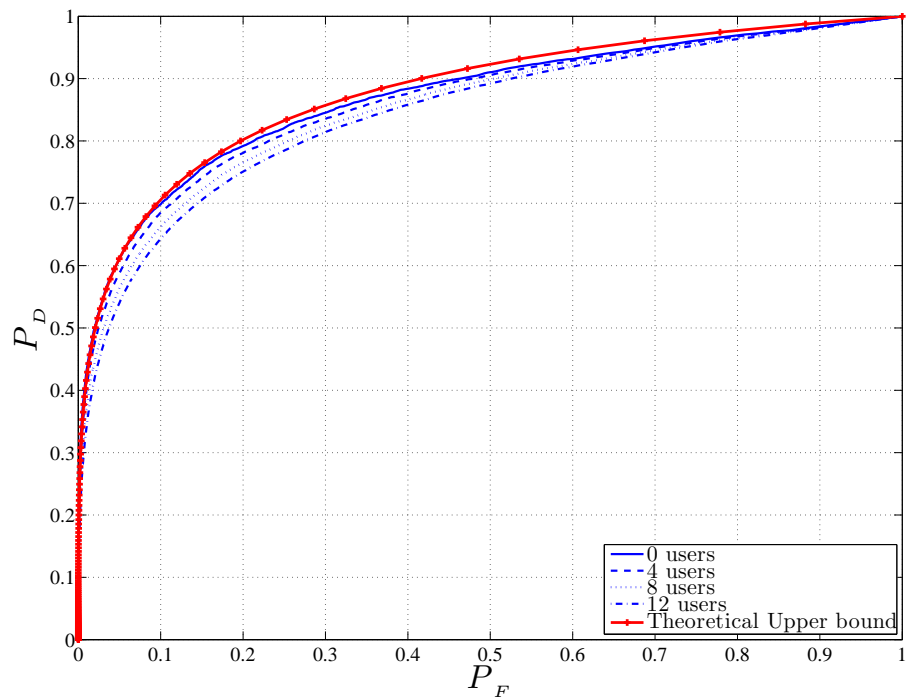


**Figure 5.4:** ROC in presence of noise (SNR = 4 dB), for 0 to 12 users and fading ( $E[a^2] = 1$ ), pilot length is ten times the spreading factor.

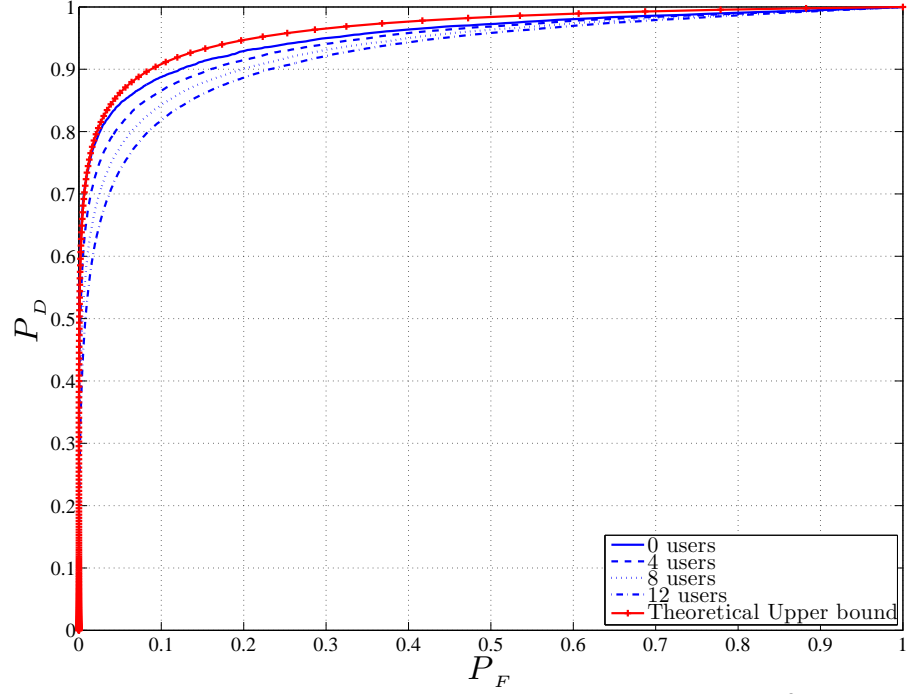


**Figure 5.5:** ROC in presence of noise (SNR = 8 dB), for 0 to 12 users and fading ( $E[a^2] = 1$ ), pilot length is ten times the spreading factor.

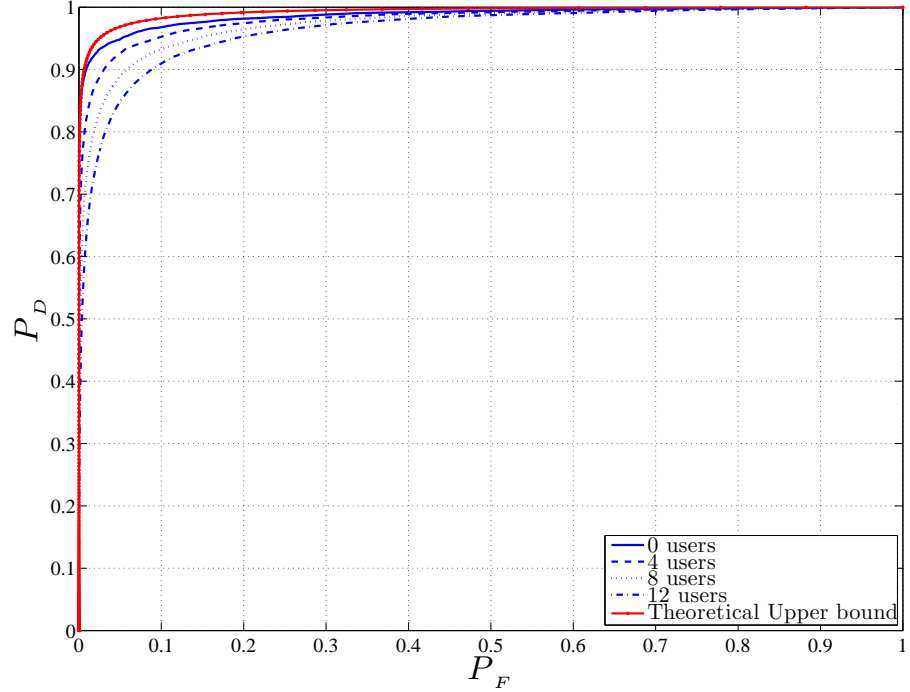


**Figure 5.6:** ROC in presence of noise (SNR = 12 dB), for 0 to 12 users and fading ( $E[a^2] = 1$ ), pilot length is ten times the spreading factor.

It is interesting to observe the effects of increasing the correlation period ( $M$  in the theoretical analysis) on the ROC in the presence of fading. In [94] it is shown that the performance of the acquisition stage improves under noise only conditions when the correlation period increases. As shown in Fig. 5.7 this is also the case when slow flat fading is present in the channel. Increasing the correlation period of the pilot signal improves the ROC only to some extent under fading conditions. There is always some residual

decrease in  $P_D$  with a fixed  $P_F$  value which cannot be overcome with increasing the correlation period. Moreover, increasing the correlation period will increase the acquisition time as the correlator has to perform more computations for each correlation value. An approach that can be used to mitigate the fading effects is the use of interleavers and de-interleavers in the transmitter and receiver respectively. Using interleaving techniques, the deep fades will be spread across several bit mitigating their effect. An investigation in using interleavers for sequence acquisition is presented in §6.

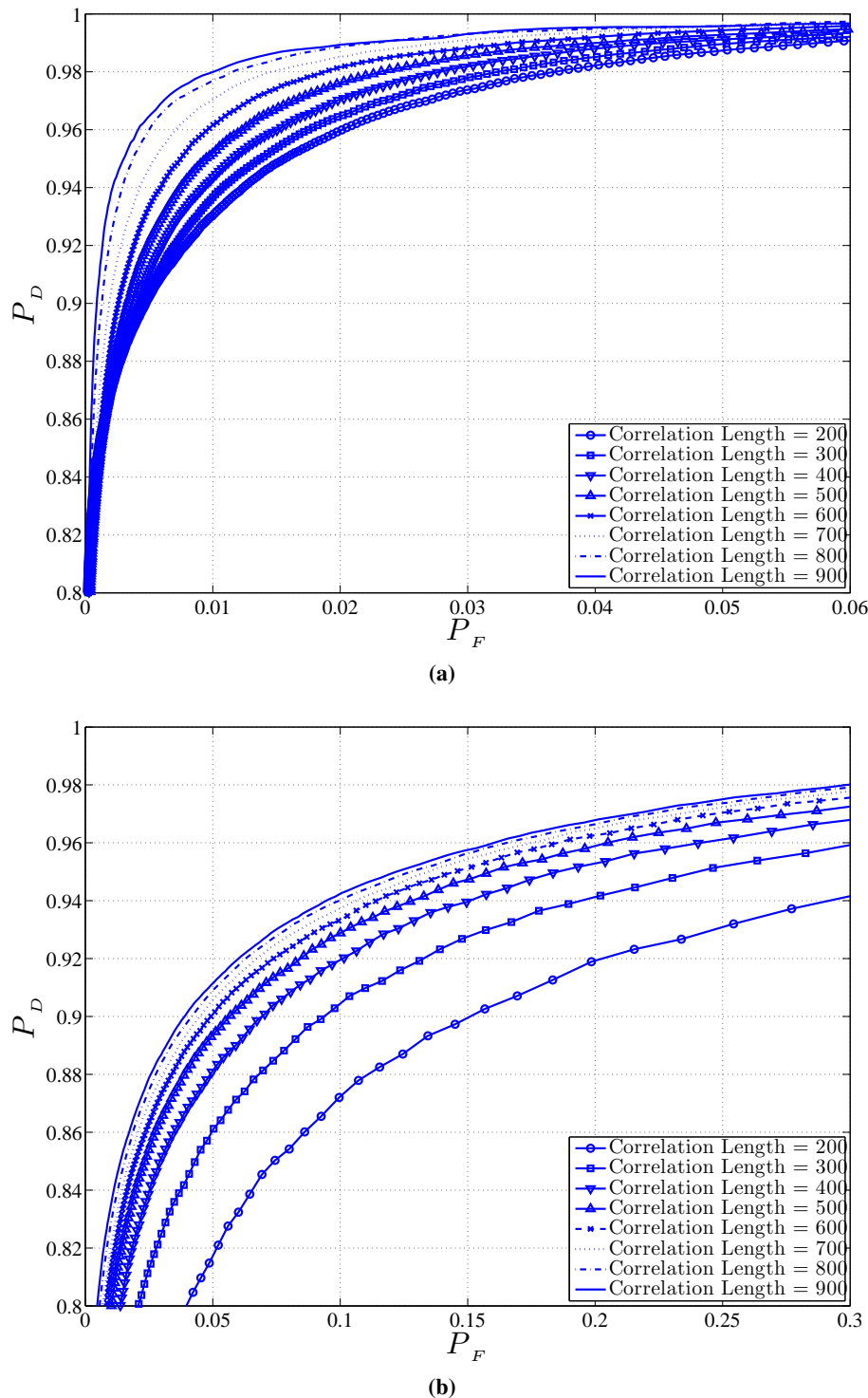


**Figure 5.7:** ROC with different correlation periods, 0 users and SNR of 8 dB (a) noise (b) noise and fading.

## 5.4 Sequence Tracking in Presence of Fading

This section is concerned with the second stage of the spreading sequence synchronisation, known as tracking stage, in presence of noise and slow frequency flat Rayleigh fading. The noise only case is presented in [167] and some analysis with a PRBS pilot is included in [94]. The pass-band loop proposed here uses the chaotic pilot sequence and has a completely different structure compared to the base-band coherent loop proposed previously in [94]. The discriminator contains two energy detectors which are neither sensitive to carrier data modulation nor carrier phase. The chaotic delay lock loop proposed in this section can be used with BPSK. The expansion of this loop to any other modulation scheme is straightforward because the analysis is done with arbitrary data and phase modulation of the carrier.

After deriving the governing equations, error curves for a filtered case as well as tracking performance plots are presented. The tracking stage is shown on the lower part of Fig. 5.1. The mathematical model adopted is for bandpass since this is the standard method of analysing such techniques [97, 107, 168].

As can be seen from Fig. 5.1 the received signal is a carrier which is modulated by data and the delayed spreading code

$$r(t) = a_t \sqrt{2} A x_t^0 (t - T_d) \cos(\omega_c t + \gamma_d(t - T_d) + \phi) + n(t) \quad (5.32)$$

where  $A$  is the amplitude of the received signal,  $x_t^0(t - T_d)$  is the delayed pilot chaotic signal in which the delay indicator  $\tau$  has been replaced with  $T_d$  to show that the acquisition stage is now finished and the delays are within the chip duration  $T_c$ ,  $\omega_c$  is the carrier angular frequency,  $\gamma_d(t - T_d)$  is a delayed arbitrary data phase modulation,  $\phi$  is the received carrier phase assumed to be random,  $n(t)$  is the received noise that is being represented by a band-limited zero mean-AWGN process which can be expressed as

$$n(t) = \sqrt{2} n_I(t) \cos(\omega_c t) - \sqrt{2} n_Q(t) \sin(\omega_c t), \quad (5.33)$$

which has a two sided power spectral density of  $\frac{N_0}{2}$  W/Hz. This means that  $n_I(t)$  and  $n_Q(t)$  are independent zero mean low pass AWGN processes.

The multi-path fading effect is expressed by  $a_t$  which is the fading coefficient that characterizes fading influence of the channel on the received signal. Fading coefficient  $a_t$  has a Rayleigh distribution given by (3.3). Since the synchronisation is partially achieved, the correlation function is near its peak. This means that the  $H_1$  hypothesis in (5.21) is in place which corresponds to a small influence from the IUI component. As a result, the IUI for tracking is not considered, since the system is in synchronisation and the effect of the IUI is negligible in this situation.

As can be seen from Fig. 5.1, the received signal is correlated with the early and late branches of the tracking loop after power division. The output of the reference local oscillator is

$$S_{LO}(t) = \sqrt{2K_1} \cos\left(\omega_c t - \omega_{IF} t + \phi'\right), \quad (5.34)$$

where  $K_1$  is a gain term,  $\omega_{IF}$  is the intermediate frequency and  $\phi'$  is the random phase of the local oscillator. The purpose of the IF bandpass filters shown in Fig. 5.1 is to filter out all the sum frequency components that resulted from the mixing of the power divided received signal with the locally generated local oscillator.

ated spread carrier signal. Therefore, these filters are assumed to have a central frequency of  $\omega_{IF}$  and a one sided noise band-width of  $B_N$  Hertz.

The two outputs of the local carrier spreading are

$$L_1(t) = 2\sqrt{K_1}x_t^0 \left( t - \hat{T}_d + \frac{\Delta}{2}T_c \right) \cos \left( \omega_c t - \omega_{IF}t + \phi' \right) \quad (5.35)$$

$$L_2(t) = 2\sqrt{K_1}x_t^0 \left( t - \hat{T}_d - \frac{\Delta}{2}T_c \right) \cos \left( \omega_c t - \omega_{IF}t + \phi' \right), \quad (5.36)$$

where  $\Delta$  is the time difference between the early and late gates normalised to the chip duration  $T_c$  and  $\hat{T}_d$  is the estimated time delay [97, 107]. Therefore bandpass filter input will be,

$$y_1(t) = L_1(t) \left\{ a_t \sqrt{2} \frac{A}{2} x_t^0 (t - T_d) \cos(\omega_c t + \gamma_d (t - T_d) + \phi) + n(t) \right\} \quad (5.37)$$

$$y_2(t) = L_2(t) \left\{ a_t \sqrt{2} \frac{A}{2} x_t^0 (t - T_d) \cos(\omega_c t + \gamma_d (t - T_d) + \phi) + n(t) \right\}. \quad (5.38)$$

After bandpass filtering and losing all the sum frequencies the output can be written as [107],

$$\begin{aligned} z_1(t) &= \sqrt{K_1} A a_t x_t^0 (t - T_d) x_t^0 \left( t - \hat{T}_d + \frac{\Delta}{2}T_c \right) \cos \left( \omega_{IF}t + \phi - \phi' + \gamma_d (t - T_d) \right) \\ &\quad + \sqrt{K_1} n_I(t) x_t^0 \left( t - \hat{T}_d + \frac{\Delta}{2}T_c \right) \cos \left( \omega_{IF}t - \phi' \right) \\ &\quad - \sqrt{K_1} n_Q(t) x_t^0 \left( t - \hat{T}_d + \frac{\Delta}{2}T_c \right) \sin \left( \omega_{IF}t - \phi' \right), \end{aligned} \quad (5.39)$$

and

$$\begin{aligned} z_2(t) &= \sqrt{K_1} A a_t x_t^0 (t - T_d) x_t^0 \left( t - \hat{T}_d - \frac{\Delta}{2}T_c \right) \cos \left( \omega_{IF}t + \phi - \phi' + \gamma_d (t - T_d) \right) \\ &\quad + \sqrt{K_1} n_I(t) x_t^0 \left( t - \hat{T}_d - \frac{\Delta}{2}T_c \right) \cos \left( \omega_{IF}t - \phi' \right) \\ &\quad - \sqrt{K_1} n_Q(t) x_t^0 \left( t - \hat{T}_d - \frac{\Delta}{2}T_c \right) \sin \left( \omega_{IF}t - \phi' \right). \end{aligned} \quad (5.40)$$

$z_{1,2}(t)$  are the sum of three distinct components. Taking  $z_1(t)$  as the example

$$z_1(t) = z_{1DC}(t) + z_{1AC}(t) + z_{1noise}(t). \quad (5.41)$$

The DC component is the desired signal which is the correlation of the two chaotic signals scaled by the power, gain and the random IF cosine function. The AC component is the signal self-noise which arises from the correlation properties of the spreading sequence. This term can be ignored provided the the chip rate is higher than the bit rate by at least two orders of magnitude and the bandpass filters are correctly adjusted. It is important to note that both  $z_{1DC}(t)$  and  $z_{1AC}(t)$  exist in the first line of equation (5.39), the next two line are the signal  $\times$  noise terms. Thus considering the signal and noise separately,

the signal components (ignoring the self-noise term) become

$$p_1(t) \simeq \sqrt{K_1} A a_t \mathbb{R} \left[ \left( \delta + \frac{\Delta}{2} \right) T_c \right] \cos \left( \omega_{IF} t + \phi - \phi' + \gamma_d(t - T_d) \right) \quad (5.42)$$

$$p_2(t) \simeq \sqrt{K_1} A a_t \mathbb{R} \left[ \left( \delta - \frac{\Delta}{2} \right) T_c \right] \cos \left( \omega_{IF} t + \phi - \phi' + \gamma_d(t - T_d) \right), \quad (5.43)$$

where  $\mathbb{R}[\cdot]$  is the auto-correlation of the chaotic sequences.

Both  $x_1(t)$  and  $x_2(t)$  are filtered with a band pass filter

The noise component can be explicitly defined to be

$$n_1(t) = \sqrt{\frac{K_1}{2}} x_t^0 \left( t - \hat{T}_d + \frac{\Delta}{2} T_c \right) n'(t) \quad (5.44)$$

$$n_2(t) = \sqrt{\frac{K_1}{2}} x_t^0 \left( t - \hat{T}_d - \frac{\Delta}{2} T_c \right) n'(t) \quad (5.45)$$

where

$$n'(t) = \sqrt{2} n_I(t) \cos(\omega_{IF} t - \phi') - \sqrt{2} n_Q(t) \sin(\omega_{IF} t - \phi'). \quad (5.46)$$

These noise processes are the products of a band limited WGN process centered at  $\omega_{IF}$  and the spreading code  $\sqrt{K_1/2} x_t^0 \left( t - \hat{T}_d \pm \frac{\Delta}{2} T_c \right)$ .

Ignoring the self-noise term and using the definition of the in-phase and quadrature noise components, the delay lock discriminator output can be expressed as the difference between the squared and low pass filtered output of the early and late branches. Therefore we have

$$\epsilon(t, \delta) = [p_2(t) + n_2(t)]_{LP}^2 - [p_1(t) + n_1(t)]_{LP}^2 \quad (5.47)$$

where  $p_{1,2}(t)$  are the approximations from equations (5.42) and (5.43) and  $\delta$  is the normalised time difference between the incoming time offset ( $T_d$ ) and the estimated timing offset ( $\hat{T}_d$ ), that is  $\delta = \frac{T_d - \hat{T}_d}{T_c}$

This is a summation of partial correlations of the pilot signal throughout the tracking period scaled by different fading coefficients. So in each complete correlation, fading coefficients with a Rayleigh distribution exist.

Since the spreading factor is high, the partial correlations can be assumed to be equal to each other. For simplicity we assume

$$R_1 \left[ \left( \delta + \frac{\Delta}{2} \right) T_c \right] = R_2 \left[ \left( \delta + \frac{\Delta}{2} \right) T_c \right] = \dots = R_m \left[ \left( \delta + \frac{\Delta}{2} \right) T_c \right] = R \left[ \left( \delta + \frac{\Delta}{2} \right) T_c \right]. \quad (5.48)$$

So the expression for  $p_1(t)$  can be simplified to

$$p_1(t) = \sum_{j=1}^m a_j A \sqrt{K_1} R \left[ \left( \delta + \frac{\Delta}{2} \right) T_c \right] \left( \cos(\omega_{IF} t + \phi - \phi' + \gamma_d(t - T_d)) \right). \quad (5.49)$$

The input to the loop filter is the squared and low pass filtered output of the two BPFs in the early and late branches. Therefore the error signal is [97, 107]:

$$\epsilon(t, \delta) = [z_2(t)]_{LP}^2 - [z_1(t)]_{LP}^2, \quad (5.50)$$

where  $z_2(t) = p_2(t) + n_2(t)$  and  $z_1(t) = p_1(t) + n_1(t)$ .

After expansion and elimination of all double frequency terms

$$\begin{aligned} \epsilon(t, \delta) = & \frac{1}{2} K_1 A^2 \left( \sum_{j=1}^m a_j \right)^2 \left\{ R^2 \left[ \left( \delta - \frac{\Delta}{2} \right) T_c \right] - R^2 \left[ \left( \delta + \frac{\Delta}{2} \right) T_c \right] \right\} \\ & + \sqrt{2K_1} A \left( \sum_{j=1}^m a_j \right) \left\{ R \left[ \left( \delta - \frac{\Delta}{2} \right) T_c \right] n_{2I}(t) \right. \\ & \left. - R \left[ \left( \delta + \frac{\Delta}{2} \right) T_c \right] n_{1I}(t) \right\} \times \cos(\phi - \phi' + \gamma_d(t - T_d)) \\ & + \sqrt{2K_1} A \left( \sum_{j=1}^m a_j \right) \left\{ R \left[ \left( \delta - \frac{\Delta}{2} \right) T_c \right] n_{2Q}(t) \right. \\ & \left. - R \left[ \left( \delta + \frac{\Delta}{2} \right) T_c \right] n_{1Q}(t) \right\} \times \sin(\phi - \phi' + \gamma_d(t - T_d)) \\ & + \{n_{2I}(t)\}^2 + \{n_{2Q}(t)\}^2 - \{n_{1I}(t)\}^2 - \{n_{1Q}(t)\}^2. \end{aligned} \quad (5.51)$$

The expression above shows the effect of fading on the tracking loop phase discriminator output. If the fading effect is ignored ( $a_j = 1$  for all  $j$ ) then the formula will reduce to the expression given in the literature for the non-coherent tracking loop [97, 107].

As can be seen from the expression above, the first line is a DC value which is the desired error function. The rest of the values are low pass filtered signal  $\times$  noise and noise  $\times$  noise terms. This  $\epsilon(t, \delta)$  will then go through the tracking loop filter which ideally has a band-width suitably adjusted to reject nearly all the noise and phase modulated sinusoidal terms. The input to the voltage controlled oscillator (VCO) is  $\frac{1}{2} K_1 A^2 \left( \sum_{j=1}^m a_j \right)^2 D_\Delta(\delta)$  where  $D_\Delta(\delta)$  is the difference of the squared values of partial correlation, which is ideally a DC term that is  $D_\Delta(\delta) = R^2 \left[ (\delta - \frac{\Delta}{2}) T_c \right] - R^2 \left[ (\delta + \frac{\Delta}{2}) T_c \right]$  [97, 107].

If normalised  $D_\Delta(\delta)$  is plotted, the resulting curve is known as the tracking loop S-curve<sup>1</sup> which is shown in Fig. 5.8 and indicated as *Error Signal*. Fig. 5.8 also shows the squared early, late and on time correlation results as well as the calculated salient points for chaotic signals. These salient points have never been presented in literature for chaotic signals before. As can be seen in Fig. 5.8, the peak of the correlation function is  $2A^2 \bar{P}(M)^2$ , where  $\bar{P}$  is the average power of chaotic sequences which is 0.5 for the Logistic map.

The tracking of signal timing is performed by adjusting the speed of the VCO by the amount indicated in the linear region of the S-curve; that is, the most important part of the S-curve is the zero crossing of the

<sup>1</sup>In this thesis, tracking loop S-curve and tracking loop error curve are used interchangably and have the same meaning.

Error Signal. In the next section, an attempt is made to statistically model the effect of noise and fading, in the placement of this zero crossing.

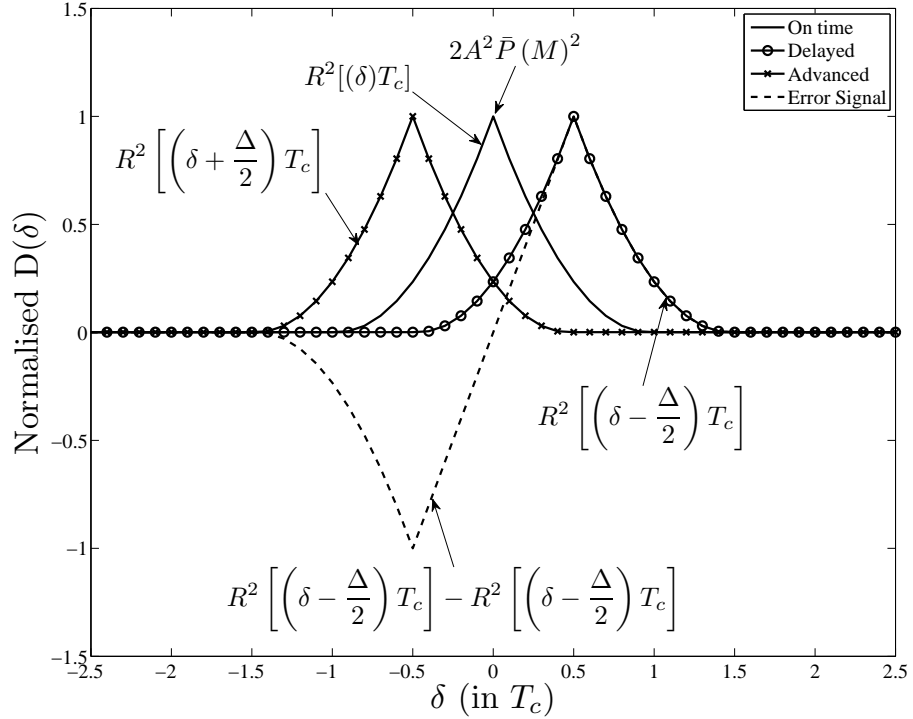


**Figure 5.8:** Tracking loop output for a chaotic pilot when  $\Delta = 1$ .

As can be seen from the derivation above, the useful tracking signal (input to the VCO) can be extracted from the non-coherent chaotic delay lock loop [97, 107]. This means that chaotic signals can indeed be tracked non-coherently. This allows for the replacement of the model presented in [94] which assumes the tracking spreading code to be PRBS with a chaotic spreading code for the tracking stage. The system considered here uses only one spreading code for both acquisition and tracking, minimises complexity by eliminating the PRBS code generation which is used in [94, 95], and increases security of signal transmission.

Before the phase discriminator output can be used for the VCO, it has to go through the loop filter. The reason is that only the DC part of the signal can be used for tracking the incoming sequence. Therefore in most tracking loops, the loop filter is an averaging integrator which effectively extracts the DC component from (5.51).

Assuming the filtering effectively removes the sinusoidal components from (5.51), the input to the VCO is [97, 107]:

$$\begin{aligned} \epsilon_{\text{filtered}}(t, \delta) &= \frac{1}{2} K_1 A^2 \left( \sum_{j=1}^m a_j \right)^2 \left\{ R^2 \left[ \left( \delta - \frac{\Delta}{2} \right) T_c \right] - R^2 \left[ \left( \delta + \frac{\Delta}{2} \right) T_c \right] \right\} \\ &\quad + \{n_{2I}(t)\}^2 + \{n_{2Q}(t)\}^2 - \{n_{1I}(t)\}^2 - \{n_{1Q}(t)\}^2. \end{aligned} \quad (5.52)$$

The expression presented in (5.52) consists of different random variables. To gain suitable understanding of the tracking loop behaviour (5.52), which is the input to the VCO, has to be statistically examined.

Each  $a_j$  is a random variable with a Rayleigh distribution. The noise components ( $n_{1I}(t)$ ,  $n_{1Q}(t)$ ,  $n_{2I}(t)$ ,  $n_{2Q}(t)$ ), are all zero mean random variables with a Gaussian distribution.

The effect of these random variables is examined individually and then the overall effect on the tracking loop is evaluated. Noting that in the operation of the tracking loop,  $\sum_{j=1}^m a_j$  is essentially the summation of independent, identically distributed random variables with a Rayleigh distribution since each of the constituents of the summation takes a different random value on every tracking loop trial. Therefore:

$$\mu = E \left[ \sum_{j=1}^m a_j \right] = mE [a_j] = mb\sqrt{\frac{\pi}{2}}, \quad (5.53)$$

and

$$\sigma^2 = var \left[ \sum_{j=1}^m a_j \right] = m^2 \sigma_{a_j}^2 = m^2 b^2 \left( 2 - \frac{\pi}{2} \right). \quad (5.54)$$

Using the CLT,  $\sum_{j=1}^m a_j$  is assumed to be a Gaussian distributed random variable with the mean and variance given in the equations above.

As (5.51) shows, the desired DC part of the discriminator output is influenced to some degree by the square of the summation of fading coefficients as well as the noise. In order to accurately model the discriminator output statistically, having acquired the distribution of  $(\sum_{j=1}^m a_j)$  it is essential to find out the distribution of  $(\sum_{j=1}^m a_j)^2$ .

It is shown in the above that the distribution of  $(\sum_{j=1}^m a_j)$  can be written as:

$$f_G(g) = \frac{1}{\sqrt{2\pi\sigma^2}} \exp \left( -\frac{(g - \mu)^2}{2\sigma^2} \right), \quad (5.55)$$

where  $\mu$  and  $\sigma^2$  are shown in (5.53) and (5.54) respectively.

If a random variable  $G$  has a Gaussian distribution, denoted by,  $f_G(g)$  then the distribution of random variable  $H$  where  $H = G^2$  is given by a non-central chi-square distribution with one degree of freedom and with a non-centrality parameter of  $\lambda = \frac{\pi}{4-\pi}$ .

The same theory is applied for the Gaussian noise components that are squared in the phase discriminator output expression given above. However, those are chi-square distributions because the noise has a zero mean. They all have one degree of freedom.

The analysis above shows that in presence of noise and fading, the DC value used for tracking is an addition of five chi-square distributions. Using the CLT again, it is hypothesised that  $\epsilon_{\text{filtered}}(0, 0)$  (input to the VCO), will fluctuate around its mean with a Gaussian distribution.

To confirm this the system is simulated and the distribution of  $\epsilon_{\text{filtered}}(0, 0)$  around the mean is observed.

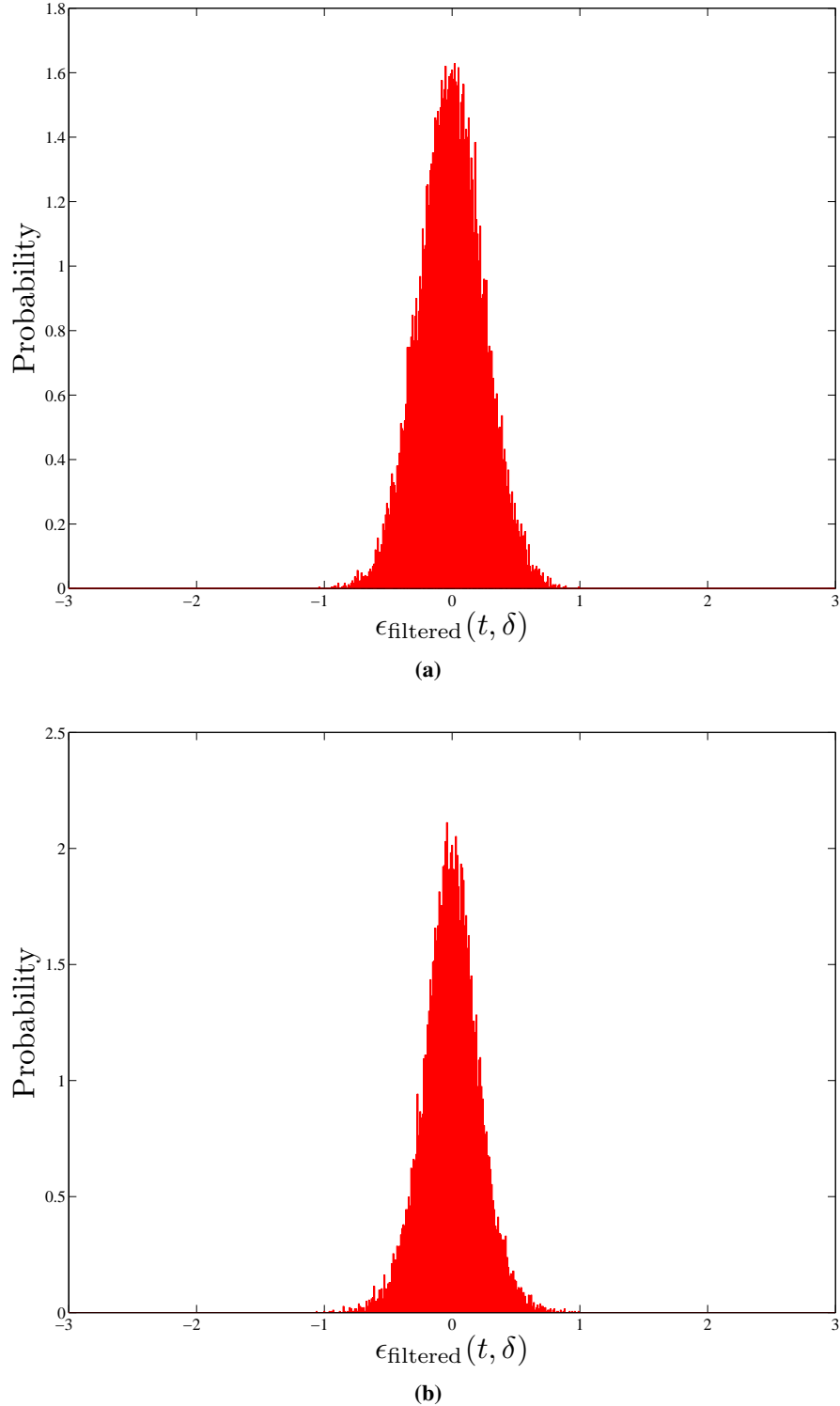


**Figure 5.9:** The PDF of  $\epsilon_{\text{filtered}}(t, \delta)$  at  $t = 0$  and  $\delta = 0$  (a) in presence of noise only and (b) in presence of noise and fading (SNR = 6 dB both cases).

As can be seen from Fig 5.9 (a) and (b), the presence of Rayleigh fading does not affect the PDF of  $\epsilon_{\text{filtered}}(0, 0)$ . This is because of the very small value of  $R^2 \left[ \left( \delta - \frac{\Delta}{2} \right) T_c \right] - R^2 \left[ \left( \delta + \frac{\Delta}{2} \right) T_c \right]$  when  $\delta = 0$  which effectively removes the squared sum of fading coefficients. This experiment confirms the theory based assumption that the values of the error on the zero crossing point of the S-curve are going to be normally distributed if there is fading present in the channel.

The non-coherent tracking loop investigated above is now used for tracking the incoming signal. The cumulative and instantaneous estimations are shown for both noiseless and noisy conditions in Fig. 5.10. The tracking loop for both cases is set to run for 40 iterations. In the noiseless case, it is evident that the non-coherent tracking loop has an optimal performance because the random jitter ( $T_d$ ) is tracked for all iterations and each estimation ( $\hat{T}_d$ ) is the same as the value of jitter for the previous step. In the noisy case, the incoming jitter is not tracked optimally because of the presence of noise which affects the correlation function. As can be seen the cumulative values for  $T_d$  and  $\hat{T}_d$  diverge. If the difference between the cumulative values becomes more than a chip duration, the acquisition stage has to be restarted as the synchronisation is lost. The work presented in [94], only presented the noiseless tracking loop performance which is unrealistic in real communication channels. The figures below however, show the effect of channel impurities on the actual tracking of signals.

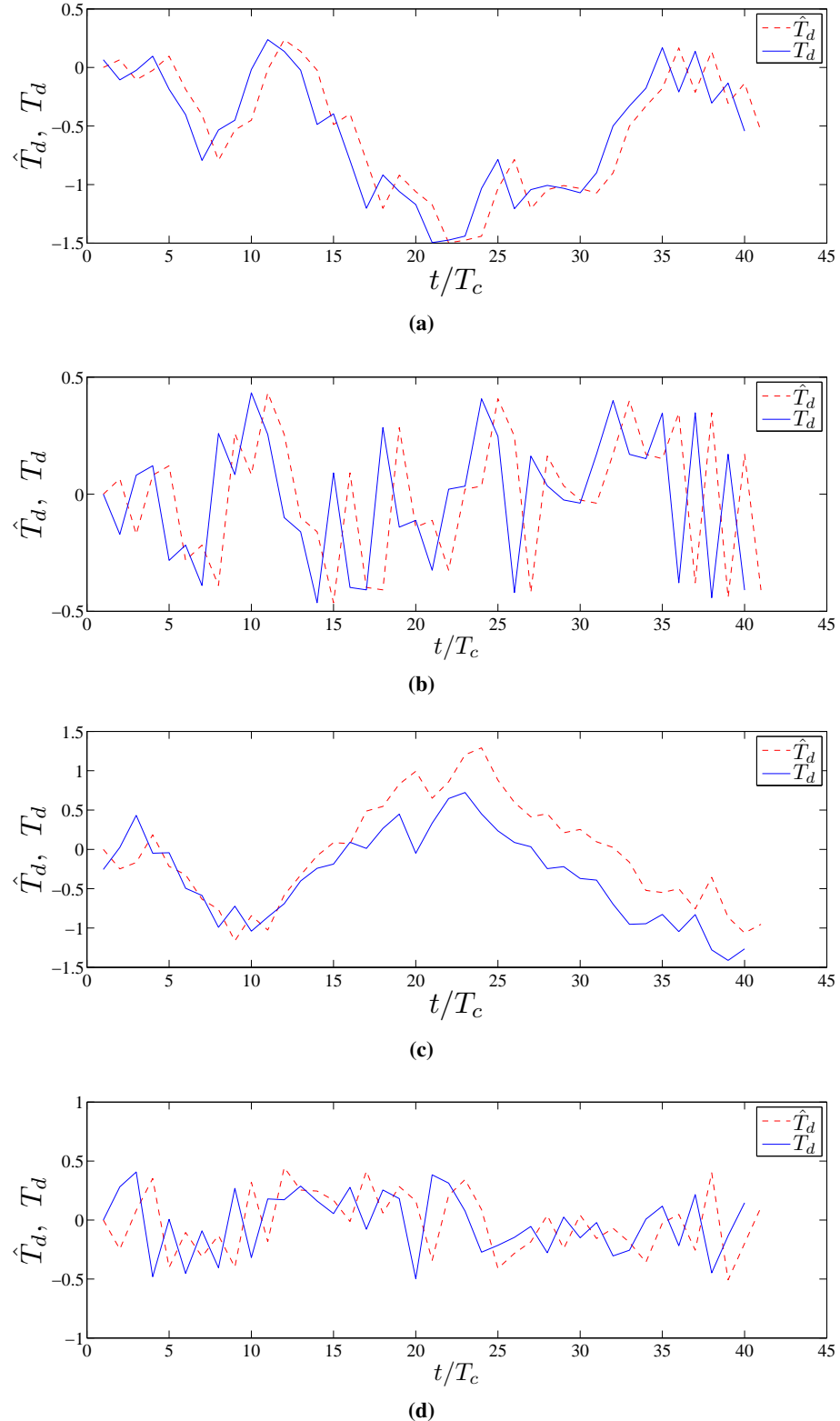


**Figure 5.10:** Timing jitter,  $T_d$  and its estimation  $\hat{T}_d$ , (a) cumulative values and (b) instantaneous values, (c) and (d) show the same values for a noisy environment ( $\text{SNR} = 8 \text{ dB}$ ). Both  $T_d$  and  $\hat{T}_d$  are normalised by  $T_c$ .

### 5.4.1 Control law derivation

In order to address the practical side of the tracking loop, the control law relating to the chaos-based non-coherent tracking loop is derived. It is assumed that only noise is present in the channel. This section presents the derivation of the control law based on the correlation properties of the chaotic signals and extends the analysis presented in [94] to include the square law devices. It is assumed that the chaotic pilot will be tracked non-coherently over its entire period. The linear region gradient is now expressed by

$$m = \frac{A^2 \bar{P} (M - 1)^2 T_c}{T_c/2} = 2A^2 \bar{P} (M - 1)^2, \quad (5.56)$$

where  $\bar{P}$  is the average power of the logistic map and  $M$  is the correlation period used for the early and late gates of the tracking loop. Consequently, the tracking loop operation is governed by the following equation,

$$\begin{aligned} & \mathbb{R}^2 \left[ \left( \delta - \frac{\Delta}{2} \right) T_c \right] - \mathbb{R}^2 \left[ \left( \delta + \frac{\Delta}{2} \right) T_c \right] \\ &= m\delta T_c = 2A^2 \bar{P} (M - 1)^2 \left( T_d - \hat{T}_d \right). \end{aligned} \quad (5.57)$$

Solving for  $\hat{T}_d$ ,

$$\hat{T}_d = T_d - \frac{\mathbb{R}^2 \left[ \left( \delta - \frac{\Delta}{2} \right) T_c \right] - \mathbb{R}^2 \left[ \left( \delta + \frac{\Delta}{2} \right) T_c \right]}{2A^2 \bar{P} (M - 1)^2}. \quad (5.58)$$

Since both  $T_d$  and  $\hat{T}_d$  are time variables, equation (5.58) has to be rewritten to reflect the time steps in  $T_c$ , therefore

$$\hat{T}_d(nT_c) = T_d(nT_c) - \frac{\mathbb{R}_1^2(nT_c) - \mathbb{R}_2^2(nT_c)}{2A^2 \bar{P} (M - 1)^2}, \quad (5.59)$$

where  $\mathbb{R}_1^2 = \mathbb{R}^2 \left[ \left( \delta - \frac{\Delta}{2} \right) T_c \right]$  and  $\mathbb{R}_2^2 = \mathbb{R}^2 \left[ \left( \delta + \frac{\Delta}{2} \right) T_c \right]$ . If the timing offset has been acquired to within  $\pm \frac{T_c}{2}$ , every new value of time offset can be iteratively calculated. Assuming that the acquired time (passed on from the acquisition stage) at the start of the tracking stage is  $T_a$  two scenarios can be envisaged. The first is  $T_a = T_d$ , meaning that  $\hat{T}_d(1T_c)$  will take the value of  $T_a$  which when substituted into equation (5.59) will give

$$\hat{T}_d(T_c) - T_a = - \frac{\mathbb{R}_1^2(nT_c) - \mathbb{R}_2^2(nT_c)}{2A^2 \bar{P} (M - 1)^2}. \quad (5.60)$$

If indeed  $T_a = T_d$ , then  $\mathbb{R}_1^2(nT_c) - \mathbb{R}_2^2(nT_c)$  to become zero in the above equation. The second is  $T_a \neq T_d$ , when it was assumed that  $T_a = T_d$ , in this case  $\hat{T}_d(1T_c)$  takes the actual value of  $T_d$  at the beginning of the tracking loop cycle because the right hand side of equation (5.60) gives the difference between the acquired and the actual time offset i.e.  $T_a - T_d$  [94]. This means that

$$\hat{T}_d(T_c) - T_a = -(T_a - T_d) \Rightarrow \hat{T}_d(T_c) = T_d. \quad (5.61)$$

Therefore equation (5.60) can be rewritten as

$$\hat{T}_d(nT_c + T_c) = \hat{T}_d(nT_c) - \frac{\mathbb{R}_1^2(nT_c) - \mathbb{R}_2^2(nT_c)}{2A^2\bar{P}(M-1)^2}, \quad (5.62)$$

where  $\hat{T}_d(0) = T_a$ .

### 5.4.2 Effects of filtering and noise on the tracking loop properties

In order to perform code tracking for DS-CDMA signals, it is necessary to have the notion of a chip duration ( $T_c$  in this case), with a sufficiently high resolution so that the tracking stage which is concerned with time delays in the order of a fraction of chip, can perform its task. However, throughout the literature related to the tracking stage of the synchronisation block for DS-CDMA systems, it is assumed that the spreading chips keep a constant value over the chip duration (rectangular pulse). The tracking stage error curves presented in [8, 107, 168] for classical DS-CDMA and in [94] for the chaos-based case, did not take into account the filtering that is included in the system. Moreover, rectangular pulses lead to an increase in the transmission band-width which is not desirable. In order to address this issue the tracking stage of the synchronisation block has been modeled with interpolated chaotic samples that have the same band-width as the original un-sampled signal since they have been low pass filtered at the end of the interpolation process. The error curve results for various values of  $\Delta$  are given in Figs. 5.11-5.14. As can be seen, the filtering has a direct effect on the shape of the errors curves, also, increasing the value of  $\Delta$  to twice the chip length (Fig. 5.14) will introduce a point with a zero slope. This is highly undesirable because it introduces errors in the tracking process and has to be avoided.

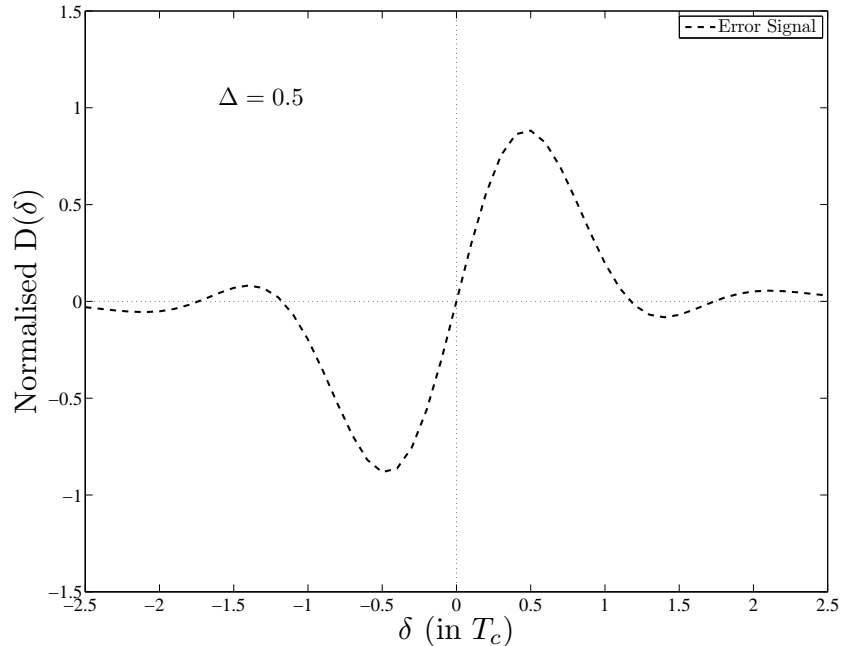


**Figure 5.11:** Non-coherent tracking loop error curve with filtered pulses for  $\Delta = 0.5$ .

Fig. 5.15 shows the effect of noise for the two types of filtering used for the tracking loop. As can be seen, the linear region of the loop is affected by noise and it no longer crosses the zero line at the correct

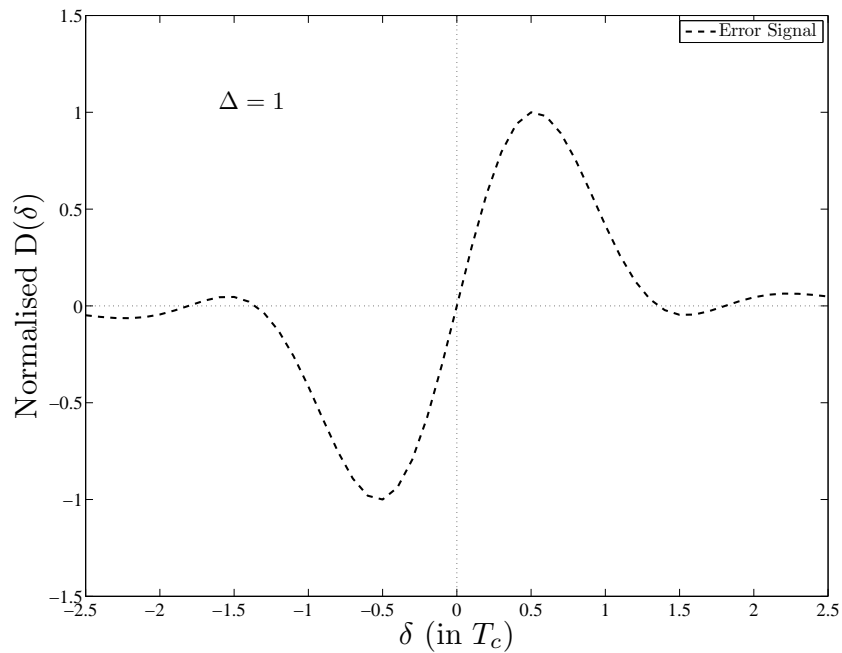


**Figure 5.12:** Non-coherent tracking loop error curve with filtered pulses for  $\Delta = 1$ .

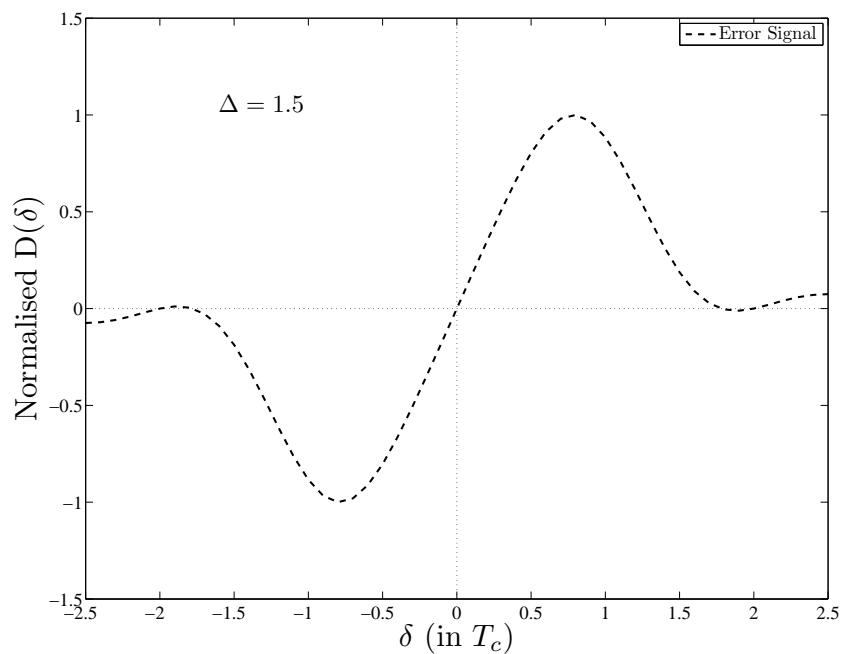


**Figure 5.13:** Non-coherent tracking loop error curve with filtered pulses for  $\Delta = 1.5$ .

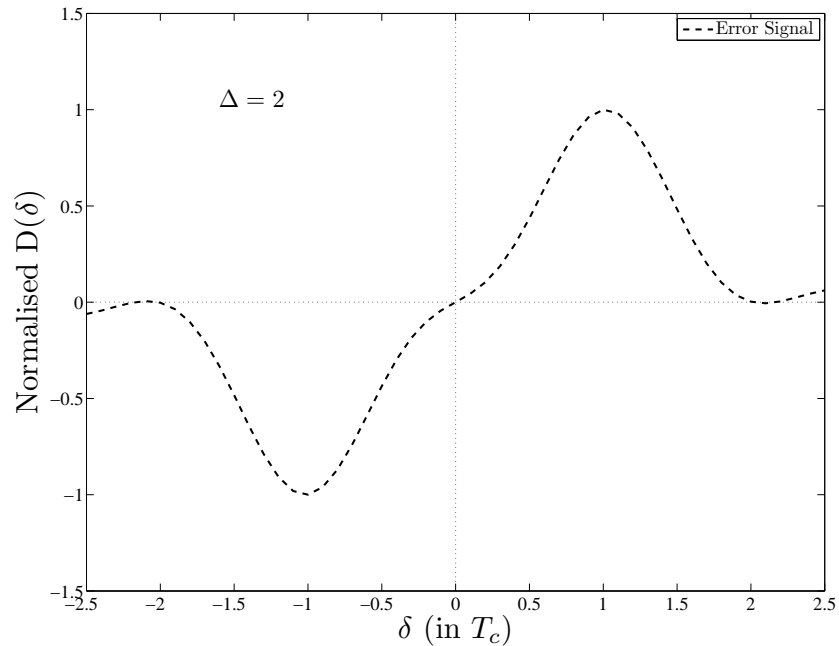


**Figure 5.14:** Non-coherent tracking loop error curve with filtered pulses for  $\Delta = 2$ .

time. Noisy conditions introduce errors in the tracking process which could ultimately result in the loss of synchronisation.

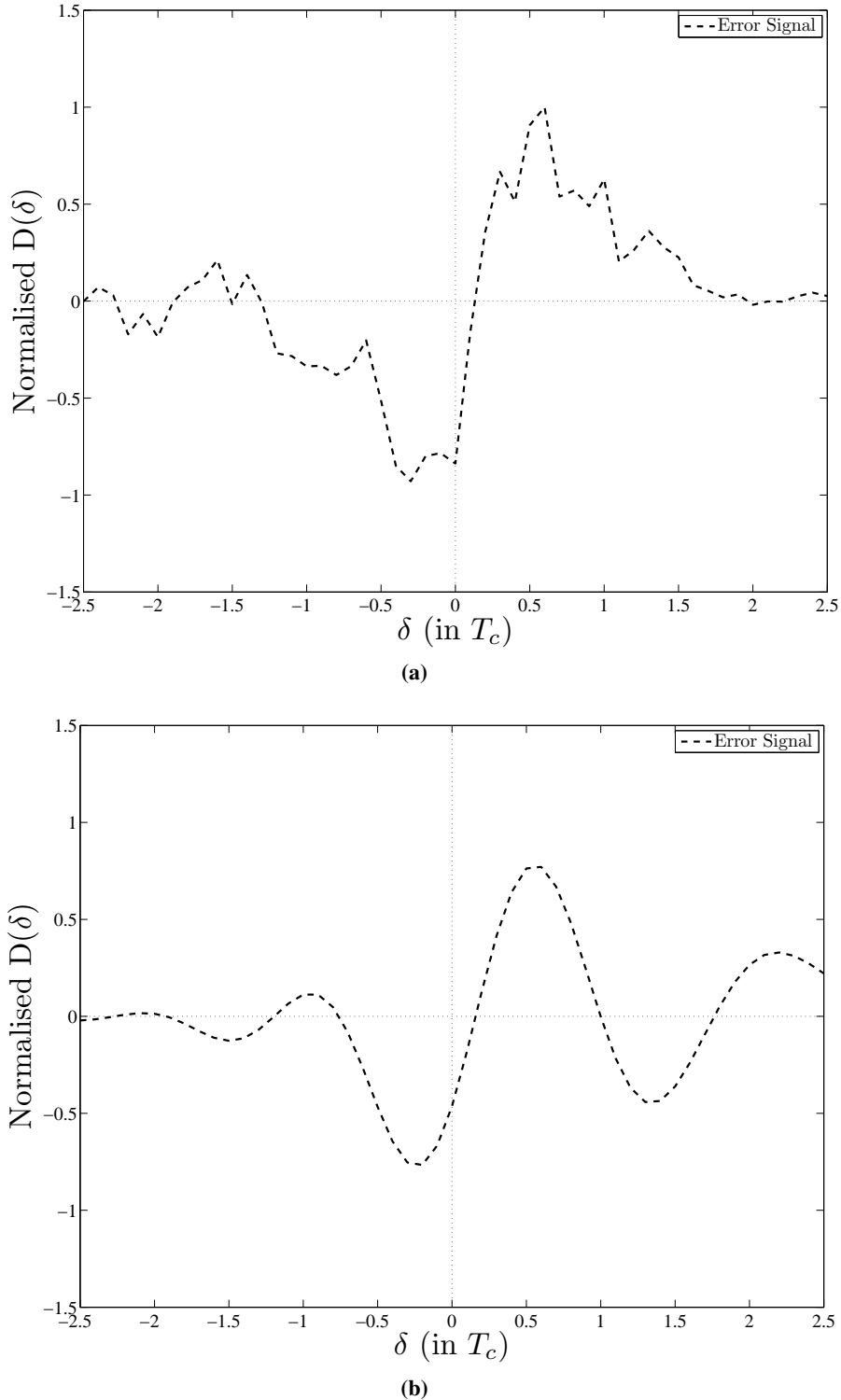


**Figure 5.15:** Tracking loop error signal for (a) noisy rectangular chaotic sequences and (b) noisy interpolated chaotic sequences (SNR = 6 dB both cases).

## 5.5 Summary

The first approximation to the synchronisation of a CDS-SS system in the presence of fading was presented in this chapter. The difference between the analysis presented in this chapter and other recent

works in this area were expressed. Both the sequence acquisition and tracking were investigated in presence of fading, and upper bounds on the performance of the acquisition stage as well as the theoretical framework for the tracking stage performance in the presence of fading have been presented. The analysis is then supported by numerical results for both stages of synchronisation.

Although the issue of fading is now treated, there is still a gap between the simulation and theoretical results. That is why the results presented for acquisition have an upper-bound. The reason for this is related to the way the system has been modelled using the existing mathematical models for the binary spreading codes. The conventional model for synchronisation assumes that the correlation function (denoted as  $R(\tau)$  and  $R(\delta)$  in this chapter) is a fixed value irrespective of the sequence. This means that the conventional binary sequence theory is not suitable for application in synchronisation analysis for a CDS-SS system. As a result there is a need to change the way the CDS-SS synchronisation is analysed, taking into account the characteristics of the chaotic sequences.

A new accurate statistical model encompassing noise, fading performance for chaos-based correlation and its application to acquisition is the subject for the next chapter. Also the next chapter will present a way to mitigate the effect of fading in order to improve acquisition performance.



# Chapter 6

## Statistical Analysis of CDS-SS Acquisition

### 6.1 Introduction

So far, §5 has highlighted the need for an accurate method in analysing the synchronisation of CDS-SS systems and that the existing method, which is borrowed from the conventional system analysis, is not suitable. This is because the existing method does not take into account the unique characteristics of the chaotic spreading codes. Also, the WCDMA system normally uses a separate synchronisation and control channel. Also, the pilot synchronisation is achieved in a certain time-slot which is free from the inter-user-interference (IUI). As a result of this the effect of IUI is not considered on the pilot synchronisation. However, if the effect of the IUI is to be considered for purely theoretical reasons, it can easily be added into the existing model proposed in this chapter without loss of generality.

This chapter presents a new approach that attempts to accurately analyse the synchronisation of chaotic sequences. This new method is rooted in the statistical characterisation of the correlation function of chaotic sequences and is termed chaotic correlation statistics (CCS). First, §6.2 presents the theoretical framework used for the CCS method. Following that, §6.3 presents the application of the CCS method in the sequence acquisition problem. To show the versatility of the suggested method, three different channel scenarios are considered. The probabilities of detection and failure ( $P_D$  and  $P_F$  respectively) are derived for each of the scenarios. §6.4 presents the comparison between the analytical and simulation results as well as a discussion. The analysis and findings in this chapter appear in [169].

### 6.2 Chaotic Correlation Statistics (CCS)

As mentioned in §2.3.3, the iterative function for the Logistic map is  $x_{n+1} = 2x_n^2 - 1$  [170], and is bounded between  $(-1, 1)$ . The initial condition for this map can be any value within  $(-1, 1)$  except  $\frac{-1}{2}$ ,  $\frac{1}{2}$  and 0. Considering the probability density function (PDF) of the Logistic map given by [170],

$$P_x(x) = \frac{1}{\pi \left( \sqrt{1 - x^2} \right)}, \quad (-1 < x < 1), \quad (6.1)$$

the values for the mean and variance of the Logistic map can be calculated as 0 and  $\frac{1}{2}$  respectively.

The correlation function of the chaotic pilot sequence generated from the Logistic map is given by,

$$z[j] = \sum_{i=1}^L (x_{i-\tau} x_{i-j}), \quad (6.2)$$

where  $z$  is the discrete correlation result,  $j$  is the time index of the correlation i.e. the phase delay corresponding to the locally generated chaotic pilot sequence,  $\tau$  is the time lag between the two sequences due to propagation, and  $L$  is the number of chips in the correlation. The value of  $\tau$  in acquisition phase is assumed to be a discrete multiple of a chip duration.

Over a large set of chaotic values generated using different initial conditions, it can be assumed each  $x_{i-\tau}$  and  $x_{i-j}$ , are random variables with PDFs given by (6.1). As a result, the correlation output can be considered a random variable consisting of the summation of the product of the two chaotic sequences over  $L$  chips. If  $L$  is a small value, the correlation function will not follow a Gaussian distribution [171]. However, given  $L$  is usually more than 50 chips for coherent CDS-SS schemes [46], it can be assumed that each value of the correlation function (i.e. each  $z[j]$ ) is the sum of a large number of independent, identically distributed random variables, and therefore can be accurately modeled by a Gaussian distribution by invoking the central limit theorem (CLT).

Two possibilities arise; first,  $j \neq \tau$  which corresponds to the two chip sequences being out of synchrony. Since chaotic sequences are orthogonal, this corresponds to the cross-correlation of the two sequences. Therefore, for  $N \gg 1$  trials, the cross-correlation result for non-aligned sequences is a Gaussian random variable denoted by  $Z_{h_0}$ .

Noting the orthogonality of chaotic sequences, the mean of  $Z_{h_0}$  can be calculated as

$$\mathbb{E}[Z_{h_0}] = \mathbb{E}\left[\sum_{i=1}^L (x_{i-\tau} x_{i-j})\right] \quad (6.3)$$

Given that the  $(x_{i-\tau} x_{i-j})$  term can be assumed to be independent random variables for each  $i$ ,

$$\begin{aligned} \mathbb{E}[Z_{h_0}] &= \sum_{i=1}^L \mathbb{E}[(x_{i-\tau} x_{i-j})] \\ &= \sum_{i=1}^L 0 \\ &= 0. \end{aligned} \quad (6.4)$$

Since the variance of the summation of  $L$  independent identically distributed Gaussian random variables that have the same variance is the same as  $L$  times the variance of one of them, the variance of  $Z_{h_0}$  can

be calculated as

$$\begin{aligned}
\text{Var}[Z_{h_0}] &= \text{Var} \left[ \sum_{i=1}^L (x_{i-\tau} x_{i-j}) \right] \\
&= \sum_{i=1}^L \text{Var}[(x_{i-\tau} x_{i-j})] \\
&= \sum_{i=1}^L \left\{ \text{E}[(x_{i-\tau} x_{i-j})^2] - \text{E}^2[(x_{i-\tau} x_{i-j})] \right\} \\
&= \sum_{i=1}^L \text{E}[x_{i-\tau}^2] \text{E}[x_{i-j}^2] - 0 \\
&= \frac{L}{4},
\end{aligned} \tag{6.5}$$

where  $\text{E}[x_{i-\tau}^2] = \frac{1}{2}$  is explained in Appendix B. Given the above mean and variance and the knowledge that  $Z_{h_0}$  follows a Gaussian distribution, the model for  $Z_{h_0}$  becomes  $Z_{h_0} \sim G(0, \frac{L}{4})$ .

The second possibility is  $j = \tau$ , which corresponds to the auto-correlation peak of the two sequences. For  $N \gg 1$  trials, the correlation result for aligned sequences can be assumed to be a Gaussian random variable corresponding to the variation of the auto-correlation peak.

The mean of  $Z_{h_1}$  can be calculated as

$$\begin{aligned}
\text{E}[Z_{h_1}] &= \text{E} \left[ \sum_{i=1}^L (x_{i-\tau} x_{i-\tau}) \right] \\
&= \text{E} \left[ \sum_{i=1}^L (x_{i-\tau}^2) \right]
\end{aligned} \tag{6.6}$$

Given that each  $(x_{i-\tau}^2)$  term can be assumed to be independent random variable for each  $i$

$$\begin{aligned}
\text{E}[Z_{h_1}] &= \sum_{i=1}^L \text{E}[(x_{i-\tau}^2)] \\
&= \sum_{i=1}^L \frac{1}{2} \\
&= \frac{L}{2}.
\end{aligned} \tag{6.7}$$

Since the variance of the summation of  $L$  independent identically distributed Gaussian random variables that have the same variance is the same as  $L$  times the variance of one of them, the variance of  $Z_{h_1}$  can

be calculated as

$$\begin{aligned}
\text{Var}[Z_{h_1}] &= \text{Var} \left[ \sum_{i=1}^L (x_{i-\tau}^2) \right] \\
&= \sum_{i=1}^L \text{Var}[(x_{i-\tau}^2)] \\
&= \sum_{i=1}^L \left\{ \text{E}[(x_{i-\tau}^2)^2] - \text{E}^2[(x_{i-\tau}^2)] \right\} \\
&= \sum_{i=1}^L (\text{E}[x_{i-\tau}^4] - \text{E}^2[x_{i-\tau}^2]) \\
&= L \times \left( \frac{3}{8} - \frac{1}{4} \right) \\
&= \frac{L}{8},
\end{aligned} \tag{6.8}$$

where  $\text{E}[x_{i-\tau}^4] = \frac{3}{8}$  is explained in Appendix B. Given the above mean and variance and the knowledge that  $Z_{h_1}$  follows a Gaussian distribution, the model for  $Z_{h_1}$  becomes  $Z_{h_1} \sim \mathcal{G}\left(\frac{L}{2}, \frac{L}{8}\right)$ .

The subscripts  $h_0$  and  $h_1$  refer to the non-synchronised and synchronised hypotheses respectively. Fig. 6.1 shows a comparison between the statistical models proposed and the computed distributions of  $Z_{h_0}$  and  $Z_{h_1}$ . The average error between the distributions and the statistical models is also shown verifying the statistical characterisation presented. It should be noted that  $Z$  is a random variable with a Gaussian distribution and  $z[j]$  is the  $j$ -th value of the correlator output array.

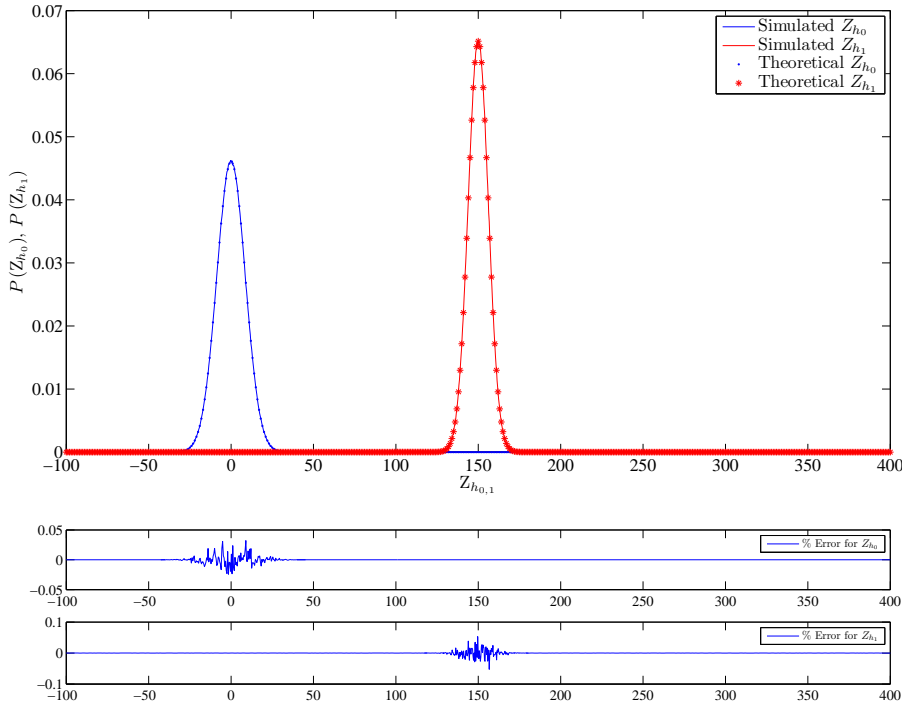


**Figure 6.1:** Comparison between the statistical models and simulated distributions of  $Z_{h_0}$  and  $Z_{h_1}$ .

The Logistic map is from the family of Chebychev maps all of which have the same PDF given by (6.1) [170]. So if any of the maps from the Chebychev family are used in the CDS-SS system, the analysis presented in this chapter can be readily applied. If other chaotic maps with different statistical properties are used, the general approach used in this chapter can still be applied to them if a large correlation length ( $L > 20$ ) is used, the mean and variances of the Gaussian distributions have to be recalculated however. This investigation indicates that, with a sufficiently large correlation length, the cross- and auto-correlation peaks are not constant, but follow Gaussian distributions.

Over  $N \gg 1$  trials, the noise value added to each chip can be considered a random variable with a Gaussian distribution and zero mean. If  $n_i$  is the noise value added to each chip then

$$n_i \sim G(0, \sigma_n^2), \quad (6.9)$$

where  $\sigma_n^2 = \frac{N_0}{2}$ , and  $N_0$  is the one sided noise power spectral density.

Since for every correlator output value  $L$  chips are summed and each chip is affected by AWGN, the cumulative effect of the noise has to be accounted for every correlator output value. Given the AWGN in this case has a zero mean ( $E[n_i] = 0$ ), it will not affect the mean of  $Z_{h_0}$  and  $Z_{h_1}$ . For the correlation length of  $L$  chips, the variance of  $Z_{h_0}$  and  $Z_{h_1}$  will be affected by the variance of the signal  $\times$  noise term. Given that the noise and the chaotic chips are independent random variable

$$\begin{aligned} \text{Var} \left[ \sum_{i=1}^L (n_i x_{i-j}) \right] &= \sum_{i=1}^L \text{Var}[(n_i x_{i-j})] \\ &= \sum_{i=1}^L (\text{Var}[(x_{i-j})] \text{Var}[(n_i)]) \\ &= L \times \frac{1}{2} \times \sigma_n^2 \\ &= \frac{L\sigma_n^2}{2}. \end{aligned}$$

Now that the correlator output is statistically modelled for both synchronised and non-synchronised cases and in noisy conditions, the CCS can be applied to different channel scenarios. This is the subject of the next section.

### 6.3 Accurate Analysis of Code Acquisition Using CCS

The base-band acquisition block diagram is shown in Fig. 6.2. The transmitter sends a periodic chaotic chip sequence as the pilot signal, which is time delayed by a random propagation delay  $\tau$ , and corrupted in the wireless channel. This pilot is modulated by a continuous set of +1 bits. Normally, the time delay between the transmitter and receiver is not an exact multiple of the chip duration. However, the role of the acquisition is to find the time delay to the nearest chip. The rest of the operation will be handled by the tracking phase described in §7. Therefore  $\tau$  is assumed to be a multiple of the chip duration for acquisition. A sliding correlator, a square law device and a threshold in a loop formation are used to

perform the signal acquisition. The sliding correlator can perform correlation on all, or a fraction, of the pilot sequence. Once the output of the square law device exceeds the threshold  $Z_{Th}$ , synchronisation is declared and the system will enter the tracking mode. If the synchronisation is lost whilst the system is in the tracking mode, i.e. when information is being transmitted, the system reverts back to acquisition and the synchronisation process will restart.

The investigation presented in this section is performed in base-band; however, the extension to pass-band would be relatively simple because, the square law device which will be used in a pass-band system to eliminate the phase difference between the incoming and locally generated carriers is taken into account. Also, it is assumed that other users are not transmitting at the time of acquisition. Therefore inter-user interference (IUI) is not considered in this section.

In order to establish the validity of the CCS approach, three separate scenarios involving noise, fading, and blind chip interleaving are considered in the following subsections. For the noise only case, the fading coefficient and the interleaver blocks presented in Fig. 6.2 have to be ignored. Similarly, for the noise and fading case, the interleaving blocks in Fig. 6.2 have to be ignored. The third scenario presents a blind interleaver/de-interleaver pair that are used to mitigate the effect of fading in acquisition performance. The assumptions used for the fading are the same as §5.

### 6.3.1 Scenario 1, noise only

Given the system is only corrupted by noise, the received signal can be written as  $r_i = x_{i-\tau} + n_i$ , which after correlation with the local replica can be written as,

$$z[j] = \sum_{i=1}^{2\beta} (x_{i-\tau} x_{i-j}) + \sum_{i=2\beta+1}^{4\beta} (x_{i-\tau} x_{i-j}) + \cdots + \sum_{i=2\beta(k-1)+1}^{2\beta k} (x_{i-\tau} x_{i-j}) + \sum_{i=1}^{2\beta k} (n_i x_{i-j}), \quad (6.10)$$

where  $2\beta$  is the spreading factor and  $k$  is the number of pilot bits in the correlation function. The correlation function is being analysed on a per bit basis because it is more convenient when the fading scenarios are considered. The expression presented in (6.10) is one realisation of random variable  $Z_h$  which will be one of the two forms of  $h_1$  or  $h_0$  depending on whether the sequences are synchronised or non-synchronised respectively.

Using the derivations presented in §6.2, the statistical representation of the correlator output non-synchronised case can be shown as

$$Z_{h_0} \sim G \left( 0, \frac{L}{4} + \frac{L\sigma_n^2}{2} \right), \quad (6.11)$$

and for the synchronised case as

$$Z_{h_1} \sim G \left( \frac{L}{2}, \frac{L}{8} + \frac{L\sigma_n^2}{2} \right). \quad (6.12)$$

where  $L = 2k\beta$  in this case. Fig. 6.3 shows the visual representation of the correlator output in presence of noise for  $N \gg 1$  experiments.

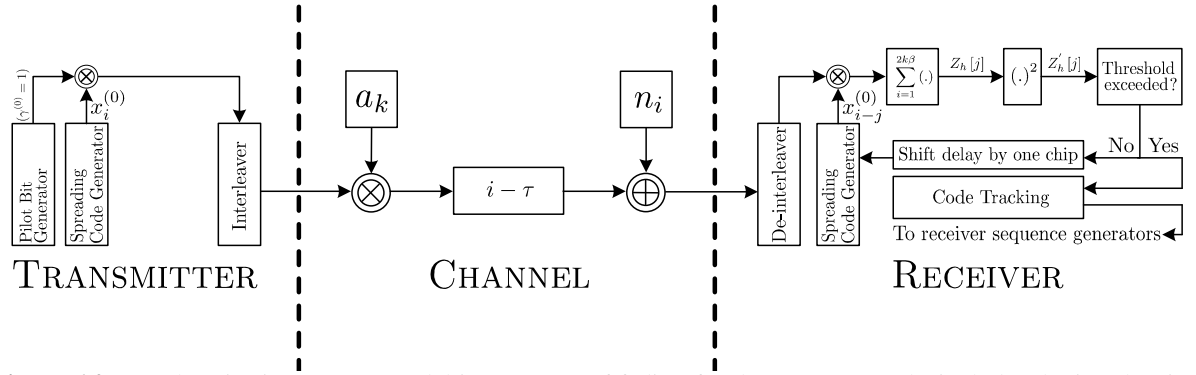


**Figure 6.2:** Synchronisation system model in presence of fading for the new approach (includes the interleaving block).

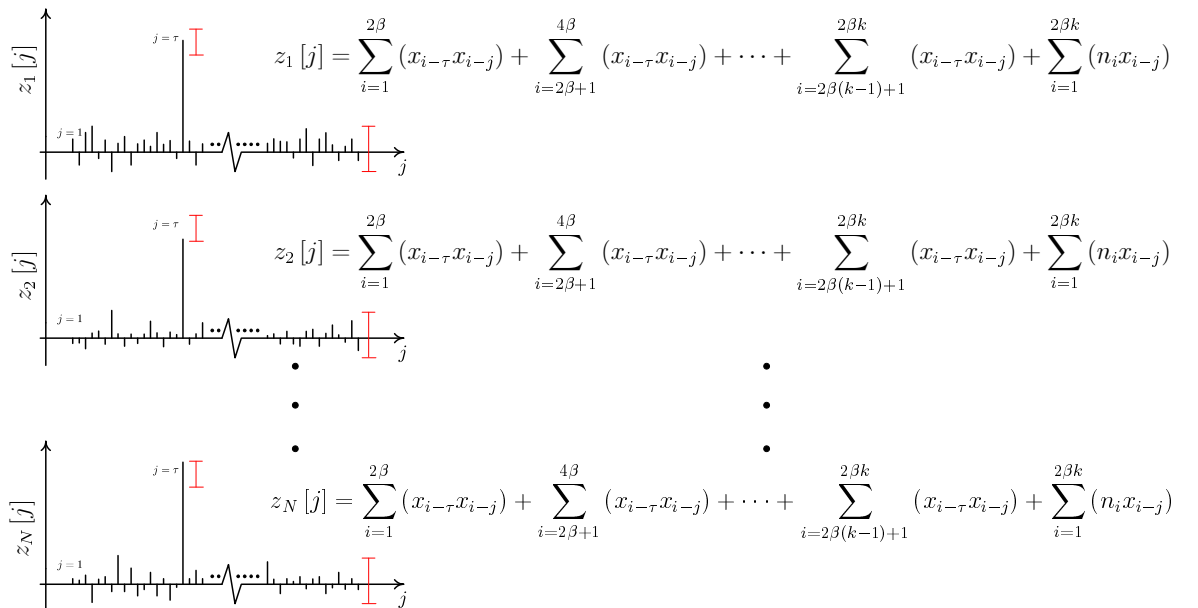


**Figure 6.3:** The chaotic correlator output for many experiments.

For every  $j$ , the correlation values go through the square law device. This affects the statistical distributions of the correlator output. To address this, the effect of the square law device on  $Z_{h_0}$  and  $Z_{h_1}$  is examined separately.

For the non-synchronised case, the variable with a zero mean Gaussian distribution is squared and takes the form of a chi-square distribution which can be expressed as

$$p(Z'_{h_0}, 1) = \frac{1}{\sqrt{2\pi Z'_{h_0}}} \exp\left(\frac{-Z'_{h_0}}{2}\right), \quad (6.13)$$

where  $Z'_{h_0} = \frac{Z_{h_0}^2}{\sigma_{Z_{h_0}}^2}$  is the squared and normalised random variable.

Similarly the synchronised case will square the random variable with a non-zero mean Gaussian distribution. The new variable will have a non-central chi-square distribution shown as

$$p(Z'_{h_1}, 1, \lambda) = \frac{1}{2} \exp\left(\frac{-(Z'_{h_1} + \lambda)}{2}\right) \left(\frac{Z'_{h_1}}{\lambda}\right)^{-\frac{1}{4}} I_{-\frac{1}{2}}\left(\sqrt{Z'_{h_1} \lambda}\right), \quad (6.14)$$

where  $Z'_{h_1} = \frac{Z_{h_1}^2}{\sigma_{Z_{h_1}}^2}$  is the squared and normalised random variable,  $I(\cdot)$  is a modified Bessel function of the first kind, and  $\lambda$  is the non centrality parameter. It is well known that the non-centrality parameter can be calculated as

$$\lambda_{\text{Noise}} = \frac{E^2[Z_{h_1}]}{\text{Var}[Z_{h_1}]} = \frac{2L}{1 + 4\sigma_n^2}. \quad (6.15)$$

Fig. 6.4 shows a comparison between the statistical models shown in (6.13) and (6.14) and the computed distributions of  $Z'_{h_0}$  and  $Z'_{h_1}$ . The average error between the distributions and the statistical models is also shown verifying the statistical characterisation presented.

### 6.3.2 Scenario 2, noise and fading

Since slow fading is assumed, the fading coefficient only changes once every bit. The correlator output for each trial can be expressed as

$$z[j] = \underbrace{a_{1,1} \sum_{i=1}^{2\beta} (x_{i-\tau} x_{i-j})}_{\text{Bit 1}} + \underbrace{a_{2,1} \sum_{i=2\beta+1}^{4\beta} (x_{i-\tau} x_{i-j})}_{\text{Bit 2}} + \dots + \underbrace{a_{k,1} \sum_{i=2\beta(k-1)+1}^{2\beta k} (x_{i-\tau} x_{i-j})}_{\text{Bit } k} + \sum_{i=1}^{2\beta k} (n_i x_{i-j}), \quad (6.16)$$

where  $a_{k,1}$  is the fading coefficient for the  $k$ -th bit of the first trial.

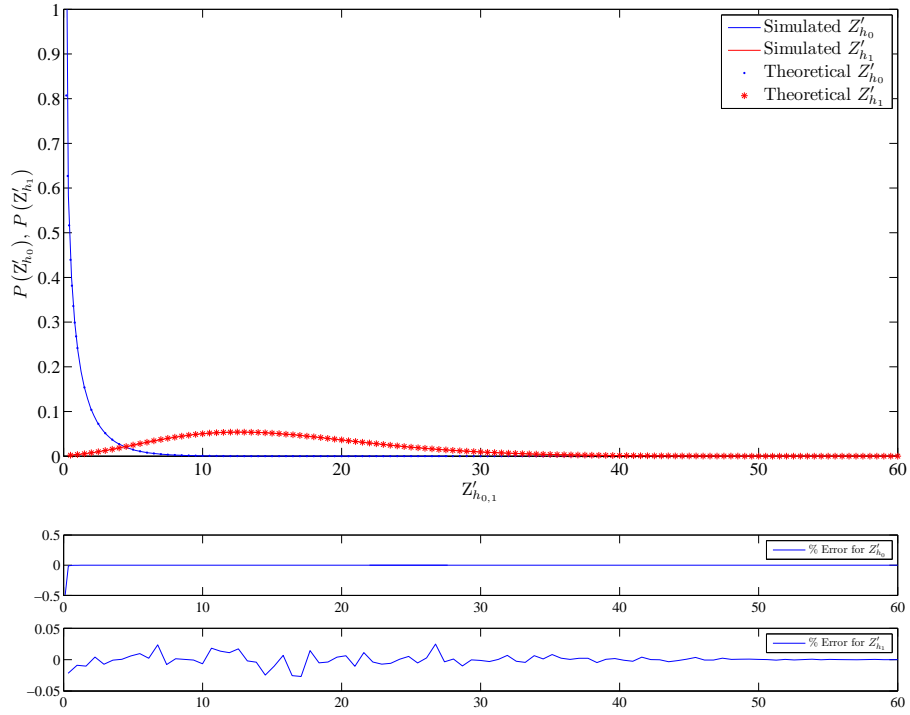


**Figure 6.4:** Comparison between the statistical models and simulated distributions of  $Z'_{h_0}$  and  $Z'_{h_1}$ .

Initially assuming that the pilot is one bit long, i.e.  $k = 1$ , and if the correlation is evaluated many times (i.e.  $N \gg 1$  trials) using different chaotic sequences and fading coefficients, the correlation function can be written as

$$Z_{h_0} = AX_{h_0} + N, \quad (6.17)$$

where  $Z_{h_0}$ ,  $A$ ,  $X_{h_0}$  and  $N$  are random variables representing the faded correlation function, Rayleigh fading envelope, the  $\sum_{i=1}^L (x_{i-\tau} x_{i-j})$  and  $\sum_{i=1}^L (n_i x_{i-j})$  terms respectively. For the non-synchronised case, it has been shown in §6.3 that  $X_{h_0}$  and  $N$  have zero mean Gaussian distributions. Assuming that  $Z_{h_0}$  has a Gaussian distribution for the fading case, and the fading coefficients are statistically independent from the correlation function, the mean and variance of  $Z_{h_0}$  can be found as

$$\begin{aligned} E[Z_{h_0}] &= E[A] E\left[\underbrace{\sum_{i=1}^L (x_{i-\tau} x_{i-j})}_{X_{h_0}}\right] + E\left[\underbrace{\sum_{i=1}^L (n_i x_{i-j})}_N\right] \\ &= E[A] E[X_{h_0}] + E[N] \\ &= b \sqrt{\frac{\pi}{2}} \times 0 + 0. \\ &= 0, \end{aligned}$$

$$\begin{aligned}
\text{Var}[Z_{h_0}] &= \text{Var}[AX_{h_0}] + \text{Var}[N] \\
&= \text{Var}[X_{h_0}]E^2[A] + \text{Var}[A]E^2[X_{h_0}] + \text{Var}[X_{h_0}]\text{Var}[A] + \text{Var}[N] \\
&= 0 + \frac{L}{4}\frac{b^2\pi}{2} + \frac{L}{4}\frac{b^2(4-\pi)}{2} + L\sigma_n^2 \\
&= \frac{L}{2}(b^2 + 2\sigma_n^2),
\end{aligned}$$

where  $b$  is the mode of the Rayleigh distribution given in (3.3). The derivation of  $E[A]$  and  $\text{Var}[A]$  is presented in Appendix C.

Therefore, assuming that  $Z_{h_0}$  is Gaussian its PDF can be expressed as

$$Z_{h_0} \sim G\left(0, \frac{L}{2}(b^2 + 2\sigma_n^2)\right). \quad (6.18)$$

The exact distribution of  $Z_{h_0}$  for this scenario is given in [172] and is presented in Appendix D. Fig. 6.5 provides a comparison between the exact solution provided in [172], and the Gaussian expression presented in (6.18). It can be seen that the assumption is close to the exact solution.

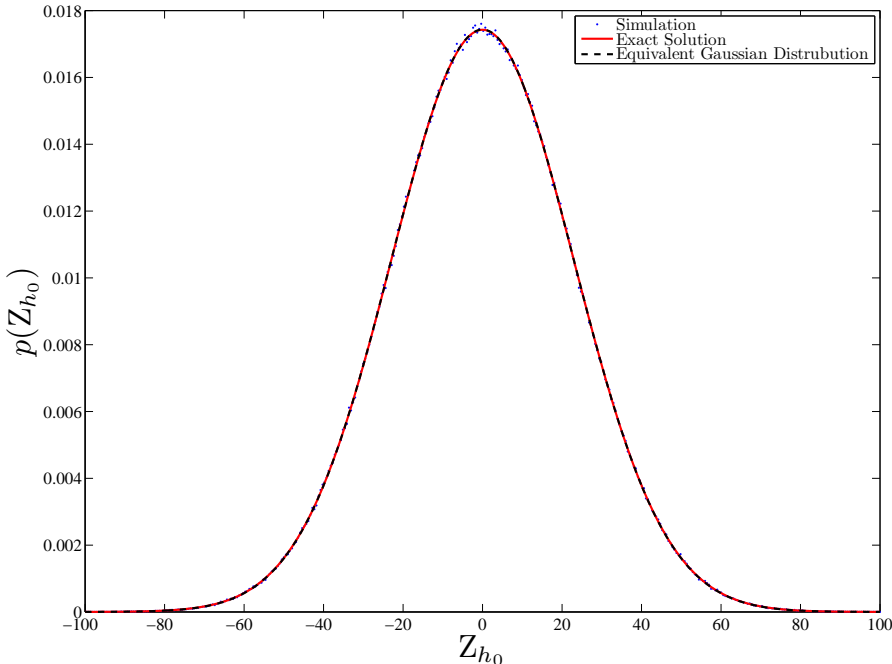


**Figure 6.5:** Comparison between the exact distribution of  $Z$  given in (6.17), Gaussian approximation and simulation.

Without the loss of generality, it can be assumed that for  $k > 1$ , each bit has the same distribution given in (6.18), and the mean and variance of the resulting  $Z_{h_0}$  is the summation of the means and variances of the individual bits. Since the means are zero, the PDF of  $Z_{h_0}$  for  $k$  bits can be expressed as

$$Z_{h_0} \sim G\left(0, \frac{kL}{2}(b^2 + 2\sigma_n^2)\right). \quad (6.19)$$

Therefore, having proven that  $Z_{h_0}$  can be accurately approximated as a random variable with a Gaussian distribution, it can be concluded that the square law device output for the non-synchronised case has a PDF shown in (6.13). For  $k > 1$  the normalisation factor for  $Z'_{h_0}$  changes to  $\frac{kL}{2} (b^2 + 2\sigma_n^2)$ .

The synchronised case is more involved, in that, there are no analytical closed form expressions for the PDF of  $Z_{h_1}$  when

$$Z_{h_1} = AX_{h_1} + N, \quad (6.20)$$

where  $X_{h_1}$  has a non-zero mean Gaussian distribution. The first attempt is to find a suitable statistical model for (6.20) when the correlation is only one bit long i.e. there is only one fading coefficient. If the auto-correlation experiment is repeated  $N$  times, a promising hypothesis is to consider the  $AX_{h_1}$  term in (6.20) a non-zero mean Gaussian distribution which is multiplied by a coefficient for each trial based. As a result of this multiplication, the mean and variance of the Gaussian distribution are going to be affected. However, it is assumed that the distribution of  $AX_{h_1}$  still remains Gaussian.

If  $N \gg 1$ , the distribution of  $AX_{h_1}$  can be modelled by affecting the mean and variance of  $X_{h_1}$  by the mean and variance of  $A$  using the approach described in [173]; therefore it is hypothesised that  $Z_{h_1}$  is a Gaussian distribution with the mean and variance of

$$\begin{aligned} E[Z_{h_1}] &= E[A] E \left[ \underbrace{\sum_{i=1}^L (x_{i-j} x_{i-j})}_{X_{h_1}} \right] + E[N] \\ &= E[A] E[X_{h_1}] + E[N] \\ &= b \sqrt{\frac{\pi}{2}} \times \frac{L}{2} + 0 \\ &= \frac{Lb}{2} \sqrt{\frac{\pi}{2}}, \end{aligned}$$

and

$$\begin{aligned} \text{Var}[Z_{h_1}] &= \text{Var}[AX_{h_1}] + \text{Var}[N] \\ &= \text{Var}[X_{h_1}] E^2[A] + \text{Var}[A] E^2[X_{h_1}] + \text{Var}[X_{h_1}] \text{Var}[A] + \text{Var}[N] \\ &= \frac{L}{8} \left( b \sqrt{\frac{\pi}{2}} \right)^2 + \frac{b^2 (4 - \pi)}{2} \left( \frac{L}{2} \right)^2 + \frac{Lb^2 (4 - \pi)}{16} + \frac{L}{2} \sigma_n^2 \\ &= \frac{L^2 b^2}{8} (4 - \pi) + \frac{L}{2} \sigma_n^2, \end{aligned}$$

where  $L = 2\beta$  since only one bit is considered in this case.

Therefore

$$Z_{h_1} \sim G \left( \frac{Lb}{2} \sqrt{\frac{\pi}{2}}, \frac{L^2 b^2}{8} (4 - \pi) + \frac{L}{2} \sigma_n^2 \right). \quad (6.21)$$

Furthermore, it is assumed that for  $k > 1$ , each bit has the same distribution given in (6.21), and the mean and variance of the resulting  $Z_{h_1}$  is the summation of the means and variances of the individual bits. Therefore the PDF of  $Z_{h_1}$  for  $k$  bits can be expressed as

$$Z_{h_1} \sim G\left(\frac{kLb}{2}\sqrt{\frac{\pi}{2}}, \frac{kL^2b^2}{8}(4 - \pi) + \frac{kL}{2}\sigma_n^2\right). \quad (6.22)$$

Since this distribution is hypothesised to be a non-zero mean Gaussian random variable, the random variable  $Z'_{h_1}$  has to follow the same distribution given in (6.14). Also because the statistical properties of the different pilot bits remain the same, the overall squared correlation function will be the sum of individual one bit correlation functions all squared. As a result the non-centrality parameter for the fading scenario can be found and adjusted for different number of pilot bits with a  $k$  coefficient. Therefore

$$\lambda_{\text{Fading}} = \frac{E^2[Z_{h_1}]}{\text{Var}[Z_{h_1}]} = \frac{k\pi}{(4 - \pi) + \frac{2}{L} + \frac{4\sigma_n^2}{Lb^2}}. \quad (6.23)$$

In order to verify the hypothesis used above, a comparison between the non-central chi-square distributions resulting from substituting values of  $k = 1, 2, 3, \dots, 10$  in (6.23) and simulation results have to be performed. To control the comparison, a non-linear regression method to find the best possible fit to the simulation data is also used to find a vector for  $\lambda_{\text{Fading}}$  which is then used to predict  $p(Z'_{h_1}, 1, \lambda)$ .

The comparison between the values generated from substituting  $\lambda_{\text{Fading}}$  values in (6.14), non-linear regressive data fitting and simulation results are shown in Fig. 6.6. As can be seen in Fig. 6.6,  $p(Z'_{h_1}, 1, \lambda)$  can be accurately predicted in the presence of noise and fading by calculating  $\lambda_{\text{Fading}}$  for different number of pilot bits. The average error between the simulation and theoretical results is 2.3%.

### 6.3.3 Scenario 3, noise and fading with interleaving

In this scenario, the system uses a block chip interleaver de-interleaver pair to combat the effect of multi-path fading. Interleaving smears the fade power across the whole pilot sequence. The interleaver chosen for this chapter is a block chip interleaver. The interleaving depth is assumed to be higher than the coherence time of the channel in such a way that after interleaving, the adjacent chips have different fading coefficients. More information regarding interleaving can be found in Appendix E. Using interleavers for mitigating the effects of fading in the channel (which were highlighted in §5) is especially effective when the pilot length is small and a good quality of synchronisation is desired. At the front end of the receiver, the acquisition phase blindly de-interleaves the transmitted signal having knowledge of the bit and chip durations.

It is assumed that pass-band carrier synchronisation has already been achieved. Initially there is no chip synchronisation, so the de-interleaver will not work correctly because it performs based on faulty assumptions regarding the chip that starts a new block. The de-interleaved chip sequence is correlated with the locally generated sequence the same way as the previous two scenarios. The de-interleaving, correlation and time shifting will continue serially until the correct time shift has been reached indicating the synchronisation has been achieved. In that instance, the blind de-interleaver will re-arrange the chips

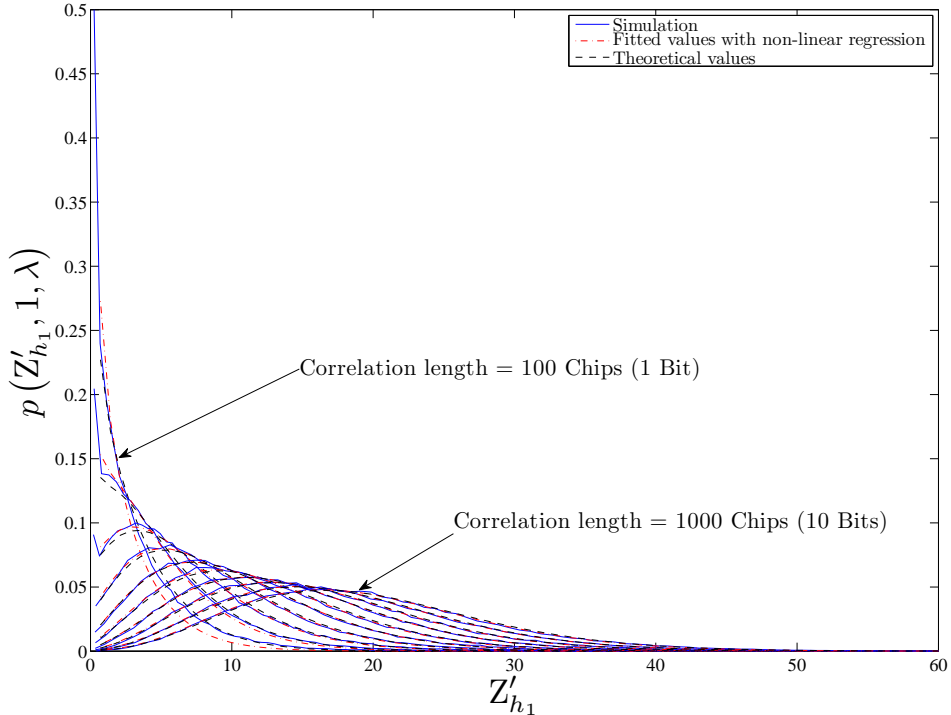


**Figure 6.6:** Comparison between the hypothesised, non-linear regression and simulation for predicting  $P(Z'_{h_1}, 1, \lambda)$ .

for every pilot bit correctly. The correlation result will then be higher than the threshold, and successful acquisition will be declared. The aim now is to derive the statistical models relating to  $Z_{h_0}$  and  $Z_{h_1}$ .

The correlator output for each trial can be expressed as

$$\begin{aligned} z[j] = & \sum_{i=1}^{2\beta} (a_i x_{i-\tau} x_{i-j}) + \sum_{i=2\beta+1}^{4\beta} (a_i x_{i-\tau} x_{i-j}) + \dots + \\ & \sum_{i=2\beta(k-1)+1}^{2\beta k} (a_i x_{i-\tau} x_{i-j}) + \sum_{i=1}^{2\beta k} (n_i x_{i-j}), \end{aligned} \quad (6.24)$$

where  $a_i$  is the fading coefficient for the  $i$ -th chip.

Given that now each transmitted chip is multiplied by a different fading coefficient, the approach to define  $Z_{h_0}$  and  $Z_{h_1}$  statistically is very similar to scenario 1. The only difference is in taking into account the statistical contribution of fading to the correlation function.

Therefore the mean and variance of  $Z_{h_0}$  for this scenario can be expressed as

$$\begin{aligned} E[Z_{h_0}] &= E \left[ \sum_{i=1}^L (a_i x_{i-\tau} x_{i-j}) \right] + E \left[ \sum_{i=1}^L (n_i x_{i-j}) \right] \\ &= \sum_{i=1}^L E[x_{i-\tau}] E[x_{i-j}] E[a_i] + \sum_{i=1}^L E[n_i x_{i-j}] \\ &= 0. \end{aligned}$$

$$\begin{aligned}
\text{Var}[Z_{h_0}] &= \text{Var} \left[ \sum_{i=1}^L (a_i x_{i-\tau} x_{i-j}) \right] + \text{Var} \left[ \sum_{i=1}^L (n_i x_{i-j}) \right] \\
&= \sum_{i=1}^L \mathbb{E}[x_{i-\tau}^2] \mathbb{E}[x_{i-j}^2] \mathbb{E}[a_i^2] - 0 + \sum_{i=1}^L \mathbb{E}[n_i^2] \mathbb{E}[x_{i-j}^2] - 0 \\
&= \frac{Lb^2}{2} + \frac{L\sigma_n^2}{2}.
\end{aligned}$$

So

$$Z_{h_0} \sim G \left( 0, \frac{L}{2} (b^2 + \sigma_n^2) \right). \quad (6.25)$$

As  $Z_{h_0}$  is a Gaussian distribution,  $Z'_{h_0}$  follows the same distribution given in (6.13). The only difference between the two scenarios is the variance of  $Z_{h_0}$ , which is normalised in any case.

The mean and variance of  $Z_{h_1}$  for this scenario can be expressed as

$$\begin{aligned}
\mathbb{E}[Z_{h_1}] &= \mathbb{E} \left[ \sum_{i=1}^L a_i (x_{i-\tau}^2) \right] + \mathbb{E} \left[ \sum_{i=1}^L (n_i x_{i-j}) \right] \\
&= \sum_{i=1}^L L \mathbb{E}[a_i] \mathbb{E}[x_{i-\tau}^2] + \sum_{i=1}^L \mathbb{E}[n_i x_{i-j}] \\
&= \frac{Lb}{2} \sqrt{\frac{\pi}{2}} + 0.
\end{aligned}$$

$$\begin{aligned}
\text{Var}[Z_{h_1}] &= \text{Var} \left[ \sum_{i=1}^L (a_i x_{i-j} x_{i-j}) \right] + \text{Var} \left[ \sum_{i=1}^L (n_i x_{i-j}) \right] \\
&= \mathbb{E} \left[ \sum_{i=1}^L a_i^2 (x_{i-\tau}^2)^2 \right] - \mathbb{E}^2 \left[ \sum_{i=1}^L a_i (x_{i-\tau}^2) \right] + \sum_{i=1}^L \mathbb{E}[n_i^2] \mathbb{E}[x_{i-j}^2] - 0 \\
&= \sum_{i=1}^L \left( \mathbb{E}[a_i^2 x_{i-\tau}^4] - \left( \frac{b}{2} \sqrt{\frac{\pi}{2}} \right)^2 \right) + \frac{L\sigma_n^2}{2} \\
&= L \left\{ \frac{b^2 (6 - \pi) + 4\sigma_n^2}{8} \right\},
\end{aligned}$$

where  $L = 2k\beta$  in this case and  $k = 1, 2, 3, \dots$  represents the number of pilot bits used in the correlation function.

So

$$Z_{h_1} \sim G \left( \frac{Lb}{2} \sqrt{\frac{\pi}{2}}, L \left\{ \frac{b^2 (6 - \pi) + 4\sigma_n^2}{8} \right\} \right), \quad (6.26)$$

which, after squaring will follow the distribution given in (6.14), with a non-centrality parameter of

$$\lambda_{\text{Interleaving}} = \frac{L\pi}{(6 - \pi) + \frac{4\sigma_n^2}{b^2}}. \quad (6.27)$$

### 6.3.4 Probability of false alarm, accurate statistical analysis

The probability of false alarm ( $P_F$ ) was introduced in §4.2. This part presents the approach used to calculate the  $P_F$  when acquisition is analysed using the CCS. The visual representation of  $P_F$  is shown in Fig.6.7. It is clear that  $P_F$  can be expressed by integrating the expression presented in (6.13) from the threshold ( $Z_{Th}$ ) to infinity. Therefore

$$P_F = \int_{Z_{Th}}^{\infty} p(Z'_{h_0}, 1) dZ'_{h_0}. \quad (6.28)$$

Since  $Z'_{h_0}$  follows a central chi-square distribution, the integral can be found as

$$P_F = \int_{Z_{Th}}^{\infty} \frac{1}{\sqrt{2\pi Z'_{h_0}}} \exp\left(\frac{-Z'_{h_0}}{2}\right) dZ'_{h_0}$$

Let  $\sqrt{Z'_{h_0}} = x \Rightarrow \frac{1}{2\sqrt{Z'_{h_0}}} dZ'_{h_0} = dx$  then  $\frac{1}{2x} dZ'_{h_0} = dx \Rightarrow dZ'_{h_0} = 2x dx$ .

Rewriting the integrand

$$\begin{aligned} P_F &= \frac{2}{\sqrt{2\pi}} \int_{Z_{Th}}^{\infty} e^{-\frac{x^2}{2}} dx \\ &= \frac{2}{\sqrt{2\pi}} \sqrt{\frac{\pi}{2}} \operatorname{erf}\left(\frac{x}{\sqrt{2}}\right) \end{aligned}$$

So

$$\begin{aligned} P_F &= \operatorname{erf}\left(\frac{\sqrt{Z'_{h_0}}}{\sqrt{2}}\right) \Big|_{Z_{Th}}^{\infty} \\ &= 1 - \operatorname{erf}\left(\frac{\sqrt{Z_{Th}}}{\sqrt{2}}\right). \end{aligned} \quad (6.29)$$

### 6.3.5 Probability of detection, accurate statistical analysis

The probability of detection ( $P_D$ ) was introduced in §4.2. This part presents the approach used to calculate the  $P_D$  when acquisition is analysed using the CCS. The visual representation of  $P_D$  is shown in Fig.6.7. It is clear that  $P_D$  can be expressed by integrating the expression presented in (6.14) from the threshold to infinity. Therefore the probability of detection ( $P_D$ ) can be expressed as

$$\begin{aligned} P_D &= \int_{Z_{Th}}^{\infty} p(Z'_{h_1}, 1, \lambda) dZ'_{h_1} \\ &= \int_{Z_{Th}}^{\infty} \frac{1}{2} \exp\left(\frac{-Z'_{h_1} + \lambda}{2}\right) \left(\frac{Z'_{h_1}}{\lambda}\right)^{-\frac{1}{4}} I_{-\frac{1}{2}}\left(\sqrt{Z'_{h_1} \lambda}\right) dZ'_{h_1} \end{aligned}$$

Let  $\sqrt{\lambda Z'_{h_1}} = x \Rightarrow \frac{\sqrt{\lambda}}{2\sqrt{Z'_{h_1}}} dZ'_{h_1} = dx$  then  $\frac{\lambda}{2x} dZ'_{h_1} = dx \Rightarrow dZ'_{h_1} = \frac{2x}{\lambda} dx$ .

Rewriting the integrand

$$\begin{aligned}
&= \frac{2}{\lambda} \int_{Z_{Th}}^{\infty} \exp\left(\frac{-\frac{x^2}{\lambda} + \lambda}{2}\right) x \left(\frac{x^2}{\lambda^2}\right)^{-\frac{1}{4}} I_{-\frac{1}{2}}(x) dx \\
&= \frac{2}{\lambda} \int_{Z_{Th}}^{\infty} \exp\left(\frac{-(x^2 + \lambda^2)}{2\lambda}\right) \frac{xx^{-\frac{1}{2}}}{\lambda^{-\frac{1}{2}}} I_{-\frac{1}{2}}(x) dx \\
&= \frac{2}{\lambda} \int_{Z_{Th}}^{\infty} \exp\left(\frac{-(x^2 + \lambda^2)}{2\lambda}\right) \sqrt{x\lambda} I_{-\frac{1}{2}}(x) dx.
\end{aligned}$$

Since  $I_{-\frac{1}{2}}(x) = \sqrt{\frac{2}{\pi}} \frac{\cosh(x)}{\sqrt{x}}$ ,

$$P_D = \frac{\sqrt{\lambda}}{\lambda} \sqrt{\frac{2}{\pi}} \int_{Z_{Th}}^{\infty} \exp\left(\frac{-(x^2 + \lambda^2)}{2\lambda}\right) \sqrt{x} \frac{\cosh(x)}{\sqrt{x}} dx.$$

Since  $\cosh(x) = \frac{\exp(x) + \exp(-x)}{2}$ ,

$$\begin{aligned}
P_D &= \frac{\sqrt{\lambda}}{2\lambda} \sqrt{\frac{2}{\pi}} \int_{Z_{Th}}^{\infty} \exp\left(\frac{-(x^2 + \lambda^2)}{2\lambda}\right) (\exp(x) + \exp(-x)) dx \\
&= \frac{\sqrt{\lambda}}{2\lambda} \sqrt{\frac{2}{\pi}} \left\{ \int_{Z_{Th}}^{\infty} \exp\left(\frac{-(x^2 + \lambda^2)}{2\lambda}\right) \exp(x) dx + \int_{Z_{Th}}^{\infty} \exp\left(\frac{-(x^2 + \lambda^2)}{2\lambda}\right) \exp(-x) dx \right\} \\
&= \frac{\sqrt{\lambda}}{2\lambda} \sqrt{\frac{2}{\pi}} \left\{ \int_{Z_{Th}}^{\infty} \exp\left(\frac{-(x - \lambda)^2}{2\lambda}\right) dx + \int_{Z_{Th}}^{\infty} \exp\left(\frac{-(x + \lambda)^2}{2\lambda}\right) dx \right\}
\end{aligned}$$

Since  $\frac{d\text{erf}(y)}{dx} = 2 \frac{\exp(-y^2)}{\sqrt{\pi}}$  it can be shown that  $\int_{Z_{Th}}^{\infty} \exp\left(-\frac{y^2}{n}\right) dy = \frac{\sqrt{\pi}}{2} \sqrt{n} \text{erf}\left(\frac{x}{\sqrt{n}}\right)$ . So for the first integral  $y = \lambda - x \Rightarrow dx = -dy$ , as a result the first integral can be evaluated as

$$-\int_{Z_{Th}}^{\infty} \exp\left(\frac{y^2}{2\lambda}\right) dy = -\frac{\sqrt{\pi}}{2} \sqrt{2\lambda} \text{erf}\left(\frac{y}{\sqrt{2\lambda}}\right) = -\sqrt{\frac{\pi}{2}} \sqrt{\lambda} \text{erf}\left(\frac{\lambda - x}{\sqrt{2\lambda}}\right)$$

The second integral can be similarly evaluated as  $\sqrt{\frac{\pi}{2}} \sqrt{\lambda} \text{erf}\left(\frac{\lambda + x}{\sqrt{2\lambda}}\right)$  by choosing  $y = \lambda + x$ . Therefore the overall result is

$$\begin{aligned}
P_D &= \frac{\sqrt{\lambda}}{2\lambda} \sqrt{\frac{2}{\pi}} \sqrt{\lambda} \left( \text{erf}\left(\frac{\lambda + x}{\sqrt{2\lambda}}\right) - \text{erf}\left(\frac{\lambda - x}{\sqrt{2\lambda}}\right) \right) \\
&= \frac{1}{2} \left( \text{erf}\left(\frac{\lambda + x}{\sqrt{2\lambda}}\right) + \text{erf}\left(\frac{x - \lambda}{\sqrt{2\lambda}}\right) \Big|_{Z_{Th}}^{\infty} \right), \quad x = \sqrt{\lambda Z'_{h_1}} \\
&= \frac{1}{2} \left( \text{erf}\left(\sqrt{\frac{Z'_{h_1}}{2}} + \sqrt{\frac{\lambda}{2}}\right) + \text{erf}\left(\sqrt{\frac{Z'_{h_1}}{2}} + \sqrt{\frac{\lambda}{2}}\right) \Big|_{Z_{Th}}^{\infty} \right) \\
&= 1 - \frac{\text{erf}\left(\sqrt{\frac{Z_{Th}}{2}} - \sqrt{\frac{\lambda}{2}}\right) + \text{erf}\left(\sqrt{\frac{Z_{Th}}{2}} + \sqrt{\frac{\lambda}{2}}\right)}{2}.
\end{aligned} \tag{6.30}$$

The expression given in (6.30) can be used for any of the three scenarios presented in this chapter. For each scenario, the value of  $\lambda$  has to be calculated using (6.15), (6.23), or (6.27) depending on what scenario is being considered.

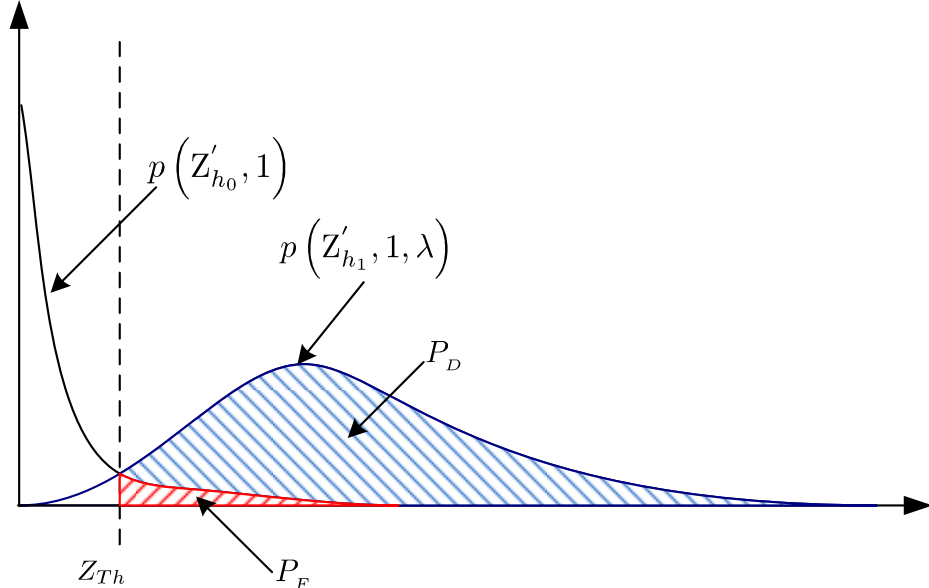


**Figure 6.7:** Visual representation of  $P_D$  and  $P_F$  based on  $p\left(Z'_{h_0}, 1\right)$  and  $p\left(Z'_{h_1}, 1, \lambda\right)$ .

## 6.4 Results and Discussion

In the previous section, the output of the square law device was statistically modeled for different scenarios. The difference in performance between each scenario can now be predicted analytically using only the non-centrality parameter. As a result, the performance benchmarks ( $P_F$  and  $P_D$ ) can be calculated using the exact expressions given in (6.13) and (6.14). This section presents a comparison between the simulation results and the analytical expressions and discusses the findings.

Modeling the acquisition phase is fundamentally a statistical problem, therefore, the system was simulated using the Monte Carlo method. The square of the correlation function was computed for each trial with different spreading sequences as well as fading coefficients and noise samples. For each realisation of the correlation function, a thersholding and counting operation was performed. Initially, a threshold value of zero was used and the number of false alarms ( $Z'_{h_0} > Z_{Th}$ ) and detections ( $Z'_{h_1} > Z_{Th}$ ) were recorded. The threshold was then increased by a step-size of 10, and the process was repeated. Finally the values of detections and false alarms were normalised, giving  $P_D$  and  $P_F$  respectively. The correlation length of the pilot has also been altered to observe its effects on acquisition performance. For the signal-to-noise ratio (SNR) of interest, the noise variance is adjusted by the value of the energy per bit  $E_b$  and the number of bits used in the correlator of the acquisition phase. The value of the fading mode is fixed to  $b = \sqrt{\frac{1}{2}}$ , causing the average power of the fading coefficients to be unity [174, 175]. It should be noted that the theoretical expressions derived in this contribution give accurate results for all values of  $b$ .

The simulated ROC plots are compared to the analytical results obtained by substituting the appropriate value of  $\lambda$ , into (6.30) and plotting it against  $P_F$  calculated from (6.29). Ideally,  $P_F$  is 0; however, a residual  $P_F$  exists due to noise, fading and the self-interference of chaotic sequences, the effects are particularly strong for lower values of  $P_D$ . As a result an acceptable region of operation for acquisition is usually defined. In this thesis this region of operation is  $P_F \in [0, 0.1]$ ; that is, a probability of false alarm between 0 and 10%.

The simulation results presented in this section, can be compared to the ones presented in Figs. 5.3-5.6 for the fading case only. However, it should be noted that Figs. 5.3-5.6 only present a theoretical upper-bound whereas the theoretical results presented in this chapter, not only match each simulation results, they cover, noise, fading and interleaving scenarios.

The simulations are designed to verify two issues; first, that for all three scenarios considered, the analytical and approximate results agree with the simulation results; and second, to quantify the improvement gained by the chip-interleaving technique, for small correlation lengths.

Fig. 6.8 presents the ROC results for an SNR of 2dB and a correlation length of 100 chips. It is observed that in the region of low  $P_F$ , ( $P_F \in [0, 0.1]$ ) the probability of detection is also low. Furthermore, as the fading coefficients reduce the correlation peak, they increase the probability of false alarm pulling the curves down. The interleaved result presented show that by using chip interleaving, the performance can be improved by approximately 12% at  $P_F = 0.1$ . The maximum error between the statistical approach and simulation is 2.0%. The error is attributed to the number of trials and is expected the decrease with larger trial sets.

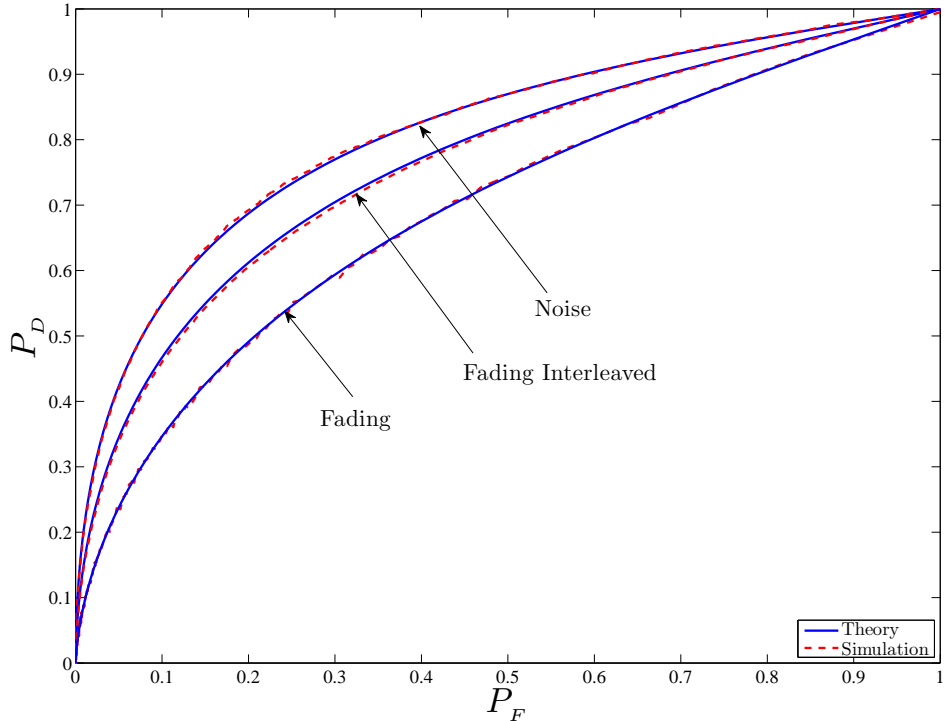
Fig 6.9 presents the ROC results for an SNR of 8dB and a correlation length of 100 chips ( $k= 1$ ). The noise only result shows a significant improvement over the 2 dB result (shown in Fig. 6.8), as expected. However, it should be noted that the fading result has not improved significantly due to the multiplicative way fading coefficients affect correlation results. However, the improvement introduced by interleaving is significant. It is observed that the performance is improved by approximately 27%, which is significant given that the correlator has only 1 bit (100 chips) to work with. The maximum error between the statistical approach and simulation is 1.2% .

Fig 6.10 presents the ROC results for an SNR of 8dB and a correlation length of 300 chips ( $k= 3$ ). In this case each correlation period has more than one fading coefficient. The first observation is that the performance for the fading scenario without interleaving has improved compared to Fig. 6.9. This is attributed to the changing of Rayleigh fading coefficients within the correlation length which reduces the adverse effects of fading on the correlation of chaotic sequence. The noise only and interleaved scenario performances have improved as expected, since there is more information available to the correlator. The maximum error between the statistical approach and simulation for this ROC result is 1.1%.

The results shown in Figs. 6.8, 6.9 and 6.10 are directly comparable to those presented in §5.3 and [93, 94]. In these references, only the upper-bound results were presented.

Fig. 6.11 presents a 3D rendition of the percentage improvement in  $P_D$  attained by applying the interleaver for various values of  $k$ . The improvement window is widest for  $P_F \in [0, 0.1]$  which is highly desirable. Also, as the value of  $k$  increases, the region of improvement decreases. However, this is of no concern as with the increase in correlation length, the performance improves. The 20-30% improvement

gained for  $P_F \in [0, 0.1]$  with  $k < 3$  is very useful when fast synchronisation is desired in a fading channel.



**Figure 6.8:** ROC plot with three scenarios, for SNR = 2 dB and correlation length = 100 chips.

## 6.5 Summary

This chapter presented a new statistical analysis method, called the CCS, to accurately model the correlation function of the chaotic sequences. The CCS is then used to model the acquisition stage performance in a noise, faded and interleaved channel. It was shown that the performance can be mathematically predicted by adjusting the non-centrality parameter in the probability distribution of the correlator output. It was shown that fading degrades the acquisition stage performance. It was also shown that a blind interleaver/de-interleaver pair mitigates the effects of fading on the channel, especially if the correlation length used for the acquisition phase is short.

The tracking stage always follows sequence acquisition in the synchronisation for CDS-SS systems. Since the tracking stage also relies on correlation, it is important to apply the CCS approach to the tracking stage to be able to determine the statistical behaviour of the tracking stage error curves. Applying the CCS method to the tracking stage is the subject of the next chapter.

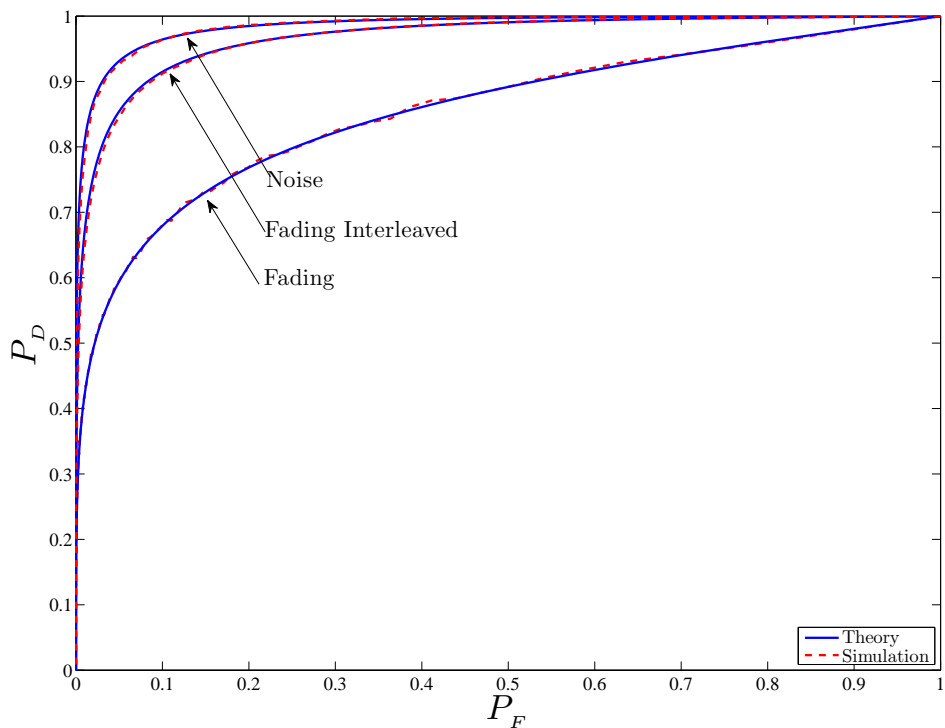


**Figure 6.9:** ROC plot with three scenarios, for SNR = 8 dB and correlation length = 100 chips.

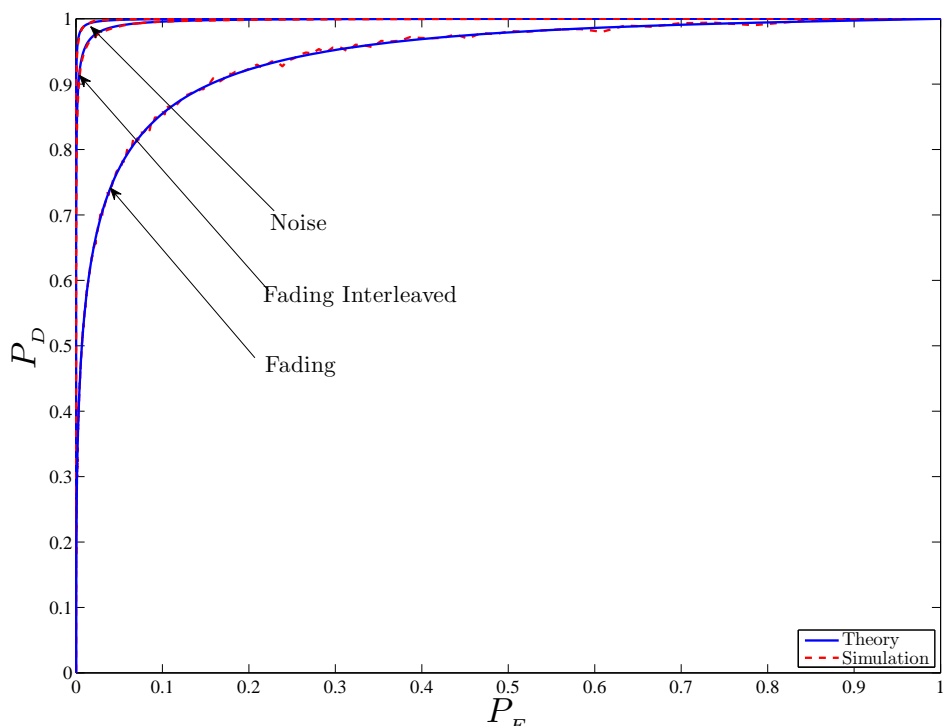


**Figure 6.10:** ROC plot with three scenarios, for SNR = 8 dB and correlation length = 300 chips.

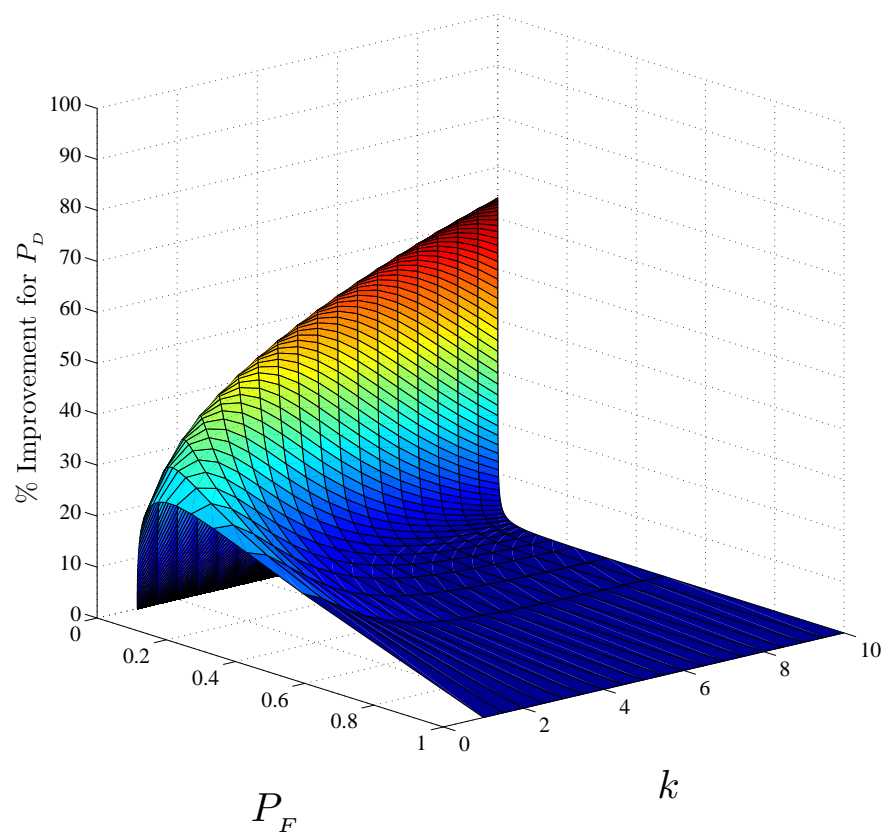


**Figure 6.11:** Percentage improvement for  $P_D$  as a result of using the interleaver/de-interleaver pair. The improvement is measured based on the noise only performance. The SNR in this case is 4 dB.



# Chapter 7

## Statistical Analysis of CDS-SS Tracking

### 7.1 Introduction

The chaotic correlation statistics (CCS) approach was introduced in §6.2 and applied to the acquisition stage in §6.3. This chapter highlights the need for an accurate statistical analysis for the CDS-SS tracking stage by comparing the conventional binary sequence based tracking loop error curves with the non-binary chaos-based ones. Moreover, the application of CCS to the tracking stage and derivation of the statistical properties of different points of the error curve are presented in this chapter. This is achieved by statistically describing the chaos-based correlation function using CCS. The aim of this chapter is to examine the chaos-based non-coherent tracking loop using CCS for the first time. The accuracy of CCS is shown to be very high when compared to the simulation results. The material presented in this chapter also appears in [176] First §7.2 applies the CCS analysis method to the tracking loop and presents the results. Then the comparison of the simulation and analytical results are presented in §7.3. Finally §7.4 summarises the chapter.

### 7.2 Code Tracking, An Accurate Statistical Analysis Using CCS

The tracking loop analysis presented in §5.4 utilises correlation of chaos-based sequences. The central issue in that analysis is the assumption that the correlation function of the chaotic sequence remains constant for different chaotic spreading codes generated from the same chaotic map. However, this assumption is based on the treatment of conventional spreading codes such as PN codes, Walsh functions etc. that are binary. Chaotic spreading codes on the other hand, are non-binary and can take any value between two set bounds. Therefore, for different initial conditions the chaotic correlation function changes. This means that applying the conventional theoretical models to chaotic spreading codes can only give an approximation to the true behaviour of the chaos-based correlation function.

This section applies the CCS analysis previously derived to a non-coherent delay lock tracking loop. The correlation function of the Logistic map is revisited first for convenience and the results of that analysis are then used to derive the statistical models related to the critical points of the S-curve. The PDF of the

Logistic map is given in (6.1) and the mean and variance of it have been previously shown to be 0 and  $\frac{1}{2}$  respectively.

Figs. 7.1 (a) and (b) show the correlation function and square of the correlation function for different initial conditions of the Logistic map respectively. Unlike the previous treatments of chaos-based correlation, the correlation function presented here has a distribution and the correlation peak has a different distribution compared to the rest of the correlation function.

Given the statistical properties above, the statistical correlation function of the chaotic map can be written in discrete form as

$$\mathbf{R}_h [\delta] = \sum_{i=1}^L (x_{i-\tau} x_{i-\delta}), \quad (7.1)$$

where  $\mathbf{R}_h [.]$  denotes the statistical correlation function which is acquired over  $h$  trials,  $\delta$  is the normalised time delay previously introduced,  $L$  is the correlation length,  $x_{i-\tau}$  is the transmitter pilot sequence which is being tracked and  $x_{i-\delta}$  is the receiver, locally generated, pilot sequence. The difference between  $R[.]$  given in (5.51) and  $\mathbf{R}_h [.]$  given above is that  $R[.]$  is the conventional correlation function used for binary spreading codes and therefore has the same value if the same correlation length is used, whereas  $\mathbf{R}_h [.]$  is a random vector with different distributions along its length.

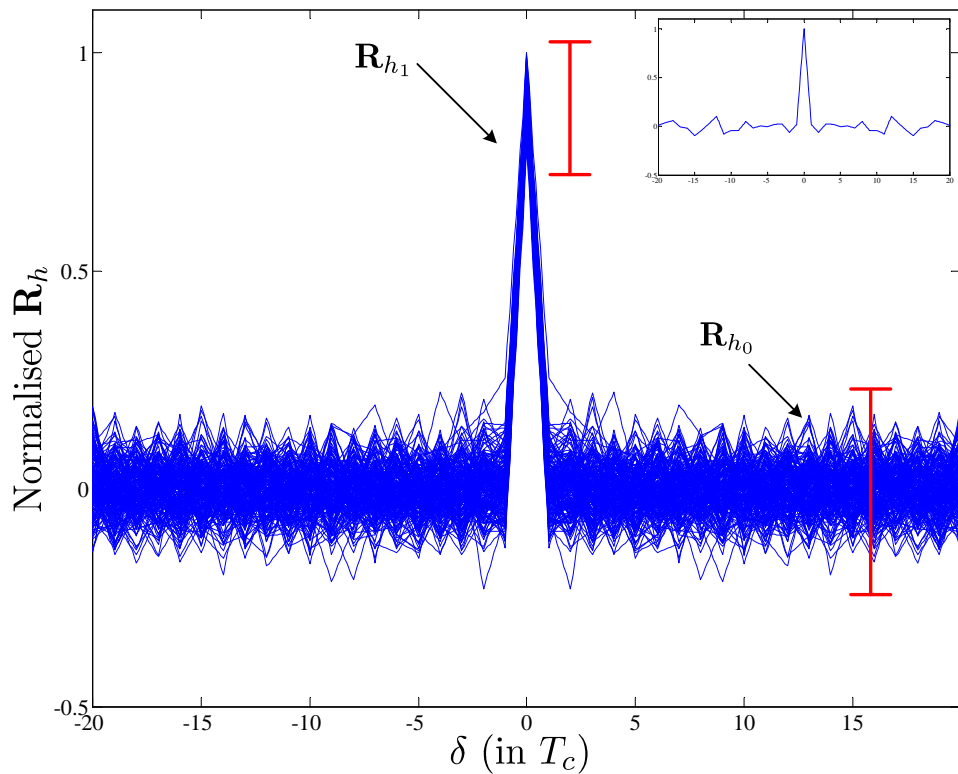
It is clear from (7.1) that there are two types of  $\mathbf{R}_h [.]$  values. The first type is generated when  $x_{i-\tau}$  and  $x_{i-\delta}$  are not aligned in time, i.e.  $\delta \neq \tau$ . Given the orthogonality of chaotic sequences, the resulting value for  $\mathbf{R}_h [.]$  has to be close to zero. The second type is generated when  $x_{i-\tau}$  and  $x_{i-\delta}$  are aligned in time, i.e.  $\delta = \tau$ . This corresponds to the auto-correlation peak. As a result the correlation function can be rewritten as

$$\mathbf{R}_{h_0} = \mathbf{R}_h [\delta \neq \tau] = \sum_{i=1}^L (x_{i-\tau} x_{i-\delta}), \quad (7.2)$$

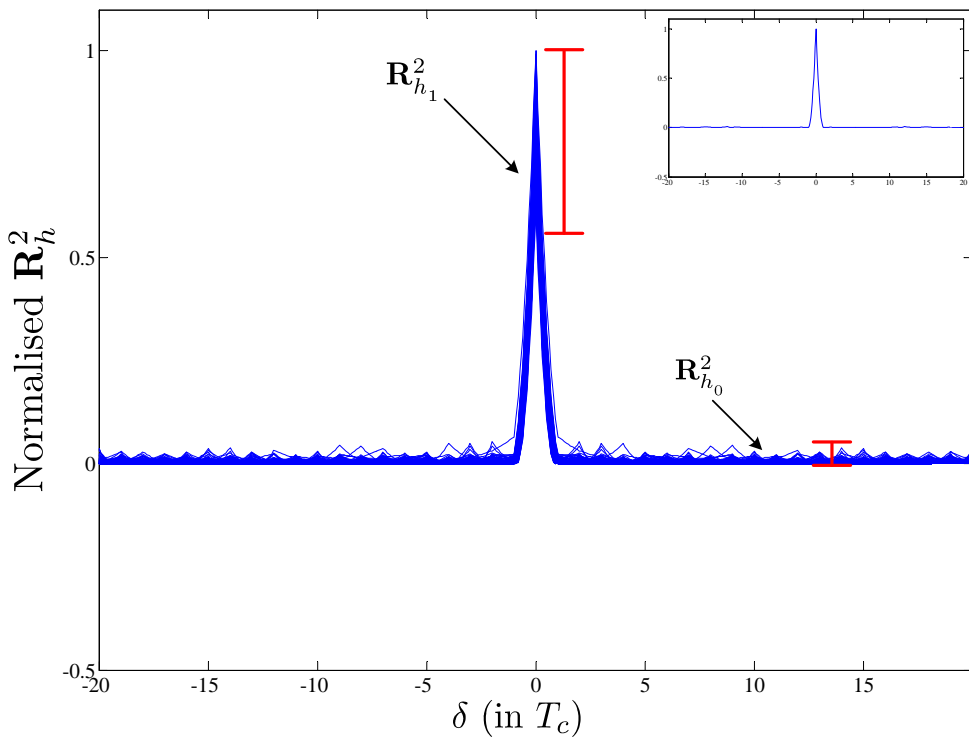
$$\mathbf{R}_{h_1} = \mathbf{R}_h [\delta = \tau] = \sum_{i=1}^L (x_{i-\tau} x_{i-\tau}), \quad (7.3)$$

where  $h_0$  denotes events that the spreading codes are not aligned and  $h_1$  denotes events in which the spreading codes are aligned. Although for each realisation of the pilot sequence  $x_{i-\tau}$  and  $x_{i-\delta}$  are known, when all the possible chaotic pilot realisations are being examined,  $x_{i-\tau}$  and  $x_{i-\delta}$  will be random variables with the PDF given in (5.51). Now  $\mathbf{R}_h [\delta]$  can be statistically modelled for both  $h_0$  and  $h_1$ .

Considering (7.2), it is clear that  $\mathbf{R}_{h_0}$  is the product of chaotic values summed for the correlation length for each trial. Given that for  $h$  trials both  $x_{i-\tau}$  and  $x_{i-\delta}$  are independent random variables, it is possible to find the distribution of the product of these and subsequently find the distribution of  $\mathbf{R}_{h_0}$ . However, noting that the correlation in tracking is performed over a large correlation period (typically  $L > 100$ ), the correlation result will be the sum of many independent, identically distributed, random variables. As a result, central limit theorem can be invoked with a high degree of accuracy which gives the PDF of (7.2) as Gaussian.



(a) Normalised correlation function



(b) Output of the square-law device for one branch.

**Figure 7.1:** Normalised correlation function (a) and square of the correlation function (b) for different initial conditions of the Logistic map. The assumption used in [93, 95, 166, 177] are shown in the top right of both figures for comparison.

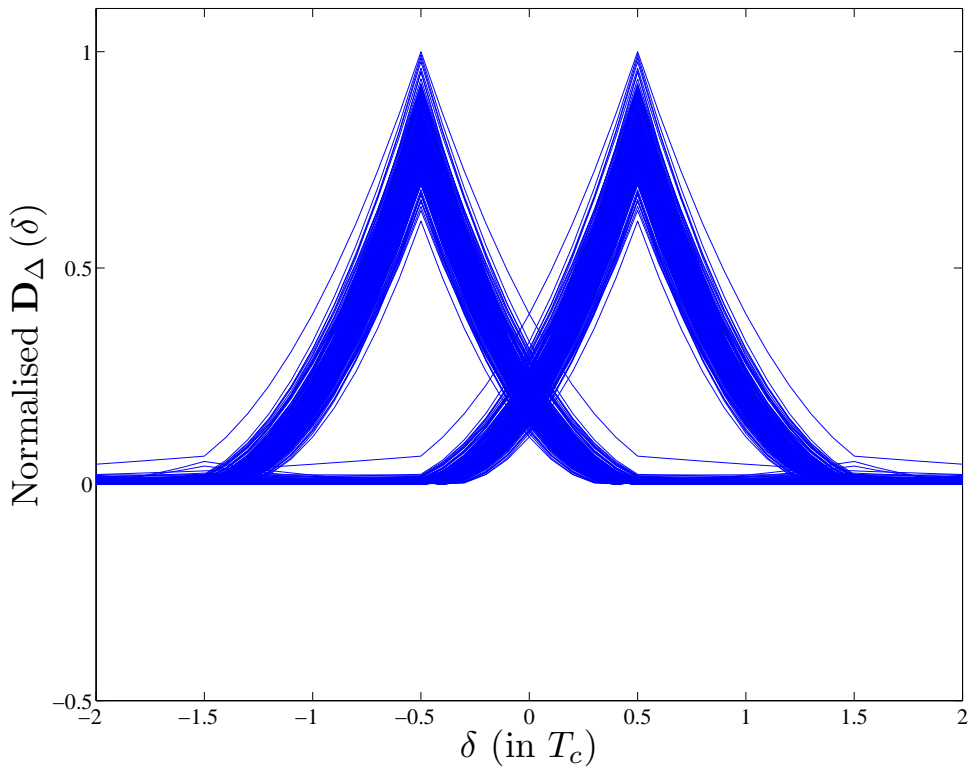


**Figure 7.2:** The outputs of the square-law devices for the two branches of the tracking loop. When one correlation is at its peak the other one has a small value.

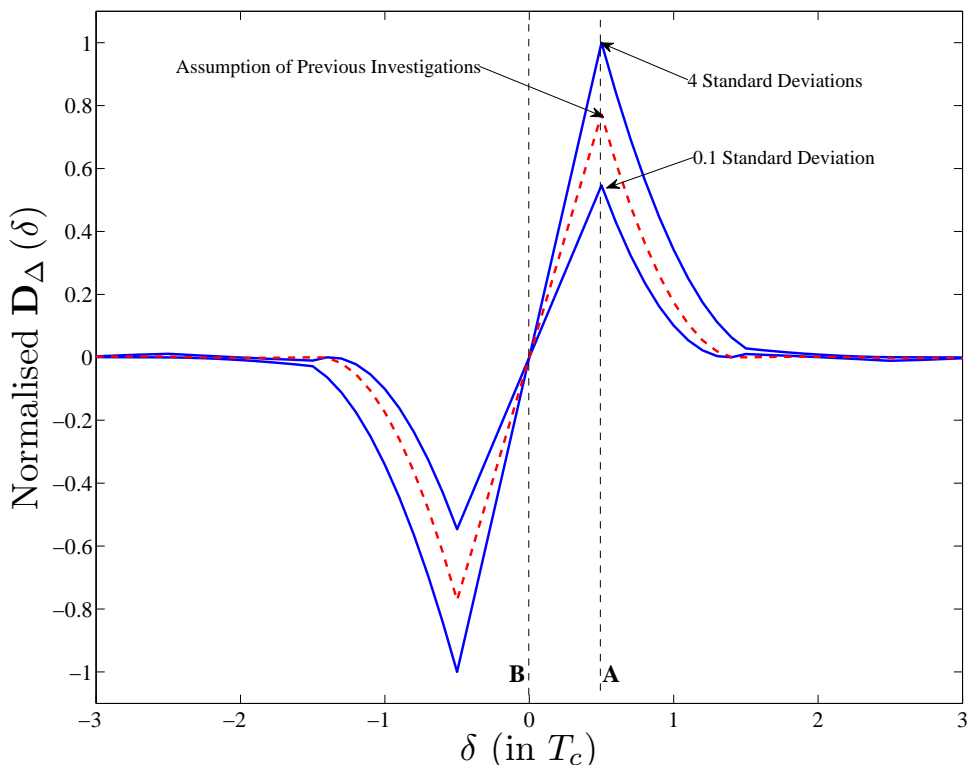


**Figure 7.3:** Upper and lower limits of the S-curve as well as the chosen points for the distribution. The assumption used [46, 167] is shown with a dashed line.

In order to describe (7.2) statistically, the mean and variance are also needed. Therefore

$$\begin{aligned} E[\mathbf{R}_{h_0}] &= E \left[ \sum_{i=1}^L (x_{i-\tau} x_{i-\delta}) \right] \\ &= L \times E[x_{i-\tau}] E[x_{i-\delta}] \\ &= 0, \end{aligned} \quad (7.4)$$

where  $E[\cdot]$  denotes the expected value.

The variance can be determined as follows

$$\begin{aligned} \sigma_{\mathbf{R}_{h_0}}^2 &= E[\mathbf{R}_{h_0}^2] - E^2[\mathbf{R}_{h_0}] \\ &= \sum_{i=1}^L E[x_{i-\tau}^2] E[x_{i-\delta}^2] \\ &= \frac{L}{4}. \end{aligned} \quad (7.5)$$

In the above formula since  $E[x] = 0$ ,  $E[x^2] = \sigma_x^2$ .

Given the above,

$$\mathbf{R}_{h_0} \sim G \left( 0, \frac{L}{4} \right), \quad (7.6)$$

which is a Gaussian distribution that describes the statistical behavior of  $\mathbf{R}_h[\delta \neq \tau]$ .

Similarly considering (7.3),  $\mathbf{R}_{h_1}$  can be modeled as a random variable with a Gaussian distribution with the mean and variance of

$$\begin{aligned} E[\mathbf{R}_{h_1}] &= E \left[ \sum_{i=1}^L (x_{i-\tau}^2) \right] \\ &= \frac{L}{2}, \end{aligned} \quad (7.7)$$

and

$$\begin{aligned} \sigma_{\mathbf{R}_{h_1}}^2 &= E[\mathbf{R}_{h_1}^2] - E^2[\mathbf{R}_{h_1}] \\ &= \sum_{i=1}^L \{E[x_{i-\tau}^4] - E^2[x_{i-\tau}^2]\} \\ &= L \left\{ \frac{3}{8} - \frac{1}{4} \right\} \\ &= \frac{L}{8}, \end{aligned} \quad (7.8)$$

respectively.

Therefore  $\mathbf{R}_{h_1}$  can be statistically expressed as

$$\mathbf{R}_{h_1} \sim G \left( \frac{L}{2}, \frac{L}{8} \right), \quad (7.9)$$

which is a Gaussian distribution that describes the statistical behavior of the auto-correlation peak of the chaotic spreading codes.

Considering the case where additive white Gaussian noise (AWGN) is present in the channel, the two PDFs can be re-expressed as

$$\mathbf{R}_h[\delta] \sim \begin{cases} G\left(0, \frac{L}{4} + \frac{L\sigma_N^2}{2}\right) & \delta \neq \tau \\ G\left(\frac{L}{2}, \frac{L}{8} + \frac{L\sigma_N^2}{2}\right) & \delta = \tau \end{cases}, \quad (7.10)$$

where  $\sigma_N^2$  is the residual noise variance and it is assumed that  $E[\mathbf{N}] = 0$ .

Since the tracking loop is non-coherent, each branch has a square-law device that squares every sample of  $\mathbf{R}_h[\delta]$  given above. The PDF of the squared correlation function can be expressed for  $\mathbf{R}_{h_0}$  and  $\mathbf{R}_{h_1}$  separately.

If  $\mathbf{R}_{h_0}$  is squared and then normalised by its variance, the result is a chi-square distribution with one degree of freedom with the PDF

$$P\left(\mathbf{R}'_{h_0}, 1\right) = \frac{1}{\sqrt{2\pi\mathbf{R}'_{h_0}}} \exp\left(\frac{-\mathbf{R}'_{h_0}}{2}\right), \quad (7.11)$$

where  $\mathbf{R}'_{h_0} = \frac{\mathbf{R}_{h_0}^2}{\sigma_{\mathbf{R}_{h_0}}^2}$ .

If  $\mathbf{R}_{h_1}$  is squared and then normalised by its variance, the resulting distribution is non-central chi-square with one degree of freedom and the non-centrality parameter  $\lambda$ . The PDF can then be expressed as (7.12) where  $\mathbf{R}'_{h_1} = \frac{\mathbf{R}_{h_1}^2}{\sigma_{\mathbf{R}_{h_1}}^2}$ ,  $\lambda = \frac{2L}{1+4\sigma_N^2}$ , and  $I(.)$  is the modified Bessel function of the first kind.

$$P\left(\mathbf{R}'_{h_1}; 1, \lambda\right) = \frac{1}{2} \exp\left(\frac{-\mathbf{R}'_{h_1} + \lambda}{2}\right) \left(\frac{\mathbf{R}'_{h_1}}{\lambda}\right)^{-\frac{1}{4}} I_{\frac{-1}{2}}\left(\sqrt{\mathbf{R}'_{h_1}\lambda}\right) \quad (7.12)$$

As can be seen from the derivation above, the correlation function of a chaotic spreading code is now expressed using a statistical model. Given that the correlation function of the chaotic codes changes with every trial, this statistical approach is much more useful in describing the behavior as opposed to the traditional method of expressing the correlation function used for binary type spreading codes. The analysis presented above is valid for long sequence lengths. It has been shown in [171] that the short sequence length does not follow a Gaussian distribution. However, normally the sequence length for tracking has to be long enough to allow sufficient resolution for *fine synchronisation*.

Now that the statistical model of the correlation function is in place, it can be applied to the chaos-based non-coherent tracking loop. The statistical correlation function method is not limited to chaos-based systems, and it can be applied to all non-binary spreading codes.

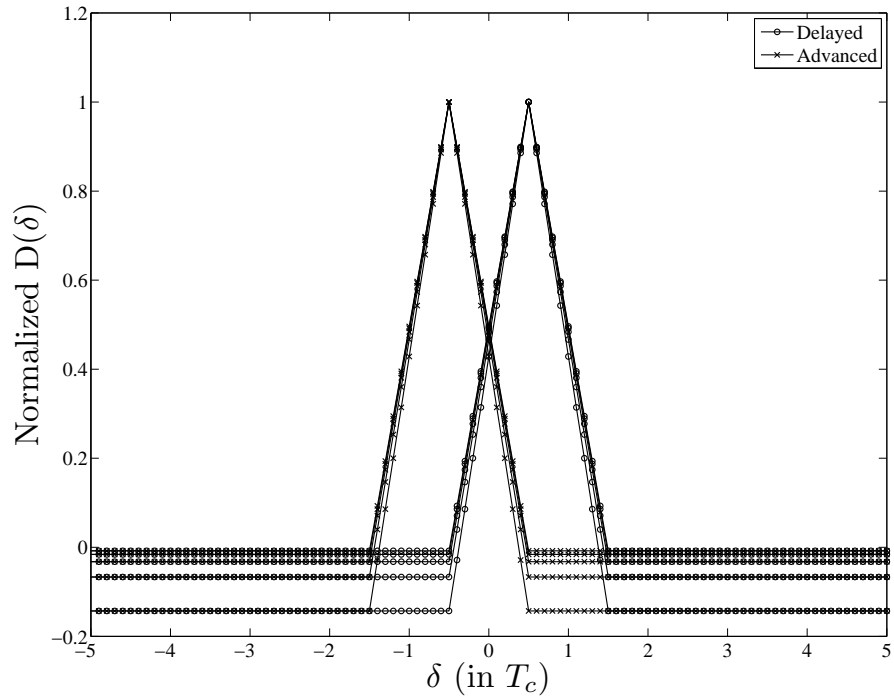


**Figure 7.4:** Early and late correlation functions for correlation lengths of 8, 16, 32, 64 and 128 before the square law device.

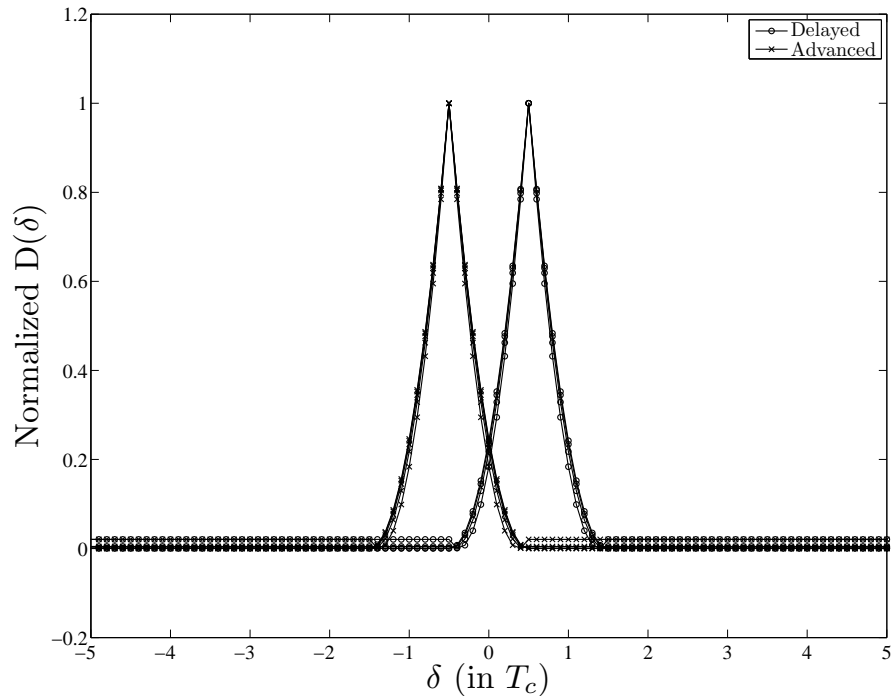


**Figure 7.5:** Early and late correlation functions for correlation lengths of 8, 16, 32, 64 and 128 after the square law device.

There are two issues to be considered here; first, the tracking loop filters cannot attenuate all the noise terms to zero and there always remains some residue noise which has to be taken into account in the statistical analysis of  $D_{\Delta}(\delta)$ . Therefore from now on, the statistical analysis will focus on  $D_{\Delta}(\delta)$  with the understanding that the correlation functions will have some residue noise in them.

Second, although  $D_\Delta(\delta)$  is ideally a DC term for conventional binary spreading codes, for chaotic spreading codes it is only so for one representation of the tracking loop. If many experiments are performed for the same chaotic map,  $D_\Delta(\delta)$  will have a distribution even in the noiseless case because the correlation function of chaotic spreading codes varies with the change of the spreading code.

The statistical error signal will be denoted by  $\mathbf{D}_\Delta(\delta)$ . It has to be noted that  $D_\Delta(\delta)$  which was explained in §5.4 is only one instance of  $\mathbf{D}_\Delta(\delta)$ . The statistical input to the voltage controlled oscillator,  $\mathbf{D}_\Delta(\delta)$ , is expressed as

$$\mathbf{D}_\Delta(\delta) = \mathbf{R}^2 \left[ \left( \delta - \frac{\Delta}{2} \right) T_c \right] - \mathbf{R}^2 \left[ \left( \delta + \frac{\Delta}{2} \right) T_c \right]. \quad (7.13)$$

The above expression is the difference of two statistical correlation functions that are squared. Noting the discussion presented above, the square of each correlation function follows the distributions given in (7.11) and (7.12) depending on the spreading code alignment. That is, the peaks of the correlation function follow the non-central chi-square distribution given in (7.12) and the other values in the correlation function, follow the central chi-square distribution given in (7.11).

It has to be noted that the two functions have a relative time delay. This is a crucial fact in determining the distribution of the various points of the tracking loop S-curve. It is assumed that the time separation between the advanced and delayed correlators equals one chip duration, i.e.  $\Delta = 1$ . This is the most common value used in literature [107] and the analysis is similar for all  $\Delta$  as long as  $0 < \Delta \leq 1$ .

It is observed from (7.13) that when in the one correlator  $\delta = \tau$ , in the other  $\delta \neq \tau$ . In other words, when one correlator is at its peak, the other one has a small value. This is illustrated in Fig. 7.2 which shows the output of the two square-law devices with a time difference of one chip duration, that is  $\Delta = 1$ .

To statistically model  $\mathbf{D}_\Delta(\delta)$ , it is sufficient to find the distribution of two points on the S-curve. Fig. 7.3 shows these points as A and B. Point A represents the instance that  $\delta = 0.5$  and point B represents  $\delta = 0$  instance. Fig. 7.3 also presents the chosen statistical bounds of 0.1 and 4 standard deviations as well as the common assumption about the S-curve presented in [46, 167, 177].

It is now clear that the value at the positive peak (point A) can be found by subtracting  $\mathbf{R}'_{h_0}$  from  $\mathbf{R}'_{h_1}$ , which means that the distribution at this point can be found by convolving the distributions of  $\mathbf{R}'_{h_0}$  and  $\mathbf{R}'_{h_1}$  which are given in (7.11) and (7.12) respectively. This is shown in the form of a convolution integral in (7.14) where  $*$  denotes convolution. The negative peak can be analysed in exactly the same way with a change of sign. The solution of the convolution integral given in (7.14) is not tractable therefore, a numerical solution is performed with the result given in Section 7.3.

Similarly, the value at point B in Fig. 7.3 is the subtraction of  $\mathbf{R}'_{h_0}$  in one correlation function from the other. The distribution at point B can be found by convolving two distributions of  $\mathbf{R}'_{h_0}$  given in (7.11). It has to be noted that since the convolution of two central chi-square distributions is another chi-square distribution with the summation of degrees of freedom [178], then the distribution of the centre part of  $\mathbf{D}_\Delta(\delta)$  can be expressed as (7.15) without the need to do the actual integration.

$$\begin{aligned} P\left(\mathbf{R}'_{h_1}; 1, \lambda\right) * P\left(\mathbf{R}'_{h_0}, 1\right) &= \frac{1}{2} \int_{-\infty}^{\infty} \frac{1}{\sqrt{2\pi(\mathbf{R}'_h - \tau)}} \exp\left(\frac{-(\mathbf{R}'_h - \tau)}{2}\right) \times \\ &\quad \left\{ \exp\left(\frac{-(\tau + \lambda)}{2}\right) + \left(\frac{\tau}{\lambda}\right)^{-\frac{1}{4}} + I_{\frac{-1}{2}}\sqrt{\tau\lambda} \right\} d\tau. \end{aligned} \quad (7.14)$$

$$\begin{aligned}
P(\mathbf{R}'_{h_0}, 1) * P(\mathbf{R}'_{h_0}, 1) &= P(\mathbf{R}'_{h_0}, 2) \\
&= \frac{1}{2} \exp\left(\frac{-(\mathbf{R}'_{h_0})}{2}\right) \\
\lim_{\mathbf{R}'_{h_0} \rightarrow +\infty} P(\mathbf{R}'_{h_0}, 1) * P(\mathbf{R}'_{h_0}, 1) &= 0.
\end{aligned} \tag{7.15}$$

It is important to compare the correlation properties of the chaos-based sequences with the conventional binary ones. This comparison can be done by mathematically describing the correlation function and the S-curve for binary sequences and comparing them to what was presented in this Section. In this chapter, the maximal length sequences (m-sequences) has been chosen for the comparison.

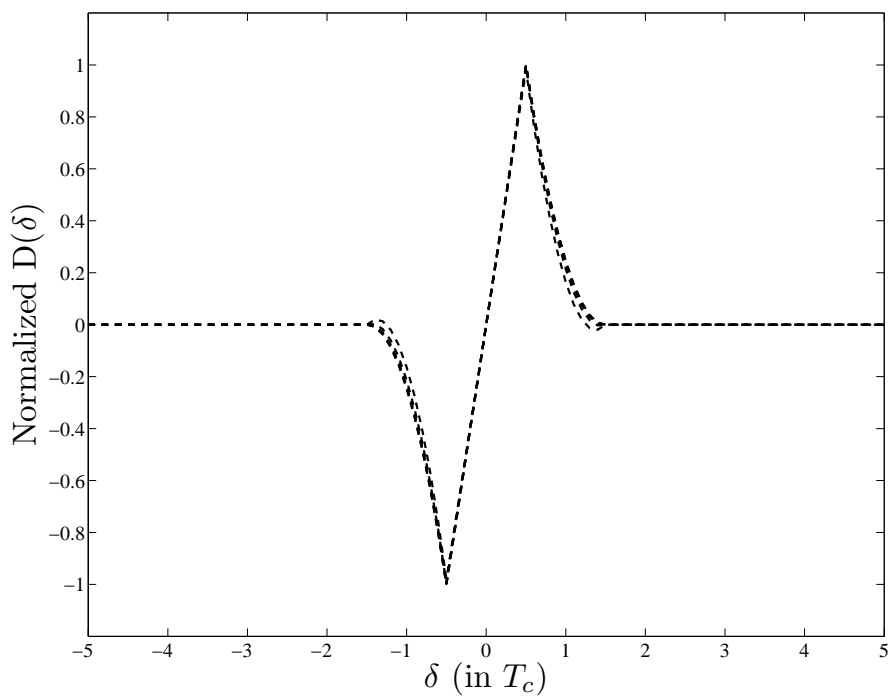
The first point to consider is that the correlation function of m-sequences is only dependent on the correlation length and will remain fixed if another m-sequence is used. This is unlike the chaotic sequences which have slightly different correlation function values for different sequences. The early and late correlation functions for m-sequences are presented in Fig. 7.4. It should be noted that these correlation functions are before the square law-device. As can be seen in Fig. 7.4 different correlation lengths affect the DC offset of the correlation functions; however, the peak of the correlation functions remain at 1 no matter what the correlation length is.

In non-coherent tracking, square law devices have to be used and the early-late correlation functions presented in Fig. 7.4 will change to the ones presented in Fig. 7.5. Two matters are of interest in Fig. 7.5, the first is the non-linearity which is introduced to the correlation functions, and the second is the change in the DC offset for the correlation functions; both of these are expected because of the squaring.

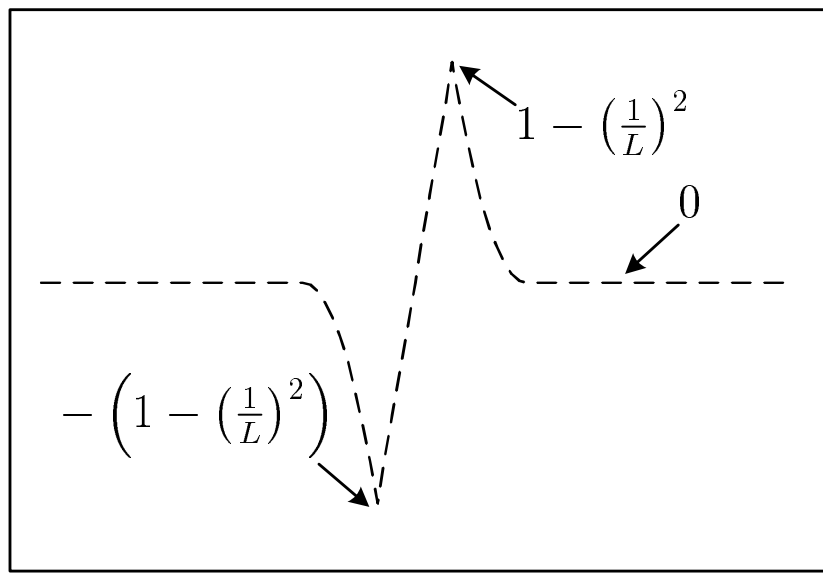
To clearly distinguish the S-curves of binary from the chaotic sequences,  $D_{\Delta_b}(\delta)$  is used as the notation referring to the binary S-curve. Using this notation, it can be seen in Fig. 7.6 that the only factor that changes the  $D_{\Delta_b}(\delta)$  is the correlation length which has been changed in the range of 8-128 chips. The main difference between the  $D_{\Delta_b}(\delta)$  presented in Fig. 7.6 and  $\mathbf{D}_{\Delta}(\delta)$  presented in Fig. 7.3 is the fact that the chaotic S-curve has to be described with a statistical distribution, whereas the  $D_{\Delta_b}(\delta)$  is a fixed entity. Finally, Fig. 7.7 shows the theoretical values for  $D_{\Delta_b}(\delta)$  in the non-coherent scenario.

### 7.3 Theoretical Findings

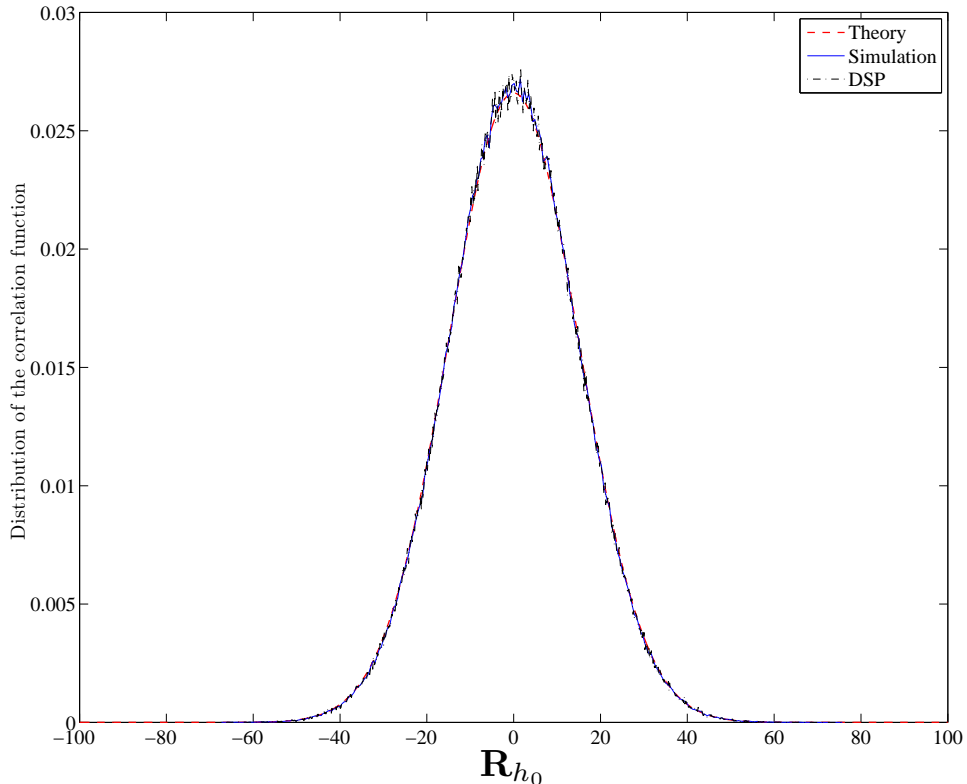
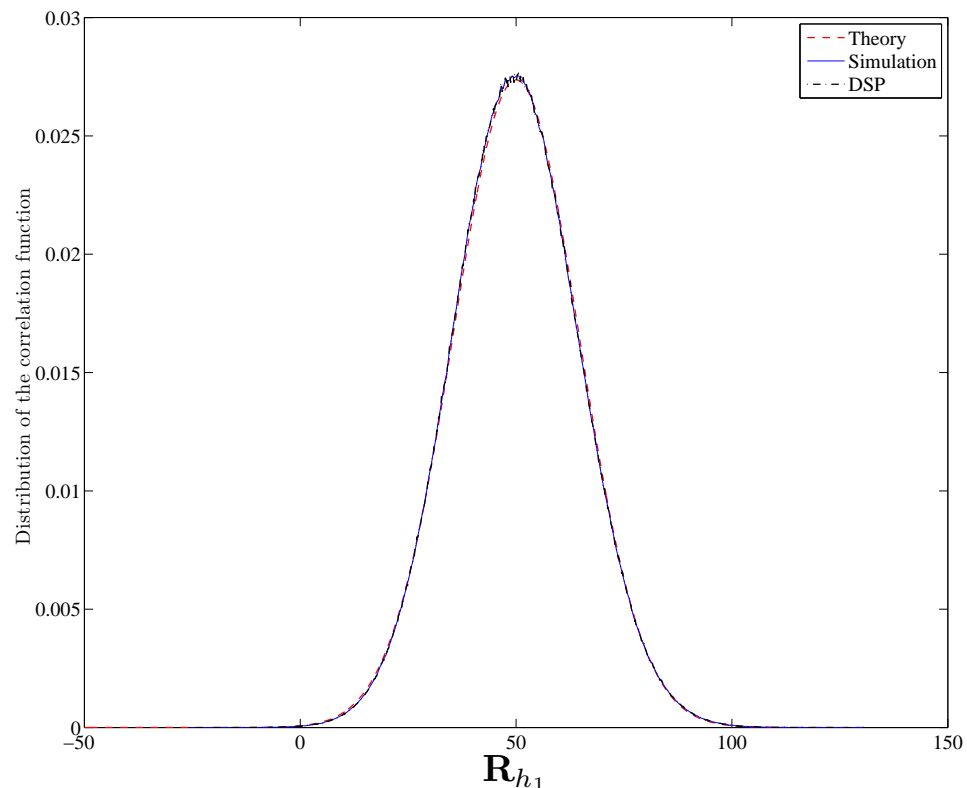
In order to verify the theoretical findings, simulations were performed for each stage of the statistical analysis. The results of these simulations were then compared to the theoretical results derived in §7.2 as well as hardware implementation results. As can be seen from Fig. 7.8, the statistical method applied in this chapter has a very high accuracy for predicting the distributions of the chaotic correlation function. The mean and variances predicted are followed closely by the simulation for both  $\mathbf{R}_{h_0}$  and  $\mathbf{R}_{h_1}$ . Also, the chi-square distributions closely match the squared values which are taken from the tracking loop.



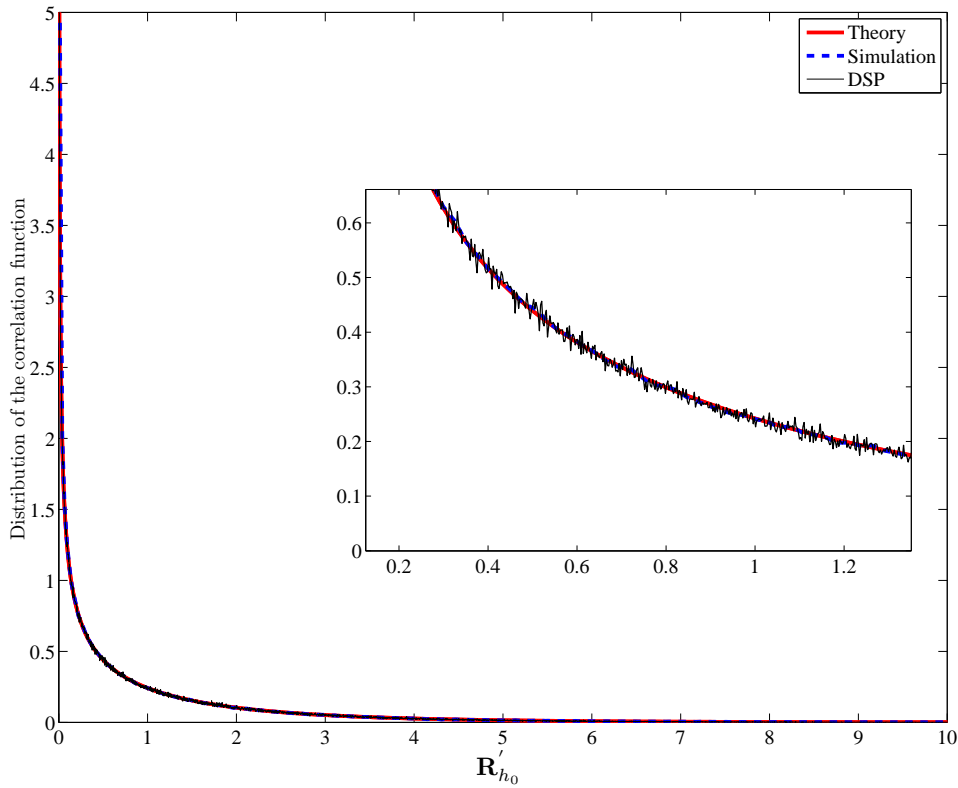
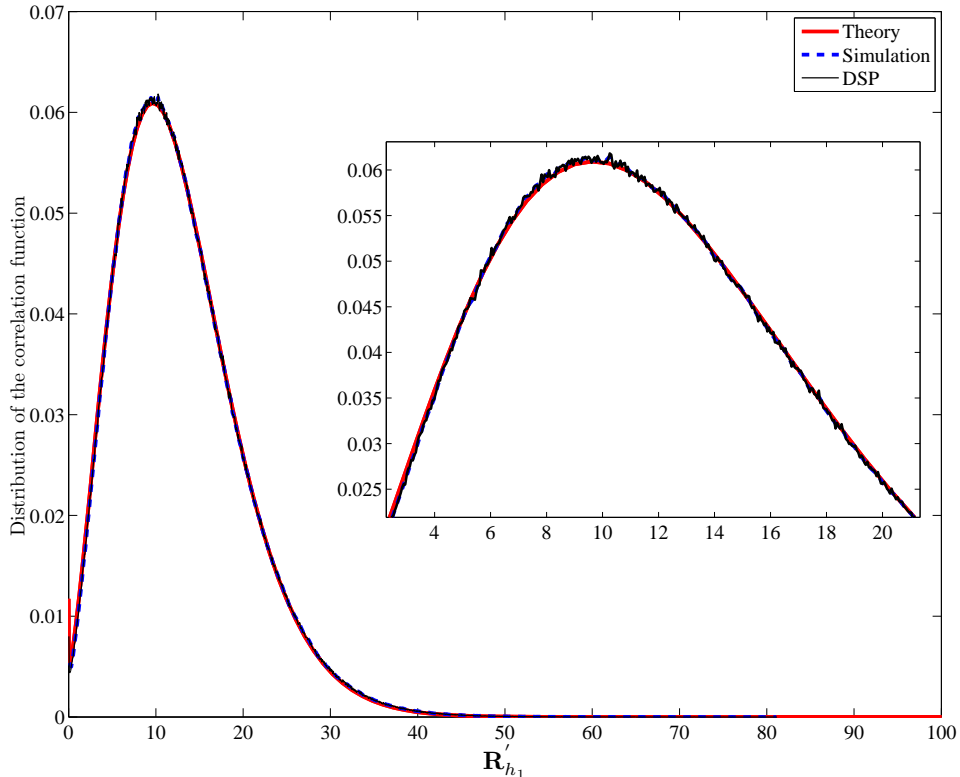
**Figure 7.6:**  $D_{\Delta_b}(\delta)$  for correlation lengths of 8, 16, 32, 64 and 128.



**Figure 7.7:** Theoretical values for  $D_{\Delta_b}(\delta)$  in a non-coherent scenario.

(a) Theoretical and simulation results for  $\mathbf{R}_{h_0}$ .(b) Theoretical and simulation results for  $\mathbf{R}_{h_1}$ .

**Figure 7.8:** Comparison between the statistical model predictions of the correlation function of chaotic spreading codes with the simulation results before square law device.

(a) Theoretical and simulation results for  $R'_{h_0}$ .(b) Theoretical and simulation results for  $R'_{h_1}$ .

**Figure 7.9:** Comparison between the statistical model predictions of the correlation function of chaotic spreading codes with the simulation results after square law device.

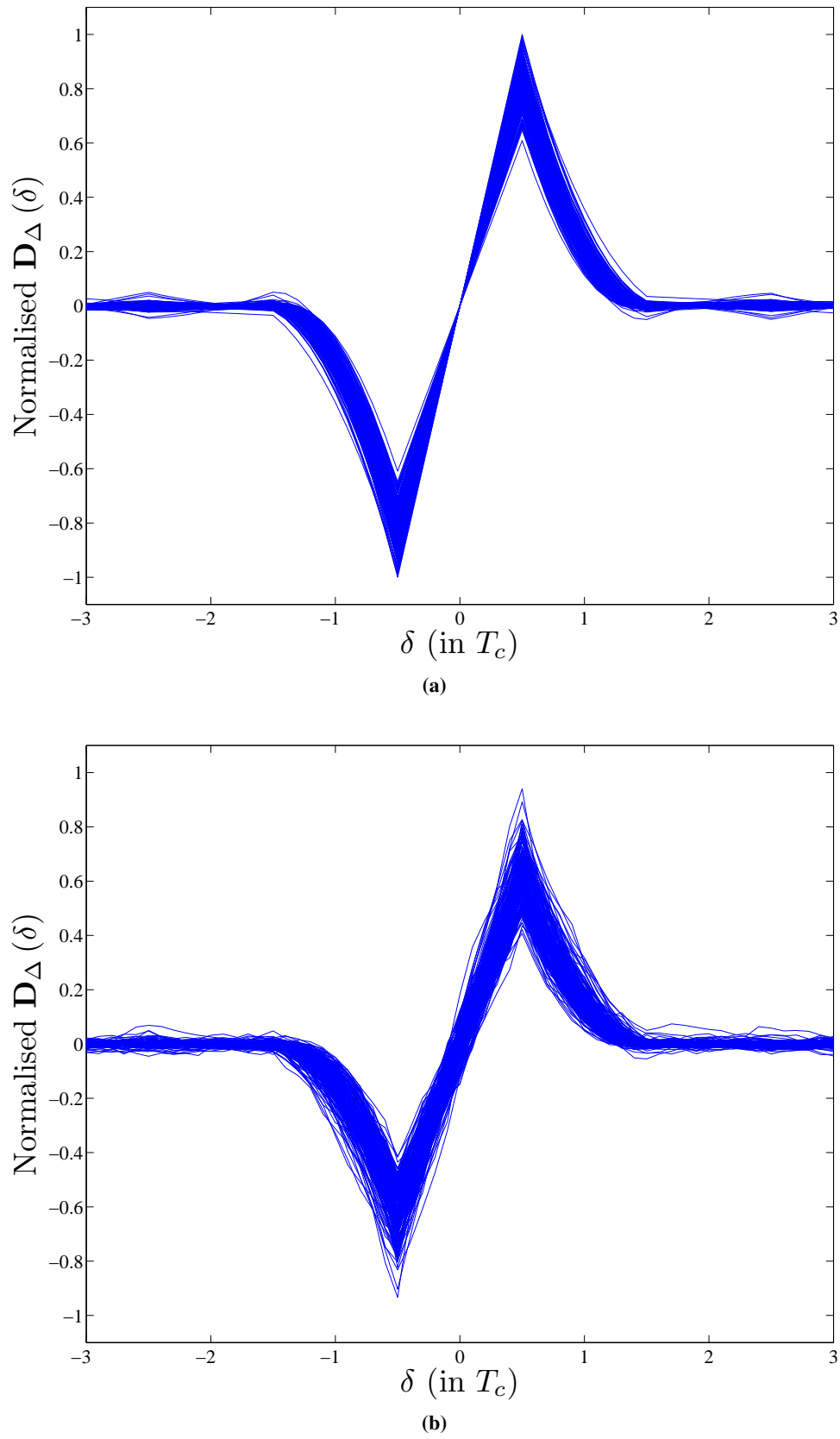


**Figure 7.10:**  $D_{\Delta}(\delta)$  in the chaos-based non-coherent tracking loop, noiseless (a) and SNR= -12dB (b)

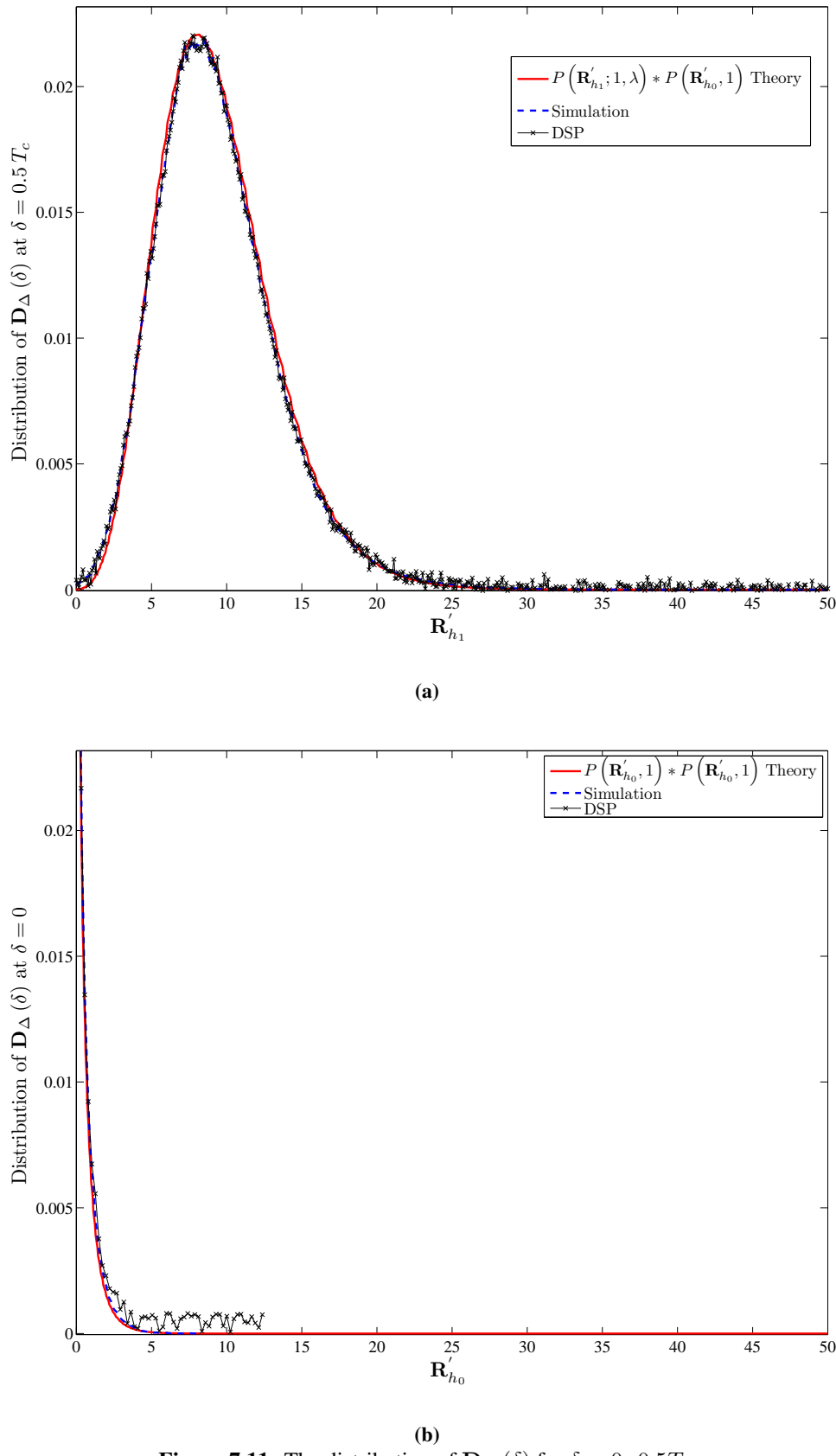


**Figure 7.11:** The distribution of  $\mathbf{D}_\Delta(\delta)$  for  $\delta = 0, 0.5T_c$ .

The first set of results are presented to show the accuracy of the CCS method used. To simulate this, a statistically significant number of chaotic-correlation functions were formed from the Logistic map using different initial conditions. The cross-correlation and auto-correlation peaks of these functions were then recorded and their distributions were drawn with the correlation length chosen to be 100 ( $L = 100$ ). The distribution of  $\mathbf{R}_{h_0}$  is shown in Fig. 7.8(a) and is a zero mean Gaussian distribution. The theoretical prediction is followed closely by the implementation and simulation results. Fig. 7.8(b) shows the distribution for  $\mathbf{R}_{h_1}$  with the mean in this case being  $\frac{L}{2} = 50$ . The two distributions will go through the square-law device. Figs. 7.9(a) and (b) show the distributions for  $\mathbf{R}'_{h_0}$  and  $\mathbf{R}'_{h_1}$  respectively. In order to show the accuracy of the proposed method, insets are provided within these figures showing a more detailed rendition of the area of interest.

The simulation setup for the chaos-based non-coherent tracking loop involved generating a statistically significant number of S-curves and observing their distributions at the points shown in Fig. 7.3. Fig. 7.10(a) shows the noiseless  $\mathbf{D}_\Delta(\delta)$  values for  $\Delta = 1$ . It can be observed that, even in the noiseless case, the peaks of  $\mathbf{D}_\Delta(\delta)$  have a distribution. It also should be noted that the slope in the linear region of the noiseless graph, changes because of the distribution of the peaks, unlike the previous assumptions in literature. The effect of noise in Fig. 7.10(b) is shown as the horizontal movement of the S-curves. It has to be noted that noise changes the place of the zero crossing on the  $\mathbf{D}_\Delta(\delta)$  curve. Also, the SNR of -12dB is calculated using the chip energy value that is,  $\frac{E_c}{N_0} = -12$  dB.

Another point relates to the multiple access SS (MA-SS) systems and their relationship with the current analysis here. It has to be noted that the addition of other users' spreading codes to the pilot which is being tracked only adds to the validity of the Gaussian analysis presented here. The only statistical effect which adding multiple users will cause is an increase in the variance of the correlation function which is a manifestation of inter-user-interference and is detrimental to the system performance.

Fig. 7.11(a) shows the comparison between the theoretical results obtained by evaluating the integral given in (7.14) numerically and the simulation and implementation results which have been obtained by subtracting the values of the two correlators over a large experiment space. Similarly Fig. 7.11(b) shows the same comparison but for the integral given in (7.15). As can be seen the results match closely, the slight differences are due to the numerical evaluation of the integral as well as the resolution of the implementation. The DSP results for the lower part of the central chi-square distribution are small but are slightly above zero. This is attributed to the shorter sequence lengths that is generated by the DSP compared to the longer sequences generated by the simulator. The theoretical expression assumes infinite sequence length.

## 7.4 Summary

This chapter used the CCS analysis introduced in §6.2 for analysing the non-coherent code tracking. It has been shown that the chaos-based tracking loop can only be accurately modelled if CCS is used. The critical points of the S-curve have been statistically modelled using the CCS method and the theoretical analysis results have been confirmed by simulation and hardware implementation results. It has to be noted that no matter how accurate the tracking is, there still remains a residual time mismatch between transmitter and the receiver, which is resulted form the errors that the tracking loop makes. Investigating

the overall system performance in the presence of this type of tracking loop error is the subject of the next chapter.

# Chapter 8

## CDS-SS Performance with Tracking Errors

### 8.1 Introduction

Now that the CDS-SS tracking loop has been accurately modelled in §7, the BPSK modulated CDS-SS system can be viewed in its entirety. It has been shown that tracking errors occur in presence of noise and fading and as a result it is important to be able to predict the CDS-SS system performance when the tracking errors exist. This chapter examines the overall performance of the BPSK modulated CDS-SS system, assuming that the tracking of the signal has not been perfect and there is some residual error. This chapter will present the BER expression for such a system when tracking errors are present. The tracking errors can be regarded as a random variable and cause slight chip misalignment which contribute to the overall increase in the system bit error rate (BER). The material presented in this chapter also appears in [179]. The structure of this chapter is as follows, §8.2 presents the overall CDS-SS system with interleavers and synchronisation block. The concept of chip misalignment and its effect on the chip energy are discussed in §8.3. The BER equations for partial chip overlap are derived for three channel scenarios in §8.4. The results from §8.4 are then used to derive the BER equations when the tracking errors are constant in §8.5 and for random errors which follow uniform and Gaussian distributions in §8.6. The derived theoretical results are compared with the simulation results in §8.7. Finally §8.8 summarises the chapter.

### 8.2 System Outline

Fig. 8.1 shows the system block diagram for the base-band BPSK modulated CDS-SS system. The chaotic sequence generated in the transmitter is multiplied with the data and sent through the channel in which it is affected by noise, fading and time delay. The receiver has the same chaotic sequence which has some timing misalignment compared to the transmitted sequence. It is assumed that the acquisition stage has correctly estimated the time difference between the transmitter and receiver to within a chip duration.

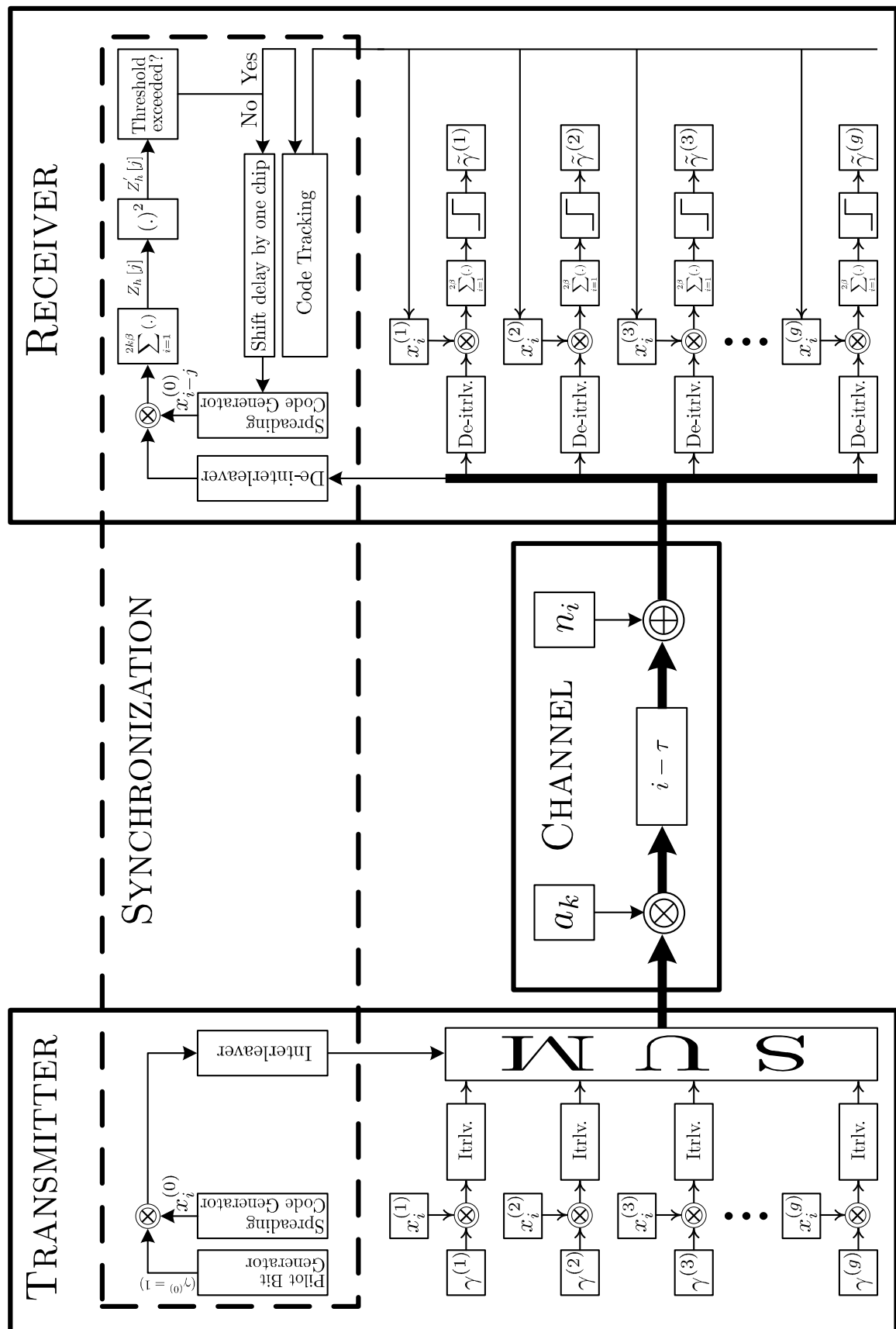


Figure 8.1: System block diagram.

It is also assumed that once the acquisition stage has performed its task, the tracking stage starts by trying to minimise the timing misalignment between the incoming sequence and the locally generated one. As shown previously, this process is not perfect and there are some tracking errors which affect the system performance. This system is designed to investigate the bit-error-rate (BER) performance when tracking loop errors are present.

Given that the main focus is with time windows within a chip duration, the chips have to be sampled. Assuming zero order hold sampling, all the calculations in the correlation functions have to be done with respect to the number of samples in a chip. Moreover, the partial alignments of the chips reduces the auto-correlation peak which has to be taken into account in order to derive an accurate expression for the BER.

### 8.3 Chip Misalignment

First, the effect of timing mismatch on one individual chip energy,  $E_c$ , is investigated. This result can then be generalised to examine the energy per bit,  $E_b$ .

Fig. 8.2 presents a single chip which is discretely sampled say 10 times, i.e.  $R_s = 10$  sa/chip. In this case, the energy per chip can be expressed as

$$E_c = \sum_{l=1}^{R_s} a_l^2 T_s, \quad (8.1)$$

where  $a_l$  are the individual zero order hold samples of the chaotic sequence and  $T_s = \frac{1}{R_s}$ . It should be noted that the above is equal to the conventional  $E_c$ , this is because it is not possible to have more energy by sampling the signal with a higher rate. Also, it should be noted that the bit duration is finite and as a result, the value of  $E_c$  at a high sampling rate will approach the value for a finite bit interval.

Now it is assumed that there is a certain timing mismatch between two chips  $a$  and  $b$ . Let  $c$  be the chip that immediately follows  $b$ . As shown in Fig. 8.2 when the two chips are misaligned by one sample ( $\tau = T_s$ ),  $E_c$  is

$$E_c = a_1 b_2 + a_2 b_3 + a_3 b_4 + \cdots + a_9 b_{10} + a_{10} c_1. \quad (8.2)$$

As a result, for a misalignment of  $\tau$ , where  $-R_s < \tau < R_s$ ,  $E_c$  can be expressed as

$$E_c = \left( \sum_{l=1}^{R_s - |\tau|} a_l^2 T_s + \sum_{m=1}^{|\tau|} (a_{m+(R_s - |\tau|)}) c_m T_s \right), \quad (8.3)$$

where the first part of the expression is the correctly aligned part of the chip and the second part is the multiplication of the chip samples with the adjacent chip samples.

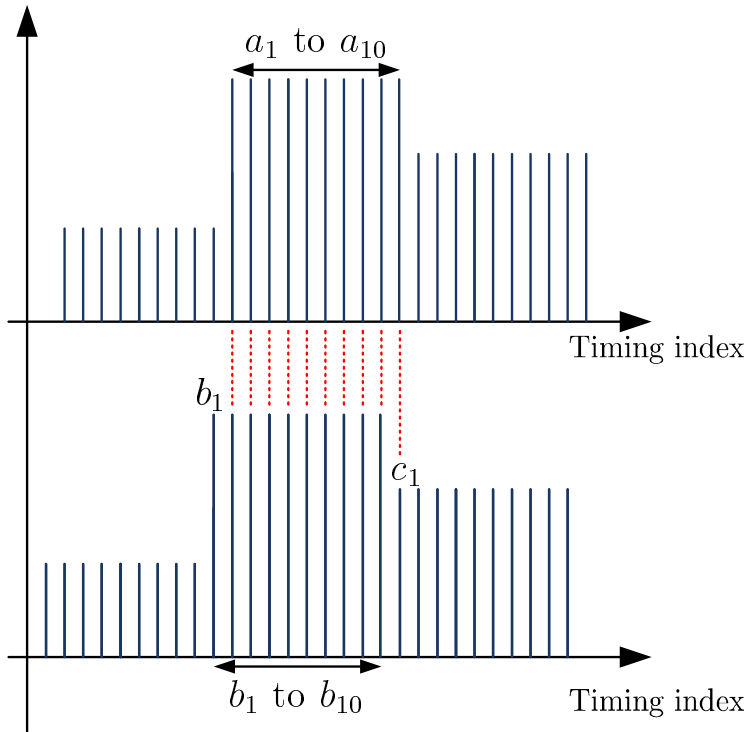


**Figure 8.2:** Chip misalignment

## 8.4 Derivation of the BER Expression With Partial Chip Overlap

Looking at Fig. 8.1 it can be seen that the output of the correlator for the  $i$ -th bits of the  $g$ -th user is

$$z_i^{(g)} = z_{i_A}^{(g)} + z_{i_B}^{(g)} + z_{i_C}^{(g)}, \quad (8.4)$$

where  $z_{i_A}^{(g)}$  is the signal part,  $z_{i_B}^{(g)}$  is the inter-user-interference (IUI), and  $z_{i_C}^{(g)}$  is the signal  $\times$  noise component. In order to determine the BER expression,  $z_i^{(g)}$  is assumed to be Gaussian by invoking the central limit theorem (CLT). The expectation and variance of  $z_i^{(g)}$  for an additive white Gaussian noise (AWGN) scenario have been calculated when perfect synchronisation is assumed in [65]. However, if there is a partial chip overlap, the expression derived in [65] is not accurate anymore.

To find the BER expression for the case when there is a timing mismatch of  $\tau$  between the transmitter and receiver, the expectation and variance of  $z_{i_A}$ ,  $z_{i_B}$ , and  $z_{i_C}$  have to be found when the timing mismatch of  $\tau$  exists. To do this, the formula derived for the energy of a partially overlapped chip shown in (8.3) is used. The following three parts examine the correlator output for AWGN, AWGN and fading, and interleaving scenarios respectively.

### 8.4.1 Scenario 1, AWGN

For  $z_{i_A}^{(g)}$

$$z_{i_A}^{(g)} = \sum_{k=1}^{2\beta} \left\{ \sum_{l=1}^{R_s - |\tau|} \left( x_{k_l}^{(g)} \right)^2 + \sum_{m=1}^{|\tau|} \left( x_k^{(g)} \right)_{m+(R_s - |\tau|)} x_{(k+1)_m}^{(g)} \right\}, \quad (8.5)$$

where  $2\beta$  is the spreading factor,  $k$  is the chip index,  $l$  is the sample index for each chip pertaining to the aligned samples, and  $m$  is the index for non-aligned samples.

The expectation of  $z_{i_A}^{(g)}$  is  $E[z_{i_A}^{(g)}]$

$$\begin{aligned} E[z_{i_A}^{(g)}] &= \sum_{k=1}^{2\beta} \left\{ E \left[ \sum_{l=1}^{R_s - |\tau|} \left( x_{k_l}^{(g)} \right)^2 \right] + E \left[ \sum_{m=1}^{|\tau|} \left( x_k^{(g)} \right)_{m+(R_s - |\tau|)} x_{(k+1)_m}^{(g)} \right] \right\} \\ &= 2\beta (R_s - |\tau|) E \left[ \left( x_{k_l}^{(g)} \right)^2 \right] + 0 \\ &= 2\beta (R_s - |\tau|) P_c. \end{aligned} \quad (8.6)$$

Before examining the variance of  $z_{i_A}^{(g)}$ , it has to be noted that  $\forall R_s \rightarrow x_{k_1}^{(g)} = x_{k_2}^{(g)} = x_{k_3}^{(g)} = \dots = x_{k_{R_s}}^{(g)}$ , as a result  $\sum_{l=1}^{R_s} \left( x_{k_l}^{(g)} \right)^2 = (R_s) \left( x_{k_l}^{(g)} \right)^2$  and consequently

$$\text{VAR} \left[ \sum_{l=1}^{R_s} \left( x_{k_l}^{(g)} \right)^2 \right] = (R_s)^2 \text{VAR} \left[ \left( x_{k_l}^{(g)} \right)^2 \right]. \quad (8.7)$$

The variance therefore is

$$\begin{aligned} \text{VAR} \left[ z_{i_A}^{(g)} \right] &= \text{VAR} \left[ \sum_{k=1}^{2\beta} \sum_{l=1}^{R_s - |\tau|} \left( x_{k_l}^{(g)} \right)^2 \right] + \text{VAR} \left[ \sum_{k=1}^{2\beta} \sum_{m=1}^{|\tau|} \left( x_k^{(g)} \right)_{m+(R_s - |\tau|)} x_{(k+1)_m}^{(g)} \right] \\ &= 2\beta (R_s - |\tau|)^2 \text{VAR} \left[ \left( x_{k_l}^{(g)} \right)^2 \right] + 2\beta |\tau|^2 \text{VAR} \left[ \left( x_k^{(g)} \right)_{m+(R_s - |\tau|)} x_{(k+1)_m}^{(g)} \right] \\ &= \beta P_c^2 \left\{ \left( (R_s - |\tau|)^2 \right) + 2|\tau|^2 \right\}. \end{aligned} \quad (8.8)$$

If all the users transmit with the same power then

$$z_{i_B}^{(g)} = \sum_{j=1}^N \sum_{k=1}^{2\beta} \sum_{l=1}^{R_s} x_{k_l}^{(j)} x_{k_l}^{(g)}, \quad (8.9)$$

where  $N$  is the number of users.

The expectation of  $z_{i_B}^{(g)}$  is

$$E[z_{i_B}^{(g)}] = \sum_{j=1}^N \sum_{k=1}^{2\beta} \sum_{l=1}^{R_s} E \left[ x_{k_l}^{(j)} x_{k_l}^{(g)} \right] \quad (8.10)$$

$$= 0. \quad (8.11)$$

The variance of  $z_{i_B}^{(g)}$  has already been derived by [65] for the case of perfect synchronisation. As cross-correlation is being considered here, the timing mismatch is not going to have any impact on the cross-correlation of the chaotic sequences. The only difference with the conventional case is the introduction of samples for every chip which affects the variance by the square of the samples per chip. So the variance can be expressed as

$$\text{VAR} \left[ z_{i_B}^{(g)} \right] = R_s^2 2\beta (N - 1) (P_c)^2, \quad (8.12)$$

which is the same as what was derived in [65].

The mean of  $z_{i_C}^{(g)}$  is

$$\begin{aligned} \mathbb{E} \left[ z_{i_C}^{(g)} \right] &= \sum_{k=1}^{2\beta} \sum_{l=1}^{R_s} \mathbb{E} \left[ \xi_{kl} x_{kl}^{(g)} \right] \\ &= 0. \end{aligned} \quad (8.13)$$

The variance of  $z_{i_C}^{(g)}$  is

$$\text{VAR} \left[ z_{i_C}^{(g)} \right] = R_s^2 \beta N_o P_c, \quad (8.14)$$

where  $N_o$  is the noise power spectral density. The above expression is the same as what was derived in [65].

So in general the correlator output for the AWGN case can be expressed as

$$\begin{aligned} z_i^{(g)} \sim & G \left( 2\beta (R_s - |\tau|) P_c, \beta P_c^2 \left\{ (R_s - |\tau|)^2 + 2|\tau|^2 \right\} + \right. \\ & \left. R_s^2 2\beta (N - 1) (P_c)^2 + R_s^2 \beta N_o P_c \right) \end{aligned} \quad (8.15)$$

#### 8.4.2 Scenario 2, AWGN and fading

If slow flat Rayleigh distributed fading is present in the channel, the mean and variance of the received signal will change. However, it is possible to find an expression for the BER with the presence of both the random tracking error as well as fading if the correlator output is statistically modelled. Such a task is simplified since the tracking error and fading random variables are independent and their joint probability is the same as the multiplication of their PDFs.

For faded  $z_{i_A}^{(g)}$

$$z_{i_A}^{(g)} = a \sum_{k=1}^{2\beta} \left\{ \sum_{l=1}^{R_s - |\tau|} \left( x_{kl}^{(g)} \right)^2 + \sum_{m=1}^{|\tau|} \left( x_k^{(g)} \right)_{m+(R_s - |\tau|)} x_{(k+1)m}^{(g)} \right\}, \quad (8.16)$$

where  $a$  is the fading coefficient with a Rayleigh distribution,  $P_A(a) = \frac{a}{b^2} \exp\left(-\frac{a^2}{2b^2}\right)$ ,  $2\beta$  is the spreading factor,  $k$  is the chip index,  $l$  is the sample index for each chip pertaining to the aligned samples, and  $m$  is the index for non-aligned samples.

The expectation of  $z_{i_A}^{(g)}$  is  $E \left[ z_{i_{\gamma=1}}^{(g)} \right]$

$$\begin{aligned} E \left[ z_{i_A}^{(g)} \right] &= a \sum_{k=1}^{2\beta} \left\{ E \left[ \sum_{l=1}^{R_s - |\tau|} \left( x_{k_l}^{(g)} \right)^2 \right] + E \left[ \sum_{m=1}^{|\tau|} \left( x_k^{(g)} \right)_{m+(R_s - |\tau|)} x_{(k+1)_m}^{(g)} \right] \right\} \\ &= \frac{a}{R_s} 2\beta (R_s - |\tau|) \left( x_{k_l}^{(g)} \right)^2 + 0 \\ &= 2a\beta (R_s - |\tau|) P_c. \end{aligned} \quad (8.17)$$

Using (8.7) the variance can be expressed as

$$\begin{aligned} \text{VAR} \left[ z_{i_A}^{(g)} \right] &= \text{VAR} \left[ a \sum_{k=1}^{2\beta} \sum_{l=1}^{R_s - |\tau|} \left( x_{k_l}^{(g)} \right)^2 \right] + \text{VAR} \left[ a \sum_{k=1}^{2\beta} \sum_{m=1}^{|\tau|} \left( x_k^{(g)} \right)_{m+(R_s - |\tau|)} x_{(k+1)_m}^{(g)} \right] \\ &= 2a^2\beta (R_s - |\tau|)^2 \text{VAR} \left[ \left( x_{k_l}^{(g)} \right)^2 \right] + 2a^2\beta |\tau|^2 \text{VAR} \left[ \left( x_k^{(g)} \right)_{m+(R_s - |\tau|)} x_{(k+1)_m}^{(g)} \right] \\ &= a^2\beta P_c^2 \left\{ \left( (R_s - |\tau|)^2 \right) + 2|\tau|^2 \right\}. \end{aligned} \quad (8.18)$$

If all the users transmit with the same power then

$$z_{i_B}^{(g)} = a \sum_{j=1}^N \sum_{k=1}^{2\beta} \sum_{l=1}^{R_s} x_{k_l}^{(j)} x_{k_l}^{(g)}, \quad (8.19)$$

where  $N$  is the number of users.

The expectation of  $z_{i_B}^{(g)}$  is

$$\begin{aligned} E \left[ z_{i_B}^{(g)} \right] &= a \sum_{j=1}^N \sum_{k=1}^{2\beta} \sum_{l=1}^{R_s} E \left[ x_{k_l}^{(j)} x_{k_l}^{(g)} \right] \\ &= 0. \end{aligned} \quad (8.20)$$

So the variance in the presence of fading can be expressed as

$$\text{VAR} \left[ z_{i_B}^{(g)} \right] = R_s^2 2a^2\beta (N-1) (P_c)^2. \quad (8.21)$$

The mean and variance of  $z_{i_C}^{(g)}$  are shown in (8.13) and (8.14) respectively.

So in general the correlator output in the slow fading case can be expressed as

$$\begin{aligned} z_i^{(g)} &\sim G \left( 2a\beta (R_s - |\tau|) P_c, a^2\beta P_c^2 \left\{ \left( (R_s - |\tau|)^2 \right) + 2|\tau|^2 \right\} + \right. \\ &\quad \left. a^2 R_s^2 2\beta (N-1) (P_c)^2 + R_s^2 \beta N_o P_c \right) \end{aligned} \quad (8.22)$$

### 8.4.3 Scenario 3, AWGN and fading with interleaving

Since multi-path fading has an adverse effect on the system performance, it is desirable to mitigate these effects as much as possible. Out of the various possible ways of mitigating the fading effects, the chip interleaving is chosen because it requires the least amount of change in the system and it uses the spread spectrum characteristics of the system to spread the fading power over the same bandwidth as the transmitted signal. This ensures that no complete bit, or series of bits, is exposed to sever fades. In order to achieve this, interleavers and de-interleavers are employed on the transmitter and receiver sides respectively.

It is assumed that a block interleaver of dimensions  $2\beta \times 2\beta$  is used. This ensures that each chip in the bit is subjected to a different fading coefficient. Having this in mind, the receiver correlator output can be re-derived.

For faded and interleaved  $z_{i_A}^{(g)}$

$$z_{i_A}^{(g)} = \sum_{k=1}^{2\beta} \left\{ \sum_{l=1}^{R_s - |\tau|} a_{kl} \left( x_{kl}^{(g)} \right)^2 + \sum_{m=1}^{|\tau|} \left( a_k x_k^{(g)} \right)_{m+(R_s - |\tau|)} x_{(k+1)m}^{(g)} \right\}, \quad (8.23)$$

The expectation of  $z_{i_A}^{(g)}$  can be calculated as

$$\begin{aligned} E[z_{i_A}^{(g)}] &= E \left[ \sum_{k=1}^{2\beta} \left\{ \sum_{l=1}^{R_s - |\tau|} a_{kl} \left( x_{kl}^{(g)} \right)^2 + \sum_{m=1}^{|\tau|} \left( a_k x_k^{(g)} \right)_{m+(R_s - |\tau|)} x_{(k+1)m}^{(g)} \right\} \right] \\ &= E \left[ \sum_{k=1}^{2\beta} \sum_{l=1}^{R_s - |\tau|} a_{kl} \left( x_{kl}^{(g)} \right)^2 \right] + E \left[ \sum_{k=1}^{2\beta} \sum_{m=1}^{|\tau|} \left( a_k x_k^{(g)} \right)_{m+(R_s - |\tau|)} x_{(k+1)m}^{(g)} \right] \\ &= 2\beta (R_s - |\tau|) E \left[ a_{kl} \left( x_{kl}^{(g)} \right)^2 \right] + 2\beta \tau E \left[ \left( a_k x_k^{(g)} \right)_{m+(R_s - |\tau|)} x_{(k+1)m}^{(g)} \right], \end{aligned} \quad (8.24)$$

since  $a$  and  $x$  are independent random variables, their joint probability is zero, so the expectation of their product can be rewritten as

$$\begin{aligned} E \left[ a_{kl} \left( x_{kl}^{(g)} \right)^2 \right] &= E[a_{kl}] + E \left[ \left( x_{kl}^{(g)} \right)^2 \right] \\ &= b \sqrt{\frac{\pi}{2}} P_c. \end{aligned}$$

For the non-aligned part, the expectation is

$$\begin{aligned} E \left[ \left( a_k x_k^{(g)} \right)_{m+(R_s - |\tau|)} x_{(k+1)m}^{(g)} \right] &= E \left[ \left( a_k \right)_{m+(R_s - |\tau|)} \right] E \left[ \left( x_k^{(g)} \right)_{m+(R_s - |\tau|)} \right] E \left[ x_{(k+1)m}^{(g)} \right]. \\ &= 0. \end{aligned}$$

So

$$E \left[ z_{i_A}^{(g)} \right] = 2\beta (R_s - |\tau|) b \sqrt{\frac{\pi}{2}} P_c. \quad (8.25)$$

Using (8.7) the variance can be expressed as

$$\text{VAR} \left[ z_{iA}^{(g)} \right] = \text{VAR} \left[ \sum_{k=1}^{2\beta} \left\{ \sum_{l=1}^{R_s - |\tau|} a_{kl} \left( x_{kl}^{(g)} \right)^2 + \sum_{m=1}^{|\tau|} \left( a_k x_k^{(g)} \right)_{m+(R_s - |\tau|)} x_{(k+1)m}^{(g)} \right\} \right],$$

since each chip is uncorrelated with the next one

$$\text{VAR} \left[ z_{iA}^{(g)} \right] = \text{VAR} \left[ \sum_{k=1}^{2\beta} \sum_{l=1}^{R_s - |\tau|} a_{kl} \left( x_{kl}^{(g)} \right)^2 \right] + \text{VAR} \left[ \sum_{k=1}^{2\beta} \sum_{m=1}^{|\tau|} \underbrace{\left( a_k x_k^{(g)} \right)_{m+(R_s - |\tau|)}}_D x_{(k+1)m}^{(g)} \right]$$

As an aside, it is clear that  $\text{E}[D] = 0$  and  $\text{VAR}[D] = b^2$ .

Therefore,

$$\begin{aligned} \text{VAR} \left[ z_{iA}^{(g)} \right] &= 2\beta (R_s - |\tau|)^2 \text{VAR} \left[ a_{kl} \left( x_{kl}^{(g)} \right)^2 \right] + \\ &\quad 2\beta |\tau|^2 \text{VAR} \left[ \left( a_k x_k^{(g)} \right)_{m+(R_s - |\tau|)} x_{(k+1)m}^{(g)} \right] \\ &= 2\beta (R_s - |\tau|)^2 \left\{ \text{E}^2 [a_{kl}] \text{VAR} \left[ \left( x_{kl}^{(g)} \right)^2 \right] + \right. \\ &\quad \left. \text{E}^2 \left[ \left( x_{kl}^{(g)} \right)^2 \right] \text{VAR} [a_{kl}] + \text{VAR} [a_{kl}] \text{VAR} \left[ \left( x_{kl}^{(g)} \right)^2 \right] \right\} + \\ &\quad 2\beta |\tau|^2 \left\{ \text{E}^2 [D] \text{VAR} \left[ x_{(k+1)m}^{(g)} \right] + \text{E}^2 \left[ x_{(k+1)m}^{(g)} \right] \text{VAR} [a_{kl}] + \right. \\ &\quad \left. \text{VAR} [D] \text{VAR} \left[ x_{(k+1)m}^{(g)} \right] \right\} \\ &= 2\beta (R_s - |\tau|)^2 \frac{b^2}{8} \{6 - \pi\} + 2\beta |\tau|^2 b^2 P_c \\ &= 2\beta (R_s - |\tau|)^2 b^2 P_c^3 \{6 - \pi\} + 2\beta |\tau|^2 b^2 P_c \end{aligned} \tag{8.26}$$

Assuming that all the users transmit with the same power,

$$z_{iB}^{(g)} = \sum_{j=1}^N \sum_{k=1}^{2\beta} \sum_{l=1}^{R_s} a_{kl} x_{kl}^{(j)} x_{kl}^{(g)}, \tag{8.27}$$

where  $N$  is the number of users.

The expectation of  $z_{iB}^{(g)}$  is

$$\begin{aligned} \text{E} \left[ z_{iB}^{(g)} \right] &= \sum_{j=1}^N \sum_{k=1}^{2\beta} \sum_{l=1}^{R_s} \text{E} \left[ a_{kl} x_{kl}^{(j)} x_{kl}^{(g)} \right] \\ &= 0. \end{aligned} \tag{8.28}$$

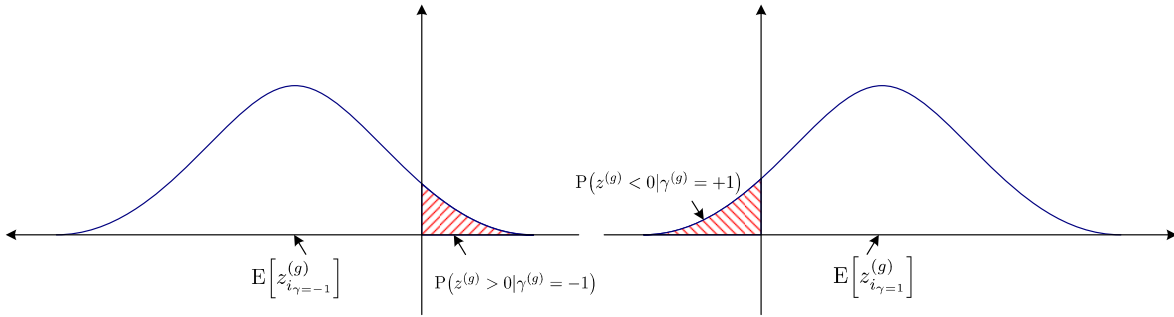


**Figure 8.3:** Probability of error given  $z_i^{(g)}$ .

The variance of this part can be expressed as

$$\begin{aligned} \text{VAR} [z_{i_B}^{(g)}] &= \text{VAR} \left[ \sum_{j=1}^N \sum_{k=1}^{2\beta} \sum_{l=1}^{R_s} a_{kl} x_{kl}^{(j)} x_{kl}^{(g)} \right] \\ &= \sum_{j=1}^N \sum_{k=1}^{2\beta} \sum_{l=1}^{R_s} \text{VAR} [a_{kl} x_{kl}^{(j)} x_{kl}^{(g)}] \\ &= 4\beta(N-1) R_s^2 P_c^2 b^2. \end{aligned} \quad (8.29)$$

The expectation and variance of  $z_{i_C}^{(g)}$  are shown in (8.13) and (8.14) respectively.

So in general the correlator output in the interleaved fading case can be expressed as

$$\begin{aligned} z_i^{(g)} \sim G &\left( 2\beta(R_s - |\tau|) b \sqrt{\frac{\pi}{2}} P_c, 2\beta(R_s - |\tau|)^2 b^2 P_c^3 \{6 - \pi\} + \right. \\ &\left. 2\beta|\tau|^2 b^2 P_c + 4\beta(N-1) R_s^2 P_c^2 b^2 + R_s^2 \beta N_o P_c \right) \end{aligned} \quad (8.30)$$

## 8.5 Derivation of the BER for Constant Tracking Errors

This part presents the results of the BER derivation for each of the three scenarios. The detailed derivation can be found in Appendix F. As shown in Fig. 8.3 the probability of error for each bit of the  $g$ -th user is

$$\begin{aligned} P_e &= \frac{1}{2} P(z^{(g)} < 0 | \gamma^{(g)} = +1) + \frac{1}{2} P(z^{(g)} > 0 | \gamma^{(g)} = -1) \\ &= \frac{1}{2} \text{erfc} \frac{\mathbb{E}[z^{(g)} | \gamma^{(g)} = +1]}{\sqrt{2 \text{VAR}[z^{(g)} | \gamma^{(g)} = +1]}}. \end{aligned} \quad (8.31)$$

The probability of error for scenarios 1, 2 and, 3 can be found by substituting equations (8.15), (8.22) and, (8.30) into (8.31) respectively.

For scenario 1 the probability of error is

$$P_e = \frac{1}{2} \text{erfc} \left( \frac{\psi}{\beta} + \frac{1}{C^2} \left( \frac{D^2}{\beta} + \frac{(N-1)}{\beta} + \frac{N_o}{E_b} \right) \right)^{-\frac{1}{2}}, \quad (8.32)$$

where  $\psi$  is the equivalent of  $\frac{\text{VAR}[x^2]}{\text{E}^2[x^2]}$ , and  $C = \frac{R_s - |\tau|}{R_s}$  and  $D = \frac{|\tau|}{R_s}$ . It should be noted that (8.32) simplifies to the expression reported in [65] when  $\tau = 0$ .

For scenario 2 the probability of error is

$$P_e = \int_0^\infty \frac{1}{2} \operatorname{erfc} \left( \frac{\psi}{\beta} + \frac{1}{C^2} \left( \frac{D^2}{\beta} + \frac{(N-1)}{\beta} + \frac{N_o}{a^2 E_b} \right) \right)^{-\frac{1}{2}} \frac{a}{b^2} \exp \left( -\frac{a^2}{2b^2} \right) da. \quad (8.33)$$

This solution is not in the closed form and will simplify to 8.32 if the fading does not exist in the channel.

For scenario 3 the probability of error is

$$P_e = \frac{1}{2} \operatorname{erfc} \left( \frac{(6-\pi)}{\pi\beta} + \frac{4|\tau|^2}{\pi\beta(R_s - |\tau|)^2} + \frac{R_s^2}{(R_s - |\tau|)^2} \left\{ \frac{4(N-1)}{\pi\beta} + \frac{2}{\pi b^2} \left( \frac{E_b}{N_o} \right)^{-1} \right\} \right)^{-\frac{1}{2}}. \quad (8.34)$$

## 8.6 Derivation of the BER for Random Tracking Errors

The BER expressions presented in (8.32), (8.33) and, (8.34) are only valid when the chip timing mismatch is fixed. In reality however, this is not the case and the error between the estimated and real chip times is a random variable with a certain PDF. In what follows, it is assumed that the chip timing mismatch will change from bit to bit and the BER can be evaluated for different PDFs.

For a noise only case the overall BER expression for a random chip timing mismatch can be found using the following expression

$$\text{BER}_{\text{Total}} = \int_{\tau=\tau_{\min}}^{\tau=\tau_{\max}} P_e(\tau) P_T(\tau) d\tau, \quad (8.35)$$

where  $P_e(\tau)$  is the probability of error presented in (8.32), and  $P_T(\tau)$  is the PDF of  $\tau$ .

If  $\tau$  follows a uniform distribution with equal probabilities in the range of  $[-R_s, R_s]$ , then the PDF of  $\tau$  can be written as,

$$P_T(\tau) = \begin{cases} \frac{1}{R_s - (-R_s)}, & -R_s \leq \tau \leq R_s \\ 0, & \text{otherwise} \end{cases}. \quad (8.36)$$

Since  $P_T(\tau)$  is constant for all  $\tau$  then (8.35) can be expressed as

$$\text{BER}_{\text{Total}_{\text{uniform}}} = \frac{1}{2R_s + 1} \int_{\tau=-R_s}^{\tau=R_s} \frac{1}{2} \operatorname{erfc} \left( \frac{\psi}{\beta} + \frac{1}{C^2} \left( \frac{D^2}{\beta} + \frac{(N-1)}{\beta} + \frac{N_o}{E_b} \right) \right)^{-\frac{1}{2}} \delta[\tau - kT_s] d\tau. \quad (8.37)$$

which is a summation of weighted PDFs multiplied by the probability of error for that particular timing mismatch.

This can be computed using discrete summation expressed as

$$\text{BER}_{\text{Total}_{\text{uniform}}} = \frac{1}{2R_s + 1} \sum_{\tau=-R_s}^{\tau=R_s} \frac{1}{2} \operatorname{erfc} \left( \frac{\psi}{\beta} + \frac{1}{C^2} \left( \frac{D^2}{\beta} + \frac{(N-1)}{\beta} + \frac{N_o}{E_b} \right) \right)^{-\frac{1}{2}}. \quad (8.38)$$

If  $\tau$  follows a bounded and discrete Gaussian distribution, (8.35) can be expressed as

$$\begin{aligned} \text{BER}_{\text{Total}_{\text{Gaussian}}} &= \frac{1}{2} \int_{\tau=-R_s}^{\tau=R_s} \delta(\tau - kT_s) \frac{1}{\sqrt{2\pi\sigma_\tau^2}} \exp \frac{-(\tau - \mu_\tau)^2}{2\sigma_\tau^2} \times \\ &\quad \operatorname{erfc} \left( \frac{\psi}{\beta} + \frac{1}{C^2} \left( \frac{D^2}{\beta} + \frac{(N-1)}{\beta} + \frac{N_o}{E_b} \right) \right)^{-\frac{1}{2}} d\tau, \end{aligned} \quad (8.39)$$

which suggests that  $\tau$  follows a Gaussian distribution with a mean of  $\mu_\tau$  and variance  $\sigma_\tau^2$ . Since  $\tau$  can only take discrete values of the Gaussian distribution, it has been multiplied by  $\delta[t - \tau]$  pulse train.

Eqn. (8.39) can be computed using a discrete summation expressed as

$$\begin{aligned} \text{BER}_{\text{Total}_{\text{Gaussian}}} &= \frac{1}{2} \sum_{\tau=-R_s}^{\tau=R_s} \frac{1}{\sqrt{2\pi\sigma_\tau^2}} \exp \frac{-(\tau - \mu_\tau)^2}{2\sigma_\tau^2} \times \\ &\quad \operatorname{erfc} \left( \frac{\psi}{\beta} + \frac{1}{C^2} \left( \frac{D^2}{\beta} + \frac{(N-1)}{\beta} + \frac{N_o}{E_b} \right) \right)^{-\frac{1}{2}}. \end{aligned} \quad (8.40)$$

For a fading case the overall BER expression for a random chip timing mismatch can be found using the following expression

$$\text{BER}_{\text{Total}} = \int_0^\infty \int_{\tau=\tau_{\min}}^{\tau=\tau_{\max}} P_e(\tau) P_T(\tau) P_A(a) d\tau da, \quad (8.41)$$

where  $P_A(a)$  is the PDF of  $a$ .

If  $\tau$  follows a uniform distribution then (8.41) can be expressed as

$$\begin{aligned} \text{BER}_{\text{Total}_{\text{uniform}}} &= \frac{1}{2R_s + 1} \int_0^\infty \int_{\tau=-R_s}^{\tau=R_s} \frac{1}{2} \operatorname{erfc} \left( \frac{\psi}{\beta} + \frac{1}{C^2} \left( \frac{D^2}{\beta} + \frac{(N-1)}{\beta} + \frac{N_o}{E_b} \right) \right)^{-\frac{1}{2}} \times \\ &\quad \frac{a}{b^2} \exp \left( -\frac{a^2}{2b^2} \right) \delta[\tau - kT_s] d\tau da. \end{aligned} \quad (8.42)$$

which is a summation of weighted PDFs multiplied by the probability of error for that particular timing mismatch.

This can be computed using discrete summation expressed as

$$\begin{aligned} \text{BER}_{\text{Total}_{\text{uniform}}} &= \frac{1}{2R_s + 1} \sum_0^\infty \sum_{\tau=-R_s}^{\tau=R_s} \frac{1}{2} \operatorname{erfc} \left( \frac{\psi}{\beta} + \frac{1}{C^2} \left( \frac{D^2}{\beta} + \frac{(N-1)}{\beta} + \frac{N_o}{a^2 E_b} \right) \right)^{-\frac{1}{2}} \times \\ &\quad \frac{a}{b^2} \exp \left( -\frac{a^2}{2b^2} \right) \end{aligned}$$

If  $\tau$  follows a bound and discrete Gaussian distribution, (8.41) can be expressed as

$$\text{BER}_{\text{TotalGaussian}} = \frac{1}{2} \int_0^{\infty} \int_{\tau=-R_s}^{\tau=R_s} \delta[\tau - kT_s] \frac{1}{\sqrt{2\pi\sigma_\tau^2}} \exp \frac{-(\tau - \mu_\tau)^2}{2\sigma_\tau^2} \times \text{erfc} \left( \frac{\psi}{\beta} + \frac{1}{C^2} \left( \frac{D^2}{\beta} + \frac{(N-1)}{\beta} + \frac{N_o}{a^2 E_b} \right) \right)^{-\frac{1}{2}} \times \frac{a}{b^2} \exp \left( -\frac{a^2}{2b^2} \right) d\tau da. \quad (8.43)$$

Eqn. (8.43) can be computed using a discrete summation expressed as

$$\text{BER}_{\text{TotalGaussian}} = \frac{1}{2} \sum_{\tau=-R_s}^{\tau=R_s} \frac{1}{\sqrt{2\pi\sigma_\tau^2}} \exp \frac{-(\tau - \mu_\tau)^2}{2\sigma_\tau^2} \times \text{erfc} \left( \frac{\psi}{\beta} + \frac{1}{C^2} \left( \frac{D^2}{\beta} + \frac{(N-1)}{\beta} + \frac{N_o}{E_b} \right) \right)^{-\frac{1}{2}} \times \frac{a}{b^2} \exp \left( -\frac{a^2}{2b^2} \right). \quad (8.44)$$

For the interleaved fading case, with  $\tau$  following a uniform distribution then (8.35) can be expressed as

$$\text{BER}_{\text{Totaluniform}} = \frac{1}{2R_s + 1} \int_{\tau=-R_s}^{\tau=R_s} \frac{1}{2} \text{erfc} \left( \frac{(6-\pi)}{\pi\beta} + \frac{4|\tau|^2}{\pi\beta(R_s - |\tau|)^2} + \frac{R_s^2}{(R_s - |\tau|)^2} \left\{ \frac{4(N-1)}{\pi\beta} + \frac{2}{\pi b^2} \left( \frac{E_b}{N_o} \right)^{-1} \right\} \right)^{-\frac{1}{2}} \delta[\tau - kT_s] d\tau. \quad (8.45)$$

which is a summation of weighted PDFs multiplied by the probability of error for that particular timing mismatch.

This can be computed using discrete summation expressed as

$$\text{BER}_{\text{Totaluniform}} = \frac{1}{2R_s + 1} \sum_{\tau=-R_s}^{\tau=R_s} \frac{1}{2} \text{erfc} \left( \frac{(6-\pi)}{\pi\beta} + \frac{4|\tau|^2}{\pi\beta(R_s - |\tau|)^2} + \frac{R_s^2}{(R_s - |\tau|)^2} \left\{ \frac{4(N-1)}{\pi\beta} + \frac{2}{\pi b^2} \left( \frac{E_b}{N_o} \right)^{-1} \right\} \right)^{-\frac{1}{2}} \delta(\tau - kT_s) d\tau. \quad (8.46)$$

If  $\tau$  follows a bound and discrete Gaussian distribution, (8.35) can be expressed as

$$\text{BER}_{\text{TotalGaussian}} = \frac{1}{2} \int_{\tau=-R_s}^{\tau=R_s} \delta[\tau - kT_s] \frac{1}{\sqrt{2\pi\sigma_\tau^2}} \exp \frac{-(\tau - \mu_\tau)^2}{2\sigma_\tau^2} \times \text{erfc} \left( \frac{(6-\pi)}{\pi\beta} + \frac{4|\tau|^2}{\pi\beta(R_s - |\tau|)^2} + \frac{R_s^2}{(R_s - |\tau|)^2} \left\{ \frac{4(N-1)}{\pi\beta} + \frac{2}{\pi b^2} \left( \frac{E_b}{N_o} \right)^{-1} \right\} \right)^{-\frac{1}{2}} d\tau. \quad (8.47)$$

Eqn. (8.47) can be computed using a discrete summation expressed as

$$\text{BER}_{\text{TotalGaussian}} = \frac{1}{2} \sum_{\tau=-R_s}^{\tau=R_s} \frac{1}{\sqrt{2\pi\sigma_\tau^2}} \exp \frac{-(\tau - \mu_\tau)^2}{2\sigma_\tau^2} \times \text{erfc} \left( \frac{(6-\pi)}{\pi\beta} + \frac{4|\tau|^2}{\pi\beta(R_s - |\tau|)^2} + \frac{R_s^2}{(R_s - |\tau|)^2} \left\{ \frac{4(N-1)}{\pi\beta} + \frac{2}{\pi b^2} \left( \frac{E_b}{N_o} \right)^{-1} \right\} \right)^{-\frac{1}{2}} \quad (8.48)$$

## 8.7 Theoretical Findings

This section provides the analytical and simulated BER curves for various systems parameters. The first result presented is the theoretical 3D BER surface in which the BER is calculated for various  $\frac{\tau}{R_s}$  values. This is shown in Fig. 8.4.

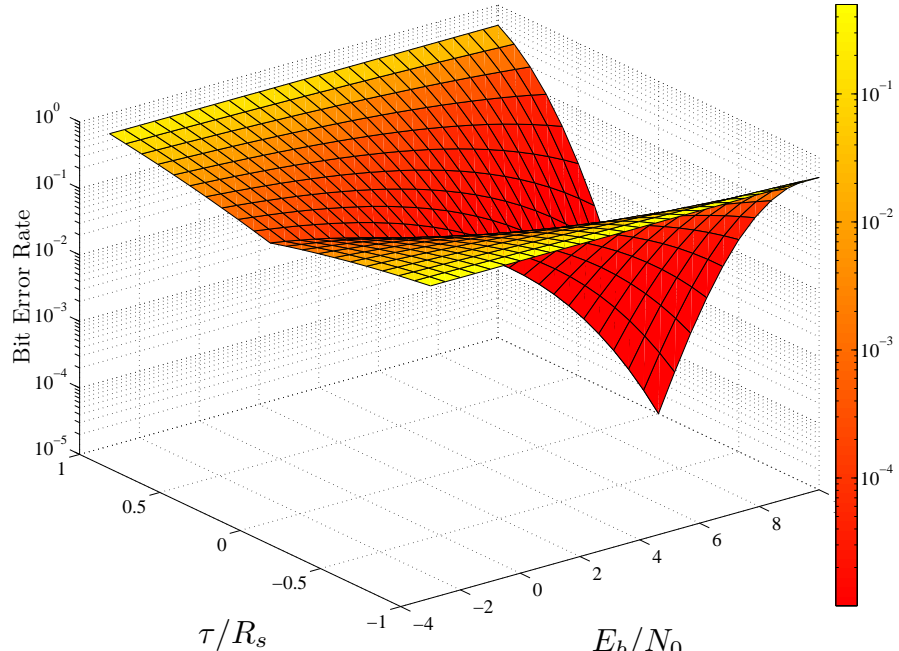
The next set of results shows the comparison between the BER simulation and derivation results when the timing mismatch value is kept constant for the whole simulation. Fig. 8.5 presents the BER performance in presence of AWGN for 1 and 16 user cases. The theoretical BER curves for the perfectly synchronised cases are also shown. As can be seen, the constant 30%<sup>1</sup> timing mismatch has a detrimental effect on the system performance on the two cases. The theoretical BER curve expressed in (8.32) (shown in green) shows very close agreement with the simulation results. As expected, an increase in the number of users results in a worse performance due to the increase in the level of inter-user interference (IUI).

Fig. 8.6 presents the BER performance for a single user when random jitter with uniform distribution exists. The fading and AWGN cases are compared to show the detrimental effect of fading on the system performance. It can be seen that the uniformly distributed random jitter can be predicted with close agreement with (8.37) and (8.42) for AWGN and fading cases respectively.

Fig. 8.7 compares the BER performance for fading and interleaving cases with uniformly distributed timing jitter. As can be seen, interleaving improves the system performance significantly. Moreover, the system performance is accurately predicted with the derived equations for the interleaving case.

---

<sup>1</sup>A 30% timing mismatch means that the two corresponding chips have a constant 70% overlap.



**Figure 8.4:** 3D BER for various  $\frac{\tau}{R_s}$  values.

Fig. 8.8 presents the BER performance when Gaussian distributed random jitter exists for a single user case. As can be seen the simulation and theoretical results agree for the Gaussian distributed jitter case. The comparison between the AWGN and fading cases highlights the worsening in the system performance when fading exists in the channel. The main finding of this chapter is a set of BER equations that predict the system performance in case of timing misalignment between the transmitter and receiver, in various channel scenarios. All the equations are simplified to the ones reported in the literature if  $\tau = 0$  and they all will give a result of 0.5 if  $\tau = R_S$ .

## 8.8 Summary

This chapter examined the system performance when tracking loop errors are present. To do this analysis, the energy per chip was derived assuming that the chips are sampled using zero order hold sampling. The BER for a fixed timing mismatch was derived subsequently. Because the tracking error changes many times during transmission, it has to be assumed that it is a random variable with a certain distribution. As a result, two different distributions were examined and the BER for them was derived. All the theoretically derived expressions were then confirmed by their close agreement with the simulations.

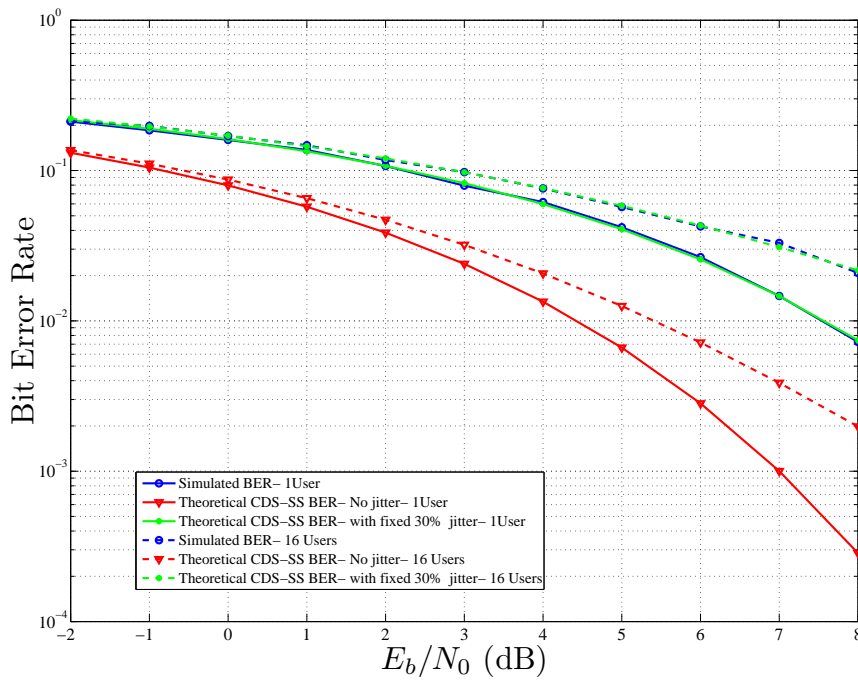


Figure 8.5: BER performance for AWGN, 1 and 16 user, constant jitter case.

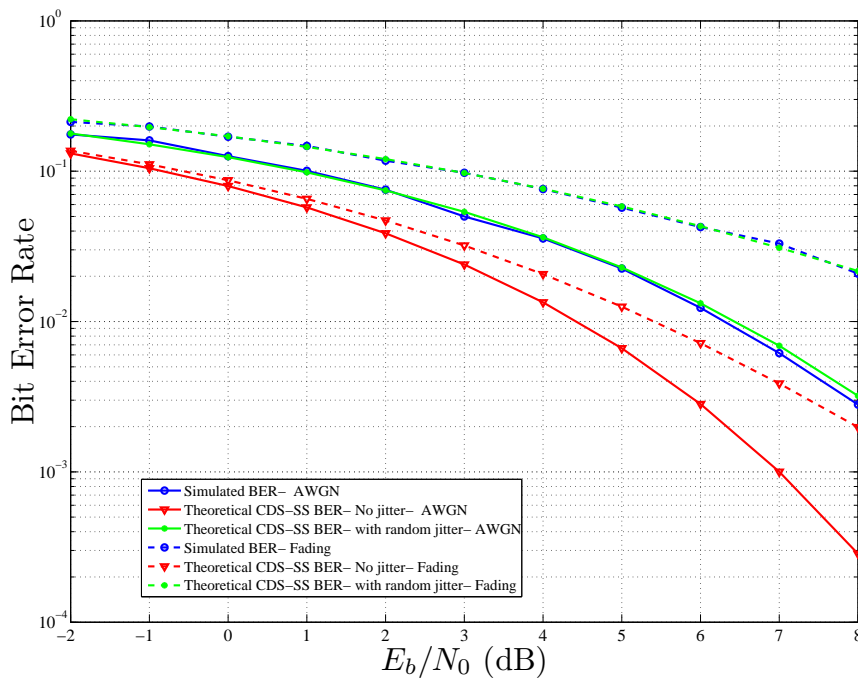


Figure 8.6: BER performance for AWGN and fading, 1 user, uniform jitter case.

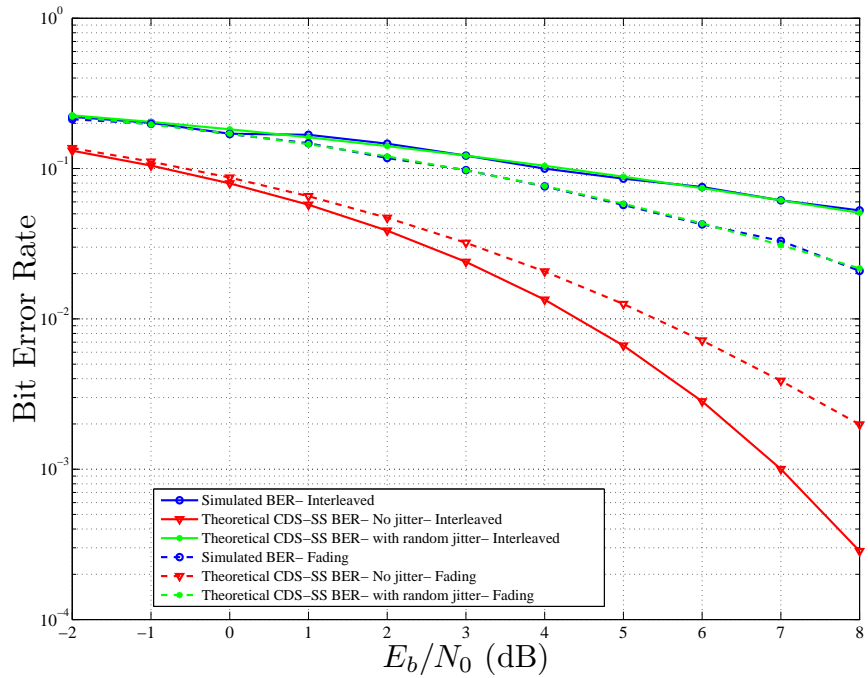


Figure 8.7: BER performance for fading and interleaved scenarios, 1 user, uniform jitter case.

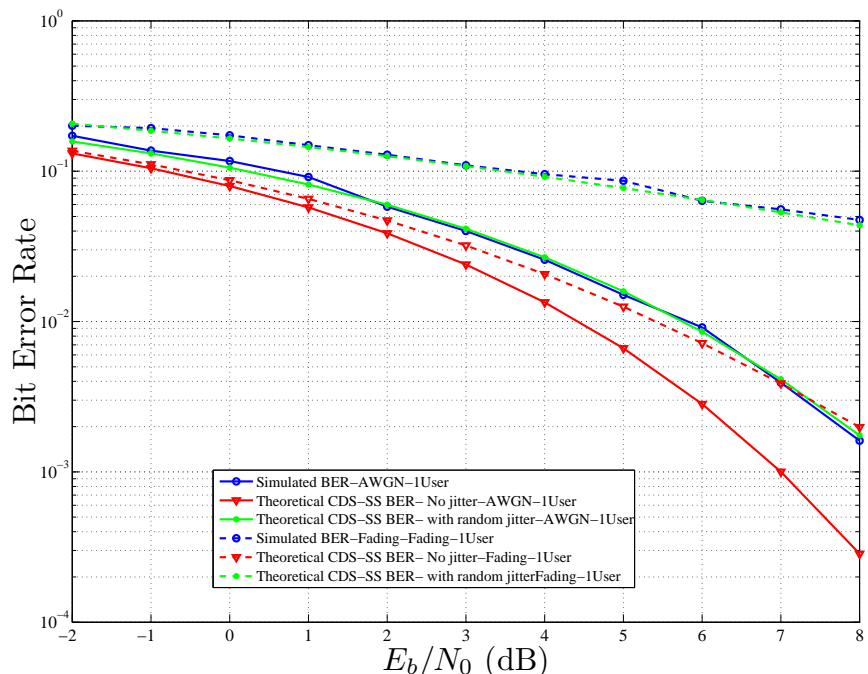


Figure 8.8: BER performance for AWGN and fading, 1 user, Gaussian distributed jitter case.



# **Chapter 9**

## **Implications and Prospects**

### **9.1 Introduction**

Now that the contributions of this thesis are fully examined in the previous chapters, it is time to look at the impact of this thesis on the state of the art and suggest possible directions of continuing this work. To re-iterate, the primary aim of this thesis is to examine the problem of synchronising chaotic spreading codes over a wireless channel. The chaotic spreading codes are used in a chaos-based direct sequence spread spectrum (CDS-SS) system. This problem is now fully analysed yielding interesting results which have been presented in the previous chapters. The primary aim of this chapter is to consider the broad implications of this thesis on the literature in existence today. Moreover, given that the CDS-SS synchronisation is an active area of research, some promising paths to continue this work have been proposed as a secondary goal of this chapter. To that end, §9.2 presents the effects of the finding on the state of the art and §9.3 presents the possible future that is based on this thesis.

### **9.2 The Effects of the Findings on the State of the Art**

The importance of synchronisation on the performance of the wireless spread spectrum systems has been highlighted in previous chapters. To summarise, without robust methods for synchronisation, the spread spectrum system performance will be adversely affected. This is because a delay of more than one chip duration will result in the auto-correlation peak of the chaotic sequence collapsing and a correlator output of close to zero. This will result in a bit error rate (BER) of 0.5.

At the outset of this research undertaking, the theory used for finding the synchronisation performance of the chaotic systems was simply adopted from the conventional spread spectrum codes which are universally binary. Essentially, the previous research assumed that the correlation function of the chaotic sequences is constant irrespective of the chaotic sequence used. This assumption is rooted in the fact that maximal length sequences have fixed correlation characteristics which only depends on their length. This assumption is not true for non-binary codes which include chaotic sequences. Because of this faulty assumption the theoretical analysis and simulation results presented in the CDS-SS synchronisation related literature did not show close agreement.

To examine the synchronisation performance of chaotic sequences, the correlation function had to be accurately modelled. An iterative map of a chaotic sequence can have infinite initial conditions which (ideally<sup>1</sup>) yield an infinite number of spreading sequences. Having this in mind, it became clear that a statistical approach has to be adopted for modelling the correlation function of the chaotic sequences. Through theoretical analysis and simulations, it was shown that when the number of chips in the correlation function is large<sup>2</sup>, the central limit theorem (CLT) can be invoked to model the correlation result as two Gaussian distributions. This way of looking at a correlation function of chaotic sequences had not been reported in the literature before and was termed chaotic correlation statistics (CCS).

Introducing the CCS to model the correlation of the chaotic chips has significant impact on the way that the chaotic chips are treated in CDS-SS systems. The CCS concept was used to examine acquisition performance in a variety of channel scenarios. The theoretical and simulation results from this analysis showed very close agreement unlike the previous results that appear in the literature. Moreover, the CCS has made accurate statistical modelling of the CDS-SS tracking loops possible. This statistical modelling was confirmed by simulation results. Overall, the CCS is an important tool for the analysis of CDS-SS systems that use correlation. This tool can be used in the future to analyse various other configurations.

Chaos-based communication, as a physical layer security method, has a valuable place in wireless applications in which security is of high importance. Moreover, because chaotic communications elevate the need for encryption algorithms which are costly in terms of processing and power consumption. As a result, in applications such as wireless sensor network security, chaos-based communication methods can be very beneficial and the present CCS method is an important step in the realisation of such methods.

### 9.3 Possible Enhancements to the Existing Work

The analysis and results presented in this thesis are limited by the research time frame. As a result there is room for expansion on the contents of this thesis. The CCS method can be used as a basis for describing any non-binary system that uses the correlation function. Specific future research directions that have their roots in this thesis are described below.

#### 9.3.1 Expansion to QPSK

The model presented for the BPSK in this thesis can be easily expanded to the QPSK case given that the statistical properties of the square of the chaotic spreading sequence are taken into account. In a QPSK setting, the in-phase and quadrature correlation results can be statistically found and then combined for the final result. The QPSK acquisition stage is already covered in literature for conventional sequences and finding out the performance of a chaos-based system and comparing to the conventional systems is instructive.

<sup>1</sup>Of course having an infinite number of spreading sequences is not possible in hardware as the number resolution becomes an issue; however, it is still possible to generate many sequences using existing hardware.

<sup>2</sup>For an acceptable level of performance, it has been assumed that the CDS-SS system uses a spreading factor of at least 50 chips.

### 9.3.2 Use of RAKE receiver

This thesis assumed that the multi-path fading is frequency flat; however, when frequency selective fading is assumed, then a receiver that can make use of the multi-path phenomenon is desirable. A RAKE receiver has been suggested in the literature for systems that use correlator receivers [87–89]. A RAKE receiver consists of a few parallel correlators (fingers) that isolate each particular version of the received signal by aligning their sequence generators with the exact path delays. The energy of each path can then be combined using various combining methods one of which is maximal ratio combining (MRC). MRC assigns the maximum weight to the path with the highest power.

The CCS method can be used to model the correlation outcome of each finger and the results can be extended to include synchronisation errors as well. It will be instructive to find the BER of a CDS-SS system that uses a RAKE receiver in a frequency selective channel.

### 9.3.3 Adaptive chaos-based synchronisation

The literature review into DS-SS acquisition and tracking showed many interesting suggestions for adaptive acquisition and tracking approaches [39, 180–184]. For example adaptive filters and equalisers can be used to improve the acquisition and tracking performance of correlator based CDS-SS systems. Another possible approach is to use the synchronised pilot signal to estimate the value of the noise in the channel in real time and change the correlation length depending on the real time channel SNR. This approach can lead into shorter acquisition times as well as faster tracking loop response times for CDS-SS systems. The application of adaptive methods within a CDS-SS system can lead to increased performance as well as an increased insight into the co-existence of non-binary spreading sequences and adaptive methods.

### 9.3.4 Other non-binary spreading sequences

The contributions of this thesis are also applicable to the systems that use non-binary sequences that do not fall into the CDS-SS category. For example, DS-SS systems that use noise-like sequences have been suggested recently. They are known as noise phase shift keying (NPSK) or DS-SS systems with random spreading. These systems use non-binary spreading codes that resembles AWGN statistically. Some preliminary research has been conducted in the synchronisation of these systems [185, 186]; however, some issues such as dealing with the un-bounded nature of the sequences have to be examined.

### 9.3.5 Hardware implementation and design

During the course of this research, various parts of the CDS-SS system were implemented in hardware in the form of a digital signal processor (DSP). Some of the results from the implementation are presented in [176, 185, 187]. The details of the hardware design and implementation is covered in Appendix G. Expansion of the hardware implementation of the system into the RF domain is instructive since it will allow real deployment measurement of the system performance. This will enable the researchers to compare the theoretically derived performance with the measurements.

## 9.4 Summary

This chapter presented the impact of the contributions of this thesis on the state of the art and suggested possible paths for continuing the current work in the future. It was explained that the CCS approach has impacted the state of the art in a significant way because it can be used in all the scenarios that involve the correlation function of non-binary sequences. The possible avenues to continue the current work include expansion to QPSK, use of a RAKE receiver, adaptive synchronisation, examining other non-binary sequences and expansion of the hardware implementation into the RF domain. The next chapter will conclude this thesis.

# **Chapter 10**

## **Conclusions**

The need for robust methods of wireless communication has been a driving force for research, invention and innovation since Marconi transmitted the first transatlantic signal using wireless technology on December 12, 1901. Since then, many different wireless communication schemes have been introduced and used. With the growing reliance on wireless communication, the sensitivity of information entrusted to the radio waves has also increased. The problem of transmitting sensitive information using wireless techniques highlights the need for secure wireless communication methods. Moreover, where transmission of secure information is concerned, there should be protection from hostile parties that actively seek to disrupt communications using methods such as jamming. As a result there is a need for robust and secure wireless communication schemes.

Although encryption and spread spectrum communication have been traditionally used for securing wireless communication systems, many scenarios exist in which encryption is not the best method because of limitations in computational power or energy constraints. Moreover, having access to an additional layer of security is desirable, since on many occasions one would like to hide not only the data but even the fact that wireless communication has taken place. The use of chaotic signals has been suggested for exactly these scenarios. The chaotic signals, which are random looking, wide-band and easy to generate have proven to be an ideal candidate for spreading sequences in spread spectrum communications including direct sequence spread spectrum systems DS-SS.

In order to design and operate a chaos-based DS-SS (CDS-SS) system successfully, it is imperative to have access to a robust way of synchronising the chaotic spreading sequences. This is because accurate synchronisation of chaotic sequences has a direct impact on the system performance. As a result, ensuring robust synchronisation of chaotic sequences is critical in CDS-SS system usability. To this end, the exact behaviour of chaotic sequences in the context of synchronisation (acquisition and tracking) has to be understood.

This thesis addressed the problems of acquisition and tracking of chaotic sequences in a spread spectrum context, where a transmitted pilot is used to acquire accurate timing between the transmitter and receiver. The aims of this thesis were to first study the state of the art in CDS-SS synchronisation and identify the existing shortcomings. The investigation in this thesis indicated that the previous analysis performed on the synchronisation of CDS-SS has not been accurate because it did not take into account the issue of the channel fading in the first instance. A deeper investigation revealed that the existing literature

on the CDS-SS subject, failed to produce accurate expressions for synchronisation performance because the approach used for system analysis had simply been borrowed from the conventional spreading code systems.

Hence the second aim of this thesis was defined as finding a more accurate approach for analysing CDS-SS system synchronisation that takes the unique nature of chaotic sequences into account. This thesis showed that an analytical approach which relies on statistically modelling the chaotic correlation function is a suitable way to model the synchronisation block of the CDS-SS system. This approach has been termed chaotic correlation statistics (CCS).

This thesis modelled the correlation of the chaotic signals as two Gaussian random variables. One with a zero mean which relates to the distribution of the correlation function when the two identical transmitted pilot and locally generated sequences are not aligned in time; and the other, a non-zero mean Gaussian random variable when the two sequences are in perfect alignment which corresponds to the auto-correlation peak. The variances of both these parts of the correlation function were then found analytically and confirmed using simulation. As the next step, the effect of additive white Gaussian noise (AWGN) and the square law device on the correlation was worked into the Gaussian model.

It was shown that the CCS can be used to accurately predict the acquisition stage performance of the CDS- SS synchronisation block in the presence of AWGN in terms of probability of detection  $P_D$  and probability of failure  $P_F$ . As a second channel scenario, the effect of slow flat fading was worked into the Gaussian model showing that the CCS model can accurately predict the acquisition stage performance when slow frequency flat fading is present. This was confirmed by the close agreement of the simulated receiver operating characteristics (ROC) results with the theoretical predictions. The reduction of the acquisition stage performance in the presence of fading lead to an investigation in chip interleaving techniques to mitigate fading. As a result, for a third channel scenario, a blind block chip interleaving/de-interleaving pair was incorporated into the acquisition stage. The resulting statistical model using the CCS approach showed close agreement with the simulated ROC results. This means that the acquisition performance can now be accurately predicted in a number of different channel scenarios.

As part of the second goal of this thesis, an investigation was conducted into the tracking stage of the CDS-SS synchronisation block. The major objective for this part was to model the peak of the tracking loop S-curve (error curve) statistically. Since the tracking loop follows a delayed lock structure in which two correlators with a certain delay are used, the CCS approach can be employed. It was shown that the CCS approach can be used to accurately model the statistical properties of the tracking loop S-curve. The distribution of the peaks of the S-curve were derived theoretically and confirmed by simulation results. This is significant because the existing literature on CDS-SS tracking traditionally assumed the tracking S-curve to be constant. This thesis showed that this is not the case as the S-curve changes form sequence to sequence. This means that the statistical approach used in this thesis for modelling the S-curve is more suitable and accurate.

After modelling the tracking stage of the CDS-SS system synchronisation block, it became apparent that there were slight tracking errors resulting from the random timing changes (known as timing jitter). As a result, this thesis focused on the effect of tracking errors on the overall system performance. To begin with, the energy reduction form a partial chip overlap was calculated and linked to the amount of misalignment. This was then used to re-derive the probability of error equations for partially overlapped

chips. The validity of this approach was confirmed by comparing the theoretical bit error rate (BER) curves with the simulation results. Once the validity of this approach was established for an AWGN case, the work was expanded to include a fading channel as well as a system utilising a chip interleaver/de-interleaver pair. The accuracy of both these cases was verified by simulation. As a final investigation, the level of timing jitter was assumed to be random and to follow a uniform distribution and a Gaussian distribution with known variance. The resulting probability of error equations do not have a closed form but they accurately predict the system performance as was shown by the close agreement with the simulation results.

Overall, this thesis has proven that synchronisation of chaotic spreading sequences for a CDS-SS system is possible. Moreover, this thesis has suggested a suitable modelling technique for the correlation function of chaotic spreading sequences. The suggested technique was tested and found to be able to predict the synchronisation block performance accurately for both acquisition and tracking stages in a variety of channel scenarios. This technique can be used in any future extension of chaotic communication that relies on finding the correlation function of chaotic sequences.



## Appendix A

### Logistic map

The Logistic map has its roots in modelling nonlinear dynamical systems that appear in ecological studies [15]. An example of an ecological system is the insect population in a given environment. Assuming that the insect breeds seasonally and the generations are not overlapping, the average population  $P_{n+1}$  of the next  $n + 1$ -th generation will be determined by the present population  $P_n$  so

$$P_{n+1} = F(P_n), \quad (\text{A.1})$$

which is a first order difference equation that can be rewritten as a linear relation

$$P_{n+1} = AP_n. \quad (\text{A.2})$$

This linear difference equation can be solved by letting

$$P_{n+1} = A^a P_n, \quad (\text{A.3})$$

which means that if each insect lays  $A$  eggs on average and all the eggs hatch, the insect population will grow exponentially given  $A > 1$ . Of course if this happens the population will explode and cover the whole environment. The controlling mechanism triggers when then the insect population is large. The controlling mechanism can take the forms of insects fighting for resources, killing each other, being affected by contagious diseases, etc. Fighting or disease transmission involves two insects and the number of such events is proportional to  $\frac{1}{2}P_{n+1}(P_{n+1} - 1)$ . This can be approximated to  $P_{n+1}^2$  when  $P_{n+1}$  is sufficiently large. As a result (A.2) can be modified to

$$P_{n+1} = AP_n - BP_{n+1} - P_n^2. \quad (\text{A.4})$$

The expression above, though simple in appearance, exhibits complicated dynamical behaviour. One of the  $A$  and  $B$  parameters can be normalised reshaping the general equation to

$$X_{n+1} = 1 - \mu X_n^2, \quad X \in (-1, +1), \quad \mu \in (0, 2]. \quad (\text{A.5})$$

This first order difference equation describes the time evolution of the normalised population  $X_n$ . Starting from a number  $X_n$  belonging to the interval  $I = (-1, +1)$ , this equation generates the next number  $X_{n+1}$  in the same interval in a deterministic manner. This means that the non-linear transformation  $f(X, \mu) \equiv 1 - \mu x^2$ , maps the interval  $I$  into itself. The equation given in (A.5) is normally referred to as the Logistic map in the literature. This function is shown in Fig. A.1.

In order to visualise the Logistic map, the parameter range for  $\mu \in (0, 2)$  are changed by small steps and the iterates of (A.5) are calculated for each step. If this is plotted, in a  $X - \mu$  coordinate system, the resulting image is known as the *bifurcation diagram*. A bifurcation diagram is essentially an attractor diagram because nearly all initial points are attracted to the points shown in the diagram. The bifurcation diagram for the Logistic map is shown in Fig. A.2.

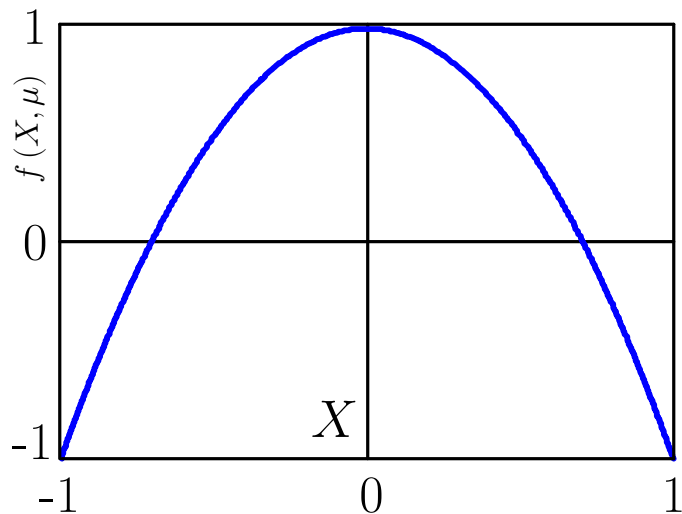


**Figure A.1:** The Logistic map function adapted from [15].

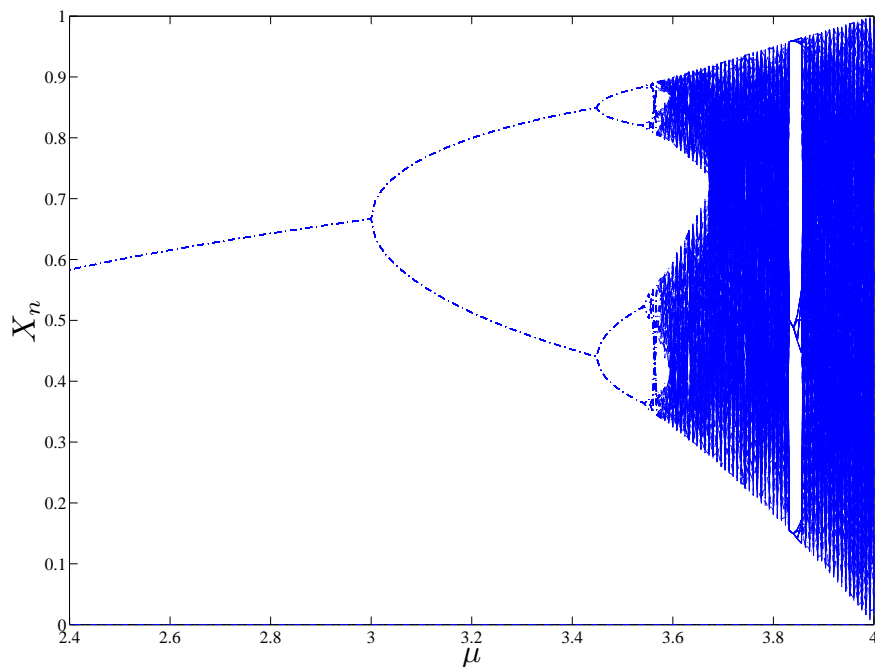


**Figure A.2:** The bifurcation diagram for the Logistic map.

## Appendix B

### Statistical derivations

#### B.1 Derivation of $E[x_k^2]$

$$\begin{aligned} E[x_k^2] &= \int_{-1}^1 x_k^2 P_X(x_k) dx_k \\ &= \int_{-1}^1 \frac{x_k^2}{\pi \sqrt{1 - x_k^2}} dx_k \\ &= \left. \frac{\frac{1}{2} \sin^{-1}(x_k) - \frac{1}{2} x_k \sqrt{(1 - x_k^2)}}{\pi} \right|_{-1}^1 \\ &= \frac{1}{4} - \left( -\frac{1}{4} \right) \\ &= \frac{1}{2} \end{aligned}$$

## B.2 Derivation of $E[x_k^4]$

$$\begin{aligned}
 E[x_k^4] &= \int_{-1}^1 x^4 P_X(x_k) dx_k \\
 &= \int_{-1}^1 \frac{x_k^4}{\pi \sqrt{1 - x_k^2}} dx_k \\
 &= \left. \frac{\frac{3}{8} \sin^{-1}(x_k) + \left(-\frac{x_k^3}{4} - \frac{3x_k}{8}\right) \sqrt{(1 - x_k^2)} \right|_{-1}^1 \\
 &= \frac{3}{8} \times \frac{1}{2} - \left(-\frac{3}{8} \times \frac{1}{2}\right) \\
 &= \frac{3}{8}
 \end{aligned}$$

## Appendix C

# Mean and Variance of the Rayleigh Random Variable

The distribution of  $a$  is given as  $f_A(a) = \frac{a}{b^2} \exp\left(\frac{-a^2}{2b^2}\right)$ . The mean and variance are therefore

$$\begin{aligned} E[a] &= \int_{-\infty}^{\infty} a \cdot f_A(a) da \\ &= \int_0^{\infty} \frac{a^2}{b^2} \exp\left(\frac{-a^2}{2b^2}\right) da \\ &= b \sqrt{\frac{\pi}{2}} \end{aligned}$$

$$\begin{aligned} \text{Var}[a] &= E[a^2] - E^2[a] \\ &= \frac{4 - \pi}{2} b^2 \end{aligned}$$



## Appendix D

# Product of Rayleigh and Gaussian Distributions

This appendix considers the pdf of  $Z_{h_0}$  variable analytically to prove that it can be approximated with Gaussian.

Assuming that  $Y$  is the random variable which is the result of the product of zero mean Gaussian and Rayleigh. That is

$$Y = AX, \quad (D.1)$$

literature, [172], shows that the pdf of  $Y$  is

$$f_Y(y) = \frac{1}{2\sigma_1\sigma_2} \exp\left(-\frac{|z|}{\sigma_1\sigma_2}\right) \quad (D.2)$$

where  $\sigma_1 = \sqrt{\frac{L}{4}}$  which is the standard deviation of  $X$  and  $\sigma_2$  is the mode of  $A$ .

The following figure shows the pdf of the simulated parameters and the theoretical results coming from the above equation.

It can be seen that there is close agreement between the theoretical and simulation results.

For the case of  $Z = AX + N$ , where  $N$  represents the signal  $\times$  noise part which is assumed to be Gaussian, there also exist an analytical solution given in the formula below. The simulation results with the analytical one presented in the formula are compared below. This is also compared with a Gaussian distribution with the same mean and variance as the theoretical curve. This helps to justify our choice of a chi-square distribution later on.

The pdf of  $Z_{h_0}$  is given by

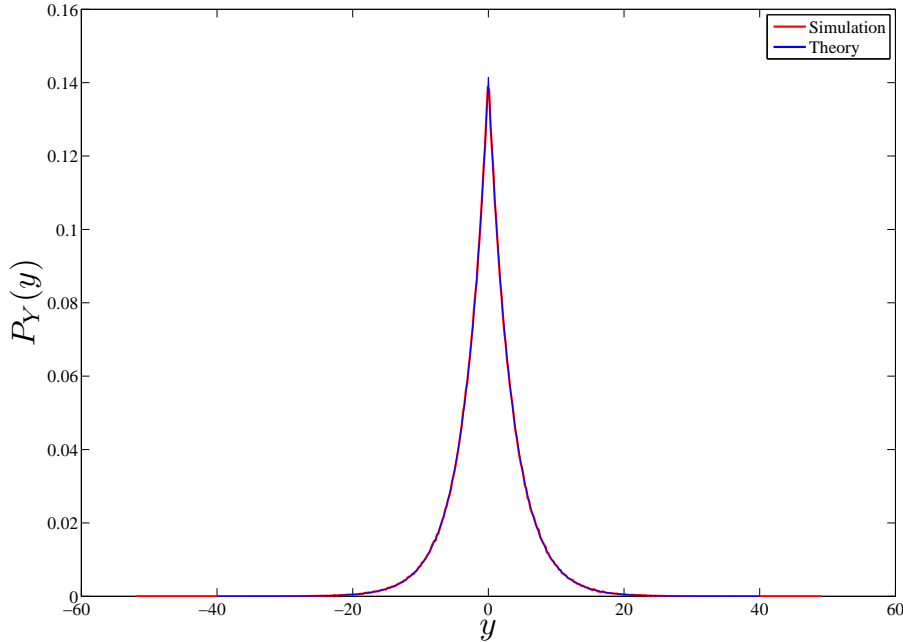


**Figure D.1:** Theory and simulation comparison for the product of Rayleigh and Gaussian.

$$f_Z(z) = \frac{1}{2\sigma_1\sigma_2} \exp \left[ \left( \frac{\sigma_3}{\sigma_1\sigma_2} \right)^2 + \frac{z}{\sigma_1\sigma_2} \right] Q \left( \frac{\sigma_3}{\sigma_1\sigma_2} + \frac{z}{\sigma_1\sigma_2} \right) + \exp \left[ \left( \frac{\sigma_3}{\sigma_1\sigma_2} \right)^2 + \frac{z}{\sigma_1\sigma_2} \right] Q \left( \frac{\sigma_3}{\sigma_1\sigma_2} + \frac{z}{\sigma_1\sigma_2} \right), \quad (\text{D.3})$$

where  $Q(\cdot)$  denotes the Q-function and  $\sigma_3$  is the standard deviation of the signal  $\times$  noise term which is  $\sqrt{\frac{L}{2}}\sigma_n$ .

The following figure shows the comparison of the results. As can be seen the three curves are close, so the resulting distribution can be closely approximated by a Gaussian distribution. As a result, the square of the cross-correlation variable can be considered to be a chi-square distribution with one degree of freedom.

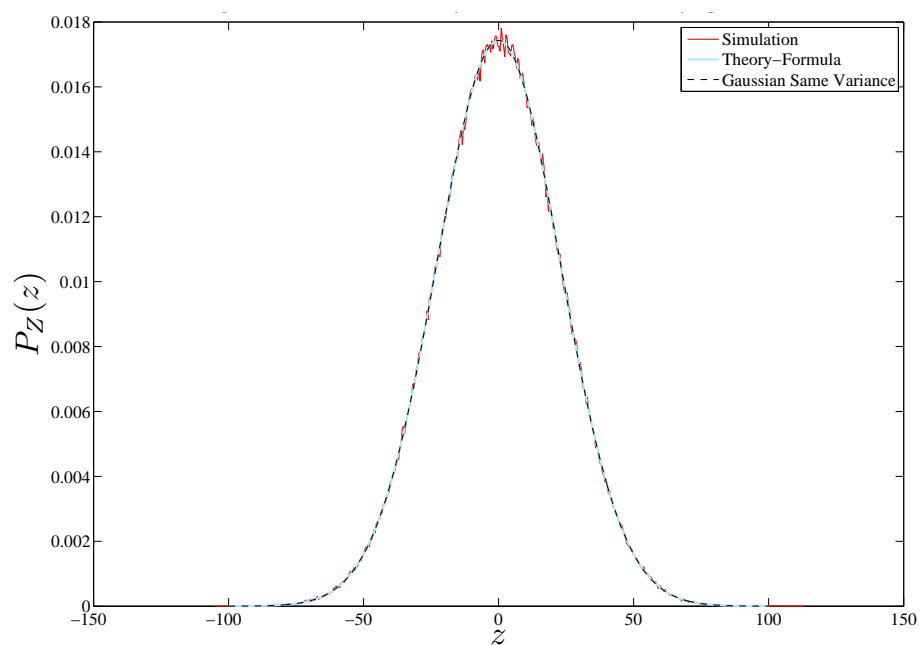


**Figure D.2:** Theory and simulation comparison for Rayleigh $\times$ Gaussian+Gaussian.



## Appendix E

# Chip-interleaving

Interleaving is a technique to eliminate (or at least mitigate) bursts of error in time. This is done by using the concept of time diversity. In chip-interleaving, a sequence of chips is permuted or interleaved before being transmitted over a channel that introduces burst errors (a channel with deep fades for example) [8]. This concept can be exploited for mitigation of the effect of fading on the system. There are various ways that the chips can be interleaved/de-interleaved, the simplest of which is the block interleaving method. Fig. E.1 presents the basic operation of a block interleaver/de-interleaver pair. Essentially, in a block interleaving scenario, the chips are transmitted by the column, that is, the first chip of the first bit is placed next to the first chip of the second bit and so on. When the message has passed through the channel, the chips are rearranged to the original form. That way, if a fading coefficient corresponding to a deep fade was to occur over bit, its fading effect would be smeared across many bits and can be compensated by the correlation function to some degree. Using interleaving techniques introduces some system delay which has to be considered for the design.



**Figure E.1:** Block chip interleaver/de-interleaver pair.



## Appendix F

# BER Derivation

### F.1 In presence of noise

$$\begin{aligned}
P_e &= \frac{1}{2} \operatorname{erfc} \frac{2\beta(R_s - |\tau|)P_c}{\sqrt{2(\beta P_c^2 \{(R_s - |\tau|)^2\} + 2|\tau|^2) + R_s^2 2\beta(N-1)(P_c)^2 + R_s^2 \beta N_o P_c}}} \\
&= \frac{1}{2} \operatorname{erfc} \left( \frac{2\beta P_c^2 \{(R_s - |\tau|)^2\} + 2|\tau|^2 + 4\beta P_c^2 R_s^2 (N-1) + 2\beta P_c R_s^2 N_o}{4\beta^2 P_c^2 (R_s - |\tau|)^2} \right)^{-\frac{1}{2}} \\
&= \frac{1}{2} \operatorname{erfc} \left( \frac{2\beta P_c^2 \{(R_s - |\tau|)^2\} + 2|\tau|^2}{4\beta^2 P_c^2 (R_s - |\tau|)^2} + \right. \\
&\quad \left. \frac{4\beta P_c^2 R_s^2 (N-1)}{4\beta^2 P_c^2 (R_s - |\tau|)^2} + \frac{\{2\beta P_c R_s^2 N_o\}}{4\beta^2 P_c^2 (R_s - |\tau|)^2} \right)^{-\frac{1}{2}} \\
&= \frac{1}{2} \operatorname{erfc} \left( \frac{\psi}{\beta} + \left( \frac{R_s}{R_s - |\tau|} \right)^2 \left\{ \frac{|\tau|^2}{\beta R_s^2} + \frac{(N-1)}{\beta} + \frac{N_o}{2\beta P_c} \right\} \right)^{-\frac{1}{2}} \\
&= \frac{1}{2} \operatorname{erfc} \left( \frac{\psi}{\beta} + \frac{1}{C^2} \left( \frac{D^2}{\beta} + \frac{(N-1)}{\beta} + \frac{N_o}{E_b} \right) \right)^{-\frac{1}{2}}. \tag{F.1}
\end{aligned}$$

## F.2 In presence of noise and fading

$$\begin{aligned}
P_e &= \frac{1}{2} \operatorname{erfc} \frac{2a\beta(R_s - |\tau|)P_c}{\sqrt{2 \left( a^2\beta P_c^2 \left\{ (R_s - |\tau|)^2 \right\} + 2|\tau|^2 \right) + R_s^2 2a^2\beta(N-1)(P_c)^2 + R_s^2\beta N_o P_c}} \\
&= \frac{1}{2} \operatorname{erfc} \left( \frac{2\beta a^2 P_c^2 \left\{ (R_s - |\tau|)^2 \right\} + 2|\tau|^2 + 4a^2\beta P_c^2 R_s^2 (N-1) + 2\beta P_c R_s^2 N_o}{4a^2\beta^2 P_c^2 (R_s - |\tau|)^2} \right)^{-\frac{1}{2}} \\
&= \frac{1}{2} \operatorname{erfc} \left( \frac{2a^2\beta P_c^2 \left\{ (R_s - |\tau|)^2 \right\} + 2|\tau|^2}{4a^2\beta^2 P_c^2 (R_s - |\tau|)^2} + \right. \\
&\quad \left. \frac{4a^2\beta P_c^2 R_s^2 (N-1)}{4a^2\beta^2 P_c^2 (R_s - |\tau|)^2} + \frac{2\beta P_c R_s^2 N_o}{4a^2\beta^2 P_c^2 (R_s - |\tau|)^2} \right)^{-\frac{1}{2}} \\
&= \frac{1}{2} \operatorname{erfc} \left( \frac{\psi}{\beta} + \left( \frac{R_s}{R_s - |\tau|} \right)^2 \left\{ \frac{|\tau|^2}{\beta R_s^2} + \frac{(N-1)}{\beta} + \frac{N_o}{2a^2\beta P_c} \right\} \right)^{-\frac{1}{2}} \\
&= \frac{1}{2} \operatorname{erfc} \left( \frac{\psi}{\beta} + \frac{1}{C^2} \left( \frac{D^2}{\beta} + \frac{(N-1)}{\beta} + \frac{N_o}{a^2 E_b} \right) \right)^{-\frac{1}{2}}. \tag{F.2}
\end{aligned}$$

## F.3 In presence of noise and interleaved fading

$$\begin{aligned}
P_e &= \frac{1}{2} \operatorname{erfc} \frac{2\beta(R_s - |\tau|)b\sqrt{\frac{\pi}{2}}P_c}{\sqrt{2 \left( 2\beta(R_s - |\tau|)^2 b^2 P_c^3 \{6 - \pi\} + 2\beta|\tau|^2 b^2 P_c + 2\beta(N-1)R_s^2 P_c^2 2b^2 + R_s^2\beta N_o P_c \right)}} \\
&= \frac{1}{2} \operatorname{erfc} \left( \frac{4\beta P_c^3 b^2 (R_s - |\tau|)^2 (6 - \pi) + 4\beta|\tau|^2 b^2 P_c + 8\beta(N-1)R_s^2 P_c^2 b^2 + 2\beta P_c R_s^2 N_o}{4\beta^2 (R_s - |\tau|)^2 b^{\frac{\pi}{2}} P_c^2} \right)^{-\frac{1}{2}} \\
&= \frac{1}{2} \operatorname{erfc} \left( \frac{4\beta P_c^3 b^2 (R_s - |\tau|)^2 (6 - \pi) + 4\beta|\tau|^2 b^2 P_c +}{4\beta^2 (R_s - |\tau|)^2 b^{\frac{\pi}{2}} P_c^2} \right. \\
&\quad \left. \frac{8\beta(N-1)R_s^2 P_c^2 b^2}{4\beta^2 (R_s - |\tau|)^2 b^{\frac{\pi}{2}} P_c^2} + \frac{2\beta P_c R_s^2 N_o}{4\beta^2 (R_s - |\tau|)^2 b^{\frac{\pi}{2}} P_c^2} \right)^{-\frac{1}{2}} \\
&= \frac{1}{2} \operatorname{erfc} \left( \frac{(6 - \pi)}{\pi\beta} + \frac{4|\tau|^2}{\pi\beta(R_s - |\tau|)^2} + \frac{R_s^2}{(R_s - |\tau|)^2} \left\{ \frac{4(N-1)}{\pi\beta} + \frac{2}{\pi b^2} \left( \frac{E_b}{N_o} \right)^{-1} \right\} \right)^{-\frac{1}{2}}. \tag{F.3}
\end{aligned}$$

## Appendix G

# DSP Design

### G.1 DSP Specification and Justification

The reasons for choosing a DSP platform to implement the CDS-SS system were twofold. Firstly, the number of logic elements needed to implement the systems on FPGA is high which prevents implementations with higher numbers of users. Secondly, the sequential nature of instruction flow in the DSP enables Monte Carlo testing with larger amounts of data which results in a more accurate examination of the DSP performance. The main results of this implementation along with a comparison with a multi-user detector are submitted for publication in [187]. The multi-user detector part presented in [187] is not a contribution of this thesis.

The DSP chosen for the realisation of the chaos-based DS-SS system presented here is the ADSP-TS201S TigerSHARC from Analog Devices which is designed with signal processing and large scale telecommunication tasks in mind. This DSP supports single-precision IEEE 32-bit and extended-precision 40-bit floating-point data formats as well as 8-, 16-, 32-, and 64-bit fixed-point data formats. Based on the tests performed, a word length of 32 was chosen as it contained sufficient precision for the generation of the chaotic samples while allowing for the realisation of a multi-user system. The DSP also has a sufficiently wide dynamic range to allow the implementation of an AWGN generator. Furthermore, in order to maximise the allowable user capacity of the system, a fast processor is needed. The chosen DSP has a processor clock speed of 600 MHz and is capable of executing 2400MIPS, 3600MFLOPS, and 1200MMACS. Overall, the capabilities of this DSP were deemed sufficient for the purposes of prototyping the DS-SS systems presented [188].

Although floating-point devices have been historically more expensive than the fixed-point ones, this price gap is narrowing due to the increase in manufacturing capacity for new and emerging technologies which rely on higher resolution of the DSPs. Moreover, previous studies [189] show that the fixed point realizations of chaotic systems are not as secure because they introduce very short periodicity into the spreading code generators. As a result, a floating-point device is deemed desirable for applications which require a higher degree of security.

The CDS-SS realisation presented in this appendix was developed using the TS201S EZ-KIT Lite evaluation board for the TigerSHARC processor as well as the VisualDSP++ development environment. The

prototypes were defined in software using high-level C programming language, which was then fed into the processor as assembly code by VisualDSP++. In order to measure the performance of the prototype, a test bench for BER performance was defined and used. The loading of the code onto the DSP platform as well as executing them was controlled by the PC connected to the evaluation board.

## G.2 Design and Implementation of the CDS-SS System

A modular approach was used in the design and the implementation of the CDS-SS system with correlator receiver. The tasks of the transmitter and receiver were broken into sub-tasks which were then specified in functions. Also, the design included a test bench to measure the BER performance of the system. Fig. G.1 presents the functional block diagram of the DSP implementation. The rest of this part gives more detail about each function.

### Test Bit Generator

In order to accurately measure the system performance, known data bits have to be transmitted and their estimate is to be compared with the original bits in order to obtain an accurate BER. The normal way of generating bits in telecommunication test bed applications is using linear feedback shift-registers (LFSR). In the present implementation, the test bit generator block shown in Fig.G.1 employs a 16 bit Fibonacci LFSR with taps on bits 11, 13, 14 and 16 where the 10-th bit is used as the user message. This block generates the message for each user and is part of the test bench. The test bench has a replica of this block available for BER measurement.

### PNRZ Encoder

As mentioned in the introduction, the message bits are encoded using PNRZ. That is, all the 0 outputs of the test bit generator are encoded to  $-1$ .

### Chaotic Generator

The chaotic generator uses the Logistic map given in (2.4) to generate a set of chaotic spreading codes with which to modulate the message. Each user will have a unique spreading sequence generated by uniquely assigned initial condition (IC).

Given that the DSP has a finite resolution, the chaotic spreading codes generated will eventually become periodic. As a result, the period of the chaotic samples as well as their variation depending on the IC are of interest. Based on the periodicity tests conducted in [190], 256 initial conditions yielding the longest sequences were chosen for the users. The chaotic generators are designed in such a way that they reset themselves just before the sequences become periodic.

### AWGN Generator

The AWGN generator consists a white Gaussian sample generator and a scaling factor calculator. The white Gaussian sample generator is implemented using the Box-Muller method presented in [191]. This method generates AWGN samples by first obtaining two independent random samples ( $n_1, n_2$ ) which are uniformly distributed over  $[0, 1]$  from the normalized rand() function which exists in the C language library. These two samples are then used to calculate  $n$ , where  $n \sim N(0, 1)$  using the following equation.

$$n = \left( \sqrt{-\ln(n_1)} \right) \left( \sqrt{2} \cos(2\pi n_2) \right). \quad (\text{G.1})$$

In order to evaluate the performance of the noise generator, the above equation was used to generate  $10^9$  noise samples on the DSP and the results were then examined up to  $4\sigma$ . The average relative deviation from the true Gaussian distribution is 0.2%. Fig.G.2 shows the result of the test conducted to verify the AWGN generator.

The scaling factor calculator scales the generated noise. This function uses the value of the current SNR as well as the energy per bit ( $E_b$ ) for each transmitted bit to calculate the appropriate scaling factor ( $\sigma$  value) for the AWGN.

### Correlator

This function performs two tasks; firstly, it multiplies the received signal samples with the locally generated spreading sequence; secondly, it sums the multiplication result for one bit duration. The correlation result will, ideally, be a large positive number for the case that a  $\{+1\}$  is transmitted and a large negative number if a  $\{-1\}$  is transmitted.

### Decision Circuit

The decision circuit acquires the output of the correlator and simply compares the received value with the threshold. The recovered message is the output of the decision circuit.

### BER Calculator

This function is part of the test bench. Essentially, for each SNR value the system is run until a certain number of errors is detected. After the error threshold is reached, the BER calculator simply calculates the ratio of the erroneous bits to the total number of bits sent. This will then be transferred into a text file for display purposes.

## G.3 System Results

This section presents the results obtained from the DSP implementation of the chaos-based DS-SS systems. The chaos-based DS-SS system implementation was benchmarked against the conventional BPSK

system using the test bench specified in the C language. The performance was measured for multiple spreading factors as well as different numbers of users in terms of the BER for SNR levels of -2 to 8 dB; the SNR is expressed as  $\frac{E_b}{N_0}$ . As can be seen from Figs. G.3 and G.4 the theoretical results presented in [192] are confirmed by the realisation presented here for changes in the spreading factor and the number of users. As expected, the BER decreases as the spreading factor is increased. This is because there is more information available to the receiver for every bit. Also, as is evident from Fig. G.3, with a fixed spreading factor an increase in the number of users increases the BER. This is also expected because with an increased number of users there is more interference, and detecting the messages would become increasingly difficult as more users use the system.

## G.4 Acquisition Results

The receiver operating characteristics (ROC) plot is presented in G.5. As can be seen the simulation and implementation results show close agreement.

## G.5 Visual Transmission Results

To prove that the acquisition of the chaotic sequences is possible to implement, a CDS-SS system was implemented which used an acquisition stage to synchronise the chips. To this system a stream of PNRZ encoded bits (a small picture) were fed and the system was allowed to synchronise. The received message was then reconstructed into the picture as can be seen in Fig. G.6, the places that the system loses synchronisation are seen as random patches.

## G.6 Speed Test Result

In this test, the speed of the CDS-SS systems is measured and compared with each other. A spreading factor of 20 was chosen and the processing speed was measured for different numbers of users when  $10^4$  message bits were transmitted and received. This was done by measuring the clock cycles needed to execute the relevant code for sending and receiving the said bits. The clock cycles were then converted to the bit rate using (G.2).

$$\text{Bit Rate} = \frac{\text{Number of bits sent} \times \text{Clock frequency}}{\text{Clock cycles} \times \text{Number of users}}. \quad (\text{G.2})$$

Fig. G.7 shows the results of the speed estimation for both receivers. As expected, if the number of users increases, the system speed decreases.

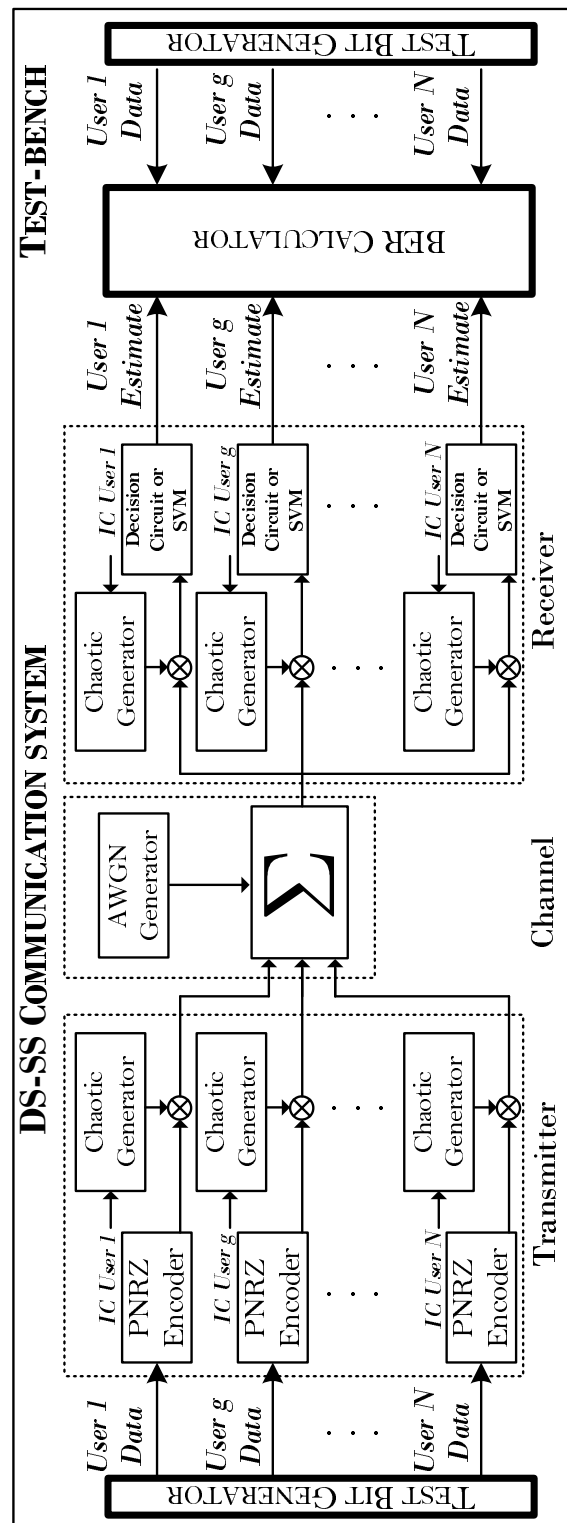


**Figure G.1:** The functional block diagram of the DS-SS system as implemented on the DSP.

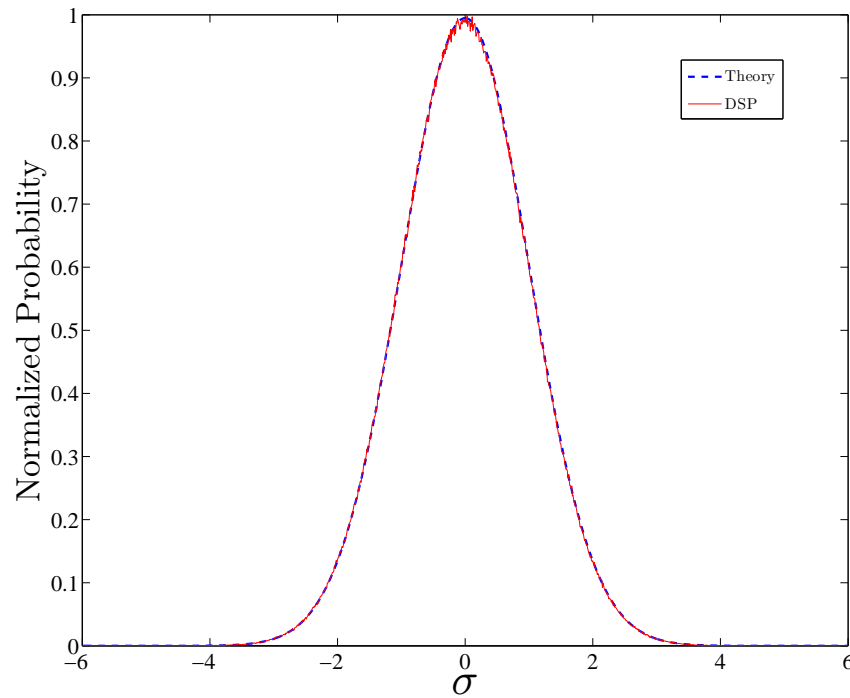


**Figure G.2:** Comparison between a theoretical Gaussian PDF and the DSP implementation.

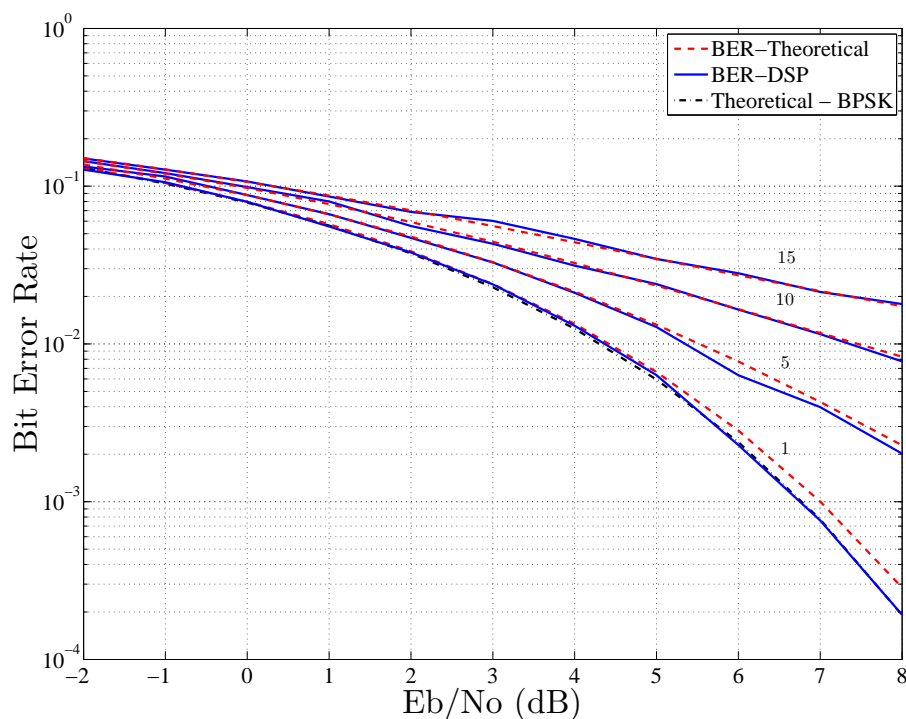


**Figure G.3:** BER for a 1, 5, 10 and 15 user DS-SS system, spreading factor of 100.

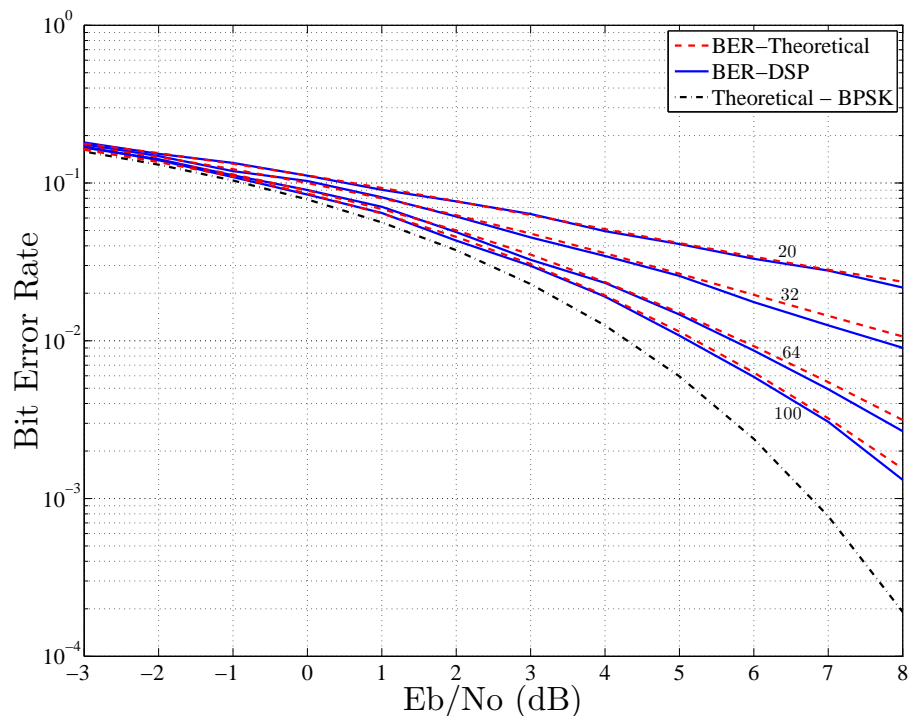


**Figure G.4:** BER for a four-user DS-SS system using spreading factors 20, 32, 64 and 100.

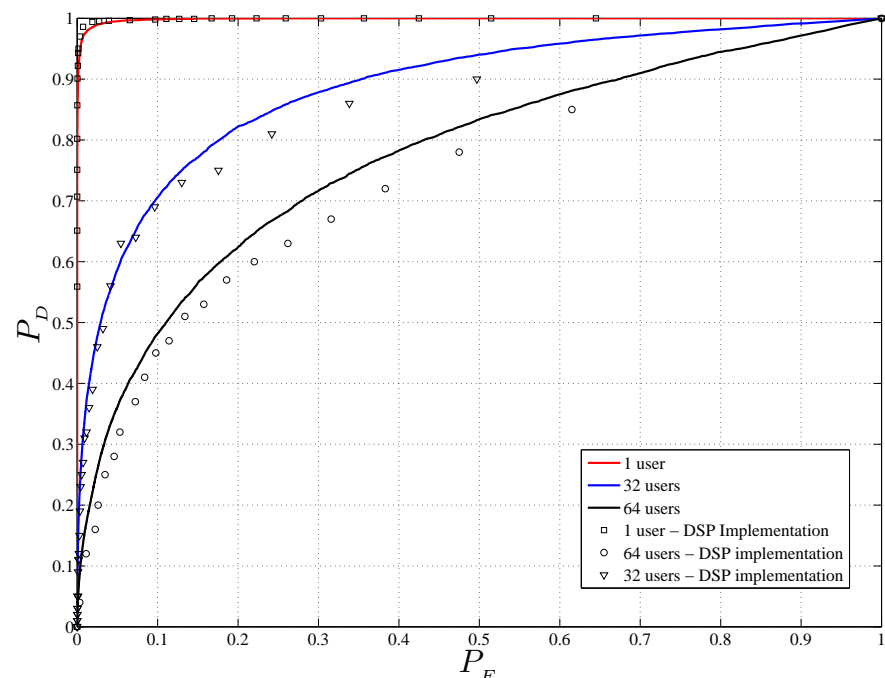


**Figure G.5:** ROC results form the DSP.



**Figure G.6:** Visual results for transmission of information.

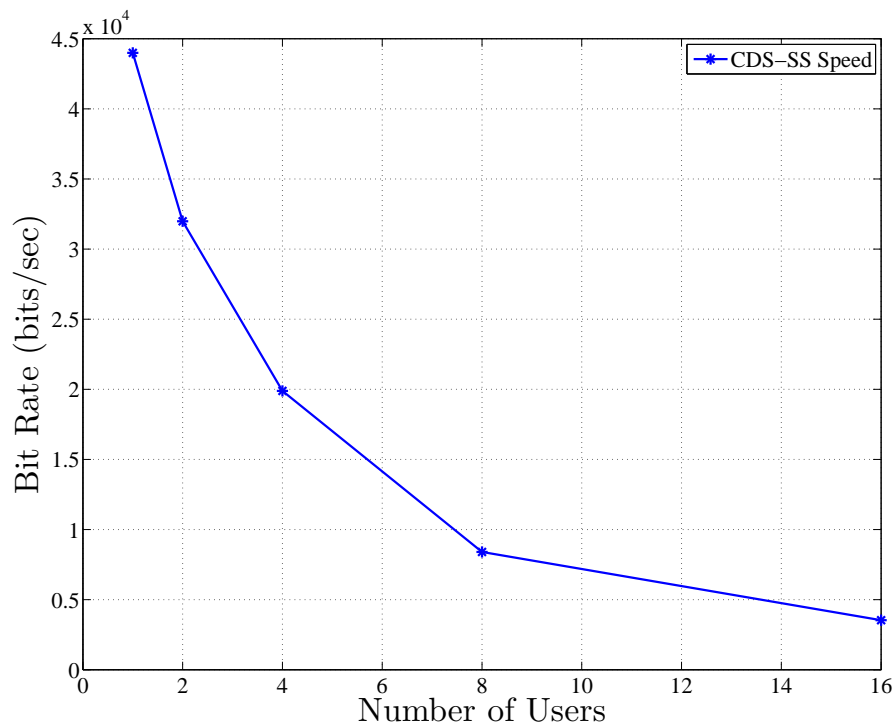


**Figure G.7:** Bit rate comparison for correlator and SVM receivers for various number of users.

# References

- [1] R. S. Baker, “Marconi’s achievement. Telegraphing across the ocean without wires.” *McClure’s Magazine*, pp. 291–299, Feb. 1902.
- [2] D. Steinbock, *Wireless Horizon: Strategy and Competition in the Worldwide Mobile Marketplace*. AMACOM, 2003.
- [3] R. W. Burns, Ed., *Communications: An International History of Formative Years*. The Institution of Electrical Engineers, 2004.
- [4] J. M. Cattell, “How the zeppelin raiders are guided by radio signals,” *Popular Science Monthly*, pp. 632–634, Apr. 1918.
- [5] H. Gernsback, “Seven zeppelins were lured to death by radio,” *Electrical Experimenter*, pp. 708–709, Nov. 1919.
- [6] R. Walters, *Spread Spectrum: Hedy Lamarr and the Mobile Phone*. BookSurge, LLC, 2005.
- [7] (2010, July) Over 5 billion mobile phone connections worldwide. Online. BBC. [Online]. Available: <http://www.bbc.co.uk/news/10569081>
- [8] J. S. Lee and L. E. Miller, *CDMA Systems Engineering Handbook*, ser. Mobile Communications. London: Artech House, 1998.
- [9] R. E. Zeimer and R. L. Peterson, *Introduction to Digital Communication*. Upper Saddle River, NJ: Prentice Hall, 2001.
- [10] J. G. Proakis, *Digital communications*. McGraw-Hill, 2001.
- [11] J. G. Proakis and M. Salehi, *Communication Systems Engineering*. Prentice Hall, 1994.
- [12] (2003, May) An introduction to jitter in communications systems. Online. Maxim Integrated Products. Sunnyvale, California, USA. [Online]. Available: <http://www.maxim-ic.com/app-notes/index.mvp/id/1916/CMP/WP-34>
- [13] “Worldwide mobile market forecasts: 2006-2011,” Portio Research, 2006.
- [14] N. Tesla, “Method of signaling,” United States of America Patent US0 723 188, Mar., 1903.
- [15] B. L. Hao, *Elementary symbolic dynamics and chaos in dissipative systems*. World Scientific Publishin Co, 1989.

- [16] E. N. Lorenz, “Deterministic nonperiodic flow,” *Journal of the Atmospheric Sciences*, vol. 20, pp. 130–141, 1963.
- [17] T. Matsumoto, “A chaotic attractor from Chua’s circuit,” *IEEE Transactions on Circuits and Systems*, vol. 12, pp. 1055–1058, 1984.
- [18] O. E. Rossler, “An equation for continuous chaos,” *Physics Letters*, vol. 57A (5), pp. 397–398, 1976.
- [19] C. E. Shannon, “Communication theory of secrecy systems,” *Bell Systems Technical Journal*, vol. 28, pp. 656–715, 1949.
- [20] A. Abel and W. Schwarz, “Chaos communications-principles, schemes, and system analysis,” *Proceedings of the IEEE*, vol. 90, no. 5, pp. 691 –710, May 2002.
- [21] L. M. Pecora and T. L. Carroll, “Synchronisation in chaotic systems,” *Physical Review Letters*, vol. 64, 19 Feb 1990.
- [22] ——, “Driving systems with chaotic signals,” *Phys. Rev. A*, vol. 44, no. 4, pp. 2374–2383, Aug 1991.
- [23] K. M. Cuomo and A. V. Oppenheim, “Circuit implementation of synchronized chaos with applications to communications,” *Phys. Rev. Lett.*, vol. 71, no. 1, pp. 65–68, Jul 1993.
- [24] H. Dedieu, M. Kennedy, and M. Hasler, “Chaos shift keying: modulation and demodulation of a chaotic carrier using self-synchronizing Chua’s circuits,” *IEEE Trans. Circuits Syst. I Analog and Digital Signal Processing*, vol. 40, no. 10, pp. 634–642, Oct. 1993.
- [25] D. R. Frey, “Chaotic digital encoding: an approach to secure communication,” *Circuits and Systems II: Analog and Digital Signal Processing, IEEE Transactions on*, vol. 40, no. 10, pp. 660–666, Oct. 1993.
- [26] K. Murali and M. Lakshmanan, “Transmission of signals by synchronization in a chaotic Van der Pol-Duffing oscillator,” *Phys. Rev. E*, vol. 48, no. 3, pp. R1624–R1626, Sep. 1993.
- [27] S. Kay and V. Nagesha, “Methods for chaotic signal estimation,” *Signal Processing, IEEE Transactions on*, vol. 43, no. 8, pp. 2013 –2016, Aug 1995.
- [28] L. Kocarev and U. Parlitz, “General approach for chaotic synchronization with applications to communication,” in *Controlling Chaos*. San Diego: Academic Press, 1996, pp. 161–164.
- [29] S. Isabelle and G. Wornell, “Statistical analysis and spectral estimation techniques for one-dimensional chaotic signals,” *Signal Processing, IEEE Transactions on*, vol. 45, no. 6, pp. 1495 –1506, Jun. 1997.
- [30] S. Starkov and S. Yemetz, “Digital communication systems using chaos,” *Control of Oscillations and Chaos, 1997. Proceedings., 1997 1st International Conference*, vol. 2, pp. 207–210 vol.2, Aug 1997.

- [31] C. Zhou and T. Chen, "Robust communication via chaotic synchronization based on contraction maps," *Physics Letters A*, vol. 225, no. 1-3, pp. 60–66, 1997.
- [32] ———, "Extracting information masked by chaos and contaminated with noise: Some considerations on the security of communication approaches using chaos," *Physics Letters A*, vol. 234, no. 6, pp. 429–435, 1997.
- [33] T. Carroll and L. Pecora, "Using multiple attractor chaotic systems for communication," *Electronics, Circuits and Systems, 1998 IEEE International Conference on*, vol. 1, pp. 103–106 vol.1, 1998.
- [34] S. Penaud, J. Guittard, P. Bouysse, and R. Quere, "DSP implementation of self-synchronised chaotic encoder-decoder," *Electronics Letters*, vol. 36, no. 4, pp. 365–366, Feb 2000.
- [35] T. Kohda, "Information sources using chaotic dynamics," *Proceedings of the IEEE*, vol. 90, no. 5, pp. 641 –661, may 2002.
- [36] H. Leung, H. Yu, and K. Murali, "Ergodic chaos-based communication schemes," *Phys. Rev. E*, vol. 66, no. 3, p. 036203, Sep 2002.
- [37] J. Lu, X. Wu, and J. Lu, "Synchronization of a unified chaotic system and the application in secure communication," *Physics Letters A*, vol. 305, no. 6, pp. 365 – 370, 2002.
- [38] M. Feki, B. Robert, G. Gelle, and M. Colas, "Secure digital communication using discrete-time chaos synchronization," *Chaos, Solitons & Fractals*, vol. 18, no. 4, pp. 881–890, 2003.
- [39] M. Feki, "An adaptive chaos synchronization scheme applied to secure communication," *Chaos, Solitons & Fractals*, vol. 18, no. 1, pp. 141–148, 2003.
- [40] A. Khadra, "Impulsive control and synchronization of chaos-generating-systems with applications to secure communication," Ph.D. dissertation, Waterloo, Ontario, 2004.
- [41] C. M. Kim, W. H. Kye, S. Rim, and S. Y. Lee, "Communication key using delay times in time-delayed chaos synchronization," *Physics Letters A*, vol. 333, no. 3-4, pp. 235–240, 2004.
- [42] J. G. Lu, "Multiple access chaotic digital communication based on generalized synchronization," *Chaos, Solitons & Fractals*, vol. 25, no. 1, pp. 221–227, 2005.
- [43] A. Loria and A. Zavala-Rio, "Adaptive tracking control of chaotic systems with applications to synchronization," *Circuits and Systems I: Regular Papers, IEEE Transactions on*, vol. 54, no. 9, pp. 2019–2029, Sept. 2007.
- [44] B. Jovic, S. Berber, and C. P. Unsworth, "A novel mathematical analysis for predicting master-slave synchronization for the simplest quadratic chaotic flow and ueda chaotic system with application to communications," *Physica D: Nonlinear Phenomena*, vol. 213, no. 1, pp. 31–50, 2006.
- [45] B. Jovic and C. Unsworth, "Fast synchronisation of chaotic maps for secure chaotic communications," *Electronics Letters*, vol. 46, no. 1, pp. 49–50, 7 2010.

- [46] R. Vali, S. Berber, and S. Nguang, "Effect of Rayleigh fading on non-coherent sequence synchronization for multi-user chaos based DS-CDMA," *Signal Processing*, vol. 90, no. 6, pp. 1924–1939, 2010.
- [47] G. Heidari-Bateni and C. D. McGillem, "A chaotic direct-sequence spread-spectrum communication system," *IEEE Trans. Commun.*, vol. 42, no. 234, pp. 1524–1527, Feb. 1994.
- [48] U. Parlitz and S. Ergezinger, "Robust communication based on chaotic spreading sequences," *Physics Letters A*, vol. 188, no. 2, pp. 146–150, 1994.
- [49] R. Rovatti, G. Setti, and G. Mazzini, "Chaos-based spreading compared to M-sequences and Gold spreading in asynchronous CDMA communication systems," in *Proceedings of the 1997 European Conference on Circuit Theory and Design*, Budapest Hungary, 1997.
- [50] M. Coulon and D. Roviras, "Multi-user receivers for synchronous and asynchronous transmissions for chaos-based multiple-access systems," *Signal Processing*, vol. 89, no. 4, pp. 583 – 598, 2009.
- [51] M. Sushchik, L. Tsimring, and A. Volkovskii, "Performance analysis of correlation-based communication schemes utilizing chaos," *Circuits and Systems I: Fundamental Theory and Applications, IEEE Transactions on*, vol. 47, no. 12, pp. 1684 –1691, Dec. 2000.
- [52] X. Wang and J. Zhang, "Chaotic secure communication based on nonlinear autoregressive filter with changeable parameters," *Physics Letters A*, vol. 357, no. 4-5, pp. 323–329, 2006.
- [53] J. Yao and A. Lawrance, "Performance analysis and optimization of multi-user differential chaos-shift keying communication systems," *Circuits and Systems I: Regular Papers, IEEE Transactions on*, vol. 53, no. 9, pp. 2075 –2091, Sep. 2006.
- [54] G. Kolumban, G. Vizvari, W. Schwarz, and A. Abel, "Differential chaos shift keying: A robust coding for chaos communications," in *Proc. International Workshop on Nonlinear Dynamics of Electronic Systems, Seville, Spain*, 1996, pp. 92–97.
- [55] G. Kolumban, G. Kis, M. Kennedy, and Z. Jako, "FM-DCSK: A new and robust solution to chaos communications," in *Proc. International Symposium on Nonlinear Theory and Its Applications, Hawaii*, 1997, pp. 117–120.
- [56] G. Kolumban, G. Kis, and M. Kennedy, "Performance improvement of chaotic communicaion systems," 1997, pp. 248–289.
- [57] G. Kolumban, M. P. Kennedy, and L. O. Chua, "The role of synchronization in digital communications using chaos. II. chaotic modulation and chaotic synchronization," *IEEE Trans. Circuits Syst. I*, vol. 45, no. 11, pp. 1129–1140, Nov. 1998.
- [58] M. Kennedy, G. Kolumban, and G. Kis, "Simulation of the multipath performance of FM-DCSK digital communication using chaos," in *Proc. IEEE International Symposium on Circuits and Systems (ISCAS '99)*, vol. 4, 30 May – 2 June 1999, pp. 568–571.

- [59] G. Kolumban, Z. Jako, and M. Kennedy, “Enhanced versions of DCSK and FM-DCSK data transmission systems,” in *Proc. IEEE International Symposium on Circuits and Systems, (ISCAS ’99)*, vol. 4, 20 May–2 June 1999, pp. 475–478.
- [60] Z. Galias and G. Maggio, “Quadrature chaos-shift keying: theory and performance analysis,” *Circuits and Systems I: Fundamental Theory and Applications, IEEE Transactions on*, vol. 48, no. 12, pp. 1510 –1519, Dec. 2001.
- [61] F. C. M. Lau, Y. M.M., and C. K. Tse, “A multiple access technique for differential chaos shift keying,” in *Circuits and Systems, 2001. ISCAS ’01. Proceedings of the 2001 IEEE International Symposium on*, vol. 3, 6–9 May 2001, pp. 317–320.
- [62] C.-C. Chen and K. Yao, “Design of spread spectrum sequences using chaotic dynamical systems with lebesgue spectrum,” in *Proc. IEEE International Symposium on Circuits and Systems ISCAS 2001*, vol. 3, 6–9 May 2001, pp. 149–152.
- [63] C. Tse, F. Lau, K. Cheong, and S. Hau, “Return-map-based approaches for noncoherent detection in chaotic digital communications,” *Circuits and Systems I: Fundamental Theory and Applications, IEEE Transactions on*, vol. 49, no. 10, pp. 1495 – 1499, Oct. 2002.
- [64] F. C. M. Lau and C. K. Tse, “Optimum correlator-type receiver design for CSK communication systems,” *International Journal of Bifurcation & Chaos in Applied Sciences & Engineering*, vol. 12, no. 5, pp. 1029–1038, 2002.
- [65] W. Tam, F. Lau, and C. Tse, “Analysis of bit error rates for multiple access CSK and DCSK communication systems,” *Circuits and Systems I: Fundamental Theory and Applications, IEEE Transactions on*, vol. 50, no. 5, pp. 702 – 707, may 2003.
- [66] W. Tam, F. Lau, C. Tse, and A. Lawrance, “Exact analytical bit error rates for multiple access chaos-based communication systems,” *IEEE Trans. Circuits Syst. II*, vol. 51, no. 9, pp. 473–481, Sep. 2004.
- [67] Y. Xia, C. K. Tse, F. C. M. Lau, and G. Kolumban, “Performance of FM-DCSK communication system over a multipath fading channel with delay spread,” 2004, pp. 685–688.
- [68] Y. Xia, C. K. Tse, and F. C. M. Lau, “Some benchmark multipath performance data of coherent CSK digital communication systems,” 2004.
- [69] J. Yao and A. Lawrance, “Approximate optimal demodulation for multi-user binary coherent chaos-shift-keying communication systems,” May 2005, pp. 2052 – 2055 Vol. 3.
- [70] ———, “Optimal spreading in multi-user non-coherent binary chaos-shift-keying communication systems,” May 2005, pp. 876 – 879 Vol. 2.
- [71] X. Wang, M. Zhan, X. Gong, C. H. Lai, and Y. C. Lai, “Spread-spectrum communication using binary spatiotemporal chaotic codes,” *Physics Letters A*, vol. 334, no. 1, pp. 30–36, 2005.

- [72] M. B. Luca, S. Azou, G. Burel, and A. Serbanescu, “A complete receiver solution for a chaotic direct-sequence spread spectrum communication system,” in *Proc. IEEE International Symposium on Circuits and Systems ISCAS 2005*, 23–26 May 2005, pp. 3813–3816.
- [73] B. Jovic and C. Unsworth, “Chaos-based multi-user time division multiplexing communication system,” *Communications, IET*, vol. 1, no. 4, pp. 549 –555, Aug. 2007.
- [74] G. Cimatti, R. Rovatti, and G. Setti, “Chaos-based spreading in ds-uwb sensor networks increases available bit rate,” *Circuits and Systems I: Regular Papers, IEEE Transactions on*, vol. 54, no. 6, pp. 1327 –1339, Jun. 2007.
- [75] J. Yu, L. Gan, and L. Li, “Design of a real sequence chaotic direct sequence spread spectrum communication system with realizable occupied bandwidth,” Jul. 2009, pp. 282 –286.
- [76] J. Kao, V. Kecman, and S. Berber, “Blind multi-user detector for chaos-based CDMA using support vector machine,” *IEEE Neural Networks*, vol. 21, no. 8, pp. 1221 – 1231, Aug. 2010.
- [77] G. S. Sandhu, “Theoretical analysis and design of a multiuser chaos-based communication system,” Ph.D. dissertation, Faculty of Engineering, The University of Auckland New Zealand, 2009.
- [78] F. Lau and C. Tse, *Chaos-Based Digital Communicaiton Systems*. Berlin: Springer, 2004.
- [79] M. P. Kennedy, R. Rovatti, and G. Setti, *Chaotic electronics in telecommunications*. CRC Press, 2000.
- [80] S. Haykin and M. Moher, *Introduction to Analog & Digital Communications*, 2nd ed. John Wiley & Sons, Inc., 2007.
- [81] J. Gilley, “Bit-error-rate simulation using Matlab,” Transcrypt International, Inc., Tech. Rep., Aug. 2003.
- [82] T. Rappaport, *Wireless Communications: Principles and Practice*, 2nd ed. Upper Saddle River, NJ, USA: Prentice Hall PTR, 2001.
- [83] D. Parsons, *The Mobile Radio Propagation Channel*. Chichester, UK: John Wiley & Sons Ltd., 2000.
- [84] G. Arredondo, W. Chriss, and E. Walker, “A multipath fading simulator for mobile radio,” *Communications, IEEE Transactions on*, vol. 21, no. 11, pp. 1325 – 1328, nov 1973.
- [85] A. Goldsmith, *Wireless Communications*. New York, NY, USA: Cambridge University Press, 2005.
- [86] A. V. Pais, “The deployment and performance of indoor/outdoor DS-CDMA systems with multi-user detection,” Ph.D. dissertation, The University of Auckland New Zealand, 2007.
- [87] H.-S. Lee, H.-S. Oh, and C.-E. Kang, “Code acquisition for the ds-cdma rake receiver in a multipath fading channel,” Jul. 1995, pp. 215 –219.

- [88] G. Mazzini, R. Rovatti, and G. Setti, "Chaos-based asynchronous DS-CDMA systems and enhanced Rake receivers: measuring the improvements," *IEEE Trans. Circuits Syst. I*, vol. 48, no. 12, pp. 1445–1453, Dec. 2001.
- [89] Y. Suzuki, E. Kudoh, and S. Ogose, "DS-CDMA RAKE receiver with time-window control loop TWCL in multipath fading environment," *Vehicular Technology, IEEE Transactions on*, vol. 49, no. 1, pp. 167–172, Jan 2000.
- [90] A. Lawrance and G. Ohama, "Exact calculation of bit error rates in communication systems with chaotic modulation," *Circuits and Systems I: Fundamental Theory and Applications, IEEE Transactions on*, vol. 50, no. 11, pp. 1391 – 1400, Nov. 2003.
- [91] G. Kolumban, M. P. Kennedy, and L. O. Chua, "The role of synchronization in digital communications using chaos. I . fundamentals of digital communications," *IEEE Trans. Circuits Syst. I*, vol. 44, no. 10, pp. 927–936, Oct. 1997.
- [92] ———, "The role of synchronization in digital communications using chaos. III. performance bounds for correlation receivers," *IEEE Trans. Circuits Syst. I*, vol. 47, no. 12, pp. 1673–1683, Nov. 2000.
- [93] S. Berber and B. Jovic, "Sequence synchronization in a wideband CDMA system," in *Proceedings of the 2006 International Conference on Wireless Broadband and Ultra Wideband Communications (AusWireless06)*, Sydney, Australia, 13–16 March 2006, pp. 1–6.
- [94] B. Jovic, C. Unsworth, G. Sandhu, and S. Berber, "A robust sequence synchronization unit for multi-user DS-CDMA chaos-based communication systems," *Signal Processing*, vol. 87, no. 7, pp. 1692 – 1708, 2007.
- [95] G. Kaddoum, D. Roviras, P. Charge, and D. Fournier-Prunaret, "Robust synchronization for asynchronous multi-user chaos-based DS-CDMA," *Signal Processing*, vol. 89, no. 5, pp. 807–818, 2009.
- [96] P. Hopkins, "A unified analysis of pseudonoise synchronization by envelope correlation," *Communications, IEEE Transactions on*, vol. 25, no. 8, pp. 770–778, Aug 1977.
- [97] M. K. Simon, J. K. Omura, R. A. Scholtz, and B. K. Levitt, *Spread Spectrum Handbook*. McGraw-Hill, Inc., 2002.
- [98] J. Holmes and C. Chen, "Acquisition time performance of PN spread-spectrum systems," *Communications, IEEE Transactions on*, vol. 25, no. 8, pp. 778 – 784, Aug. 1977.
- [99] W. K. Alem and C. L. Weber, "Acquisition techniques of PN sequences," in *NTC '77; National Telecommunications Conference, Volume 2*, 1977.
- [100] C. L. Polydoros, A.; Weber, "Rapid acquisition techniques for direct-sequence spread spectrum systems using an analog detector," vol. 1, Nov./Dec. 1981, pp. A7.1.1–A7.1.5.

- [101] A. Polydoros and C. Weber, "A unified approach to serial search spread-spectrum code acquisition—part I: General theory," *Communications, IEEE Transactions on*, vol. 32, no. 5, pp. 542–549, 1984.
- [102] ———, "A unified approach to serial search spread-spectrum code acquisition—part II: A matched-filter receiver," *Communications, IEEE Transactions on [legacy, pre - 1988]*, vol. 32, no. 5, pp. 550–560, 1984.
- [103] D. DiCarlo and C. Weber, "Statistical performance of single dwell serial synchronization systems," *Communications, IEEE Transactions on*, vol. 28, no. 8, pp. 1382 – 1388, Aug. 1980.
- [104] ———, "Multiple dwell serial search: Performance and application to direct sequence code acquisition," *Communications, IEEE Transactions on*, vol. 31, no. 5, pp. 650 – 659, May 1983.
- [105] S. Lee, J. Kim, C. Lee, and S. Jun, "Double-dwell serial search algorithm with multi-level threshold values in DS-CDMA systems," vol. 1, 2000, pp. 522 –525 vol.1.
- [106] O.-S. Shin and K. B. Lee, "Differentially coherent combining for double-dwell code acquisition in DS-CDMA systems," *Communications, IEEE Transactions on*, vol. 51, no. 7, pp. 1046 – 1050, Jul. 2003.
- [107] R. L. Peterson, R. E. Zeimer, and D. E. Borth, *Introduction to Spread Spectrum Communication*. Englewood Cliffs, NJ: Prentice Hall, 1995.
- [108] R. Ward, "Acquisition of pseudonoise signals by sequential estimation," *Communication Technology, IEEE Transactions on*, vol. 13, no. 4, pp. 475 –483, 1965.
- [109] R. Ward and K. Yiu, "Acquisition of pseudonoise signals by recursion-aided sequential estimation," *Communications, IEEE Transactions on*, vol. 25, no. 8, pp. 784 – 794, Aug. 1977.
- [110] Y. You, J. Kim, H. Lee, and C. Kang, "Threshold decision for PN code acquisition in direct-sequence spread-spectrum packet radio systems," *Electronics Letters*, vol. 32, no. 4, pp. 306 –307, Feb. 1996.
- [111] J. Bussgang and D. Middleton, "Optimum sequential detection of signals in noise," *Information Theory, IRE Transactions on*, vol. 1, no. 3, pp. 5 –18, Dec. 1955.
- [112] A. Polydoros, "On synchronization aspects of direct-sequence spread spectrum systems," Ph.D. dissertation, University of Southern California, Los Angeles, 1982.
- [113] C. Kilgus, "Pseudonoise code acquisition using majority logic decoding," *Communications, IEEE Transactions on*, vol. 21, no. 6, pp. 772 – 774, Jun. 1973.
- [114] G. Sage, "Serial synchronization of pseudonoise systems," *Communication Technology, IEEE Transactions on*, vol. 12, no. 4, pp. 123 –127, 1964.
- [115] K. Chawla and D. Sarwate, "Parallel acquisition of PN sequences in DS/SS systems," *Communications, IEEE Transactions on*, vol. 42, no. 5, pp. 2155 –2164, May 1994.

- [116] W. Braun, "Performance analysis for the expanding search PN acquisition algorithm," *Communications, IEEE Transactions on*, vol. 30, no. 3, pp. 424 – 435, Mar. 1982.
- [117] A. Weinberg, "Generalized analysis for the evaluation of search strategy effects on PN acquisition performance," vol. 31, no. 1, Jan. 1983, pp. 37 – 49.
- [118] A. Polydoros, "Generalized serial search code acquisition: The equivalent circular state-diagram approach," vol. 2, Nov. 1983, pp. 496 – 500.
- [119] S. Soliman and R. Scholtz, "Synchronization over fading dispersive channels," *Communications, IEEE Transactions on*, vol. 36, no. 4, pp. 499 –505, Apr. 1988.
- [120] H.-S. Liaw and C. Chung, "Differentially coherent correlation technique for DS-SS code acquisition in a fast Rayleigh fading channel," *Electronics Letters*, vol. 30, no. 21, pp. 1738 –1740, Oct. 1994.
- [121] T. Ristaniemi and J. Joutsensalo, "Code timing acquisition for DS-CDMA in fading channels by differential correlations," *Communications, IEEE Transactions on*, vol. 49, no. 5, pp. 899 –910, May 2001.
- [122] B. Ibrahim and A. Aghvami, "Direct sequence spread spectrum matched filter acquisition in frequency-selective Rayleigh fading channels," *Selected Areas in Communications, IEEE Journal on*, vol. 12, no. 5, pp. 885–890, Jun. 1994.
- [123] S. Tantaratana, A. Lam, and P. Vincent, "Noncoherent sequential acquisition of PN sequences for DS/SS communications with/without channel fading," *Communications, IEEE Transactions on*, vol. 43, no. 234, pp. 1738 –1745, Apr. 1995.
- [124] E. G. Strom, S. Parkvall, S. L. Miller, and B. E. Ottersten, "DS-CDMA synchronization in time-varying fading channels," *Selected Areas in Communications, IEEE Journal on*, vol. 14, no. 8, pp. 1636–1642, 1996.
- [125] Y. You, H. Cho, M. Joo, and C. Kang, "Detection technique for a serial DS-SS code synchronisation in a fading mobile channel," *Electronics Letters*, vol. 33, no. 6, pp. 446 –447, Mar. 1997.
- [126] Y.-H. You, T.-H. Moon, J.-H. Kim, and C.-E. Kang, "Threshold decision technique for direct sequence code synchronisation in a fading mobile channel," *Communications, IEE Proceedings-*, vol. 144, no. 3, pp. 155 –160, Jun. 1997.
- [127] J. Iinatti, "Performance of DS code acquisition in static and fading multipath channels," *Communications, IEE Proceedings on*, vol. 147, no. 6, pp. 355 –360, Dec. 2000.
- [128] K.-W. Jang, T.-H. Kim, Y.-W. Park, and M. Murata, "Code acquisition system using periodic property of PN code in Rayleigh fading channel," vol. 6, 2000, pp. 2834 –2838.
- [129] L.-L. Yang and L. Hanzo, "Serial acquisition of DS-CDMA signals in multipath fading mobile channels," *Vehicular Technology, IEEE Transactions on*, vol. 50, no. 2, pp. 617 –628, Mar. 2001.

- [130] W.-H. Sheen and H.-C. Wang, "A new analysis of direct-sequence pseudonoise code acquisition on Rayleigh fading channels," *Selected Areas in Communications, IEEE Journal on*, vol. 19, no. 11, pp. 2225 –2232, Nov. 2001.
- [131] S. Vijayakumaran, T. Wong, and S. Aedudodla, "On the asymptotic performance of threshold-based acquisition systems in multipath fading channels," *Information Theory, IEEE Transactions on*, vol. 51, no. 11, pp. 3973 – 3986, Nov. 2005.
- [132] J. Moon and Y.-H. Lee, "Parallel acquisition of PN sequences in Rayleigh fading channel and the application to the multi-carrier CDMA systems," vol. 2, Sep. 2001, pp. G–6 –G–10 vol.2.
- [133] P. Shamain and L. Milstein, "Acquisition of direct sequence spread spectrum signals with correlated fading," *Selected Areas in Communications, IEEE Journal on*, vol. 19, no. 12, pp. 2406 –2419, Dec. 2001.
- [134] G. Corazza, C. Caini, A. Vanelli-Coralli, and A. Polydoros, "DS-CDMA code acquisition in the presence of correlated fading - Part I: theoretical aspects," *Communications, IEEE Transactions on*, vol. 52, no. 7, pp. 1160 – 1168, Jul. 2004.
- [135] P. Dmochowski and P. McLane, "Joint timing and pilot symbol channel estimation for diversity receivers in Rayleigh fading channels," vol. 3, Sep. 2004, pp. 1658 – 1663.
- [136] O.-S. Shin and K. B. Lee, "Utilization of multipaths for spread-spectrum code acquisition in frequency-selective Rayleigh fading channels," *Communications, IEEE Transactions on*, vol. 49, no. 4, pp. 734 –743, Apr. 2001.
- [137] H. W. Je, O.-S. Shin, and K. B. Lee, "Acquisition for DS/CDMA systems with multiple antennas in frequency-selective fading channels," *Wireless Communications, IEEE Transactions on*, vol. 2, no. 4, pp. 787 – 798, Jul. 2003.
- [138] G. Mazzini, R. Rovatti, and G. Setti, "Sequence synchronization in chaos-based DS-CDMA systems," in *Circuits and Systems, 1998. ISCAS '98. Proceedings of the 1998 IEEE International Symposium on*, vol. 4, May. 1998, pp. 485–488 vol.4.
- [139] A. J. Viterbi, *CDMA: Principles of Spread Spectrum Communications*. Addison-Wesley, 1995.
- [140] J.-P. Mangeot, F. Launay, and P. Coirault, "A multi-user transmission using chaotic carriers," *Communications in Nonlinear Science and Numerical Simulation*, vol. 14, no. 6, pp. 2709 – 2719, 2009.
- [141] B. Jovic, "Synchronisation techniques for single and multiple-access chaotic communication systems," Ph.D. dissertation, Faculty of Engineering, The University of Auckland, 2007.
- [142] J. J. Spilker and D. Magill, "The delay-lock discriminator-an optimum tracking device," *Proceedings of the IRE*, vol. 9, pp. 1403–1416, 1961.
- [143] J. J. Spilker, "Delay-lock tracking of binary signals," *Space Electronics and Telemetry, IEEE Transactions on*, vol. 9, no. 1, pp. 1 –8, Mar. 1963.

- [144] H. Meyr, "Delay-lock tracking of stochastic signals," *Communications, IEEE Transactions on*, vol. 24, no. 3, pp. 331–339, 1976.
- [145] W. J. Gill, "A comparison of binary delay-lock tracking-loop implementations," *Aerospace and Electronic Systems, IEEE Transactions on*, vol. AES-2, no. 4, pp. 415 –424, Jul. 1966.
- [146] J. Holmes and L. Biederman, "Delay-lock-loop mean time to lose lock," *Communications, IEEE Transactions on*, vol. 26, no. 11, pp. 1549 – 1557, Nov. 1978.
- [147] A. Welti and B. Bobrovsky, "Optimization of a second order PN-code tracking loop using the mean exit time criterion," Aug. 1989, pp. 487 –490.
- [148] U. Bernhard and B. Bobrovsky, "Mean exit time of a noncoherent DLL for a randomly fluctuating channel delay," vol. 3, Oct. 1993, pp. 804 –808 vol.3.
- [149] J. Hasson and B. Bobrovsky, "A comparison of the mean time to lose lock in coherent/noncoherent DLL's," Mar. 1995.
- [150] J. Moss, A. Street, D. Edwards, and M. Mehler, "Analysis of a DS-CDMA receiver DLL architecture," vol. 1, Sep. 1996, pp. 460 –464 vol.1.
- [151] K. Kiasaleh, "Channel-aided, decision-directed delay-locked loop for pilot symbol aided CDMA communications impaired by fast frequency-selective Rayleigh fading and user interference," *Vehicular Technology, IEEE Transactions on*, vol. 49, no. 4, pp. 1392–1407, 2000, 0018-9545.
- [152] M. Guenach and L. Vandendorpe, "Tracking performance of DA and DD multiuser timing synchronizers for short code DS-CDMA systems," *Selected Areas in Communications, IEEE Journal on*, vol. 19, no. 12, pp. 2452–2461, Dec. 2001.
- [153] W. Huang, I. Andonovic, and M. Nakagawa, "Code tracking of DS-CDMA systems in the presence of multiuser interference and additive noise," vol. 3, Sep. 1998, pp. 843 –847 vol.3.
- [154] S. Thayaparan, T.-S. Ng, and J. Wang, "The use of delay-locked loop signals in DS/CDMA receiver for multiple-access interference reduction," *Vehicular Technology, IEEE Transactions on*, vol. 55, no. 3, pp. 980–989, May 2006.
- [155] H.-R. Park, "Performance analysis of a decision-feedback coherent code tracking loop for pilot-symbol-aided DS/SS systems," *Vehicular Technology, IEEE Transactions on*, vol. 55, no. 4, pp. 1249 –1258, Jul. 2006.
- [156] S. Thayaparan, T.-S. Ng, and J. Wang, "Half-sine and triangular despreading chip waveforms for coherent delay-locked tracking in DS/SS systems," *Communications, IEEE Transactions on*, vol. 48, no. 8, pp. 1384 –1391, Aug. 2000.
- [157] H. Hartmann, "Analysis of a dithering loop for PN code tracking," *Aerospace and Electronic Systems, IEEE Transactions on*, vol. AES-10, no. 1, pp. 2 –9, Jan. 1974.
- [158] M. Simon, "Noncoherent pseudonoise code tracking performance of spread spectrum receivers," *Communications, IEEE Transactions on*, vol. 25, no. 3, pp. 327 – 345, Mar. 1977.

- [159] P. M. Hopkins, "Double dither loop for pseudonoise code tracking," *Aerospace and Electronic Systems, IEEE Transactions on*, vol. AES-13, no. 6, pp. 644–650, 1977.
- [160] R. Yost and R. Boyd, "A modified PN code tracking loop: Its performance analysis and comparative evaluation," *Communications, IEEE Transactions on*, vol. 30, no. 5, pp. 1027 – 1036, May 1982.
- [161] D. LaFlame, "A delay-lock loop implementation which is insensitive to arm gain imbalance," *Communications, IEEE Transactions on*, vol. 27, no. 10, pp. 1632 – 1633, Oct. 1979.
- [162] E. F. Osborne and T. Schonhof, "Delay-locked receivers with phase sensing of correlation (error) function," vol. II, Nov. 1973, pp. 26B–1–26B–6.
- [163] C.-Y. Lo, K.-C. Chen, and W.-H. Sheen, "Noncoherent DLL and TDL PN code tracking loops in Rayleigh fading channels," vol. 1, Sep. 1994, pp. 338 –342.
- [164] W.-H. Sheen and G. Stuber, "A new tracking loop for direct sequence spread spectrum systems on frequency-selective fading channels," *Communications, IEEE Transactions on*, vol. 43, no. 12, pp. 3063–3072, Dec 1995.
- [165] J.-C. Lin, "A modified PN code tracking loop for direct-sequence spread-spectrum communication over arbitrarily correlated multipath fading channels," *Selected Areas in Communications, IEEE Journal on*, vol. 19, no. 12, pp. 2381 –2395, Dec. 2001.
- [166] G. Setti, R. Rovatti, and G. Mazzini, "Synchronization mechanism and optimization of spreading sequences in chaos-based DS-CDMA systems," *IEICE Transactions on Fundamentals of Electronics, Communications and Computer Sciences*, vol. E82-A, no. 9, pp. 1737–1746, Sep. 1999.
- [167] R. Vali, S. Berber, and S. K. Nguang, "Analysis of a chaos-based non-coherent delay lock tracking loop," in *Communications (ICC), 2010 IEEE International Conference on*, 2010, pp. 1–6.
- [168] J. K. Holmes, *Spread Spectrum Systems for GNSS and Wireless Communications*, ser. GNSS technology and applications. London: Artech House, 2007.
- [169] R. Vali, S. Berber, and S. K. Nguang, "Accurate derivation of chaos-based acquisition phase performance in a fading channel," *IEEE Trans. Wireless Commun.*, submitted for publication.
- [170] T. Geisel and V. Fairen, "Statistical properties of chaos in Chebyshev maps," *Physics Letters*, vol. 105A, pp. 263–266, 1984.
- [171] G. Kaddoum, P. Charge, D. Roviras, and D. Fournier-Prunaret, "A methodology for bit error rate prediction in chaos-based communication systems," *Circuits, Systems, and Signal Processing*, vol. 28, pp. 925–944, 2009.
- [172] M. K. Simon, *Probability distributions involving Gaussian random variables*. Springer, 2002.
- [173] N. Johnson and H. Tetley, *Statistics: An Intermediate Textbook*. Cambridge University Press, 1949, vol. 1.

- [174] E. Biglieri, J. Proakis, and S. Shamai, “Fading channels: information-theoretic and communications aspects,” *IEEE Trans. Inform. Theory*, vol. 44, no. 6, pp. 2619–2692, Oct. 1998.
- [175] E. Biglieri, G. Caire, and G. Taricco, “Coding for the fading channel: a survey,” *Signal Processing.*, vol. 80, no. 7, pp. 1135–1148, 2000.
- [176] R. Vali, S. Berber, and S. K. Nguang, “Analysis of chaos-based code tracking using chaotic correlation statistics,” *IEEE Trans. Circuits Syst. I*, to be published.
- [177] ———, *Planning and Optimisation of 3G and 4G Wireless Networks*. River Publishers, 2009, ch. Synchronization, pp. 445–479.
- [178] I. Miller, *Miller and Freund's probability and statistics for engineers*, 2004.
- [179] R. Vali, S. Berber, and S. K. Nguang, “Performance of chip interleaved partially synchronised chaotic DS-SS systems,” *IEEE Trans. Wireless Commun.*, submitted for publication.
- [180] B. G. Agee, R. J. Kleinman, and J. H. Reed, “Soft synchronization of direct sequence spread-spectrum signals,” *Communications, IEEE Transactions on*, vol. 44, no. 11, pp. 1527–1536, 1996.
- [181] W. A. Al-Qaq, M. Devetsikiotis, and J. K. Townsend, “Importance sampling methodologies for simulation of communication systems with time-varying channels and adaptive equalizers,” *Selected Areas in Communications, IEEE Journal on*, vol. 11, no. 3, pp. 317–327, 1993.
- [182] A. Barbosa and S. Miller, “Adaptive detection of DS/CDMA signals in fading channels,” *Communications, IEEE Transactions on*, vol. 46, no. 1, pp. 115–124, Jan. 1998.
- [183] M. El-Tarhuni and A. Sheikh, “Performance analysis for an adaptive filter code-tracking technique in direct-sequence spread-spectrum systems,” *Communications, IEEE Transactions on*, vol. 46, no. 8, pp. 1058–1064, Aug 1998.
- [184] M. El-Tarhuni, “A modified non-coherent delay-locked loop for CDMA systems,” vol. 2, May 2004, pp. 1124–1128 Vol.2.
- [185] R. Vali and S. M. Berber, “Secure communication in asynchronous noise phase shift keying CDMA systems,” in *Spread Spectrum Techniques and Applications (ISSSTA) . 2008 IEEE 10th International Symposium on*, Aug. 2008, pp. 528–533.
- [186] ———, “Analysis of non-coherent code tracking for NPSK systems in presence of noise and fading,” May 2011, pp. 3516 –3519.
- [187] R. Vali, S. Berber, and S. K. Nguang, “Comparing DSP realizations of correlator and SVM receivers for chaos-based multi-user DS-SS,” *Signal Processing*, submitted for publication.
- [188] *ADSP-TS201S: 500/600 MHz TigerSHARC Processor Data Sheet*, Dec. 2006.
- [189] H. Kamata, Y. Umezawa, M. Dobashi, T. Endo, and Y. Ishida, “Private communications with chaos based on the fixed-point computation,” *IEICE Transactions on Fundamentals of Electronics, Communications and Computer Sciences*, vol. E83, pp. 1238–1246, 2000.

- [190] L. Simic and S. Berber, “Performance analysis of a chaos-based multi-user communication system implemented in dsp technology,” in *Proc. AusWireless '2006.*, 13-16 March 2006.
- [191] J.-L. Danger, A. Ghazel, E. Boutillon, and H. Laamari, “Efficient FPGA implementation of gaussian noise generator for communication channel emulation,” vol. 1, 2000, pp. 366–369.
- [192] W. M. Tam, F. C. M. Lau, C. K. Tse, and A. J. Lawrance, “Exact analytical bit error rates for multiple access chaos-based communication systems,” vol. 51, no. 9, pp. 473–481, Sep. 2004.